The Dissertation Committee for Diane Christine Forbes certifies that this is the approved version of the following dissertation:

pH-Responsive Polymer Nanoparticles Synthesized Using ARGET ATRP

Committee:

Nicholas Peppas, Supervisor

Donald Paul

Christopher Ellison

Lydia Contreras

Aaron Baker

pH-Responsive Polymer Nanoparticles Synthesized Using ARGET ATRP

by

Diane Christine Forbes, B.S.

Dissertation

Presented to the Faculty of the Graduate School of

The University of Texas at Austin

in Partial Fulfillment

of the Requirements

for the Degree of

Doctor Of Philosophy

The University of Texas at Austin

December 2013

To my husband and my parents

Acknowledgments

Thank you to the many people who have helped me learn and grow during my graduate studies. Your support and guidance is appreciated more than I can possibly express in words.

I thank Dr. Nicholas Peppas for his guidance and instruction, both for my research as well as my professional development. He shared his passion for polymers and biomaterials and worked tirelessly for the good of his lab.

I thank my committee members for their support and guidance. I owe a special thanks to Dr. Christopher Ellison for kindly permitting me to use his lab equipment for polymer characterization. I am grateful to Dr. Donald Paul for his helpful discussions and for giving me the opportunity to be the teaching assistant for his polymers class. Thank you to Dr. Lydia Contreras for her encouragement and suggestions. Thank you to Dr. Aaron Baker for agreeing to serve on my committee.

I am grateful for my friends and colleagues for their support during graduate school. I thank the Peppas lab post-doctoral researchers, Dr. Mar Creixell, Dr. Brenda Carrillo-Conde, and Dr. Mary Caldorera-Moore, for their help with my research. Thank you to the Peppamers who graduated during my time in the lab, Dr. Margaret Phillips, Dr. Cody Schoener, and Dr.

William Liechty, for their leadership. Thank you to my fellow labmates, Brandon Slaughter, Jennifer Knipe, Amey Puranik, Stephanie Steichen, Jonathan Peters, Michael Koetting, Heidi Culver, Lindsey Sharpe, Adam Daily, and Sarena Horava, for their suggestions and assistance which contributed to my project. I give special thanks to Hannah Frizzell, my undergraduate student, for her hard work and enthusiasm for research – mentoring you and seeing you learn has been one of the greatest delights of graduate school.

I am very thankful for the help of many other people with important experiments. I thank the Ellison lab for their generous assistance, especially Dr. Josh Katzenstein for help with my ARGET ATRP chemistry, Julie Cushen and Sunshine Zhou for help with SAXS, and Dr. Dustin Janes for assistance with FTIR. Thank you to ICMB facilities staff Julie Hayes (confocal microscopy) and Richard Salinas (flow cytometry) for all of their assistance.

I acknowledge research funding from the National Science Foundation (CBET-1033746) and additional financial support from the National Science Foundation Graduate Research Fellowship Program.

The help and support I received outside of the laboratory was just as important in my success. Thank you to Jackson Stolle and Kyle Klavetter for being such good classmates and friends. I am very grateful for the friendship and encouragement of Andrea Stolle. I am thankful for my cousin Andrew Brown and his wife, Ariel Brown, for helping Travis Forbes and me stay connected to the world outside of graduate school. Thank you to my sister, Linda Brown, for her love and support, and good luck to her in her own graduate

school career! I am thankful for my parents Roger and Rosanne Brown for their encouragement.

Most of all, I thank my husband, Travis Forbes, for all of his love and support that sustained me through graduate school. I am so blessed to have such an incredible partner walking alongside me. Congratulations from one future Dr. Forbes to another as he prepares to graduate with his Ph.D. in electrical engineering in December 2013.

pH-Responsive Polymer Nanoparticles Synthesized Using ARGET ATRP

Diane Christine Forbes, Ph.D.
The University of Texas at Austin, 2013

Supervisor: Nicholas Peppas

Polycationic nanoparticles were synthesized with an activators regenerated by electron transfer for atom transfer radical polymerization-based (ARGET ATRP-based) emulsion in water method and investigated for their utility as biomaterials for drug delivery. The polycationic nanoparticles were composed of 2-(diethylamino)ethyl methacrylate (DEAEMA) for pH-responsiveness, poly(ethylene glycol) methyl ether methacrylate (PEGMA) for improved biocompatibility, *tert*-butyl methacrylate (tBMA) to impart hydrophobicity, and a tetraethylene glycol dimethacrylate (TEGDMA) cross-linking agent for enhanced colloidal stability. Dynamic light scattering demonstrated pH-responsive swelling, and cell-based assays demonstrated pH-dependent membrane disruption. The polycationic nanoparticles demonstrated low toxicity to cells.

The polycationic nanoparticles were evaluated for use as drug delivery biomaterials by investigating the interactions with the drug and cells. Delivery remains a major challenge for translating small interfering RNA (siRNA) to the clinic, and overcoming the delivery challenge requires effective siRNA delivery vehicles. The polycationic nanoparticles demonstrated efficient siRNA loading. Evidence of siRNA-induced knockdown in cells was observed following transfection with the polycationic nanoparticle/siRNA complexes. Imaging techniques confirmed enhanced siRNA internalization using the polycationic nanoparticle/siRNA complexes compared to naked siRNA.

An array of polycationic nanoparticles synthesized using ARGET ATRP or UV-initiated polymerization methods was characterized to examine the effect of polymerization method on material properties and the connection to molecular structure. An improved understanding of molecular structure, and its connection to polymerization method and material characteristics, may aid the design of advanced materials. The ARGET ATRP polycationic nanoparticles demonstrated increased nanoscale homogeneity compared to the UV-initiated polymerization polycationic nanoparticles; increased nanoscale heterogeneity in the UV-initiated polymerization polycationic nanoparticles was associated with broader transitions.

The polycationic nanoparticles promoted cellular uptake of siRNA and induced knockdown, thus demonstrating potential as siRNA delivery vehicles. The ARGET ATRP method provides an alternative route to creating polycationic nanoparticles with improved nanoscale homogeneity.

Table of Contents

List of Tables

List of Figures

Chapter 1

Introduction and Research Objectives

1.1 Introduction

Biomaterials researchers operate at the interface between biology and materials science in order to create new materials that can aid patients by detecting, treating, or preventing disease. Drug delivery remains an active focus for biomaterials researchers as well as researchers in the area of nanomedicine, which is the medical application of nanotechnology.[1–3] Nano- or micro-scale delivery vehicles can enhance therapeutic efficacy compared to free-drug (no-carrier) by avoiding rapid clearance,[4] preventing enzymatic degradation of the therapeutic agent,[5] or bypassing efflux pumps with chemotherapeutic-loaded nanoparticles.[6]

Nano- and micro-scale stimuli-responsive polymer hydrogels may be used as drug delivery biomaterials.[7–11] Hydrogels are three-dimensional networks of cross-linked polymer chains, which, due to their hydrophilicity swell in water or biological fluids.[12;13] Stimuli-responsive polymers respond to environmental triggers, such as swelling in response to low pH values, and this response to stimuli can be used to release loaded therapeutic drugs.[14–18]

There has been renewed interest in nanoscale biomaterials for drug delivery as a result of research interest in siRNA (small interfering RNA) and RNA interference.[19–21] First reported by Fire and Mello,[22] RNAi is an innate mechanism within cells to alter gene expression in response to small RNAs; the small RNA initiates a catalytic mechanism to degrade specific mRNA molecules.[23] RNAi-based therapeutic agents offer the potential to correct aberrant gene expression to treat disease.[24–31] This impressive potential is matched by the challenges of delivery; siRNA must avoid degradation by nucleases, be internalized by the target cells, and escape the endosome in order to be active in the cytosol.[32;33] Drug delivery vehicles such as pH-responsive nanogels are one delivery strategy designed to help the siRNA overcome these delivery challenges.[34–37]

New technologies in controlled radical polymerization have created opportunities to make drug delivery biomaterials with controlled chemical structures.[38;39] Controlled radical polymerization, in contrast to traditional free radical polymerization, provides enhanced control over molecular structure by minimizing the concentration of free radicals to suppress termination reactions.[40–42] While advanced polymerization chemistries have been typically conducted in organic solvents in order to avoid side reactions that make aqueous polymerizations challenging, the reports of aqueous controlled radical polymerization reactions are growing[43–45] as are reports of advanced chemistries for the synthesis of drug delivery vehicles using hydrophilic polymers.[46–51]

ARGET ATRP (activators regenerated by electron transfer for atom

transfer radical polymerization) is a recently-reported controlled radical polymerization technique.[52;53] In contrast to traditional ATRP which makes use of a "forward" chemical mechanism with active copper(I) catalysts, reverse ATRP techniques such as ARGET ATRP make use of a "reverse" chemical initiation strategy where inactive copper(II) catalyst is reduced in order to activate the reaction.[54] The copper(II) is more air-stable than copper(I) and can be activated by the addition of a reducing agent;[55] as a result, ARGET ATRP can take place in the presence of residual air.[56]

Advances in controlled radical polymerization technology create opportunities for new, and possibly improved, biomaterials for drug delivery by enhancing control over molecular structure. New chemistries, such as ARGET ATRP, may offer advantages over previously developed technologies, but the ultimate utility of these chemistries for the synthesis of biomaterials for drug delivery will depend on careful investigations that seek to better understand the material properties and the interactions between the material and relevant biological systems.

1.2 Research objectives

In order to advance the goal of creating and investigating new ARGET ATRP-based materials and understanding their utility as biomaterials for drug delivery, the research objectives were to:

1. Develop an ARGET ATRP-based technique to synthesize polycationic

nanoparticles;

2. Evaluate the suitability of the polycationic nanoparticles for drug delivery; and

3. Examine the effect of polymerization method on material properties and the connection to molecular structure.

The objectives of this research are part of a broader research project to create an oral delivery system for siRNA therapeutics. The research to achieve this broader goal is collaborative and ongoing. The polycationic nanoparticle research represents a piece of the work to overcome the many challenges associated with creating an oral delivery system for siRNA therapeutics.The polycationic nanoparticles have utility for intracellular delivery as part of this future oral delivery system. The specific challenges associated with creating an siRNA delivery system suitable for oral administration are being tackled by another researcher; this research focuses on the polycationic nanoparticles and their interactions with siRNA and cells.

Develop an ARGET ATRP-based technique to synthesize polycationic nanoparticles This work represents the first report in the literature of polycationic nanoparticles synthesized using an ARGET ATRP-based emulsion in water synthesis method. Polycationic nanoparticles composed of 2-(diethylamino)ethyl methacrylate (DEAEMA), poly(ethylene glycol) methyl ether methacrylate (PEGMA), and *tert*-butyl methacrylate monomers with

tetraethylene glycol dimethacrylate (TEGDMA) cross-linking agent were synthesized with the ARGET ATRP-based emulsion. While the new method may offer unique properties in the resulting materials, the advantage of the new method may come from an alternative route to creating polycationic nanoparticles. The Chemistry background (Chapter 2) provides an introduction to ARGET ATRP, examples of relevant polycationic nanoparticles found in the literature, and a discussion of the toxicity of the chemicals used in synthesis. The protocol for the new synthesis technique and initial characterization results are first presented in Chapter 4.

Evaluate the suitability of the polycationic nanoparticles for drug delivery The polycationic nanoparticles synthesized using the new ARGET ATRP-based technique were investigated for use as drug delivery vehicles. The successful delivery of siRNA to cells to induce knockdown was a central goal. The siRNA background (Chapter 3) provides a discussion of the therapeutic potential of small RNA and DNA, continuing challenges in drug delivery, and a discussion of oligonucleotide oral delivery systems found in the literature. Material characterization relevant to drug delivery including size, biocompatibility, pH-responsiveness, and the loading and release of a small molecule (representing a model chemotherapeutic) is first described in Chapter 4. The polycationic nanoparticles are investigated for for siRNA delivery to an easy-to-transfect cell line and a hard-to-transfect cell line in Chapter 5. The siRNA binding is evaluated to determine loading efficiency and the uptake of siRNA

is investigated. Chapter 4 and Chapter 5 provide a comparison of four different formulations. Chapter 6 takes a closer look at a single ARGET ATRP formulation in order to better understand the interaction of the polycationic nanoparticles with siRNA and with cells.

Examine the effect of polymerization method on material properties and the connection to molecular structure. An improved understanding of molecular structure, and its connection to synthesis techniques and material properties, may facilitate the design of enhanced materials. In Chapter 7, four formulations of polycationic nanoparticles were characterized using a variety of techniques designed to probe the molecular structure. Nanoscale heterogeneity represents a critical aspect of molecular structure, as heterogeneity leads to broad transitions while homogeneity leads to sharp transitions.

1.3 References

[1] R. L. Juliano. The future of nanomedicine: Promises and limitations. *Sci. Publ. Policy*, 39(1):99–104, 2012.

[2] T. L. Doane and C. Burda. The unique role of nanoparticles in nanomedicine: imaging, drug delivery and therapy. *Chem. Soc. Rev.*, 41(7):2885–2911, 2012.

[3] M. L. Etheridge, S. A. Campbell, A. G. Erdman, C. L. Haynes, S. M. Wolf, and J. McCullough. The big picture on nanomedicine: the state of investigational and approved nanomedicine products. *Nanomed.: Nanotechnol.*, 9(1):1–14, 2013.

[4] W.B. Liechty and N.A. Peppas. Expert opinion: Responsive polymer nanoparticles in cancer therapy. *Eur. J. Pharm. Biopharm.*, 80:241–246, 2012.

[5] W.B. Liechty, D.R. Kryscio, B.V. Slaughter, and N.A. Peppas. Polymers for drug delivery systems. *Annu. Rev. Chem. Biomol.*, 1(1):149–173, 2010.

[6] M. Creixell and N. A. Peppas. Co-delivery of siRNA and therapeutic agents using nanocarriers to overcome cancer resistance. *Nano Today*, 7 (4):367–379, 2012.

[7] N. A. Peppas. Intelligent therapeutics: biomimetic systems and nan-

otechnology in drug delivery. *Adv. Drug Deliver. Rev.*, 56(11):1529–1531, 2004.

[8] M Caldorera-Moore and N.A. Peppas. Micro- and nanotechnologies for intelligent and responsive biomaterial-based medical systems. *Adv. Drug Deliver. Rev.*, 61(15):1391–1401, 2009.

[9] L. Wu, J. Zhang, and W. Watanabe. Physical and chemical stability of drug nanoparticles. *Adv. Drug Deliver. Rev.*, 63(6):456–469, 2011.

[10] S. C. Balmert and S. R. Little. Biomimetic delivery with micro-and nanoparticles. *Adv. Mater.*, 24(28):3757–3778, 2012.

[11] P. Couvreur. Nanoparticles in drug delivery: Past, present and future. *Adv. Drug Deliver. Rev.*, 65(1):21–23, 2013.

[12] N. A. Peppas, P. Bures, W. Leobandung, and H. Ichikawa. Hydrogels in pharmaceutical formulations. *Eur. J. Pharm. Biopharm.*, 50(1):27–46, 2000.

[13] N. A. Peppas, J. Z. Hilt, A. Khademhosseini, and R. Langer. Hydrogels in biology and medicine: From molecular principles to bionanotechnology. *Adv. Mater.*, 18(11):1345–1360, 2006.

[14] W. Gao, J. M. Chan, and O. C. Farokhzad. pH-responsive nanoparticles for drug delivery. *Mol. Pharm.*, 7(6):1913–1920, 2010.

[15] W.B. Liechty, M. Caldorera-Moore, M.A. Phillips, C. Schoener, and N.A. Peppas. Advanced molecular design of biopolymers for transmucosal and intracellular delivery of chemotherapeutic agents and biological therapeutics. *J. Control. Release*, 155(2):119–127, 2011.

[16] J. Yoo, D. J. Irvine, D. E. Discher, and S. Mitragotri. Bio-inspired, bioengineered and biomimetic drug delivery carriers. *Nat. Rev. Drug Discov.*, 10(7):521–535, 2011.

[17] A. K. Bajpai, Jaya Bajpai, Rajesh Saini, and Rashmi Gupta. Responsive polymers in biology and technology. *Polym. Rev.*, 51(1):53–97, 2011.

[18] A. S. Hoffman. Stimuli-responsive polymers: Biomedical applications and challenges for clinical translation. *Adv. Drug Deliver. Rev.*, 65(1):10–16, 2012.

[19] S. Ganta, H. Devalapally, A. Shahiwala, and M. Amiji. A review of stimuli-responsive nanocarriers for drug and gene delivery. *J. Control. Release*, 126(3):187–204, 2008.

[20] D. S. H. Chu, J. G. Schellinger, J. Shi, A. J. Convertine, P. S. Stayton, and S. H. Pun. Application of living free radical polymerization for nucleic acid delivery. *Acc. Chem. Res.*, 45(7):1089–1099, 2012.

[21] B. Ballarín-González, F. Dagnaes-Hansen, R. A Fenton, S. Gao, S. Hein, M. Dong, J. Kjems, and K. A Howard. Protection and systemic transloca-

tion of siRNA following oral administration of chitosan/siRNA nanoparticles. *Mol. Ther. Nucleic Acids*, 2(3):e76, 2013.

[22] A. Fire, S. Q. Xu, M. K. Montgomery, S. A. Kostas, S. E. Driver, and C. C. Mello. Potent and specific genetic interference by double-stranded RNA in *Caenorhabditis elegans*. *Nature*, 391(6669):806–811, 1998.

[23] D. Bumcrot, M. Manoharan, V. Koteliansky, and D. W. Y. Sah. RNAi therapeutics: a potential new class of pharmaceutical drugs. *Nat. Chem. Biol.*, 2(12):711–719, 2006.

[24] D. Cejka, D. Losert, and V. Wacheck. Short interfering RNA (siRNA): tool or therapeutic? *Clin. Sci.*, 110(1):47, 2006.

[25] L. Bonetta. RNA-based therapeutics: Ready for delivery? *Cell*, 136(4): 581–584, 2009.

[26] D. Castanotto and J. J. Rossi. The promises and pitfalls of RNA-interference-based therapeutics. *Nature*, 457(7228):426–433, 2009.

[27] K. Tiemann and J. J. Rossi. RNAi-based therapeutics-current status, challenges and prospects. *EMBO Mol. Med.*, 1(3):142–151, 2009.

[28] B. L. Davidson and P. B. McCray. Current prospects for RNA interference-based therapies. *Nat. Rev. Genet.*, 12(5):329–340, 2011.

[29] K. Cheng and R. I. Mahato. Biological and therapeutic applications of small RNAs. *Pharm. Res.*, 28(12):2961–2965, 2011.

[30] J.C. Burnett, J.J. Rossi, and K. Tiemann. Current progress of siRNA/shRNA therapeutics in clinical trials. *Biotechnol. J.*, 6(9):1130–1146, 2011.

[31] J. K. Watts and D. R. Corey. Silencing disease genes in the laboratory and the clinic. *J. Pathol.*, 226(2):365–379, 2011.

[32] A. Aigner. Cellular delivery *in vivo* of siRNA-based therapeutics. *Curr. Pharm. Des.*, 14(34):3603–3619, 2008.

[33] K. A. Whitehead, R. Langer, and D. G. Anderson. Knocking down barriers: advances in siRNA delivery. *Nat. Rev. Drug Discov.*, 8(2):129–138, 2009.

[34] D. W. Pack, A. S. Hoffman, S. Pun, and P. S. Stayton. Design and development of polymers for gene delivery. *Nat. Rev. Drug Discov.*, 4(7): 581–593, 2005.

[35] D. J. Gary, N. Puri, and Y. Y. Won. Polymer-based siRNA delivery: Perspectives on the fundamental and phenomenological distinctions from polymer-based DNA delivery. *J. Control. Release*, 121(1-2):64–73, 2007.

[36] K. Bruno. Using drug-excipient interactions for siRNA delivery. *Adv. Drug Deliver. Rev.*, 63(13):1210–1226, 2011.

[37] T. Wang, J. R. Upponi, and V. P. Torchilin. Design of multifunctional non-viral gene vectors to overcome physiological barriers: Dilemmas and strategies. *Int. J. Pharm.*, 427(1):3–20, 2012.

[38] D. J. Siegwart, J. K. Oh, and K. Matyjaszewski. ATRP in the design of functional materials for biomedical applications. *Prog. Polym. Sci.*, 37 (1):18–37, 2012.

[39] J. K. Oh, R. Drumright, D. J. Siegwart, and K. Matyjaszewski. The development of microgels/nanogels for drug delivery applications. *Prog. Polym. Sci.*, 33(4):448–477, 2008.

[40] K. Matyjaszewski and J. Xia. Atom transfer radical polymerization. *Chem. Rev.*, 101(9):2921–2990, 2001.

[41] N. Ayres. Atom transfer radical polymerization: a robust and versatile route for polymer synthesis. *Polym. Rev.*, 51(2):138–162, 2011.

[42] D. A. Shipp. Reversible-deactivation radical polymerizations. *Polym. Rev.*, 51(2):99–103, 2011.

[43] J. Qiu, B. Charleux, and K. Matyjaszewski. Controlled/living radical polymerization in aqueous media: homogeneous and heterogeneous systems. *Prog. Polym. Sci.*, 26(10):2083–2134, 2001.

[44] M. J. Monteiro and M. F. Cunningham. Polymer nanoparticles via living radical polymerization in aqueous dispersions: Design and applications. *Macromolecules*, 45(12):4939–4957, 2012.

[45] A. Simakova, S. E. Averick, D. Konkolewicz, and K. Matyjaszewski. Aqueous ARGET ATRP. *Macromolecules*, 45(16):6371–6379, 2012.

[46] Q. Xiong, P. Ni, F. Zhang, and Z. Yu. Synthesis and characterization of 2-(dimethylamino)ethyl methacrylate homopolymers via aqueous RAFT polymerization and their application in miniemulsion polymerization. *Polym. Bull.*, 53(1):1–8, 2004.

[47] J. K. Oh, C. Tang, H. Gao, N. V. Tsarevsky, and K. Matyjaszewski. Inverse miniemulsion ATRP: a new method for synthesis and functionalization of well-defined water-soluble/cross-linked polymeric particles. *J. Am. Chem. Soc.*, 128(16):5578–5584, 2006.

[48] J. K. Oh, F. Perineau, and K. Matyjaszewski. Preparation of nanoparticles of well-controlled water-soluble homopolymers and block copolymers using an inverse miniemulsion ATRP. *Macromolecules*, 39(23):8003–8010, 2006.

[49] J. K. Oh, D. J. Siegwart, H. Lee, G. Sherwood, L. Peteanu, J. O. Hollinger, K. Kataoka, and K. Matyjaszewski. Biodegradable nanogels prepared by atom transfer radical polymerization as potential drug delivery carriers: synthesis, biodegradation, *in vitro* release, and bioconjugation. *J. Am. Chem. Soc.*, 129(18):5939–5945, 2007.

[50] J. K. Oh, H. Dong, R. Zhang, K. Matyjaszewski, and H. Schlaad. Preparation of nanoparticles of double-hydrophilic PEO-PHEMA block copolymers by AGET ATRP in inverse miniemulsion. *J. Polym. Sci., Part A: Polym. Chem.*, 45(21):4764–4772, 2007.

[51] S. M. Paterson, D. H. Brown, T. V. Chirila, I. Keen, A. K. Whittaker, and M. V. Baker. The synthesis of water-soluble phema via arget atrp in protic media. *J. Polym. Sci., Part A: Polym. Chem.*, 48(18):4084–4092, 2010.

[52] W. Jakubowski and K. Matyjaszewski. Activators regenerated by electron transfer for atom-transfer radical polymerization of (meth)acrylates and related block copolymers. *Angew. Chem.*, 118(27):4594–4598, 2006.

[53] W. Jakubowski, K. Min, and K. Matyjaszewski. Activators regenerated by electron transfer for atom transfer radical polymerization of styrene. *Macromolecules*, 39(1):39–45, 2006.

[54] K. Matyjaszewski. Atom transfer radical polymerization (ATRP): current status and future perspectives. *Macromolecules*, 45(10):4015–4039, 2012.

[55] K. Matyjaszewski, W. Jakubowski, K. Min, W. Tang, J. Huang, W. A. Braunecker, and N. V. Tsarevsky. Diminishing catalyst concentration in atom transfer radical polymerization with reducing agents. *P. Natl. Acad. Sci.*, 103(42):15,309–15,314, 2006.

[56] K. Matyjaszewski, H. Dong, W. Jakubowski, J. Pietrasik, and A. Kusumo. Grafting from surfaces for everyone: ARGET ATRP in the presence of air. *Langmuir*, 23(8):4528–4531, 2007.

Chapter 2

Chemistry Background

2.1 Introduction to ARGET ATRP

Advances in Atom-Transfer Radical Polymerization (ATRP) technology have led to methods that combine the versatility and control of controlled radical polymerizations (CRP) with mild reaction conditions[1] more characteristic of a traditional free radical polymerization. For example, Activators ReGenerated by Electron Transfer (ARGET) ATRP can occur in the presence of limited amounts of air[1;2] and uses copper(II) catalyst, which is significantly less sensitive to oxidation compared to copper(I) catalysts.[2;3] In addition, ARGET ATRP significantly reduces the copper catalyst concentration compared to conventional ATRP; for example, reduction from a typical value of 1000 ppm to ~10 ppm was achieved for styrene polymerization with a targeted degree of polymerization of 1000 while maintaining a molecular weight polydispersity less than 1.2.[2]

The mechanisms for ARGET ATRP and traditional ATRP are shown in Figure 2.1. Both the significant reduction in catalyst concentration as well as the ability to conduct polymerizations in the presence of limited

amount of air are possible due to the addition of a reducing agent (RA) such as vitamin C,[1;3;4] glucose,[2;4] or tin(II) 2-ethylhexanoate.[1;5] The reducing agent scavenges oxygen and reduces the inactive copper(II) to the active copper(I) catalyst.[1–3] The ligand (L) complexes with the active copper(I) catalyst. Ligands such as tris[2-(dimethylamino)ethyl]amine (Me_6TREN)and tris(2-pyridylmethyl)amine (TPMA) are "10^3-10^5 times more active than the originally used CuBr/bipyridine complexes",[2] and these ligands are commercially available.[6] Improved ligand stability can improve control of the polymerization, so ligand selection is critical;[7] TPMA provided the best control for the polymerization of n-butyl acrylate.[8;9] It was also reported that increasing the excess of TPMA ligand from 3-fold to 10-fold also resulted in an increase in reaction conversion.[8]

A primary difference between traditional free radical polymerizations and those frequently termed "controlled" polymerizations is that termination reactions between free radicals are significantly reduced.[10] In traditional free radical polymerizations, growing chains are quickly terminated. In controlled radical polymerizations, active growing chains may be quickly deactivated (which is a reversible process), but they are rarely terminated.[11] A more precise designation for these "controlled" reactions is Reversible-Deactivation Radical Polymerization (RDRP), which is defined by IUPAC as a "chain polymerization, propagated by radicals that are deactivated reversibly, bringing them into active-dormant equilibria of which there might be more than one".[12] This reversibility creates opportunities for new polymer architectures such as block

copolymers via chain extension (rather than functionalization/conjugation strategies using synthesized polymer chains).

An important similarity between traditional free radical and controlled radical polymerizations such as ARGET ATRP is that for both methods, the composition of copolymers is a function of the feed composition and of the reactivity ratios. The feed composition is in turn a function of conversion. These facts lead to difference in the distribution of chain composition; in traditional free radical polymerizations, the lifetime of growing chains is very short with respect to the total reaction time, so a diverse population of chain compositions would be expected, while in controlled radical polymerizations, the lifetime of growing chains is comparable to the total reaction time and so probability suggests that the chains will have a narrower distribution of composition. Whether this difference in composition distribution as well as the difference in molecular weight distribution affects material properties (and hence, performance) for a specific application is an important question when studying which type of polymerization to use.

2.1.1 Aqueous ARGET ATRP

Reports of aqueous ARGET ATRP are growing in number, but the synthesis techniques are largely restricted to polymerization of polyethylene glycol acrylates or methacrylates. The rare exceptions are DMAEMA[13] and *N*-isopropylacrylamide,[14] for which there is a reported aqueous technique. The ARGET ATRP or AGET ATRP strategies for the polyethylene glycol acry-

lates or methacrylates include traditional copper halide catalyzed,[15–19] as well as metalloenzyme techniques[14;20;21] or iron halide catalysts.[22;23]

2.1.2 Emulsion with ARGET ATRP

Inverse miniemulsion with ARGET ATRP or AGET ATRP has been used to prepare hydrogel nanoparticles of poly(2-hydroxyethyl methacrylate)[24] and oligo(ethylene glycol) monomethyl ether methacrylate.[16;25] Such nanoparticle systems may incorporate biodegradable cross-linking agents with disulfide groups,[15;26] which are cleaved in a reductive environment. These nanoparticle systems were investigated for drug delivery applications.[27] This nanoparticle drug delivery system is composed of the hydrophilic polymer polyethylene glycol, and so lacks a responsive component to improve targeted delivery.

There are reports of standard oil-in-water miniemulsion polymerizations as well as inverse emulsion polymerizations. AGET ATRP has been used to prepare poly(butyl acrylate) in a standard miniemulsion (monomer in water) in the presence of limited air.[28] AGET ATRP and ARGET ATRP were used to prepare poly(methyl methacrylate) in a standard miniemulsion (monomer in water) using an amphiphilic ATRP initiator without additional surfactant.[29] ARGET ATRP was used to prepare butyl methacrylate in a standard miniemulsion with only 50 ppm copper(II) catalyst.[30]

Both ARGET ATRP and AGET ATRP rely upon a reducing agent such as ascorbic acid or tin(II) 2-ethylhexanoate to activate the copper(II)

catalyst, and extra reducing agent can be used to conduct reactions in the presence of limited air. In AGET ATRP, the molar amount of reducing agent is set based on the molar amount of copper with 0.1-0.5 mole reducing agent per mole copper for deoxygenated mixtures and 1.5 mol reducing agent per mole copper for mixtures with air.[28] In contrast, in ARGET ATRP, a large excess of reducing agent (50-100x) is added to "regenerate" the active catalyst throughout the reaction, and as a result, the copper concentration can be significantly reduced.[1]

2.2 Polycationic polymers

Cationic monomers such as 2-(dimethylamino)ethyl methacrylate (DMAEMA) and 2-(diethylamino)ethyl methacrylate (DEAEMA) may be used to make pH-responsive polymers and polymer hydrogels. PDMAEMA and PDEAEMA polymers find applications in various fields including waste-water treatment,[31] paints and coatings,[31] filtration techniques,[31] as well as biomaterials.[32–36] These polymers undergo a "pH-dependent hydrophobe-to-hydrophile phase shift"[37] when going from high pH values to low pH values. At low pH values, the amino group of the DMAEMA and DEAEMA is protonated and positively charged. The positively charged groups repel and the hydrogel swells. The reported pK_a of PDMAEMA is ~7.5[38;39] and reported values for the pK_a of PDEAEMA range from ~7.0-7.3[40–42] to 7.68.[43] PDMAEMA[44–48] and PDEAEMA[48] and are also temperature responsive because they have a

"characteristic temperature-dependent solubility (lower critical solution temperature, LCST) in water."[47]

There is a broad range of creative synthesis strategies for the synthesis of polycationic polymers. A survey of the strategies for making cationic nanoparticles using 2-(diethylamino)ethyl methacrylate (DEAEMA) is shown in Table 2.2. In the group of ARGET ATRP-based techniques, there are several reports for polycationic polymers synthesized with the monomer 2-(diethylamino) ethyl methacrylate (DEAEMA) as well as the related monomer 2-(dimethylamino)ethyl methacrylate (DMAEMA) (see Table 2.1). Note that both Siegwart, et al.,[5] and Dong and Matyjaszewski[49] found that DMAEMA acts as an intrinsic reducing agent to reduce copper(II) to copper(I), but that an additional reducing agent is needed in the presence of limited amounts of air.

2.3 Toxicity of chemicals used for nanoparticle synthesis

A concern of researchers regarding the use of ATRP methods to prepare polymeric biomaterials is the presence of copper in the polymerization and in the final product. The use of the heavy metal copper merits consideration of cytotoxicity effects, but careful analysis suggests the use of copper at sufficiently low concentrations may not be a barrier to use as a biomaterial.

While copper ions are an essential enzyme cofactor for oxidation-

reduction reactions,[50] copper ions are harmful at sufficiently high concentrations. As a result, it is perhaps not surprising that the body has a robust system to maintain copper homeostasis. Copper is relatively easily absorbed and excreted by most mammals, and little is stored,[50] with an exception perhaps in the livers of newborns where the copper concentration greatly exceeds that of normal adults.[51] Copper is even present in breast milk (602 µmol/L in human breast milk for the first week after birth[50]).

The use of copper as a biomaterial has been approved for use in the ParaGard® T 380A Intrauterine Copper Contraceptive device (IUD).[52] The T-shaped IUD measures 32 mm horizontally and 36 mm vertically and it contains more than 300 mg copper. The contraceptive effectiveness is enhanced as the copper is continuously released into the uterine cavity; however, the mechanism for this effectiveness is not known.[53]

Copper is present in drinking water; the EPA sets the maximum contaminant level goal (MCLG) for copper in water at 1.3 mg/ml, which means that public water systems must take action if more than 10% of tap water samples this concentration. This concentration was selected "based upon the best available science to prevent potential health problems".[54]

The daily dietary copper intake is between 0.6 and 1.6 mg, and about half is absorbed by the intestines.[50] The liver plays a primary role in copper homeostasis[55] because bile produced in the liver is the primary excretory route for excess copper.[50;55] While some of the 4.5 mg or more of copper excreted daily in the bile into the intestines will be reabsorbed, contributing to "cycling"

of copper, the copper in bile is not easily reabsorbed.[50] Copper overload is rare since the liver has an "enormous capacity" to increase copper excretion;[55] in fact, studies with intravenously injected copper in mice demonstrated that increased copper load results in increased copper in bile.[56] The liver also plays an important role by synthesizing ceruloplasmin; 95% of copper in plasma is bound to ceruloplasmin, which can carry up to six copper atoms.[55] The role of ceruloplasmin in copper transport remains unsettled;[55] what is settled is that ceruloplasmin is a multifunctional protein "that overcomes the one gene-one function concept".[57]

Nevertheless, the harmfulness of excess copper may be witnessed in the case of Wilson's disease, which is a condition where normal copper homeostasis is disrupted by the lack of a specific copper transporter protein. If untreated, Wilson's disease is fatal; the lack of transporter protein leads to an accumulation of copper in the liver exceeding 250 mg/kg (compared to healthy state concentrations below 50 mg/kg)[58] followed by damage to kidneys, brain, and eyes.[59] Toxicity studies have investigated the use of copper as a biomaterial, particularly as a component of dental alloys.[60–63] The source of the copper ions matters; pure metals released ions more slowly than copper salts, and greater toxicity was observed with increased exposure concentration.[63]

ATRP techniques typically rely on organic solvents (due to poor control[19;64;65] and problems with loss of terminal functionality[66] in water), but for the biomaterials application as a drug delivery system, concerns about minimizing toxicity led to adapting the ARGET ATRP technique to synthesis in

water. Toxicity from residual methacrylate monomer is a concern that would need to be addressed by careful purification and cytotoxicity. For example, although tetraethylene glycol dimethacrylate has a low reported health hazard (0 on both Hazardous Materials Identification System (HMIS) and National Fire Protection Association (NFPA) scales),[67] leaching from dental resin can cause inflammation of dental pump and necrosis. This is a challenge shared by all biomaterials researchers using methacrylate or acrylate monomers.[68] The TPMA ligand used for the ARGET ATRP synthesis should be less of a toxicity concern than the methacrylate monomers, both due to its low concentration and low reported health hazard (level 1 under both HMIS and NFPA systems).[69]

2.4 Tables

Table 2.1: Strategies to create polycationic polymers using DEAEMA. ARGET ATRP: activators regenerated by electron transfer atom transfer radical polymerization, CCL: core cross-linked, EGDMA: ethylene glycol dimethacrylate, PCL: poly(ε-caprolactone), PEGDMA: poly(ethylene glycol) dimethacrylate, PPGDA: poly(propylene glycol) diacrylate, RAFT: reversible addition-fragmentation chain transfer, SCL: shell cross-linked, SCVCP: self-condensing vinyl copolymerization, TEGDMA: tetra(ethylene glycol) dimethacrylate

Method	**Structure**	**Strategy**
Free radical (UV)	Cross-linked (nanogel)	Monomer-in-water emulsion using TEGDMA cross-linking agent[37;70;71]
Free radical (thermal)	Branched	"Strathclyde" approach for branching with branching agent (EGDMA) and chain transfer agent[72]
Free radical (redox)	Cross-linked (nanogel)	Monomer-in-water emulsion using EGDMA cross-linking agent[73;74]
Free radical (redox)	Cross-linked (microgel)	Monomer-in-water emulsion using PPGDA cross-linking agent[40;75]
Free radical (redox)	Cross-linked (core-shell)	Two-stage surfactant-free emulsion in water with PEGDMA cross-linking agent[76;77]
RAFT	Cross-linked (CCL micelle)	Block copolymers assembled into micelles and core cross-linked[78]
RAFT	SCL nanocapsule	Shell cross-linked nanocapsule grown on sacrificial PS template core[79]
Traditional ATRP	Branched	SCVCP using AB*-type inimer[47]
Traditional ATRP	Branched	Branched diblock PPEGMA-*b*-P(DEAEMA-*co*-EGDMA) copolymer[80]
Traditional ATRP	Cross-linked (SCL micelle)	Block copolymers assembled into micelles and shell cross-linked[81]
Traditional ATRP	Star-shaped	Arms grown from multifunctional initiator[48]
ARGET ATRP	Star-shaped	Triblock PCL-*b*-PDEAEMA-*b*-PPEGMA assembled into micelles[42]
ARGET ATRP	Cross-linked (nanogel)	Monomer-in-water emulsion using TEGDMA cross-linking agent[82]

Table 2.2: Strategies to create polycationic DEAEMA and DMAEMA polymers using ARGET ATRP. ARGET ATRP: activators regenerated by electron transfer atom transfer radical polymerization, PCL: poly(ε-caprolactone), PEGMA: poly(ethylene glycol) methyl ether methacrylate, TEGDMA: tetra(ethylene glycol) dimethacrylate

Method	**Structure**	**Strategy**
ARGET ATRP	Linear chain	DEAEMA homopolymer in anisole solvent[49]
ARGET ATRP	Cleavable linear chains	DEAEMA and DMAEMA were grown from a disulfide initiator in anisole solvent[5]
ARGET ATRP	Grafted to silk	DEAEMA grafted to silk in water solvent[13]
ARGET ATRP	Surface grafted	DMAEMA initiated from silica surface in anisole solvent[83]
ARGET ATRP	Surface grafted	DEAEMA brush grown on silica particles or wafers in ethanol/water solvent[84]
ARGET ATRP	Star-shaped (forms micelles)	DEAEMA block (of triblock PCL-*b*-PDEAEMA-*b*-PPEGMA) grown in toluene solvent[42]
ARGET ATRP	Cross-linked (nanogel)	DEAEMA/PEGMA/tBMA-in-water emulsion using TEGDMA cross-linking agent[82]

2.5 Figures

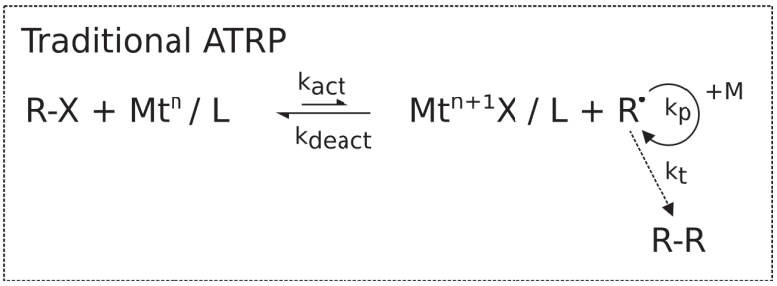

(a) Traditional ATRP

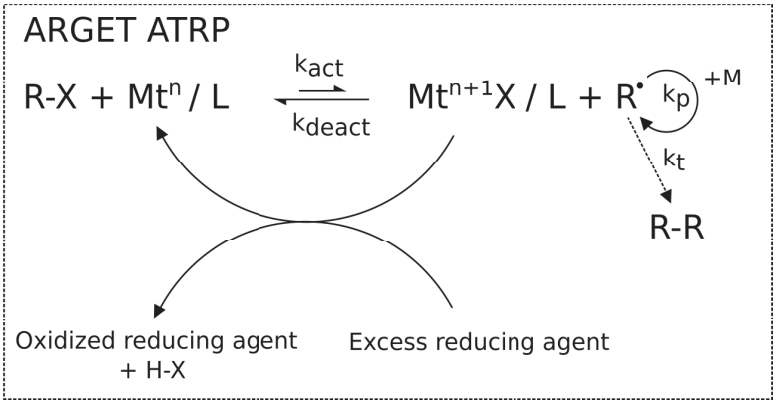

(b) ARGET ATRP

Figure 2.1: Comparison of traditional ATRP and ARGET ATRP (top) and ARGET ATRP (bottom) mechanisms. ARGET ATRP uses excess reducing agent to form the active form of the transition metal (Mt) catalyst, while traditional ATRP starts out with the active form of the catalyst added directly to the reaction. (Similar schematics appear in reports in the literature.[2;6;8;10;85;86])

2.6 References

[1] K. Matyjaszewski, H. Dong, W. Jakubowski, J. Pietrasik, and A. Kusumo. Grafting from surfaces for everyone: ARGET ATRP in the presence of air. *Langmuir*, 23(8):4528–4531, 2007.

[2] W. Jakubowski and K. Matyjaszewski. Activators regenerated by electron transfer for atom-transfer radical polymerization of (meth)acrylates and related block copolymers. *Angew. Chem.*, 118(27):4594–4598, 2006.

[3] K. Min, H. Gao, and K. Matyjaszewski. Use of ascorbic acid as reducing agent for synthesis of well-defined polymers by ARGET ATRP. *Macromolecules*, 40(6):1789–1791, 2007.

[4] Q. Lou and D. A. Shipp. Recent developments in atom transfer radical polymerization (ATRP): Methods to reduce metal catalyst concentrations. *ChemPhysChem*, 13(14):3257–3261, 2012.

[5] D.J. Siegwart, M. Leiendecker, R. Langer, and D.G. Anderson. Automated ARGET ATRP accelerates catalyst optimization for the synthesis of thiol-functionalized polymers. *Macromolecules*, 45(3):1254–1261, 2012.

[6] Y. Kwak, A. J. D. Magenau, and K. Matyjaszewski. ARGET ATRP of methyl acrylate with inexpensive ligands and ppm concentrations of catalyst. *Macromolecules*, 44(4):811–819, 2011.

[7] N. V. Tsarevsky. Catalytic activity and performance of copper-based complexes mediating atom transfer radical polymerization. *Isr. J. Chem.*, 52(3-4):276–287, 2012.

[8] K. Matyjaszewski, W. Jakubowski, K. Min, W. Tang, J. Huang, W. A. Braunecker, and N. V. Tsarevsky. Diminishing catalyst concentration in atom transfer radical polymerization with reducing agents. *P. Natl. Acad. Sci.*, 103(42):15,309–15,314, 2006.

[9] T. Pintauer and K. Matyjaszewski. Atom transfer radical addition and polymerization reactions catalyzed by ppm amounts of copper complexes. *Chem. Soc. Rev.*, 37(6):1087, 2008.

[10] R. Nicolaÿ and Y. Kwak. ATRP with alkyl pseudohalides acting as initiators and chain transfer agents: When ATRP and RAFT polymerization become one. *Isr. J. Chem.*, 52(3-4):288–305, 2012.

[11] K. Matyjaszewski. Atom transfer radical polymerization (ATRP): current status and future perspectives. *Macromolecules*, 45(10):4015–4039, 2012.

[12] A. D. Jenkins, R. G. Jones, and G. Moad. Terminology for reversible-deactivation radical polymerization previously called "controlled" radical or "living" radical polymerization (IUPAC Recommendations 2010). *Pure Appl. Chem.*, 82(2):483–491, 2010.

[13] T. Xing, S. Li, X. Xu, and G. Chen. Structure and properties of silk grafted with *N, N*-dimethylaminoethyl methacrylate via

the ARGET ATRP method. *J. Eng. Fiber Fabr.*, Retrieved from http://www.jeffjournal.org/(Special Issue: Fibers), 2012.

[14] S. J. Sigg, F. Seidi, K. Renggli, T. B. Silva, G. Kali, and N. Bruns. Horseradish peroxidase as a catalyst for atom transfer radical polymerization. *Macromol. Rapid Commun.*, 32(21):1710–1715, 2011.

[15] J. K. Oh, C. Tang, H. Gao, N. V. Tsarevsky, and K. Matyjaszewski. Inverse miniemulsion ATRP: a new method for synthesis and functionalization of well-defined water-soluble/cross-linked polymeric particles. *J. Am. Chem. Soc.*, 128(16):5578–5584, 2006.

[16] J. K. Oh, F. Perineau, and K. Matyjaszewski. Preparation of nanoparticles of well-controlled water-soluble homopolymers and block copolymers using an inverse miniemulsion ATRP. *Macromolecules*, 39(23):8003–8010, 2006.

[17] J. K. Oh, K. Min, and K. Matyjaszewski. Preparation of poly (oligo (ethylene glycol) monomethyl ether methacrylate) by homogeneous aqueous AGET ATRP. *Macromolecules*, 39(9):3161–3167, 2006.

[18] S. A. Bencherif, D. J. Siegwart, A. Srinivasan, F. Horkay, J. O. Hollinger, N. R. Washburn, and K. Matyjaszewski. Nanostructured hybrid hydrogels prepared by a combination of atom transfer radical polymerization and free radical polymerization. *Biomaterials*, 30(29):5270–5278, 2009.

[19] A. Simakova, S. E. Averick, D. Konkolewicz, and K. Matyjaszewski. Aqueous ARGET ATRP. *Macromolecules*, 45(16):6371–6379, 2012.

[20] Y. H. Ng, F. di Lena, and C. L. L. Chai. Metalloenzymatic radical polymerization using alkyl halides as initiators. *Polym. Chem.*, 2(3):589–594, 2011.

[21] Y. H. Ng, F. di Lina, and C. L. L. Chai. PolyPEGA with predetermined molecular weights from enzyme-mediated radical polymerization in water. *Chem. Commun.*, 47(22):6464–6466, 2011.

[22] W. He, L. Zhang, J. Miao, Z. Cheng, and X. Zhu. Facile iron-mediated AGET ATRP for water-soluble poly (ethylene glycol) monomethyl ether methacrylate in water. *Macromol. Rapid Commun.*, 33(12):1067–1073, 2012.

[23] J. Miao, W. He, L. Zhang, Y. Wang, Z. Cheng, and X. Zhu. AGET ATRP of water-soluble PEGMA: Fast living radical polymerization mediated by iron catalyst. *J. Polym. Sci., Part A: Polym. Chem.*, 50(11):2194–2200, 2012.

[24] J. K. Oh, H. Dong, R. Zhang, K. Matyjaszewski, and H. Schlaad. Preparation of nanoparticles of double-hydrophilic PEO-PHEMA block copolymers by AGET ATRP in inverse miniemulsion. *J. Polym. Sci., Part A: Polym. Chem.*, 45(21):4764–4772, 2007.

[25] J. K. Oh, F. Perineau, B. Charleux, and K. Matyjaszewski. AGET ATRP in water and inverse miniemulsion: A facile route for preparation of high-molecular-weight biocompatible brush-like polymers. *J. Polym. Sci., Part A: Polym. Chem.*, 47(7):1771–1781, 2009.

[26] J. K. Oh, D. J. Siegwart, H. Lee, G. Sherwood, L. Peteanu, J. O. Hollinger, K. Kataoka, and K. Matyjaszewski. Biodegradable nanogels prepared by atom transfer radical polymerization as potential drug delivery carriers: synthesis, biodegradation, *in vitro* release, and bioconjugation. *J. Am. Chem. Soc.*, 129(18):5939–5945, 2007.

[27] J. K. Oh, S. A. Bencherif, and K. Matyjaszewski. Atom transfer radical polymerization in inverse miniemulsion: A versatile route toward preparation and functionalization of microgels/nanogels for targeted drug delivery applications. *Polymer*, 50(19):4407–4423, 2009.

[28] K. Min, W. Jakubowski, and K. Matyjaszewski. AGET ATRP in the presence of air in miniemulsion and in bulk. *Macromol. Rapid Commun.*, 27(8):594–598, 2006.

[29] F. Stoffelbach, N. Griffete, C. Bui, and B. Charleux. Use of a simple surface-active initiator in controlled/living free-radical miniemulsion polymerization under AGET and ARGET ATRP conditions. *Chem. Commun.*, (39):4807–4809, 2008.

[30] A. M. Elsen, J. Burdynska, S. Park, and K. Matyjaszewski. Activators regenerated by electron transfer atom transfer radical polymerization in

miniemulsion with 50 ppm of copper catalyst. *ACS Macro Lett.*, 2(9): 822–825, 2013.

[31] M. Sahnoun, M.-T. Charreyre, L. Veron, T. Delair, and F. D'Agosto. Synthetic and characterization aspects of dimethylaminoethyl methacrylate reversible addition fragmentation chain transfer (RAFT) polymerization. *J. Polym. Sci., Part A: Polym. Chem.*, 43(16):3551–3565, 2005.

[32] M. Ranger, M. Jones, M. Yessine, and J. Leroux. From well-defined diblock copolymers prepared by a versatile atom transfer radical polymerization method to supramolecular assemblies. *J. Polym. Sci., Part A: Polym. Chem.*, 39(22):3861–3874, 2001.

[33] M. Dufresne and J. Leroux. Study of the micellization behavior of different order amino block copolymers with heparin. *Pharm. Res.*, 21(1):160–169, 2004.

[34] W. Zhang, J. He, Z. Liu, P. Ni, and X. Zhu. Biocompatible and ph-responsive triblock copolymer mPEG-b-PCL-b-PDMAEMA: Synthesis, self-assembly, and application. *J. Polym. Sci., Part A: Polym. Chem.*, 48 (5):1079–1091, 2010.

[35] K. Sui, X. Shan, S. Gao, Y. Xia, Q. Zheng, and D. Xie. Dual-responsive supramolecular inclusion complexes of block copolymer poly (ethylene glycol)-block-poly [(2-dimethylamino) ethyl methacrylate] with α-cyclodextrin. *J. Polym. Sci., Part A: Polym. Chem.*, 48(10):2143–2153, 2010.

[36] B. D. Riquelme, D. Dumas, A. Fontana, M. Delannoy, J. R. Valverde, D. Sondag, and C. Grandfils. Hemocompatibility and biofunctionality of two poly(2-(dimethylamino)ethyl methacrylate-co-poly(ethyleneglycol) copolymers. *J. Biomed. Mater. Res. Part A*, 99A(3):445–454, 2011.

[37] O. Z. Fisher, T. Kim, S. R. Dietz, and N. A. Peppas. Enhanced core hydrophobicity, functionalization and cell penetration of polybasic nanomatrices. *Pharm. Res.*, 26(1):51–60, 2008.

[38] P. van de Wetering, E. E. Moret, N. M. E. Schuurmans-Nieuwenbroek, M. J. van Steenbergen, and W. E. Hennink. Structure-activity relationships of water-soluble cationic methacrylate/methacrylamide polymers for nonviral gene delivery. *Bioconjugate Chem.*, 10(4):589–597, 1999.

[39] M. R. Simmons, E. N. Yamasaki, and C. S. Patrickios. Cationic amphiphilic model networks: Synthesis by group transfer polymerization and characterization of the degree of swelling. *Macromolecules*, 33(8): 3176–3179, 2000.

[40] J. I. Amalvy, E. J. Wanless, Y. Li, V. Michailidou, S. P. Armes, and Y. Duccini. Synthesis and characterization of novel pH-responsive microgels based on tertiary amine methacrylates. *Langmuir*, 20(21):8992–8999, 2004.

[41] B. Mao, L. Gan, Y. Gan, X. Li, P. Ravi, and K. Tam. Controlled polymerizations of 2-(dialkylamino)ethyl methacrylates and their block copoly-

mers in protic solvents at ambient temperature via atrp. *J. Polym. Sci., Part A: Polym. Chem.*, 42(20):5161–5169, 2004.

[42] Y. Q. Yang, W. J. Lin, L. J. Zhang, C. Z. Cai, W. Jiang, X. D. Guo, and Y. Qian. Synthesis, characterization and pH-responsive self-assembly behavior of amphiphilic multiarm star triblock copolymers based on PCL, PDEAEMA, and PEG. *Macromol. Res.*, 21(9):1011–1020, 2013.

[43] A. Shatkay and I. Michaeli. Potentiometric titrations of polyelectrolytes with separation of phases. *J. Phys. Chem.*, 70(12):3777–3782, 1966.

[44] F. Zeng, Y. Shen, S. Zhu, and R. Pelton. Atom transfer radical polymerization of 2-(dimethylamino) ethyl methacrylate in aqueous media. *J. Polym. Sci., Part A: Polym. Chem.*, 38(20):3821–3827, 2000.

[45] S. Liu, J. V. M. Weaver, Y. Tang, N. C. Billingham, S. P. Armes, and K. Tribe. Synthesis of shell cross-linked micelles with pH-responsive cores using ABC triblock copolymers. *Macromolecules*, 35(16):6121–6131, 2002.

[46] N. Pantoustier, S. Moins, M. Wautier, P. Degée, and P. Dubois. Solvent-free synthesis and purification of poly[2-(dimethylamino)ethyl methacrylate] by atom transfer radical polymerization. *Chem. Commun.*, (3):340–341, 2003.

[47] H. Mori, A. Walther, X. André, M. G. Lanzendörfer, and A. H. E. Müller. Synthesis of highly branched cationic polyelectrolytes via self-

condensing atom transfer radical copolymerization with 2-(diethylamino) ethyl methacrylate. *Macromolecules*, 37(6):2054–2066, 2004.

[48] A. Schmalz, M. Hanisch, H. Schmalz, and A. H. E. Müller. Double stimuli-responsive behavior of linear and star-shaped poly (*N, N*-diethylaminoethyl methacrylate) in aqueous solution. *Polymer*, 51(6): 1213–1217, 2010.

[49] H. Dong and K. Matyjaszewski. ARGET ATRP of 2-(dimethylamino) ethyl methacrylate as an intrinsic reducing agent. *Macromolecules*, 41 (19):6868–6870, 2008.

[50] M. C. Linder, L. Wooten, P. Cerveza, S. Cotton, R. Shulze, and N. Lomeli. Copper transport. *Am. J. Clin. Nutr.*, 67(5):965S–971S, 1998.

[51] G. Faa, C. Liguori, A. Columbano, and G. Diaz. Uneven copper distribution in the human newborn liver. *Hepatology*, 7(5):838–842, 1987.

[52] TEVA Pharmaceuticals USA, Inc. Paragard intrauterine copper contraceptive, 2012. http://www.paragard.com/default.aspx.

[53] TEVA Pharmaceuticals USA, Inc. *Prescribing Information: ParaGard T 380A Intrauterine Copper Contraceptive*, 2012.

[54] United States Environmental Protection Agency. Basic information about copper in drinking water, 2012. http://water.epa.gov/drink/contaminants/basicinformation/copper.cfm.

[55] N.E. Hellman and J.D. Gitlin. Ceruloplasmin metabolism and function. *Annu. Rev. Nutr.*, 22(1):439–458, 2002.

[56] D. Gitlin, W.L. Hughes, and C.A. Janeway. Absorption and excretion of copper in mice. *Nature*, 188(4745):150–151, 1960.

[57] P. Bielli and L. Calabrese. Structure to function relationships in ceruloplasmin: a 'moonlighting' protein. *Cell. Mol. Life Sci.*, 59(9):1413–1427, 2002.

[58] G. Crisponi, V. M. Nurchi, D. Fanni, C. Gerosa, S. Nemolato, and G. Faa. Copper-related diseases: from chemistry to molecular pathology. *Coord. Chem. Rev.*, 254(7-8):876–889, 2010.

[59] National Center for Biotechnology Information (NCBI), MedlinePlus. Wilson disease, 2012. http://www.nlm.nih.gov/medlineplus/wilsondisease.html.

[60] J. C. Wataha, C. T. Hanks, and R. G. Craig. The *in vitro* effects of metal cations on eukaryotic cell metabolism. *J. Biomed. Mater. Res.*, 25(9): 1133–1149, 1991.

[61] G. Schmalz, H. Langer, and H. Schweikl. Cytotoxicity of dental alloy extracts and corresponding metal salt solutions. *J. Dent. Res.*, 77(10): 1772–1778, 1998.

[62] J.C. Wataha. Biocompatibility of dental casting alloys: a review. *J. Prosthet. Dent.*, 83(2):223–234, 2000.

[63] M.C. Cortizo and M.F. Lorenzo de Mele. Cytotoxicity of copper ions released from metal. *Biol. Trace Elem. Res.*, 102(1):129–141, 2004.

[64] N. V. Tsarevsky and K. Matyjaszewski. Environmentally benign atom transfer radical polymerization: Towards "green" processes and materials. *J. Polym. Sci., Part A: Polym. Chem.*, 44(17):5098–5112, 2006.

[65] A. Simakova, M. Mackenzie, S. E. Averick, S. Park, and K. Matyjaszewski. Bioinspired iron-based catalyst for atom transfer radical polymerization. *Angew. Chem. Int. Ed.*, 2013. doi: 10.1002/anie.201306337.

[66] J. Qiu, B. Charleux, and K. Matyjaszewski. Controlled/living radical polymerization in aqueous media: homogeneous and heterogeneous systems. *Prog. Polym. Sci.*, 26(10):2083–2134, 2001.

[67] Sigma-Aldrich. Material safety data sheet: Tetraethylene glycol dimethacrylate, January 2012.

[68] E. Yoshii. Cytotoxic effects of acrylates and methacrylates: Relationships of monomer structures and cytotoxicity. *J. Biomed. Mater. Res.*, 37(4): 517–524, 1997.

[69] Sigma-Aldrich. Material safety data sheet: Tris(2-pyridylmethyl)amine, March 2012.

[70] O. Z. Fisher and N. A. Peppas. Polybasic nanomatrices prepared by UV-initiated photopolymerization. *Macromolecules*, 42(9):3391–3398, 2009.

[71] W. B. Liechty, R. L. Scheuerle, and N. A. Peppas. Tunable, responsive nanogels containing *t*-butyl methacrylate and 2-(*t*-butylamino)ethyl methacrylate. *Polymer*, 54(15):3784–3795, 2013.

[72] J. V. M. Weaver, R. T. Williams, B. J. L. Royles, P. H. Findlay, A. I. Cooper, and S. P. Rannard. pH-Responsive branched polymer nanoparticles. *Soft Matter*, 4(5):985–992, 2008.

[73] H. Hayashi, M. Iijima, K. Kataoka, and Y. Nagasaki. pH-sensitive nanogel possessing reactive PEG tethered chains on the surface. *Macromolecules*, 37(14):5389–5396, 2004.

[74] A. Tamura, M. Oishi, and Y. Nagasaki. Enhanced cytoplasmic delivery of siRNA using a stabilized polyion complex based on PEGylated nanogels with a cross-linked polyamine structure. *Biomacromolecules*, 10(7):1818–1827, 2009.

[75] D. Palioura, S. P. Armes, S. H. Anastasiadis, and M. Vamvakaki. Metal nanocrystals incorporated within pH-responsive microgel particles. *Langmuir*, 23(10):5761–5768, 2007.

[76] Y. Hu, T. Litwin, A. R. Nagaraja, B. Kwong, J. Katz, N. Watson, and D. J. Irvine. Cytosolic delivery of membrane-impermeable molecules in dendritic cells using pH-responsive core-shell nanoparticles. *Nano Lett.*, 7(10):3056–3064, 2007.

[77] Y. Hu, P. U. Atukorale, J. J. Lu, J. J. Moon, S. H. Um, E. C. Cho, Y. Wang, J. Chen, and D. J. Irvine. Cytosolic delivery mediated via electrostatic surface binding of protein, virus, or siRNA cargos to pH-responsive core- shell gel particles. *Biomacromolecules*, 10(4):756–765, 2009.

[78] S. Yusa, M. Sugahara, T. Endo, and Y. Morishima. Preparation and characterization of a pH-responsive nanogel based on a photo-cross-linked micelle formed from block copolymers with controlled structure. *Langmuir*, 25(9):5258–5265, 2009.

[79] X. Huang, D. Appelhans, P. Formanek, F. Simon, and B. Voit. Tailored synthesis of intelligent polymer nanocapsules: An investigation of controlled permeability and pH-dependent degradability. *ACS Nano*, 6(11): 9718–9726, 2012.

[80] T. He, F. Di Lena, K. C. Neo, and C. L. L. Chai. Direct synthesis of pH-responsive polymer nanoparticles based on living radical polymerization and traditional radical polymerization. *Soft Matter*, 7(7):3358–3365, 2011.

[81] H. Liu, X. Jiang, J. Fan, G. Wang, and S. Liu. Aldehyde surface-functionalized shell cross-linked micelles with pH-tunable core swellability and their bioconjugation with lysozyme. *Macromolecules*, 40(25):9074–9083, 2007.

[82] D. C. Forbes, M. Creixell, H. Frizzell, and N. A. Peppas. Polycationic

nanoparticles synthesized using ARGET ATRP for drug delivery. *Eur. J. Pharm. Biopharm.*, 84(3):472–478, 2013.

[83] L. Cao, T. Man, J. Zhuang, and M. Kruk. Poly (*N*-isopropylacrylamide) and poly (2-(dimethylamino) ethyl methacrylate) grafted on an ordered mesoporous silica surface using atom transfer radical polymerization with activators regenerated by electron transfer. *J. Mater. Chem.*, 22:6939–6946, 2012.

[84] B. T. Cheesman, A. J. G. Neilson, J. D. Willott, G. B. Webber, S. Edmondson, and E. J. Wanless. Effect of colloidal substrate curvature on pH-responsive polyelectrolyte brush growth. *Langmuir*, 29(20):6131–6140, 2013.

[85] W. Jakubowski, K. Min, and K. Matyjaszewski. Activators regenerated by electron transfer for atom transfer radical polymerization of styrene. *Macromolecules*, 39(1):39–45, 2006.

[86] K. A Payne, D. R D'hooge, P. H. M. Van Steenberge, M. Reyniers, M. F. Cunningham, R. A. Hutchinson, and G. B. Marin. ARGET ATRP of butyl methacrylate: Utilizing kinetic modeling to understand experimental trends. *Macromolecules*, 46(10):3828–3840, 2013.

Chapter 3

siRNA Background

3.1 Therapeutic potential of small RNA and DNA

Small RNA and DNA therapeutics may offer improved treatment strategies for a full range of conditions including hypercholesterolemia, glaucoma, viruses, cancer, and inflammatory bowel disease. In spite of their promise, delivery to the action site of the cytosol remains a significant obstacle. While small interfering RNAs (siRNA) have enjoyed recent popularity due to their potent and specific gene silencing, other oligonucleotides including microRNA (miRNA), antisense oligonucleotides (AS-ODNs), and transcription factor decoys also show promise for therapeutic applications. Oligonucleotides are susceptible to degradation, particularly by nucleases, so efficacy may be enhanced by polymer carrier strategies that protect the drug. Also, oligonucleotides are only effective inside the cytosol of the cell. Therefore, the delivery strategy must achieve not only cellular uptake but also evade the biological defense strategy of endosomal sequestration without activation of the immune system.

Most oligonucleotide delivery strategies in laboratory or clinical trials

are injection-based; thus, there remains a paucity of data on the development of oral delivery systems. Intravenous administration is the most common strategy, but subcutaneous, intralesional, intravitreal, and intratumoral injections are also used. From a drug delivery standpoint, the oral route of administration is advantageous because it increases patient compliance and comfort over injection, provides a simple, repeatable administration, and provides a large surface area of absorption. Efficient oral delivery of fragile biotherapeutics, such as peptides, proteins, and nucleic acids, has long been considered a challenge of drug delivery and is still one of the field's most compelling and difficult problems. Successful development of oral delivery systems for oligonucleotides such as siRNA would provide patients a powerful, specific therapeutic in a convenient form that most would consider less invasive than injections.

3.2 Small RNAs and DNAs

Small interfering RNA (siRNA), microRNA (miRNA), antisense oligonucleotides (AS-ODNs), and transcription factor decoys are oligonucleotides that can regulate gene expression when delivered to the cytosol. These four strategies all use a short sequence of nucleotides (approximately 20 base pairs), and each strategy requires intracellular delivery and endosomal escape of the oligonucleotides. The oligonucleotides differ in the nucleotide type (RNA or DNA) and the number of strands (single or double stranded), and these differences change important physicochemical properties that affect

drug delivery such as molecular weight, configuration, and stability.[1] Another difference is the mechanism of action of the oligonucleotide; decoys work by a pre-transcriptional mechanism while siRNA and AS-ODNs work by a post-transcriptional mechanism (see Figure 3.1).[2;3] Despite these differences, delivery strategies share fundamental similarities because the oligonucleotides have similarities in structure and site of action.

The pre-transcriptional mechanism of action for transcription factor decoys is distinct from the post-transcriptional regulation by RNA interference (RNAi) and antisense oligonucleotides. Transcription factor decoys imitate chromosomal DNA target sequences so that transcription factors bind to the decoy rather than to the cDNA.[4] The typical action of the transcription factor is to regulate gene expression, so some factors up-regulate while other factors down-regulate specific genes by interacting with transcriptional machinery in the nucleus.[5]

Antisense oligonucleotides may act via a stoichiometric binding approach to block translation of mRNA or by a catalytic, RNAi-like mechanism.[2;6;7] Antisense oligonucleotides are typically single-stranded DNA or chemically modified DNA derivatives.[7] In the RNAi-like mechanism, the RNA/DNA heteroduplex of mRNA and antisense oligonucleotide activates RNase H to degrade the mRNA strand.[2] The antisense oligonucleotide dissociates and is free to bind to another mRNA strand to repeat the degradation process.[6] In addition to targeting mRNA, the next generation of antisense oligonucleotides can be designed to repress over-expressed miRNA.[8] The dis-

advantage of antisense oligonucleotides is that they are less potent and shorter lasting than siRNAs.[9]

RNA interference (RNAi) has received much attention since its initial report in 1998 by Fire and Mello[10] as a powerful strategy to alter gene expression, and a number of RNAi-based therapeutic strategies have progressed to clinical trials (see Table 3.1). Inducers of the RNAi mechanism include endogenous miRNA, synthetic siRNAs, and "vector based" short hairpin RNA (shRNA). While the field of shRNA therapeutics is largely based on viral vector transfection methods,[11] a novel, orally administered, bacterial-based system may offer an improved delivery strategy (see Table 3.2 for clinical trials of shRNA-based therapeutics).[12–14] siRNA has been an intense focus of gene therapy researchers and its therapeutic potential has been likened to a "magic bullet"[15]due to its potent, catalytic-type mechanism and specific gene knockdown.

The mechanism of siRNA is characterized by degradation of a specific mRNA sequence with a perfectly complementary sequence. Translation of the mRNA sequence to proteins is therefore downregulated and gene expression is silenced. The endogenous RNAi inducers miRNA,[16] in contrast, may downregulate 250-500 different mRNA sequences that are partially complementary by translational repression. Early research focused on the cytoplasm as the site of action for RNAi, but later work has identified a role for RNAi in the cell nucleus as well.[11;17;18]

Research continues to identify similarities in the RNAi mechanisms of

siRNA and miRNA so that the basic classifications of Figure 3.1 are subject to some qualifications; each small RNA may act like the other. Perfect complementarity of the miRNA sequence results in mRNA degradation;[19] likewise, siRNA may induce off-target effects that occur via a miRNA-like mechanism through down-regulation of partially complementary mRNA sequences.[20–22] This crossover should perhaps come as no surprise since before being completely processed to mature, single-stranded miRNAs, pre-miRNAs from the nucleus are processed into siRNA-like double-stranded RNA before strand separation.[19] The crossover can result in interference with endogenous miRNA mechanisms.[23] Another complication is that there are at least 3 classes of action for siRNA, of which at least one is independent of the traditional Argo/RISC mechanism.[24]

Recent studies have demonstrated that siRNA can provoke the innate immune system into an inflammatory response,[25–28] and this is particularly troubling for the treatment of IBD whose strategy is to suppress the immune response. For example, PKR (protein kinase R) "can react to as little as 11 base pairs of dsRNA in a nonsequence-specific fashion"[27]. Particularly for the treatment of IBD which is connected with a abnormal immune response and inflammation, an effective siRNA-based therapeutic must do more than silence an important gene, it must also avoid causing an immune response and additional inflammation. Adding complexity to experimental design, since immune stimulation is sequence-dependent, the use of a "scrambled" siRNA control is insufficient to test for an innate immune response[27]. These interactions may

be hybridization-independent, meaning the interaction is not dependent on Watson and Crick RNA base pairing.[29]

3.3 Oral delivery of small RNAs and DNAs

Delivery of all types of oligonucleotides is challenging because the negatively charged (anionic), water soluble molecules are large (molecular weight ~12,500 Da with 3 nm diameter and 5 nm height for siRNA[30]) with very low membrane permeability.[31;32] If the oligonucleotide is taken up by the cell, it will still need to escape endosomal sequestration because the site of action is the cytosol. The magnitude of these challenges is being met by an impressive effort to design improved oligonucleotide delivery systems and a number of excellent reviews[22;33–47] have been published.

It is not surprising that early RNAi delivery efforts were focused on disease targets amenable to site-specific delivery (either by direct injection or topical application) such as ocular diseases where the drug could be injected into the eye for a local, rather than systemic, effect. However, a number of important disease targets are not amenable to direct injection or topical application, resulting in widespread work in systemic delivery, particularly intravenous injections.[38;48–51] Delivery with a more patient-friendly, broad-utility platform is needed.

Oral delivery systems may be less invasive than current treatments to improve patient comfort and compliance.[52] However, such systems would

only be effective if they could protect the payload during transit to ensure safe delivery of the oligonucleotide to the cytosol of the targeted cells (see Figure 3.2). An oral oligonucleotide delivery system must provide protection from the acidic gastric environment as well as from enzymatic attack from nucleases until the drug is absorbed.[52;53]

Many proposed oral delivery systems include multicomponent design with a cationic component to interact with the negatively charged siRNA. In addition, many of these proposed systems are designed for intestine-specific delivery to treat inflammatory bowel disease. A summary of the limitations of proposed siRNA oral delivery systems is found in Table 3.3.

3.3.1 Chitosan modified poly(d,l-lactide-*co*-glycolide) nanospheres (CS-PLGA NS) loaded with a transcription factor decoy

The chitosan modified poly(D,L-lactide-*co*-glycolide) nanospheres (CS-PLGA NS) for delivery of a transcription factor decoy developed by Tahara and associates[54] use classical biomaterials to achieve colon-specific oral delivery of oligonucleotides; a representation of the system is shown in Figure 3.3a. The nanospheres are formed by the emulsion solvent diffusion method (ESD) using ethanol/acetone organic phase with dissolved PLGA and complexed siRNA/DOTAP and an aqueous phase with 2% w/v polyvinyl alcohol (PVA).[55] Although widely used for transfection studies and less toxic that other cationic lipids, DOTAP can damage cells[56] and thus may be another regulatory concern. Advantages of the ESD method over other emulsion tech-

niques include “mild conditions” (ethanol/acetone versus dichloromethane organic phase) as well as the use of propeller-type stirring rather than sonication, which is more amenable to scale-up.[55]

Both chitosan modified and unmodified PLGA provided 4 hours of protection for the DNA cargo from DNase I degradation, and the chitosan modified PLGA also provided protection from acidic pH for 2 hours.[54] While both of these advantages should be noted, the use of the cationic lipid DOTAP introduces cytotoxicity concerns analogous to those for the thioketal nanoparticles developed by Wilson and associates.[57] Cytotoxicity studies *in vitro* indicated that the CS-PLGA NS showed “no adverse effects” for 2 and 24 h incubation with up to 5 mg/ml concentrations.

The transcription factor decoy-loaded CS-PLGA NS proved an effective orally administered treatment for dextran sodium sulfate (DSS)-induced experimental colitis in Wistar rats; however, dosing was high compared to other oligonucleotide studies with 2 mg oligonucleotide per rat.[54] The high dose suggests that either the transcription factor decoys are inherently less powerful than siRNA-based therapeutic strategies or that the delivery system may not be as effective as other orally administered oligonucleotide delivery systems. The high dose may be needed due to the burst release of as much as 40% of the oligonucleotide, which will likely degrade before reaching the cytosol. The author notes that an adding an enteric coating may improve the “protective effect”[54] so the oligonucleotide is less susceptible to degradation, particularly in the gastric environment. Researchers noted greater adhesion

and penetration for the nanospheres in inflamed versus non-inflamed tissues.[54] This effect may be beneficial as the work of Wilson and associates suggests that targeting delivery to sites of inflammation may improve overall efficacy.[57]

3.3.2 Eudragit® coated capsules with sodium caprate permeation enhancer minitablets loaded with antisense oligonucleotides

The antisense oligonucleotide oral delivery system developed by Isis Pharmaceuticals (Carlsbad, CA) uses two different Eudragit® coatings to achieve site-specific delivery as well as time-delayed release of the sodium caprate permeation enhancer.[32;58] *In vivo* studies in beagle dogs and humans reported an average plasma bioavailability of 1.4% (relative to IV) and 9.5% (relative to subcutaneous dose),[32] respectively, for the oligonucleotide.[58] This oral delivery systems is designed for systemic rather than intestinal delivery of oligonucleotides, unlike the other reported oral delivery systems. As a result, it may exhibit the problems associated with other systemic approaches such as off-target effects, particularly in areas of oligonucleotide accumulation such as the kidneys and liver.[58]

The Eudragit® L30 D55 (poly(methacrylic acid-co-ethyl acrylate) in 1:1 ratio) outer coating for the gelatin capsules[32] is designed for pH-specific delivery to the duodenum (first segment of the small intestine).[59] Minitablets for extended release of sodium caprate (C10) are contained within the gelatin capsule (see Figure 3.3b); the minitablets are coated with Eudragit® RS30D,[32] which is designed for time-controlled, pH-independent release and composed

of a terpolymer of ethyl acrylate, methyl methacrylate, and low content of methacrylic acid ester with quaternary ammonium groups present as salts.[60]

Sodium caprate is the sodium salt of the 10-carbon saturated fatty acid capric acid (also known as decanoic acid), which is a naturally occurring, dietary fatty acid that can be found in palm kernel and coconut oil.[61] It has been used in Japan[62] as well as Sweden (Doktacillin™)[58] to improve drug absorption; sodium caprate causes dilation of tight junctions, resulting in increased paracellular transport.[62;63] Sodium caprate has FDA approval as a food additive is an emulsifier or binder food additive.[64–67] While sodium caprate is permitted as a food additive, its use as a pharmaceutical additive must carefully evaluate its effect on intestinal epithelium. Caco-2 cell studies demonstrate transient and reversible alterations in permeability;[58] while no wounds to cells are observed, recovery may take a few hours.[62]

3.3.3 Eudragit® coated capsules with bovine serum albumin (BSA) encapsulated antisense oligonucleotides

Uddin and associates[68] created a system for antisense oligonucleotide oral delivery by microencapsulation of the antisense oligonucleotide with albumin. The antisense oligonucleotide-loaded albumin microspheres are created using a spray-drying method. First, albumin is glutaraldehyde cross-linked for 24 h with continuous stirring followed by the addition of sodium bisulphate to neutralize excess glutaraldehyde. Next, the antisense oligonucleotide drug is added, and the mixture is spray-dried using a Büchi mini spray-dryer. The pro-

cess produced 2 µm diameter spherical particles designed for ready uptake by antigen-presenting cells such as macrophages. Tablets of albumin-encapsulated oligonucleotide microspheres were coated with Eudragit L100-55 (see Figure 3.3c). The release kinetics of the enteric-coated tablets were evaluated using a standard drug dissolution experiment. The enteric coating prevented premature release and the micro-encapsulation resulted in a sustained release profile for 30+ h. The albumin microencapsulation improved the bioavailability of antisense oligonucleotide following oral delivery compared to the naked antisense oligonucleotide (70% versus 9% bioavailability).

3.3.4 β1,3-d-glucan-encapsulated siRNA particles (GeRPs) loaded with siRNA

Oral delivery of siRNA was first reported in 2009 by Aouadi and associates[69] in a β1,3-D-glucan-encapsulated siRNA particles (GeRPs). The outer β1,3-D-glucan shell was purified from baker's yeast with base and solvent extractions followed by hydrolysis of the outer cell wall and cell contents. Using a layer-by-layer approach to build the core and encapsulate the siRNA, the 2 to 3 µm porous, hollow shells were filled with negatively charged tRNA, positively charged polyethylenimine (PEI), negatively charged unmodified siRNA, and then another PEI layer, like the representation shown in Figure 3.3d. The GeRPs were targeted to the M cells of the Peyer's patches in the intestines in order to reach the gut-associated lymphatic tissue (GALT) located below. Over time, the ingested GeRPs may migrate throughout the lymphatic tissue

away from the gut;[69] the effects of this delocalization of the delivery system need to be evaluated in order to anticipate possible off-target effects.

Studies *in vitro* with 10^6 macrophages concluded that "as little as 40 pmoles siRNA within GeRPs" resulted in 70 to 80% knockdown of the targeted mRNA. Studies *in vivo* found gene silencing persisting for about 8 days in mice following 8 days of oral gavage of about 20 µg siRNA / kg in 200 µl containing about 10^8 GeRPs .[69] The results are promising; this reported mass of siRNA required to achieve knockdown per mass of mouse is competitive with the best cationic lipid systems (10 to 20 µg siRNA / kg in mice).[44] While baker's yeast is an extremely well characterized system, as with any system containing natural components, the potential for significant and unexplained batch-to-batch variation may exist. In addition, although PEI is widely used in gene therapy, the polymer is cytotoxic[70] and so may cause adverse effects.

3.3.5 Nanoparticles-in-microsphere oral system (NiMOS) loaded with siRNA

The biodegradable nanoparticles-in-microsphere oral system (NiMOS) developed by Amiji and colleagues was used for plasmid DNA delivery[71–73] before its adaptation by Kriegel for siRNA delivery[74;75]. Poly(ε-caprolactone) microspheres (2 to 4 µm diameter) were loaded with type B gelatin nanoparticles (280 nm diameter) containing "physically" encapsulated siRNA, such as the representation in Figure 3.3e. The outer poly(ε-caprolactone) is stable to acidic pH and so it protects the siRNA cargo during transit through the stomach,

and the polymer is degraded by lipases in the intestines to release the siRNA-loaded gelatin nanoparticles.[74;75] The gelatin nanoparticles are degraded by proteases to release the siRNA cargo. Early work found improved biodistribution with poly(ε-caprolactone) encapsulated gelatin nanoparticles compared to the gelatin nanoparticles alone because gelatin degrades too rapidly during gastrointestinal transit for effective delivery to the intestines.[71]

The NiMOS was evaluated in a murine model with 1.2 mg NiMOS/kg dosing in 200 µl.[74;75] While loading efficiencies of the final system are reported as over 50%,[75] the total siRNA content of the NiMOS as well as the siRNA dosing of the *in vivo* studies seem to have been omitted from the reported results. Acute colitis in mice was induced by treatment with dextran sulfate sodium (DSS). The DSS-treated mice were treated with the anti-TNF-α siRNA-loaded NiMOS which achieved significant reductions in TNF-α concentrations so that the DSS-treated mice had "similar" concentrations as the healthy control mice.[75] Another study found that a "combined" treatment using two anti-inflammatory siRNAs was able to achieve a better outcome than use of a single anti-TNF-α siRNA.[74]

An effective NiMOS for siRNA delivery to the intestines in a clinical setting would require careful tuning to the specific transit time and degradation conditions characteristic of human physiology, which vary depending on disease state. The broad, delocalized expression in both the small and large intestines, identified in earlier work with the system and transfection with plasmid DNA,[71] may be undesirable for some applications; the siRNA studies

indicate the large intestine was removed for analysis but no analysis of the small intestine was included in the reports.[74;75]

3.3.6 Thioketal nanoparticles (TKNs) loaded with siRNA

The thioketal nanoparticle (TKN) system developed by Wilson and associates[57] uses specialized polymer chemistry to protect the siRNA from degradation in the gastrointestinal tract and release the siRNA "specifically" at sites of inflammation. The poly(1,4-phenyleneacetone dimethylene thioketal) (PPADT) polymer resists acidic, basic, and enzymatic degradation but it degrades in the presence of increased concentrations of reactive oxygen species (ROS) characteristic of sites of intestinal inflammation. The 600 nm diameter PPADT nanoparticles contain siRNA complexed with DOTAP (cationic lipid 1,2-dioleoyl-3-trimethylammonium-propane) (Figure 3.3f); the DOTAP gives the nanoparticles an overall positive surface charge. The siRNA/DOTAP-loaded nanoparticles are synthesized using a single emulsion; siRNA/DOTAP complexed in dichloromethane and methanol is combined with PPADT dissolved in dichloromethane to form the organic phase and the aqueous phase is composed of 5% polyvinyl alcohol (PVA) in pH 7.4 phosphate buffer saline (PBS).[57]

Toxicity *in vitro* was reported as comparable to that of poly(lactic-*co*-glycolic acid) (PLGA) siRNA loaded nanoparticles; no toxicity was detected up to 5.0 mg/ml.[57] While these toxicity results are positive, the chemicals used in synthesis have serious known or suspected negative health effects, so regulatory

approval of the final product might prove to be challenging. Benzene and dichloromethane are the solvents used for the PPADT polymer synthesis and emulsion, respectively; while subsequent purification steps should significantly reduce the concentrations of benzene and dichloromethane to perhaps even below limits of detection, the known potent carcinogenicity of benzene, and suspected carcinogenicity of dichloromethane, mean that any residual solvent could have adverse health effects in long-term use, such as for the management of chronic disease.

Studies *in vivo* demonstrated that 5 days of oral gavage of 2.3 mg siRNA/kg and 0.23 mg siRNA/kg achieved 10-fold and 3-fold, respectively, decrease in the targeted mRNA concentration in the colon. The TKNs were more effective than β-glucan particles (similar to those used by Aouadi and associates[69]) at achieving mRNA reduction at the same 0.23 mg siRNA/kg dose; β-glucan particles do not deliver siRNA specifically to sites of inflammation, so the results suggest that targeting delivery to sites of inflammation may improve the therapeutic efficacy.[57]

3.3.7 Nanoparticles made with chitosan loaded with siRNA

There are several reports in the literature of chitosan-based nanoparticles for oral siRNA delivery. Chitosan may be chemically modified and nanoparticles are formed using a double emulsion or by ionic gelation. The chitosan nanoparticles may be used alone[76–80] (as shown in Figure 3.3g) or after encapsulation in a hydrogel for intestines-specific delivery (as shown in

Figure 3.3i).[81]

3.3.7.1 Chitosan/siRNA nanoparticles

The chitosan/siRNA nanoparticles used by Ballarín-González and associates[80] represent the most straight-forward synthesis approach of the various chitosan-based techniques; unmodified chitosan was combined with siRNA to form nanoparticle complexes in a single-step process. These complexes were approximately 150 nm in diameter, as determined using particle tracking analysis (see Figure 3.3g). Biodistribution experiments following oral administration to mice confirmed uptake of siRNA by the intestine and translocation to the liver, spleen, and kidney. The chitosan conferred enhanced stability for the siRNA, as confirmed using northern blotting and qPCR analysis. Although the report does not include confirmation of siRNA-induced knockdown, the enhanced stability and uptake of siRNA imparted by the chitosan (compared to naked siRNA) demonstrates the advantages of carrier-enhanced delivery.

3.3.7.2 Thiolated trimethyl chitosan (TTMC), galactosylated trimethyl chitosan–cysteine (GTC) nanoparticles, and mannose-modified trimethyl chitosan-cysteine (MTC) conjugate nanoparticles

Zhang, et al. used thiolated trimethyl chitosan (TTMC)[77] and galactosylated trimethyl chitosan–cysteine (GTC) nanoparticles (NPs)[78] for siRNA

delivery (two separate reports), and the GTC nanoparticles were investigated for use in siRNA oral delivery. Thiolated trimethyl chitosan (TTMC) was synthesized by adding trimethyl and thiol groups to chitosan.[77] Galactosylated trimethyl chitosan–cysteine (GTC) contains galactose modifications in addition to the trimethyl and thiol groups.[78] A related approach using chitosan modified to contain sugar, trimethyl, and thiol groups was used by He and associates[76] to create trimethyl chitosan-cysteine nanoparticles[82] and mannose-modified trimethyl chitosan-cysteine (MTC) conjugate nanoparticles.

The use of various functional groups represents an alternative approach to designing multi-component systems for siRNA delivery; rather than mixing or combining different components, the components are chemically bound along the chitosan chain. The nanoparticles were formed by ionic cross-linking of the positively charged chitosan with a negatively charged component such as thiamine pyrophosphate (TPP),[76] or in the case of the work by Zhang and associates, TPP or hyaluronic acid.[77;78] An siRNA/TPP or siRNA/hyaluronic acid solution was added drop-wise to a solution of chitosan conjugate under stirring. The nanoparticles had a positive surface charge, as determined using dynamic light scattering, and an approximate diameter of 120 nm diameter for the MTC-NPs and 150 nm for the GTC- and TTMC-NPs (see Figure 3.3g).

Both TTMC-NPs and GTC-NPs outperformed the Lipofectamine2000 (a commercially available transfection reagent) control to induce significant knockdown *in vitro* for RAW264.7 murine macrophage cells.[77;78] Biodistribution experiments confirmed that the TTMC-NPs promoted intestinal absorp-

tion of siRNA (compared to naked siRNA), and their success was attributed to enhanced intestinal stability and permeation.[77] The GTC-NPs were used for oral delivery of Map4k4 siRNA to mice with DSS-induced colitis. A dose of 250 μg Map4k4 siRNA/kg/day for seven days resulted in significant knockdown in the mRNA of Map4k4 and TNF-α in colonic tissue (92.1% and 69.0%, respectively). Treatment with MAP4k4 siRNA GTC-NPs resulted in no significant weight loss, no significant colon shortening, and improvements in histology such as minimal damage and neutraphil infiltration, as compared to significant weight loss, colon shortening, and evidence of abnormality, cell death, and neutraphil infiltration in PBS-treated mice with DSS-induced colitis.[78]

For the MTC-NPs, the knockdown efficiency *in vitro* in RAW264.7 cells of the MTC-NPs exceeded that of the Lipofectamine2000 for the knockdown of TNF-α, and the MTC nanoparticles demonstrated negligible cytotoxicity. Studies *in vivo* demonstrated increased siRNA concentration (compared to naked siRNA) in the liver, spleen, lung, and intestine of mice. Delivery of anti-TNF-α siRNA using MTC nanoparticles resulted in significant TNF-α knockdown in the liver, lung, and spleen of mice. The MTC nanoparticles outperformed β1,3-D-glucan-encapsulated siRNA particles (GeRPs) *in vivo*, requiring less siRNA (3.75 nmol/kg versus 12 nmol/kg) to achieve the same knockdown.[76]

3.3.7.3 *N*-((2-hydroxy-3-trimethylammonium) propyl) chitosan chloride (HTCC) nanoparticles

The chitosan-based system developed by Wei and associates[79] makes use of a Shirasu porous glass membrane emulsification technique for size control rather than the TPP-based ionic gelation scheme used by Zhang and associates[77;78] and He and associates.[76] The *N*-((2-hydroxy-3-trimethylammonium) propyl) chitosan chloride (HTCC) is a partially quaternized derivative of chitosan with good cell-adhesion as well as permeation-enhancing effects.[79] The 150 nm diameter nanoparticles are formed by an oil/water/oil double emulsion method which permits loading of paclitaxel nanocrystals in addition to siRNA (see Figure 3.3g).

In vitro studies with mouse telomerase reverse transcriptase (mTERT) siRNA demonstrated that the HTCC nanoparticles successfully delivered siRNA to cells to induce knockdown. In order to enhance the anti-tumor efficacy, paclitaxel was incorporated to create a dual-delivery system. Tumor-bearing mice were treated with nanoparticles with 0.2 μg siRNA/kg/day and 6.5 μg paclitaxel/kg/day, and treatment resulted in significantly inhibited tumor growth and increased survival time compared to mice treated with naked mTERT siRNA.

3.3.7.4 Chitosan/siRNA and polyethylenimine (PEI)/siRNA complexes combined with polylactide (PLA), coated with polyvinyl alcohol (PVA) and encapsulated in chitosan/alginate hydrogel

The multicomponent systems developed by Laroui and associates are designed to protect the siRNA during gastrointestinal transit and to release the payload in the colon using a pH-responsive hydrogel.[81] Synthesis is a complicated, multistep process of complexation: a single emulsion followed by a double emulsion, purification of the nanoparticles, and then encapsulation in a chitosan/alginate hydrogel.[81;83] The system's complexity (as illustrated in Figure 3.3i) represents a fundamental barrier to clinical use. The PEI-containing nanoparticles had improved loading, protection, and transfection compared to the chitosan containing nanoparticles.

The chitosan (see Figure 3.3g) and PEI (see Figure 3.3h) nanoparticles contain 9.6 ng siRNA/mg and 15.2 ng siRNA/mg, respectively. The PEI-containing nanoparticles are 300-500 nm in diameter at pH 6-7 (size of chitosan nanoparticles not given). The cationic polymer (chitosan or PEI) complexed to the siRNA is designed to reduce burst release in order to increase the fraction of drug that makes it to the delivery site; after 30 minutes in PBS buffer, only about 30% of the siRNA was released from the PEI/siRNA complexes (identified as an "optimal" result"),[81] while without a complex, a burst effect is typically observed. The PEI-containing nanoparticles were evaluated *in vitro* and they demonstrated improved cell viability and transfection compared to the

transfection agent Lipofectamine without resulting in macrophage inflammation. The siRNA-loaded PEI-containing nanoparticles in an alginate/chitosan hydrogel were administered orally in mice at 5 mg NP/ml hydrogel;[81] the total volume administered is not specified, so the total quantity of siRNA administered is unclear. The treatment significantly reduced concentrations in the colon as well as blood of the targeted TNF-α, but not liver concentrations. While the therapeutic effect was not truly site-specific to the intestines, it is promising that the treatment did not alter the concentration of TNF-α cytokines in the liver because systemic anti-TNF-α approaches using biological therapeutics have been limited by "profound systemic toxicity"[81] that alters the TNF-α expression throughout the body.

3.4 Tables

Table 3.1: Clinical trials for RNAi therapeutics. Information was gathered from a variety of sources including ClinicalTrials.gov, company press releases, and reports in the literature. Updates about the status of clinical trials can be found at ClinicalTrials.gov with the NCT number; http://clinicaltrials.gov/show/NCT#.

Category	Disease	Delivery	Excipient	Product	Sponsor	Phase I	Phase II	Phase III
Eye	AMD	IVT	n	Bevasiranib (Cand 5)	Opko Health	✓ NCT00722384	✓ NCT00259753	✗ NCT00557791 ✗ NCT00499590
Eye	DME	IVT	n	Bevasiranib (Cand 5)	Opko Health		✓ NCT00306904	
Eye	AMD	IVT	n	PF-04523655 (RTP801-14, PF-655)	Quark/Pfizer/Silence	✓ NCT00725686	✓ NCT00713518	
Eye	DME	IVT	n	PF-04523655 (RTP801i-14, PF-655)	Quark/Pfizer/Silence		NCT01445899 ✗ NCT00701181	
Eye	AMD	IVT	n	Sirna-027 (AGN211745)	Allergan/Merck–Sirna Therapeutics	✓ NCT00363714	✓ NCT00363714 ✗ NCT00395057	
Eye	Glaucoma	ophthalmic drops	n	SYL-040012	Sylentis	✓ NCT00990741 ✓ NCT01227291	✓ NCT01227291	
Eye	Glaucoma; eye injury	IVT	n	QPI-1007	Quark	NCT01064505		
Eye	Ocular pain, dry eye	Eye drops	-	SYL1001	Sylentis	NCT01438281		
Virus	RSV infection after lung transplantation	rebulizer	n	ALN-RSV01	Alnylam/Cubist/ Kyowa Kirin		✓ NCT00658086 NCT01065935	
Virus	HBV Infection	IV	Cationic lipid	NUC B1000	Nucleonics			
Renal	DGF	IV	n	QPI-1002 (Also in siNP)	Quark	NCT00802347	NCT00802347	
Asthma	Asthma	Inhaled	-	Excellair™ (ACU-ISP-001)	ZaBeCor	✓		
Skin	PC	ID/L injection	n	TD101	Trans Derm/IPCC	✓ NCT00716014		
Cancer	Liver cancer	IV	Liposome	ALN-VSP01	Alnylam			
Cancer	Liver cancer	IV	SNALP	ALN-VSP02	Alnylam/Tekmira	✓ NCT00882180 NCT01158079		
Cancer	CML	IV	anionic liposome	Bcr-abl	Univ Duisburg-Essen	✓		
Cancer	Metastatic melanoma	Ex vivo + ID	-	Proteasome siRNAs	Duke University	NCT00672542		
Cancer	Solid tumor	IV	lipid NP atuPLEX	Atu-027	Silence/Atugen AG	NCT00938574		
Cancer	Solid tumor (liver)	IV	SNALP	TKM-PLK1 (TKM-080301, ALN-PLK1)	Tekmira, Alnylam	NCT01262235 NCT01437007		
Cancer	Solid tumor	IV	CD, TF, PEG NP	CALAA-01	Calando Pharma/Alnylam	NCT00689065		
Cancer	Pancreatic cancer	EUS biopsy needle	LODER polymer	siG12D LODER (Local Drug EluteR)	Silenseed	(Phase 0) NCT01188785		
ATTR	ATTR	IV	SNALP	ALN-TTR01	Alnylam	NCT01148953		
Cholesterol	Hypercholesterolemia	IV	SNALP	ApoB SNALP (PRO-040201, TKM-ApoB-001)	Tekmira/Alnylam	✗ NCT00927459		
Cholesterol	Hypercholesterolemia	IV	SNALP	ALN-PCS02	Alnylam	NCT01437059		

Key: ✓ completed, ▬ ongoing, ✗ terminated or withdrawn, ✓ ▭ ✗ no record at ClinicalTrials.gov

Abbreviations: AMD: wet age-related macular degeneration ApoB: apolipoprotein B ARF: acute renal failure ATTR: transthyretin mediated amyloidosis CD, TF, PEG VP: cyclodextrin nanoparticle, contains transferrin (TF) for targeting and polyethylene glycol (PEG) for stealth properties CML: chronic myeloid leukemia DGF delayed graft function in kidney transplantation DME: diabetic macular edema EUS: endoscopic ultrasound Ex vivo + ID: ex vivo transfection of autologous dendritic cells with siRNA/mRNA; intradermal injection of cells HBV: Hepatitis B ID/IL: intradermal/intralesional IPCC: International Pachyonychia Congenita Consortium IV: intraveneous IVT: intravitreal LODER: Local drug EuteR n: naked siRNA NP: nanoparticle PC: Pachyonychia congenita RSV: respiratory syncytial virus SC: subcutaneous SNALP: stable nucleic acid lipid particle

Table 3.2: Clinical trials for shRNA therapeutics. Information was gathered from a variety of sources including ClinicalTrials.gov, company press releases, and reports in the literature. Updates about the status of clinical trials can be found at ClinicalTrials.gov with the NCT number; http://clinicaltrials.gov/show/NCT#.

Category	Disease	Delivery	Product	Sponsor	Clinical Trials
HIV	HIV / AIDS lymphoma	Autologous hematopoietic stem cell transplantation; cells transfected *ex vivo* by lentiviral vector	Anti-*tat/rev* shRNA (pHIV7-shI-TAR-CCR5RZ)	City of Hope National Medical Center / Benitec	✗ Phase 0 NCT01153646
Cancer	Solid tumors	Injection of autologous tumor cells following electroporation and irradiation to induce tumor cell antigen recognition using bi-functional-shRNA	FANG™ vaccine	Gradalis	Phase I NCT01061840 Phase II NCT01309230 NCT01453361
Cancer	FAP	Oral administration of entered coated capsule containing live, attenuated E. coli expressing shRNA	CEQ508	Marina Biotech	Phase I

Key for Table 1: ongoing, ✗ terminated or withdrawn, no record at ClinicalTrials.gov

Abbreviations: FAP: Familial adenomatous polyposis

Table 3.3: Disadvantages of current oral delivery systems for oligonucleotides reported in the literature.

Oral siRNA delivery systems reported in the literature	**Limitations of the reported oral siRNA delivery systems**
Chitosan modified poly(D,L-lactide-co-glycolide) nanospheres (CS-PLGA NS) with a transcription factor decoy[54;55]	- low delivery efficiency - burst release - PLGA is expensive[84]
Eudragit® coated capsules with sodium caprate permeation enhancer minitablets with antisense oligonucleotides[32;58]	- designed for systemic delivery
Eudragit® coated capsules with albumin-encapsulated antisense oligonucleotides	- designed for systemic delivery
β1,3-D-glucan-encapsulated siRNA particles (GeRPs) with siRNA[69]	- complicated, multistep, multicomponent synthesis - 5 layer system - 2 yeast-derived components
Nanoparticles-in-microsphere oral system (NiMOS) with siRNA[74;75]	- delivery not colon-specific
Thioketal nanoparticles (TKNs) with siRNA[57]	- 24 h polymer synthesis - benzene solvent
Nanoparticles made with chitosan[76–81]	- most effective systems are associated with complicated, multistep synthesis

3.5 Figures

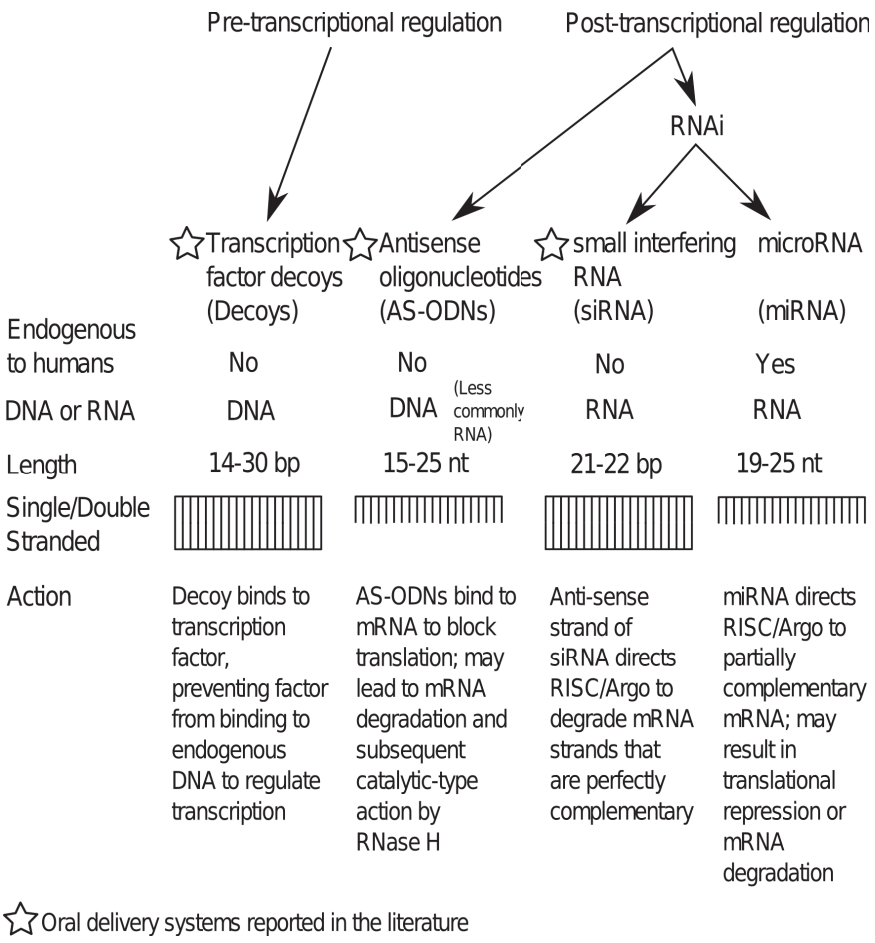

Figure 3.1: Overview of transcription factor decoys, antisense oligonucleotides, small interfering RNA and microRNA. A table by Mack[19] containing specifics for siRNA and miRNA is available in the literature. Abbreviations: bp: base pairs, nt: nucleotides, RISC: RNA induced silencing complex, Argo: Argonaute 2 protein in RISC responsible for mRNA cleavage[20]

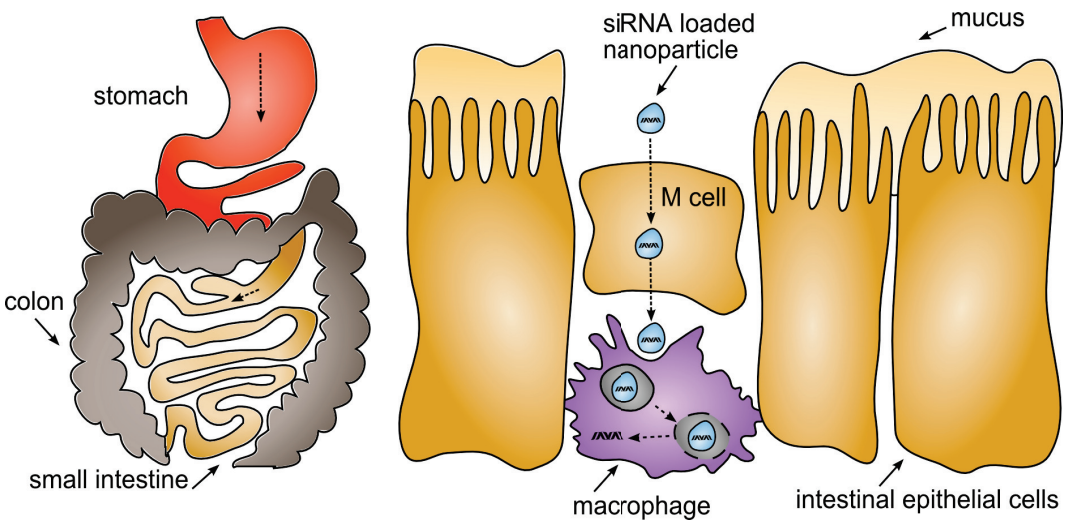

Figure 3.2: Delivery challenges for polymer carrier and oligonucleotide cargo: a) acidic pH, b) nucleases, c) mucus layer, d) cell membrane, e) endosomal membrane, for final f) release into the cytosol.

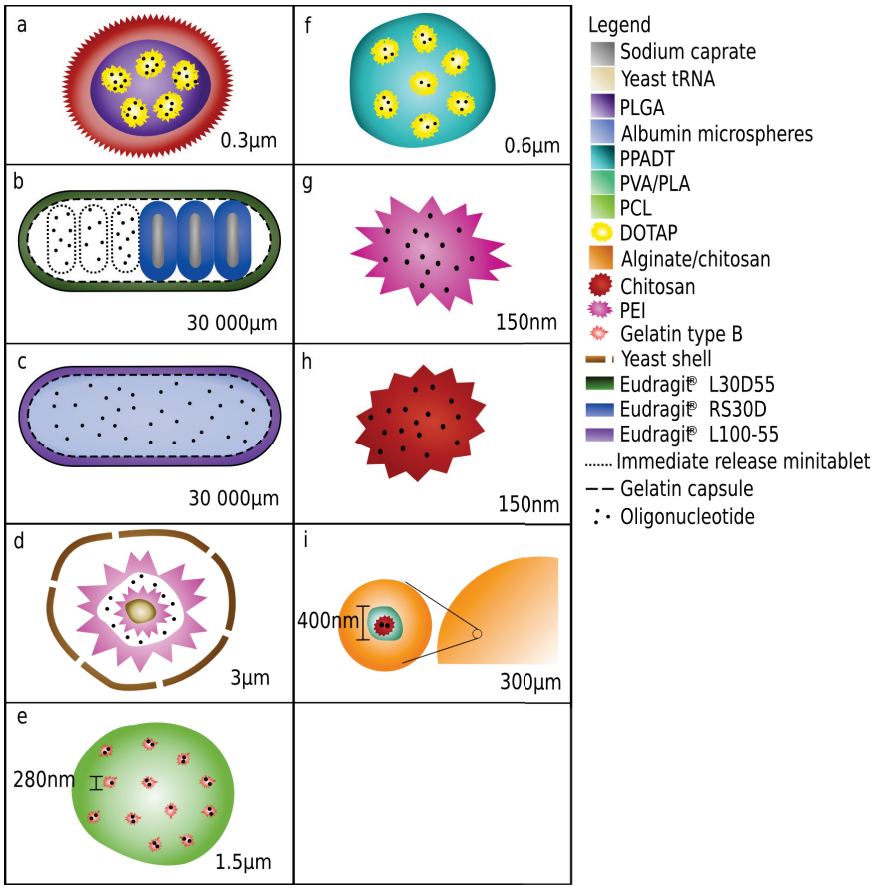

Figure 3.3: Oral delivery systems for small RNA and DNA. Images are shown as schematics and scale bars are approximate. a) Chitosan modified poly(D,L-lactide-*co*-glycolide) nanospheres (CS-PLGA NS) with transcription factor decoy oligonucleotides, b) Eudragit® coated capsules with sodium caprate permeation enhancer minitablets and antisense oligonucleotides, c) Eudragit® coated capsules with bovine serum albumin (BSA) encapsulated antisense oligonucleotides, d) β1,3-D-glucan-encapsulated siRNA particles (GeRPs) e) Nanoparticles-in-microsphere oral system (NiMOS) with siRNA, f) Thioketal nanoparticles (TKNs) with siRNA, g) chitosan nanoparticles with siRNA, h) Polyethylenimine (PEI)/siRNA complexes, i) PEI/siRNA complexes with siRNA combined with polylactide (PLA), coated with polyvinyl alcohol (PVA) and encapsulated in a chitosan/alginate hydrogel

3.6 References

[1] J. Perkel. RNAi therapeutics: A two-year update. *Science*, 326(5951): 454, 2009.

[2] C. F. Bennett and E. E. Swayze. RNA targeting therapeutics: Molecular mechanisms of antisense oligonucleotides as a therapeutic platform. *Annu. Rev. Pharmacol. Toxicol.*, 50(1):259–293, 2010.

[3] Q. Liu and Z. Paroo. Biochemical principles of small RNA pathways. *Annu. Rev. Biochem.*, 79(1):295–319, 2010.

[4] R. Morishita, G. H. Gibbons, M. Horiuchi, K. E. Ellison, M. Nakama, L. Zhang, Y. Kaneda, T. Ogihara, and V. J. Dzau. A gene therapy strategy using a transcription factor decoy of the E2F binding site inhibits smooth muscle proliferation *in vivo*. *P. Natl. Acad. Sci.*, 92(13):5855, 1995.

[5] M. J. Mann and V. J. Dzau. Therapeutic applications of transcription factor decoy oligonucleotides. *J. Clin. Invest.*, 106(9):1071–1076, 2000.

[6] S. Agrawal. *Antisense Therapeutics*. Humana Press, Totowa, NJ, 1996.

[7] C. A. Stein and J. S. Cohen. Oligodeoxynucleotides as inhibitors of gene expression: a review. *Cancer Res.*, 48(10):2659, 1988.

[8] S. Davis. Improved targeting of miRNA with antisense oligonucleotides. *Nucleic Acids Res.*, 34(8):2294–2304, 2006.

[9] M.I. Phillips. *Antisense therapeutics*. Springer, Totowa, NJ, 2005.

[10] A. Fire, S. Q. Xu, M. K. Montgomery, S. A. Kostas, S. E. Driver, and C. C. Mello. Potent and specific genetic interference by double-stranded RNA in *Caenorhabditis elegans*. *Nature*, 391(6669):806–811, 1998.

[11] D. D. Rao, J. S. Vorhies, N. Senzer, and J. Nemunaitis. siRNA vs. shRNA: Similarities and differences. *Adv. Drug Deliver. Rev.*, 61(9):746–759, 2009.

[12] H. Guo, J. Zhang, and C. Inal. Targeting tumor gene by shRNA-expressing Salmonella-mediated RNAi. *Gene Ther.*, 18(1):95–105, 2010.

[13] J.H. Fruehauf, M.B. Vaze, F.S. Laroux, and J.A. Sexton. E. coli mediated gene silencing of beta-catenin. *US Patent 2010/0189691 A1*, 2010.

[14] N. Bodyak, A. Borrelli, J. Fruehauf, J. Harborth, M. B. Vaze, C. Grillot-Courvalin, and A. Silva. Ind-enabling studies for CEQ508 targeting beta-Catenin of GI polyps: First oral RNAi drug. *Gastroenterology (Supplement 1)*, 138(5):S–79, 2010.

[15] D. Cejka, D. Losert, and V. Wacheck. Short interfering RNA (siRNA): tool or therapeutic? *Clin. Sci.*, 110(1):47, 2006.

[16] S. M. Hammond. MicroRNA therapeutics: a new niche for antisense nucleic acids. *Trends Mol. Med.*, 12(3):99–101, 2006.

[17] S. Y. Berezhna. siRNA in human cells selectively localizes to target RNA sites. *P. Natl. Acad. Sci.*, 103(20):7682–7687, 2006.

[18] G. Meister. RNA interference in the nucleus. *Science*, 321(5888):496–497, 2008.

[19] G.S. Mack. MicroRNA gets down to business. *Nat. Biotechnol.*, 25(6): 631–638, 2007.

[20] D. Bumcrot, M. Manoharan, V. Koteliansky, and D. W. Y. Sah. RNAi therapeutics: a potential new class of pharmaceutical drugs. *Nat. Chem. Biol.*, 2(12):711–719, 2006.

[21] M. Yang and J. Mattes. Discovery, biology and therapeutic potential of RNA interference, microRNA and antagomirs. *Pharmacol. Ther.*, 117(1): 94–104, 2008.

[22] R. Juliano, M.R. Alam, V. Dixit, and H. Kang. Mechanisms and strategies for effective delivery of antisense and siRNA oligonucleotides. *Nucleic Acids Res.*, 36(12):4158–4171, 2008.

[23] A. A. Khan, D. Betel, M. L. Miller, C. Sander, C. S. Leslie, and D. S. Marks. Transfection of small RNAs globally perturbs gene regulation by endogenous microRNAs. *Nat. Biotechnol.*, 27:549–555, 2009.

[24] T.A. Vickers and S.T. Crooke. siRNAs targeted to certain polyadenylation sites promote specific, RISC-independent degradation of messenger RNAs. *Nucleic Acids Res.*, 40(13):6223–6234, 2012.

[25] K. Tiemann and J. J. Rossi. RNAi-based therapeutics-current status, challenges and prospects. *EMBO Mol. Med.*, 1(3):142–151, 2009.

[26] R. Barbalat, S. E. Ewald, M. L. Mouchess, and G. M. Barton. Nucleic acid recognition by the innate immune system. *Annu. Rev. Immunol.*, 29 (1):185–214, 2011.

[27] K. A. Whitehead, J. E. Dahlman, R. S. Langer, and D. G. Anderson. Silencing or stimulation? siRNA delivery and the immune system. *Annu. Rev. Chem. Biomol.*, 2(1):77–96, 2011.

[28] B. Ballarín-González and K. A. Howard. Polycation-based nanoparticle delivery of {RNAi} therapeutics: Adverse effects and solutions. *Adv. Drug Deliver. Rev.*, 64(15):1717–1729, 2012.

[29] M. Lindow, H. Vornlocher, D. Riley, D. J. Kornbrust, J. Burchard, L. O. Whiteley, J. Kamens, J. D. Thompson, S. Nochur, H. Younis, S. Bartz, J. Parry, N. Ferrari, S. P. Henry, and A. A. Levin. Assessing unintended hybridization-induced biological effects of oligonucleotides. *Nat. Biotechnol.*, 30(10):920–923, 2012.

[30] D. V. Svintradze and G. M. Mrevlishvili. Fiber molecular model of atelocollagen-small interfering RNA (siRNA) complex. *Int. J. Biol. Macromol.*, 37(5):283–286, 2005.

[31] M. G. Ferreiro, L. G. Tillman, G. Hardee, and R. Bodmeier. Alginate/poly-L-lysine microparticles for the intestinal delivery of antisense oligonucleotides. *Pharm. Res.*, 19(6):755–764, 2002.

[32] L. G. Tillman, R. S. Geary, and G. E. Hardee. Oral delivery of antisense oligonucleotides in man. *J. Pharm. Sci.*, 97(1):225–236, 2008.

[33] D. W. Pack, A. S. Hoffman, S. Pun, and P. S. Stayton. Design and development of polymers for gene delivery. *Nat. Rev. Drug Discov.*, 4(7): 581–593, 2005.

[34] T. Park, J. Jeong, and S. Kim. Current status of polymeric gene delivery systems. *Adv. Drug Deliver. Rev.*, 58(4):467–486, 2006.

[35] D. J. Gary, N. Puri, and Y. Y. Won. Polymer-based siRNA delivery: Perspectives on the fundamental and phenomenological distinctions from polymer-based DNA delivery. *J. Control. Release*, 121(1-2):64–73, 2007.

[36] A. Aigner. Cellular delivery *in vivo* of siRNA-based therapeutics. *Curr. Pharm. Des.*, 14(34):3603–3619, 2008.

[37] E. Fattal and A. Bochot. State of the art and perspectives for the delivery of antisense oligonucleotides and siRNA by polymeric nanocarriers. *Int. J. Pharm.*, 364(2):237–248, 2008.

[38] M. Morille, C. Passirani, A. Vonarbourg, A. Clavreul, and J. P. Benoit. Progress in developing cationic vectors for non-viral systemic gene therapy against cancer. *Biomaterials*, 29(24-25):3477–3496, 2008.

[39] D. Castanotto and J. J. Rossi. The promises and pitfalls of RNA-interference-based therapeutics. *Nature*, 457(7228):426–433, 2009.

[40] Y. K. Oh and T. G. Park. siRNA delivery systems for cancer treatment. *Adv. Drug Deliver. Rev.*, 61(10):850–862, 2009.

[41] K. A. Whitehead, R. Langer, and D. G. Anderson. Knocking down barriers: advances in siRNA delivery. *Nat. Rev. Drug Discov.*, 8(2):129–138, 2009.

[42] M. R. Lares, J. J. Rossi, and D. L. Ouellet. RNAi and small interfering RNAs in human disease therapeutic applications. *Trends Biotechnol.*, 28 (11):570–579, 2010.

[43] Z. Liu, Z. Zhang, C. Zhou, and Y. Jiao. Hydrophobic modifications of cationic polymers for gene delivery. *Prog. Polym. Sci.*, 35(9):1144–1162, 2010.

[44] L. Huang and Y. Liu. *In vivo* delivery of RNAi with lipid-based nanoparticles. *Annu. Rev. Biomed. Eng.*, 13(1):507–530, 2011.

[45] C. V. Pecot, G. A Calin, R. L. Coleman, G. Lopez-Berestein, and A. K. Sood. RNA interference in the clinic: challenges and future directions. *Nat. Rev. Cancer*, 11(1):59–67, 2011.

[46] S. Akhtar and I. Benter. Toxicogenomics of non-viral drug delivery systems for RNAi: Potential impact on siRNA-mediated gene silencing activity and specificity. *Adv. Drug Deliver. Rev.*, 59(2-3):164–182, 2007.

[47] M. Dominska and D. M. Dykxhoorn. Breaking down the barriers: siRNA delivery and endosome escape. *J. Cell Sci.*, 123(8):1183–1189, 2010.

[48] A. W. Tong, C. M. Jay, N. Senzer, P. B. Maples, and J. Nemunaitis. Systemic therapeutic gene delivery for cancer: Crafting Paris' arrow. *Curr. Gene Ther.*, 9(1):45–60, 2009.

[49] M. E. Davis, J. E. Zuckerman, C. H. J. Choi, D. Seligson, A. Tolcher, C. A. Alabi, Y. Yen, J. D. Heidel, and A. Ribas. Evidence of RNAi in humans from systemically administered siRNA via targeted nanoparticles. *Nature*, 464(7291):1067–1070, 2010.

[50] X. Z. Yang, S. Dou, T. M. Sun, C. Q. Mao, H. X. Wang, and J. Wang. Systemic delivery of siRNA with cationic lipid assisted PEG-PLA nanoparticles for cancer therapy. *J. Control. Release*, 156(2):203–211, 2011.

[51] A. Malek, O. Merkel, L. Fink, F. Czubayko, T. Kissel, and A. Aigner. *In vivo* pharmacokinetics, tissue distribution and underlying mechanisms of various PEI (-PEG)/siRNA complexes. *Toxicol. Appl. Pharmacol.*, 236 (1):97–108, 2009.

[52] S. Akhtar. Oral delivery of siRNA and antisense oligonucleotides. *J. Drug Targeting*, 17(7):491–495, 2009.

[53] M.D. Bhavsar and M.M. Amiji. Polymeric nano- and microparticle technologies for oral gene delivery. *Expert Opin. Drug Del.*, 4(3):197–213, 2007.

[54] K. Tahara, S. Samura, K. Tsuji, H. Yamamoto, Y. Tsukada, Y. Bando, H. Tsujimoto, R. Morishita, and Y. Kawashima. Oral nuclear factor-κB

decoy oligonucleotides delivery system with chitosan modified poly (D,L-lactide-co-glycolide) nanospheres for inflammatory bowel disease. *Biomaterials*, 32(3):870–878, 2011.

[55] K. Tahara, T. Sakai, H. Yamamoto, H. Takeuchi, and Y. Kawashima. Establishing chitosan coated PLGA nanosphere platform loaded with wide variety of nucleic acid by complexation with cationic compound for gene delivery. *Int. J. Pharm.*, 354(1-2):210–216, 2008.

[56] M. C. Filion and N. C. Phillips. Toxicity and immunomodulatory activity of liposomal vectors formulated with cationic lipids toward immune effector cells. *Biochim. Biophys. Acta, Biomembr.*, 1329(2):345–356, 1997.

[57] D. S. Wilson, G. Dalmasso, L. Wang, S. V. Sitaraman, D. Merlin, and N. Murthy. Orally delivered thioketal nanoparticles loaded with TNF-α siRNA target inflammation and inhibit gene expression in the intestines. *Nat. Mater.*, 9(11):923–928, 2010.

[58] A. A. Raoof, P. Chiu, Z. Ramtoola, I. K. Cumming, C. Teng, S. P. Weinbach, G. E. Hardee, A. A. Levin, and R. S. Geary. Oral bioavailability and multiple dose tolerability of an antisense oligonucleotide tablet formulated with sodium caprate. *J. Pharm. Sci.*, 93(6):1431–1439, 2004.

[59] Evonik Industries. EUDRAGIT L 30 D-55, 2012. http://eudragit.evonik.com/product/eudragit/en/products-services/eudragit-products/enteric-formulations/l-30-d-55/pages/default.aspx.

[60] Evonik Industries. EUDRAGIT RS 30 D, 2012. http://eudragit.evonik.com/product/eudragit/en/products-services/eudragit-products/sustained-release-formulations/rs-30-d/pages/default.aspx.

[61] V. Dubois, S. Breton, M. Linder, J. Fanni, and M. Parmentier. Fatty acid profiles of 80 vegetable oils with regard to their nutritional potential. *Eur. J. Lipid Sci. Technol.*, 109(7):710–732, 2007.

[62] E. K. Anderberg, T. Lindmark, and P. Artursson. Sodium caprate elicits dilatations in human intestinal tight junctions and enhances drug absorption by the paracellular route. *Pharm. Res.*, 10(6):857–864, 1993.

[63] S. Maher, T. W. Leonard, J. Jacobsen, and D. J. Brayden. Safety and efficacy of sodium caprate in promoting oral drug absorption: from *in vitro* to the clinic. *Adv. Drug Deliver. Rev.*, 61(15):1427–1449, 2009.

[64] U.S. Food and Drug Administration. Everything Added to Food in the United States (EAFUS): Database, 2012. http://www.accessdata.fda.gov/scripts/fcn/fcnNavigation.cfm?rpt=eafusListing.

[65] U.S. Food and Drug Administration. Everything Added to Food in the United States (EAFUS), 2011. http://www.fda.gov/Food/FoodIngredientsPackaging/ucm115326.htm.

[66] U.S. Food and Drug Administration. CFR - Code of Federal Regulations Title 21 Sec. 172.860 Fatty acids, 2011. http://www.accessdata.fda.gov/scripts/cdrh/cfdocs/cfcfr/CFRSearch.cfm?fr=172.863.

[67] U.S. Food and Drug Administration. CFR - Code of Federal Regulations Title 21 Sec. 172.863 Salts of Fatty Acids, 2011. http://www.accessdata.fda.gov/scripts/cdrh/cfdocs/cfcfr/CFRSearch.cfm?fr=172.860.

[68] M. N. Uddin, N. J. Patel, T. Bhowmik, B. D'Souza, A. Akalkotkar, F. Etzlar, C. W. Oettinger, and M. D'Souza. Enhanced bioavailability of orally administered antisense oligonucleotide to nuclear factor kappa B mRNA after microencapsulation with albumin. *J. Drug Targeting*, 21(5):450–457, 2013.

[69] M. Aouadi, G. J. Tesz, S. M. Nicoloro, M. Wang, M. Chouinard, E. Soto, G. R. Ostroff, and M. P. Czech. Orally delivered siRNA targeting macrophage Map4k4 suppresses systemic inflammation. *Nature*, 458 (7242):1180–1184, 2009.

[70] S. Moghimi, P. Symonds, J. Murray, A. Hunter, G. Debska, and A. Szewczyk. A two-stage poly(ethylenimine)-mediated cytotoxicity: implications for gene transfer/therapy. *Mol. Ther.*, 11(6):990–995, 2005.

[71] M. D. Bhavsar and M. M. Amiji. Gastrointestinal distribution and *in vivo*

gene transfection studies with nanoparticles-in-microsphere oral system (NiMOS). *J. Control. Release*, 119(3):339–348, 2007.

[72] M. D. Bhavsar and M. M. Amiji. Oral IL-10 gene delivery in a microsphere-based formulation for local transfection and therapeutic efficacy in inflammatory bowel disease. *Gene Ther.*, 15(17):1200–1209, 2008.

[73] M. D. Bhavsar and M. M. Amiji. Development of novel biodegradable polymeric nanoparticles-in-microsphere formulation for local plasmid DNA delivery in the gastrointestinal tract. *AAPS PharmSciTech*, 9(1): 288–294, 2008.

[74] C. Kriegel and M. M. Amiji. Dual *TNF-α/Cyclin D1* gene silencing with an oral polymeric microparticle system as a novel strategy for the treatment of inflammatory bowel disease. *Clin. Transl. Gastroenterol.*, 2 (3):e2, 2011.

[75] C. Kriegel and M. M. Amiji. Oral TNF-α gene silencing using a polymeric microsphere-based delivery system for the treatment of inflammatory bowel disease. *J. Control. Release*, 150(1):77–86, 2011.

[76] C. He, L. Yin, C. Tang, and C. Yin. Multifunctional polymeric nanoparticles for oral delivery of TNF-alpha siRNA to macrophages. *Biomaterials*, 34(11):2843–2854, 2013.

[77] J. Zhang, C. He, C. Tang, and C. Yin. Ternary polymeric nanoparticles for oral siRNA delivery. *Pharm. Res.*, 30(5):1228–1239, 2013.

[78] J. Zhang, C. Tang, and C. Yin. Galactosylated trimethyl chitosan–cysteine nanoparticles loaded with *Map4k4* siRNA for targeting activated macrophages. *Biomaterials*, 34(14):3667–3677, 2013.

[79] W. Wei, P. Lv, X. Chen, Z. Yue, Q. Fu, S. Liu, H. Yue, and G. Ma. Co-delivery of mTERT siRNA and paclitaxel by chitosan-based nanoparticles promoted synergistic tumor suppression. *Biomaterials*, 34(15):3912–3923, 2013.

[80] B. Ballarín-González, F. Dagnaes-Hansen, R. A Fenton, S. Gao, S. Hein, M. Dong, J. Kjems, and K. A Howard. Protection and systemic translocation of siRNA following oral administration of chitosan/siRNA nanoparticles. *Mol. Ther. Nucleic Acids*, 2(3):e76, 2013.

[81] H. Laroui, A. L. Theiss, Y. Yan, G. Dalmasso, H. T. T. Nguyen, S. V. Sitaraman, and D. Merlin. Functional TNFα gene silencing mediated by polyethyleneimine/TNFα siRNA nanocomplexes in inflamed colon. *Biomaterials*, 32(4):1218–1228, 2011.

[82] C. He, L. Yin, C. Tang, and C. Yin. Trimethyl chitosan-cysteine nanoparticles for systemic delivery of TNF-α siRNA via oral and intraperitoneal routes. *Pharm. Res.*, 30(10):2596–2606, 2013.

[83] H. Laroui, G. Dalmasso, H. T. T. Nguyen, Y. Yan, S. V. Sitaraman, and D. Merlin. Drug-loaded nanoparticles targeted to the colon with polysaccharide hydrogel reduce colitis in a mouse model. *Gastroenterology*, 138(3):843–853.e2, 2010.

[84] F. Danhier, E. Ansorena, J. M. Silva, R. Coco, A. Le Breton, and V. Préat. PLGA-based nanoparticles: An overview of biomedical applications. *J. Control. Release*, 161(2 (Special Issue: Drug Delivery Research in Europe)):505–522, 2012.

Chapter 4

Polycationic Nanoparticles Synthesized Using ARGET ATRP for Drug Delivery

4.1 Introduction

Advances in controlled radical polymerization technology create opportunities for new biomaterials for drug delivery that have seen widespread interest. These biomaterial carriers require well-controlled, advanced preparation techniques to achieve controlled molecular structures for the final product. Both RAFT (reversible addition-fragmentation chain transfer polymerization)[1;2] and ATRP (atom transfer radical polymerization)[3;4] are used for the synthesis of these new classes of biomaterials that seek to translate improved control over architecture into improved technologies for biomedical applications. ATRP biomaterials have been reported to have improved colloidal stability,[5;6] pH-responsiveness,[5] and degradation upon inclusion of a degradable cross-linking agent as well as increased swelling ratios[6;7] compared to biomaterials produced using traditional radical polymerization techniques. These controlled radical polymerization techniques are characterized by propagating

radicals "that are deactivated reversibly" such that there is an "equilibrium" between active and dormant chains.[8] The instantaneous concentration of propagating radicals is kept low because at any time, most of the chains are in a dormant state, which in turn minimizes transfer and termination reactions.[8] In contrast, in traditional free radical polymerization, the propagating chains lack a dormant state and are instead quickly terminated irreversibly,[9] resulting in greater heterogeneity than with controlled polymerization techniques.[10]

A recently developed variety of ATRP, termed Activators ReGenerated by Electron Transfer (ARGET) ATRP, is particularly attractive for biomaterial synthesis because unlike most types of controlled radical polymerizations, it can occur in the presence of limited air[11] and requires relatively low concentrations of copper catalyst that are significantly lower than traditional ATRP.[12] ARGET ATRP avoids UV-initiation, which confers advantages including ease of conducting multiple simultaneous reactions, synthesis protocols that can be scaled without consideration of the UV light source intensity and duration, as well as the ability to use photosensitive components such as dyes or biologically derived components in the polymerization reaction.

Drug delivery carriers may increase therapeutic efficacy compared to free drug due to avoiding rapid clearance,[13] preventing enzymatic degradation of the therapeutic,[14] or bypassing efflux pumps with chemotherapeutic-loaded nanoparticles.[15] Carriers may also permit new modes of administration, such as the oral delivery of siRNA,[16] chemotherapeutic agents, or fragile proteins.[17]

In the case of nucleic acid-based therapeutics such as siRNA where

delivery remains the most important challenge,[18] drug delivery carriers can facilitate uptake of the siRNA[19] and prevent degradation by nucleases.[20] Most commonly reported siRNA carriers include synthetic cationic polymers, such as PEI,[21] or lipid-based nanoparticles;[22] however, concerns exist regarding cytotoxicity of certain cationic lipid and polymers particles.[23]

Determining if the new techniques result in better drug delivery biomaterials requires direct comparison data for the two polymerization methods. Existing comparative studies between ATRP and traditional free radical polymerizations report improved performance for traditional ATRP synthesized materials,[5–7] but additional work is needed to see if this improvement occurs in other systems that have been better optimized for traditional free radical polymerization or for ARGET ATRP synthesized biomaterials. This work converts a previously optimized traditional free radical photoemulsion nanoparticle synthesis[24;25] to an ARGET ATRP-based scheme and provides a systemic comparison of ARGET ATRP and UV-initiated nanoparticles. The ARGET ATRP synthesis in water represents, to the best knowledge of the authors, the first report of an ARGET ATRP synthesis of cross-linked polycationic nanoparticles in water[26] without an inverse (continuous oil phase) emulsion.[27] The resulting polycationic hydrogel nanoparticles may be used for the delivery of proteins such as insulin,[25] oligonucleotides such as siRNA,[13] as well as co-delivery of siRNA with small molecule drugs.

4.2 Materials and methods

4.2.1 Chemicals

Poly(ethylene glycol) methyl ether methacrylate (PEGMA) solution (M_n 2000 for PEG chain, 50 wt% in water), 2-(diethylamino) ethyl methacrylate (DEAEMA), *tert*-butyl methacrylate (tBMA), tetraethylene glycol dimethacrylate (TEGDMA), ethyl 2-bromoisobutyrate (EBIB), tris(2-pyridylmethyl)amine (TPMA), myristyltrimethylammonium bromide (MyTab), ascorbic acid, trypsin-EDTA solution, and Dulbecco's Modified Eagle's Medium (DMEM) - high glucose without L-glutamine, penicillin, streptomycin, and fluorescein were purchased from Sigma-Aldrich.

1 N Hydrochloric acid (HCl), 1 N sodium hydroxide, 10x phosphate buffered saline (PBS), sodium chloride, monosodium phosphate monohydrate, and disodium phosphate heptahydrate were purchased from Fisher Scientific, Brij-30® and Copper(II) bromide were purchased from Acros Organics, and Irgacure 2959 was purchased from Ciba Specialty Chemicals Corp. Dimethyl Sulfoxide 99+% (DMSO) was purchased from Alfa Aesar. Amicon® Centricon® centrifuge filter devices, 15 ml, MW Cut Off 30,000 were purchased from Millipore and 12,000-14,000 MW cut off Dialysis tubing was purchased from Spectra/Por® . Ultrapure water was used for all studies. All chemicals were used as received.

1xPBS without calcium and magnesium and 200 mM L-glutamine solution (MediaTech), CellTiter 96® AQ_{ueous} Non-Radioactive Cell Proliferation

Assay (MTS) and CytoTox-ONE Homogeneous Membrane Integrity Assay from Promega, Thermo Scientific HyClone USDA Tested Fetal Bovine Serum and Thermo Scientific Nunc Microwell 96-well Microplates were used for cell culture experiments. L929 and PANC-1 cells were obtained from American Type Culture Collection (ATCC) and sheep blood in citrate buffer was purchased from Hemostat Laboratories. KDalert™ GAPDH Assay Kit, Lipofectamine® 2000 Transfection Reagent, Silencer® GAPDH siRNA, and Silencer® Negative Control #1 were purchased from Life Technologies .

4.2.2 Nanoparticle synthesis and purification

This work represents the first reported use of ARGET ATRP to synthesize cationic nanoparticles, the first reported use of an oil-in-water emulsion for the ARGET ATRP synthesis of hydrogel nanoparticles, and one of the first reports of ARGET ATRP-based techniques in water. The newly reported ARGET ATRP synthesis technique stands out due to its ease of execution; it does not require rigorous exclusion of air or inhibitors and it does not require a UV source for initiation. As a result, the reaction can be conducted without applying vacuum, freeze-pump-thaw cycles, or other techniques typically required for controlled radical polymerizations. Commercially available monomers may be used without removing the inhibitor prior to the reaction. Avoiding UV-initiation confers advantages including ease of conducting multiple simultaneous reactions, synthesis protocols that can be scaled without consideration of the UV light source intensity and duration, as well as the

ability to use photosensitive components such as dyes or biologically-derived components in the polymerization reaction. The technique is relatively rapid (3 hour reaction time) and the synthesis does not make use of organic solvents.

Cross-linked polymer nanoparticles were synthesized using a UV-initiated polymerization previously developed by Fisher and colleagues[24] or a newly developed ARGET ATRP.[28] Briefly, a mixture of 2-(diethylamino) ethyl methacrylate (DEAEMA), poly(ethylene glycol) methyl ether methacrylate (where M_n of PEG chain is 2000) (PEGMA), tetraethylene glycol dimethacrylate (TEGDMA), and tert-butyl methacrylate (tBMA) was combined with an aqueous solution of 8 mg/ml Brij® 30 and 1.35 mg/ml myristyltrimethylammonium bromide (MyTab) for a 0.1 weight ratio of monomer to solvent.

For the UV-initiated polymerization, Irgacure® 2959 was added at a 0.005 weight ratio initiator to monomer. For the ARGET ATRP polymerization, copper(II) bromide ($CuBr_2$), tris(2-pyridylmethyl)amine (TPMA), and ethyl 2-bromoisobutyrate (EBIB) were added at $CuBr_2$:TPMA:EBIB::0.5:0.5:4 with respect to 100 mol of DEAEMA in the feed. See Figure 4.2 for the reagents used for nanoparticle synthesis.

Following probe sonication for 10 min at amplitude 90 using a S-4000 Misonix Ultrasonicator, the mixtures were purged with nitrogen for 20 min. The UV-initiated polymerization was reacted by exposure to a UV light source (Dymax BlueWave™ 200 UV) for 2.5 h at 140 mW/cm^2 with constant stirring. The ARGET ATRP polymerization was reacted for 3 h with constant stirring following addition of degassed ascorbic acid solution (ascor-

bic acid:DEAEMA::0.5:100). Purification was done by a technique described previously by Fisher and Peppas.[25] Briefly, 1 N hydrochloric acid (HCl) was added to the reaction mixture (equal volumes) and after 30 min, the polymer nanoparticles were precipitated with acetone. A pellet of the precipitated nanoparticles was formed by centrifugation at 3200 RCF (relative centrifugal force) and the supernatant removed. The pellet was resuspended in 0.5 N HCl and the process was repeated 4 more times. The nanoparticles were finally re-suspended in water, dialyzed, and freeze dried.

As shown in Table 4.1, 4 formulation were investigated: 30UV, 45UV, 30ARGET, 45ARGET, where the number describes the moles of tBMA in the feed per 100 mol DEAEMA, and UV or ARGET describes the polymerization technique. The 30UV formulation is analogous to that reported by Fisher et al.[24] and Liechty et al..[29] The polycationic nanoparticles are represented schematically in Figure 4.1.

4.2.3 Characterization

4.2.3.1 Light scattering

The z-average diameter and zeta potential were measured using a Malvern ZetaSizer NanoZS instrument equipped with a 633 nm laser source and MPT-2 Autotitrator. Zeta potential and the z-average diameter of 0.5 mg/ml nanoparticles were measured in water and 5 mM phosphate buffer at pH 6.5 and 7.4. The z-average diameter was also measured in pH 7.4 PBS. The

pH-responsive swelling was determined as the z-average diameters in water; the autotitrator increased the pH to 10 and then stepwise decreased the pH while measuring the z-average diameter.

4.2.3.2 TEM

Nanoparticles were imaged using a FEI Tecnai Transmission Electron Microscope (TEM) (80 kV) with 16,500x to 220,000x magnification. A 0.02 mg/ml suspension of freeze-dried particles in water was drop-cast onto a Formvar-coated 400 mesh copper grid (Electron Microscopy Sciences) and stained with 2% uranyl acetate immediately before imaging.

4.2.3.3 Cytotoxicity

Fibroblast L929 and Adenocarcinoma Pancreatic PANC-1 cells were maintained in Dulbecco's Modified Eagle Medium (DMEM) supplemented with 10% fetal bovine serum (FBS), 1% L-glutamine, and 1% penicillin and streptomycin. Cells were seeded at 10,000 cells per well in 96 well plates and incubated for 48 h before testing. For the MTS assay, following 2 h incubation of cells with nanoparticles, particles were removed and cells were rinsed 2 x with sterile PBS. Next, the cells were incubated for 3 h with the MTS assay in DMEM without phenol red with 2% FBS. The supernatant was transferred to a transparent plate, the 690 nm (background) and 490 nm (MTS assay) absorbance (A) was measured using a microplate reader (Synergy HT, BioTek Instruments, Inc.), and relative cell viability (V) was calculated as:

$$V = \frac{A_{490,\,sample} - A_{690,\,sample} - (A_{490,\,bleach} - A_{690,\,bleach})}{A_{490\,media} - A_{690,\,media} - (A_{490,\,bleach} - A_{690,\,bleach})} \quad (4.1)$$

For the CytoTox-ONE Homogeneous Membrane Integrity Assay, L929 cells were incubated with nanoparticles for 1 h, and the assay used according to the manufacturer's instructions. The fluorescence was measured using a microplate reader (Synergy HT, BioTek Instruments, Inc., Winooski, VT) at 530 nm excitation and 590 nm excitation.

4.2.3.4 Hemolysis

Hemolysis at extracellular (pH 7.4) and endosomal (pH 6.5) pH conditions[30] was done using sheep blood in 150 mM phosphate buffer. Hemolysis was used to investigate membrane disruption caused by the polycationic nanoparticles that is relevant for endosomal escape and cytotoxicity. Briefly, blood was centrifuged, the supernatant removed, and washed 3x with isotonic sodium chloride. The red blood cells were resuspended in phosphate buffer at pH 6.5 or 7.4, combined with nanoparticles suspended in phosphate buffer of the same pH, and incubated for 1 h at 37^{o}C.

Following centrifugation, the absorbance (A) of the supernatant was measured at 541 nm as an indicator of hemolytic activity or membrane disruption (HA), calculated as:

$$HA = \frac{A_{541,\,sample} - A_{541,\,phosphate\,buffer}}{A_{541,\,deionized\,water} - A_{541,\,phophate\,buffer}} \quad (4.2)$$

4.2.3.5 Fluorescein loading and release

A 10 ml suspension of 2 mg/ml nanoparticles in 10 mM (1x) PBS at pH 4.3 was confined to a dialysis bag and submerged in 91 ml of 10.9 μg/ml fluorescein in PBS at pH 4.3 for 24 h with agitation for loading of the swollen nanoparticles with fluorescein. 1 N sodium hydroxide was added to increase the pH of the solution to pH 8.4, and the loaded nanoparticles inside the dialysis bag were recovered by centrifugation with a Centricon® tube at 3500 rpm for 35 min. The centrifuged particles were recovered, resuspended in 5 ml 10 mM (1x) PBS pH 7.4, and placed in another dialysis bag for the release study (also with agitation). After 2 h of release at pH 7.4 in 50 ml PBS at pH 7.4, the pH was decreased to 4.3 using 1 N hydrochloric acid, and the release study continued. Fluorescence was measured using a microplate reader (Synergy HT, BioTek Instruments, Inc., Winooski, VT) at excitation 485 nm and emission 528 nm.

4.3 Results and discussion

Monodisperse polycationic nanoparticles were synthesized using both ARGET ATRP and UV-initiated polymerization. The best performing for-

mulations were biocompatible with membrane disruption tuned for endosomal disruption.

4.3.1 Dynamic light scattering

Dynamic light scattering (DLS) studies were performed using a Malvern ZetaSizer NanoZS instrument equipped with a 633 MPT-2 Autotitrator. The values of the z-average diameter and polydispersity index (PDI) of the formulations measured with dynamic light scattering are shown in Table 4.2. It is clear that diameter increases at lower pH; the diameter at pH 6.5 was greater than the diameter at pH 7.4. The formulations with a feed ratio of 45 mol tBMA (per 100 mol DEAEMA in the feed) had poor colloidal stability in 10 mM (1x) PBS at pH 7.4, which was observed as flocculation or aggregation upon addition of 10x PBS to non-aggregated nanoparticles in water. The AR-GET ATRP formulations had larger diameters and smaller PDI values than the corresponding UV-initiated formulations.

The pH-responsive swelling profile of the polymer nanoparticles is shown in Figure 4.3. The 30ARGET formulation appears to swell more than the corresponding UV-initiated formulation 30UV. For both 30 mol tBMA formulations 30ARGET and 30UV, the onset of pH-responsive swelling was approximately the same pH value. Note that the reported pK_{a} values for DEAEMA range from 6.68[31] to 7.0-7.3.[32] The 45UV and 45ARGET formulations were not colloidally stable at high pH values, so as a result, pH-responsive swelling could not be measuring using DLS.

The zeta potential values of the four formulations are shown in Table 4.3. All particles have positive surface charge, which will promote complexation with negatively charged siRNA. The ARGET ATRP formulations have greater surface charge than the corresponding UV-initiated formulations. Both 45 mol tBMA formulations have low cytotoxicity, but for the 30 mol tBMA formulations, decreased surface charge correlates with decreased cytotoxicity.

4.3.2 TEM

Dried nanoparticles were suspended in water at 0.02 mg/ml, drop-cast onto a Formvar-coated 400 mesh copper grid and stained with 2% uranyl acetate immediately before imaging. Transmission electron microscopy (TEM) demonstrates that the dried particles are approximately spherical as shown in Figure 4.4 and that minimal aggregation was observed.

4.3.3 MTS assay

Fibroblast (L929) and Adenocarcinoma Pancreatic (PANC-1) cells were used to determine biocompatibility of the different types of polycationic nanoparticles (see Figure 4.5). Cell viability was assessed using MTS assay after 2 h of incubation with nanoparticles. Both cell lines present similar responses when exposed to the nanoparticles, and the MTS results correlate with the LDH assay results. Formulation 45ARGET demonstrates no toxicity at low concentrations and low toxicity (80% viability for L929 and PANC-1) at the highest concentration of 5 mg/ml. Formulation 45UV presents no toxicity

at any of the concentrations studied. Cells incubated with 30UV nanoparticles present toxicity at concentrations greater than 1 mg/ml; cell viability was reduced to 0% for the highest concentration of 5 mg/ml. Formulation 30ARGET presents toxicity at all the concentrations studied, except for the lowest concentration of 0.039 mg/ml. For 30ARGET, cell viability was reduced down to 0% at 2.5 mg/ml. The half maximal inhibitory concentration (IC50) of 45ARGET and 30UV nanoparticles was found to be approximately 0.625 mg/ml and 2.5 mg/ml, respectively, for both cell lines. Formulations containing 45 mol tBMA per 100 mol DEAEMA in the feed were less toxic than the corresponding 30 mol tBMA formulations for both cell lines. ARGET ATRP synthesized nanoparticles have greater toxicity than UV-initiated formulations with corresponding feed concentrations. It appears that both tBMA content and polymerization method affect biocompatibility of the nanoparticles.

4.3.4 Membrane disruption

Hemolysis at endosomal (pH 6.5) and extracellular (pH 7.4) pH values[30] was studied using sheep blood in phosphate buffer at various concentrations exposed to nanoparticles for 1 h. The proposed delivery system for siRNA is designed for oral administration and so will not come into contact with the blood. As a result, hemolysis experiments do not have the goal of studying biocompatibility of the biomaterial with components of the blood, but instead, hemolysis is used to investigate membrane disruption caused by the polycationic nanoparticles that is relevant for endosomal escape and cytotoxicity.

All formulations except for the 30ARGET exhibited pH-dependent hemolytic activity and strong hemolytic activity at all concentrations at pH 6.5 (Figure 4.6). At endosomal pH of 6.5, the hemolytic activity of 30ARGET at concentrations lower than 0.25 mg/ml was lower than that of the other formulations; however, at pH 7.4, all concentrations of 30ARGET are more hemolytic. The strong hemolytic activity at endosomal pH (pH 6.5) and low hemolytic activity at extracellular pH (pH 7.4) was designed to minimize cytotoxicity while maximizing endosomal escape. The hemolytic activity of 45UV was negligible at all concentrations, while 30UV and 45ARGET each show some hemolytic activity at the highest concentrations of 2 mg/ml and 1 mg/ml.

The membrane disruption measured using hemolysis correlates with membrane disruption evaluated using a lactate dehydrogenase (LDH) assay (see Figure 4.7). For the CytoTox-ONE Homogeneous Membrane Integrity Assay, L929 cells were incubated with nanoparticles for 1 h, and the assay used according to the manufacturer's instructions. Lysis fraction describes the fraction of dead cells. The 30UV formulation has the greatest lysis fraction and pH 7.4 hemolytic activity. While the formulations 30UV and 45ARGET show some hemolytic activity at the highest concentrations of 2 mg/ml and 1 mg/ml, they have negligible lysis fractions. The 45UV formulation also does not cause lysis. The high membrane integrity functions correlate with low hemolytic activity at physiological conditions, showing that cytotoxicity is due to cell membrane disruption.

4.3.5 Fluorescein loading and release

Fluorescein has been widely used as a model chemotherapy drug due to its similarity in molecular weight and hydrophobicity to chemotherapeutic agents. Fluorescein loading and release using different types of previously swollen nanoparticles was studied. Such studies may be relevant for using the polycationic nanoparticles as part of a co-delivery system (siRNA and small molecule chemotherapeutic) for the treatment of cancer.

Particles were suspended in low pH buffer with fluorescein for 24 h. Nanoparticles containing 30 mol tBMA (per 100 mol DEAEMA in the feed) presented a greater loading efficiency compared with nanoparticles containing 45 mol tBMA (see Figure 4.8 and Table 4.4). As a result, the loading efficiency of fluorescein correlates with the swelling behavior. As previously discussed, nanoparticles with 30 mol tBMA have greater colloidal stability at high pH and so present a better swelling profile, regardless of the polymerization method.

Release of fluorescein from nanoparticles was studied at pH 7.4 and at low pH 4.3 (see Figure 4.9 and Table 4.4). Fluorescein release from ARGET ATRP formulations is significantly lower than particles polymerized by the UV-initiated method. Formulation 30UV releases more fluorescein than 30ARGET and 45ARGET, probably due to the fact that the loading efficiency and the swelling were greater. 45UV nanoparticles released a surprising amount of fluorescein, particularly considering that these particles loaded less fluorescein than the 30UV and their swelling profile is worse. This could be due to altered solubility due to increased hydrophobic content; recall 45UV nanopar-

ticles have less colloidal stability than 30UV. Surface charge effects could also play a role in loading and release; the nanoparticles contain DEAEMA which is protonated at low pH while fluorescein contains carboxyl groups that may also be affected by pH, hence affecting loading and release.

4.4 Conclusion

This work provides a systemic comparison of ARGET ATRP and UV-initiated polycationic nanoparticles for drug delivery of hydrophobic drugs to the cytoplasm. ARGET ATRP nanoparticles present lower biocompatibility and drug release when compared to the same formulation polymerized by UV, despite having similar loading profiles. Hydrophobic content of nanoparticles has negative consequences on the swelling and colloidal stability of the nanoparticles; however, increased hydrophobicity improves biocompatibility. These results apply to the formulations tested but should not be extended to a complete range of formulations without additional testing. This work provides a guide to deciding what type of nanoparticles have the best properties for specific applications (see Table 4.5).

4.5 Tables

Table 4.1: Key to formulation nomenclature. UV-initiated and ARGET ATRP formulations were prepared with 30 and 45 mol tBMA per 100 mol DEAEMA in the feed. The abbreviations 30UV, 45UV, 30ARGET, and 45ARGET are used throughout the text to identify the formulations.

	UV-initiated	ARGET ATRP
30 mol tBMA per 100 mol DEAEMA in the feed	30UV	30ARGET
45 mol tBMA per 100 mol DEAEMA in the feed	45UV	45ARGET

Table 4.2: Z-average diameter and polydispersity index (PDI) for the 30UV, 45UV, 30ARGET, and 45ARGET formulations. Z-average diameter and polydispersity measured using dynamic light scattering with Malvern ZetaSizer NanoZS instrument in 5mM phosphate buffer (PB) at pH 7.4 and 6.5 as well as 10 mM (1x) phosphate buffered saline (PBS) at pH 7.4.

	Z-average diameter, nm			Polydispersity index (PDI)		
Formulation	PB 7.4	PB 6.5	PBS 7.4	PB 7.4	PB 6.5	PBS 7.4
30UV	71.83	83.09	83.33	0.211	0.185	0.289
45UV	69.68	88.27	74.23	0.233	0.358	0.230
30ARGET	130.2	146.6	147.2	0.148	0.060	0.134
45ARGET	98.29	115.3	106.1	0.212	0.210	0.208

Table 4.3: Zeta potential measured with Malvern ZetaSizer NanoZS instrument in 5 mM phosphate buffer at pH 7.4 and 6.5 and water.

	Zeta potential, mV		
Formulation	PB 7.4	PB 6.5	water
30UV	6.57	14.4	38.0
45UV	5.54	6.88	40.9
30ARGET	13.3	17.9	42.4
45ARGET	13.2	21.8	45.4

Table 4.4: Fluorescein loading and release. Polycationic nanoparticles (2 mg/ml) were loaded via equilibrium partitioning with fluorescein (10.9 μg/ml) while swollen at pH 4.3 for 24 h. Release experiments were conducted in 1x PBS and at 120 min, pH was decreased from pH 7.4 to pH 4.3.

Formulation	Percent loading, %	Total release
30UV	65%	14.68 μg
45UV	42%	51.62 μg
30ARGET	56%	5.59 μg
45ARGET	53%	2.04 μg

Table 4.5: Material properties summary for the 30UV, 45UV, 30ARGET, and 45ARGET formulations. Good swelling is characterized by a colloidal stability at high pH values that permits accurate determination of the unswollen diameter using DLS. Cytotoxicity was evaluated using cancerous (PANC-1 pancreatic adenocarcinoma) and noncancerous (L929 fibroblast) cells using an MTS assay. Hemolytic activity serves as a measure of membrane disruption.

Formulation	Swelling	Cytotoxicity	Hemolysis, pH 7.4	Hemolysis, pH 6.5
30UV	Good	Medium	Low	High
45UV	Poor	Good	Low	High
30ARGET	Good	Poor	High	Medium
45ARGET	Poor	Good	Low	High

4.6 Figures

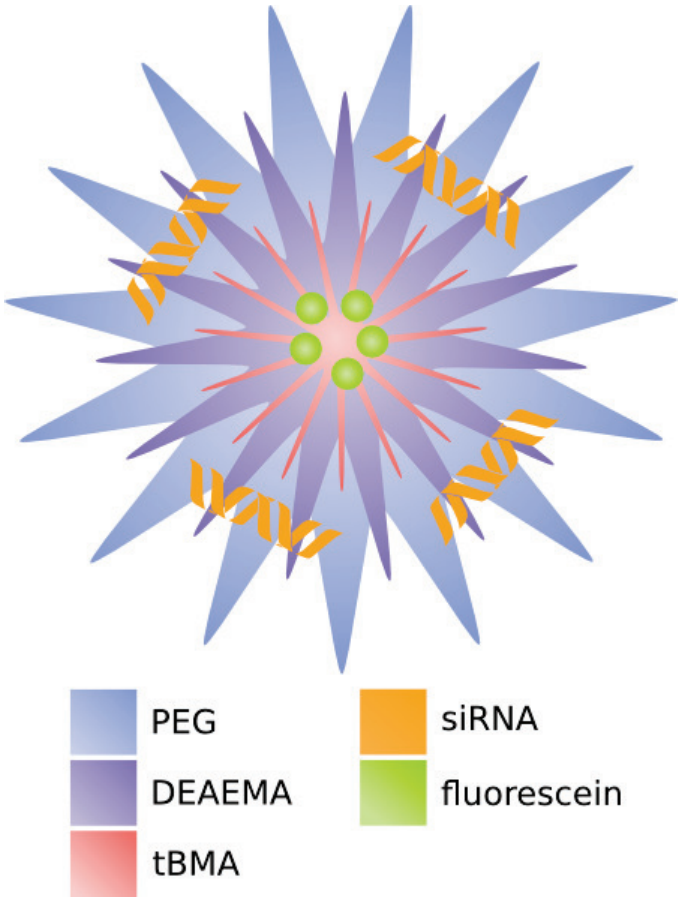

Figure 4.1: Schematic representation of the polycationic nanoparticle. The location of PEG, DEAEMA, and tBMA is influenced by hydrophobicity, with the hydrophilic PEG dominating the surface and the hydrophobic tBMA in the core. The PEG, DEAEMA, and tBMA do not form three distinct layers, as represented by the overlapping, spiked cartoon figure. The negatively charged siRNA complexes with the positively charged DEAEMA, and the hydrophobic fluorescein associates with the hydrophobic tBMA in the core.

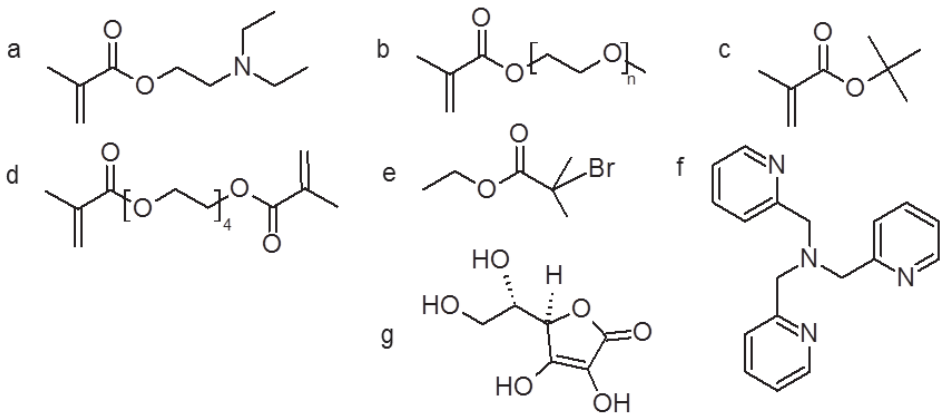

Figure 4.2: Reagents used in synthesis. Monomers: a) 2-(diethylamino) ethyl methacrylate (DEAEMA) b) poly(ethylene glycol) methyl ether methacrylate (PEGMA) (average molecular weight of PEG is 2000), c) *tert*-butyl methacrylate (tBMA). Cross-linking agent: d) tetraethylene glycol dimethacrylate (TEGDMA). Initiator: e) ethyl 2-bromoisobutyrate (EBIB). Ligand: f) tris(2-pyridylmethyl)amine (TPMA). Reducing agent: g) ascorbic acid.

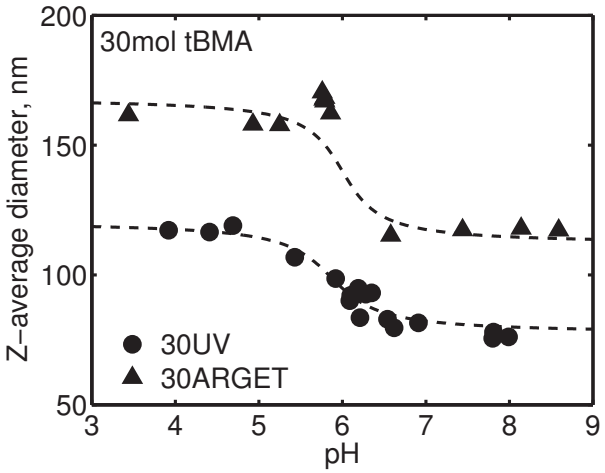

(a) Formulations with 30 mol tBMA per 100 mol DEAEMA in the feed

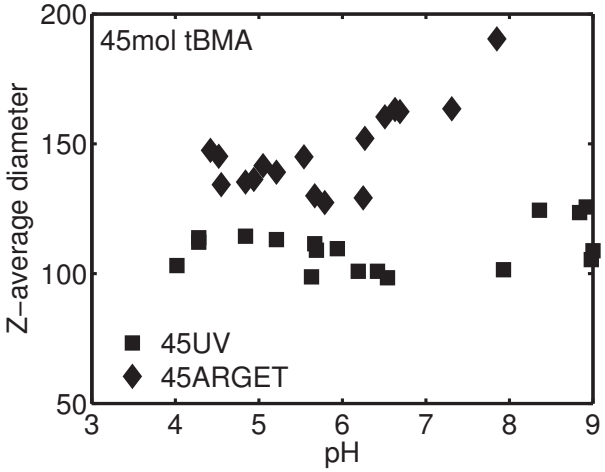

(b) Formulations with 45 mol tBMA per 100 mol DEAEMA in the feed

Figure 4.3: pH-responsive swelling of polycationic nanoparticles (0.5 mg/ml in water). Nanoparticles were prepared using UV-initiated polymerization or ARGET ATRP with 30 or 45 mol tBMA with respect to 100 mol DEAEMA in the feed. Formulations with high feed ratios of tBMA (45UV and 45ARGET) were not colloidally stable at high pH values; z-average diameters greater than 200 nm at high pH values are not shown. Z-average diameter values measured using dynamic light scattering with Malvern ZetaSizer NanoZS instrument equipped with MPT-2 Autotitrator.

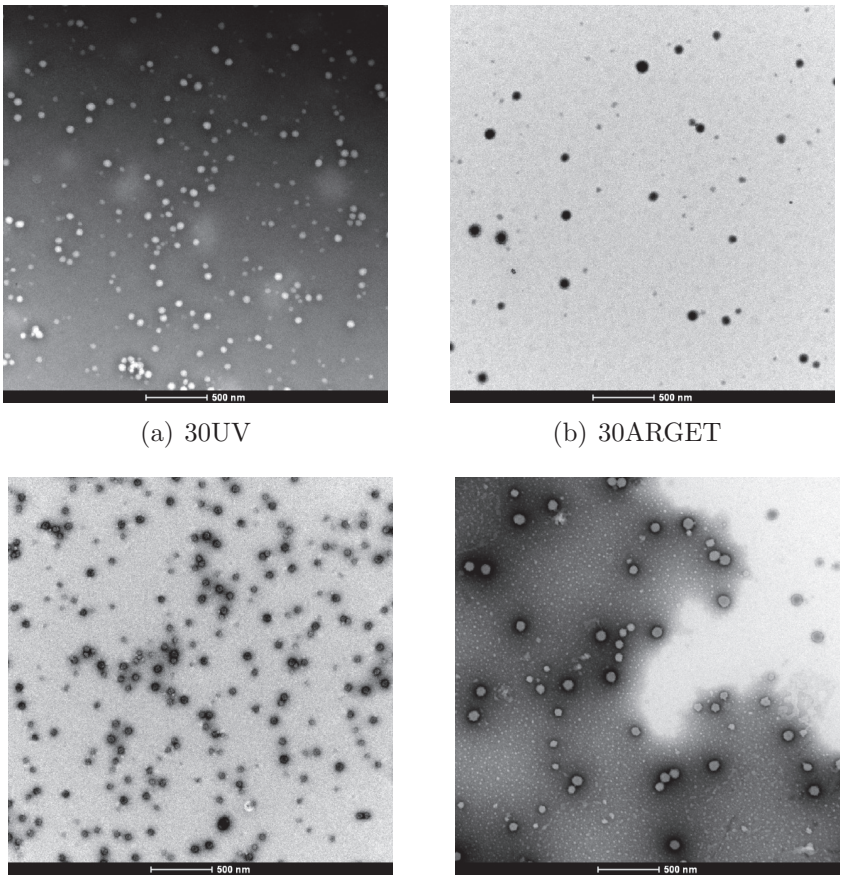

(a) 30UV (b) 30ARGET

(c) 45UV (d) 45ARGET

Figure 4.4: Transmission electron microscopy (TEM) shows spherical dried polycationic nanoparticles (magnification 26,500 x, FEI Tecnai Transmission Electron Microscope, 80 kV). A suspension of freeze-dried particles in water at 0.02 mg/ml was drop-cast onto a Formvar-coated 400 mesh copper grid and stained with 2% uranyl acetate immediately before imaging.

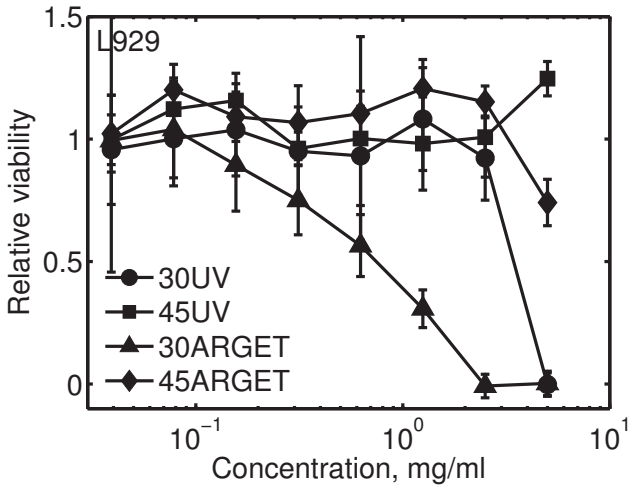

(a) L929

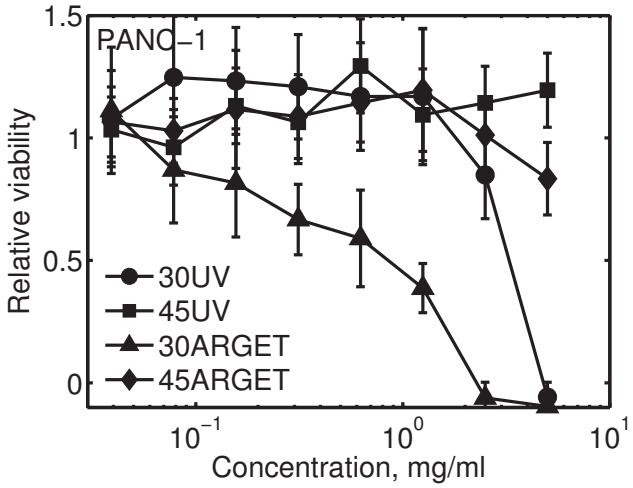

(b) PANC-1

Figure 4.5: Cytotoxicity of polycationic nanoparticles for noncancerous (L929 mouse fibroblasts) and cancerous (PANC-1 pancreatic carcinoma) cells evaluated using an MTS assay following 2 h incubation.

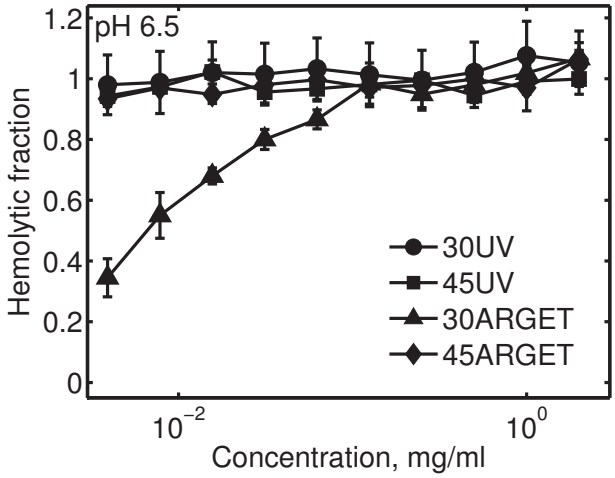

(a) Endosomal: pH 6.5

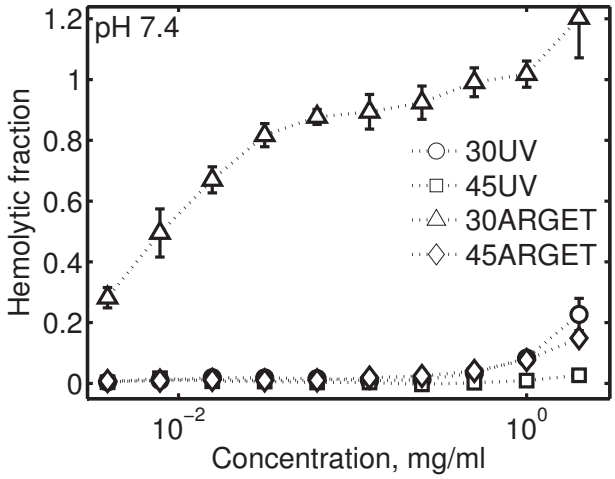

(b) Extracellular: pH 7.4

Figure 4.6: Hemolysis as measure of membrane disruption at endosomal and extracellular pH values. Sheep blood was washed with isotonic sodium chloride, resuspended in 150 mM phosphate buffer at pH 6.5 or 7.4, combined with polycationic nanoparticles suspended in phosphate buffer of the same pH, and incubated for 1 h. Membrane disruption was determined using absorbance of the hemoglobin at 541 nm.

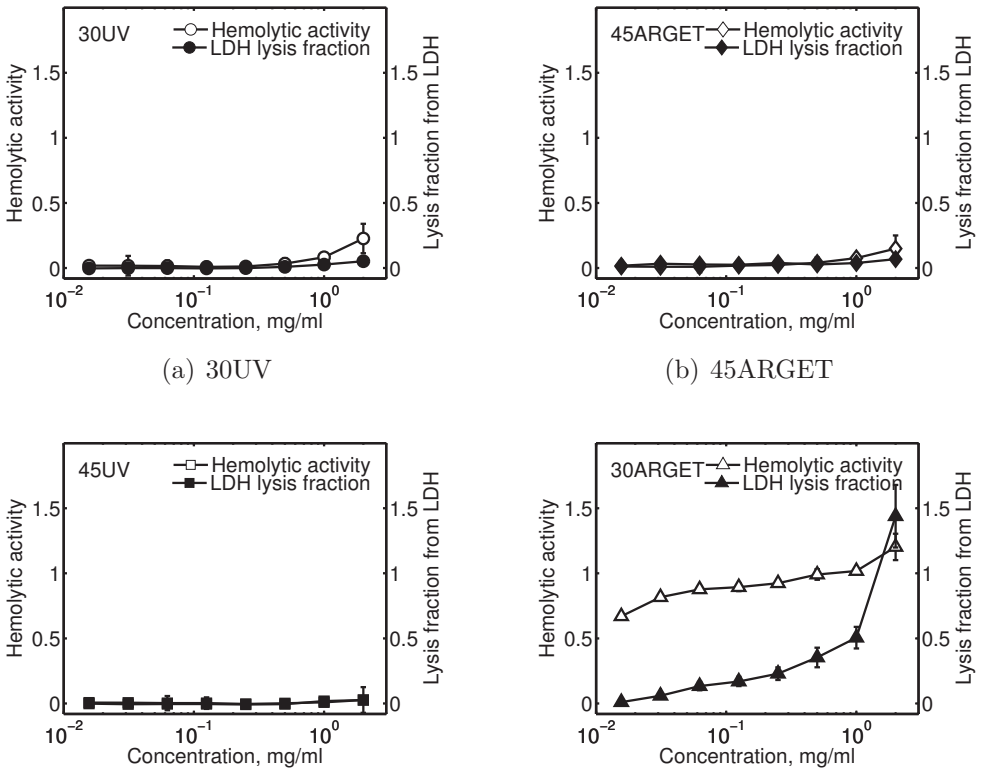

(a) 30UV

(b) 45ARGET

(c) 45UV

(d) 45ARGET

Figure 4.7: Increased hemolytic activity at pH 7.4 correlates with increased fraction of cells with membrane disruption. Hemolytic activity measured using sheep blood rinsed with isotonic sodium chloride, resuspended in phosphate buffer, and then exposed to polycationic nanoparticles. The fraction of lysed cells was determined using a CytoTox-ONE™ Homogeneous Membrane Integrity Assay with L929 cells that were exposed to polycationic nanoparticles at same concentrations and for same duration as the hemolysis assay. A lysis fraction of 0 corresponds to no lysed cells or no cytotoxicity.

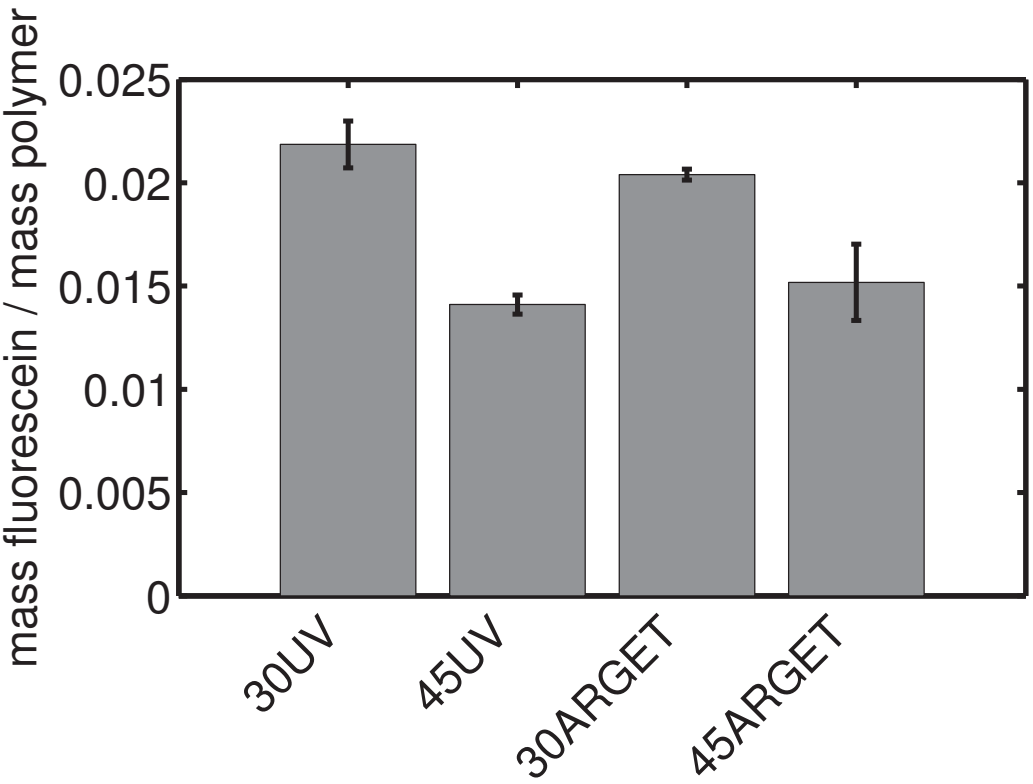

Figure 4.8: Fluorescein loading into polycationic nanoparticles. 2 mg/ml polycationic nanoparticles were loaded via equilibrium partitioning with 10.9 μg/ml fluorescein while swollen at pH 4.3 for 24 h. Following loading, the pH was increased and the polycationic nanoparticles recovered using centrifugation with a Centricon® tube.

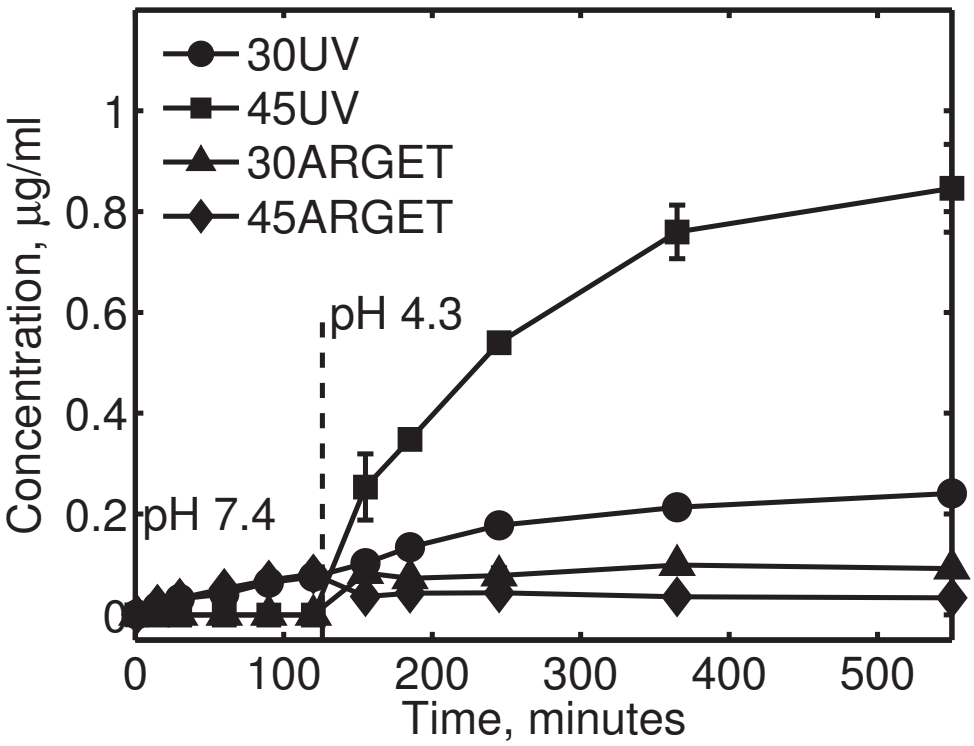

Figure 4.9: Fluorescein release from nanoparticles in 1xPBS. At 120 min, pH was decreased from pH 7.4 to pH 4.3. Fluorescence measured using a microplate reader at excitation 485 nm and emission 528 nm.

4.7 References

[1] A. Gregory and M.H. Stenzel. The use of reversible addition fragmentation chain transfer polymerization for drug delivery systems. *Expert Opin. Drug Del.*, 8(2):237–269, 2011.

[2] M.H. Stenzel. RAFT polymerization: an avenue to functional polymeric micelles for drug delivery. *Chem. Commun.*, (30):3486–3503, 2008.

[3] D. J. Siegwart, J. K. Oh, and K. Matyjaszewski. ATRP in the design of functional materials for biomedical applications. *Prog. Polym. Sci.*, 37 (1):18–37, 2012.

[4] F.J. Xu, K.G. Neoh, and E.T. Kang. Bioactive surfaces and biomaterials via atom transfer radical polymerization. *Prog. Polym. Sci.*, 34(8):719–761, 2009.

[5] T. He, F. Di Lena, K. C. Neo, and C. L. L. Chai. Direct synthesis of pH-responsive polymer nanoparticles based on living radical polymerization and traditional radical polymerization. *Soft Matter*, 7(7):3358–3365, 2011.

[6] J. K. Oh, R. Drumright, D. J. Siegwart, and K. Matyjaszewski. The development of microgels/nanogels for drug delivery applications. *Prog. Polym. Sci.*, 33(4):448–477, 2008.

[7] J. Yoon, J.K. Oh, W. Li, T. Kowalewski, and K. Matyjaszewski. *ATRP: A Versatile Tool toward Uniformly Crosslinked Hydrogels with Controlled*

Architecture and Multifunctionality, Hydrogel Micro and Nanoparticles. Wiley Online Library, 2012. 169-186 pp.

[8] A. D. Jenkins, R. G. Jones, and G. Moad. Terminology for reversible-deactivation radical polymerization previously called "controlled" radical or "living" radical polymerization (IUPAC Recommendations 2010). *Pure Appl. Chem.*, 82(2):483–491, 2010.

[9] G.G. Odian. *Principles of Polymerization*. John Wiley and Sons, Hoboken, NJ, 2004.

[10] P. C. Hiemenz and T. P. Lodge. *Polymer Chemistry, 2nd*. Boca Raton: CRC Press, 2007.

[11] K. Matyjaszewski, H. Dong, W. Jakubowski, J. Pietrasik, and A. Kusumo. Grafting from surfaces for everyone: ARGET ATRP in the presence of air. *Langmuir*, 23(8):4528–4531, 2007.

[12] W. Jakubowski and K. Matyjaszewski. Activators regenerated by electron transfer for atom-transfer radical polymerization of (meth)acrylates and related block copolymers. *Angew. Chem.*, 118(27):4594–4598, 2006.

[13] W.B. Liechty and N.A. Peppas. Expert opinion: Responsive polymer nanoparticles in cancer therapy. *Eur. J. Pharm. Biopharm.*, 80:241–246, 2012.

[14] W.B. Liechty, D.R. Kryscio, B.V. Slaughter, and N.A. Peppas. Polymers for drug delivery systems. *Annu. Rev. Chem. Biomol.*, 1(1):149–173, 2010.

[15] M. Creixell and N. A. Peppas. Co-delivery of siRNA and therapeutic agents using nanocarriers to overcome cancer resistance. *Nano Today*, 7 (4):367–379, 2012.

[16] D. C. Forbes and N. A. Peppas. Oral delivery of small RNA and DNA. *J. Control. Release*, 162(2):438–445, 2012.

[17] W.B. Liechty, M. Caldorera-Moore, M.A. Phillips, C. Schoener, and N.A. Peppas. Advanced molecular design of biopolymers for transmucosal and intracellular delivery of chemotherapeutic agents and biological therapeutics. *J. Control. Release*, 155(2):119–127, 2011.

[18] Y. Zhang, A. Satterlee, and L. Huang. *In vivo* gene delivery by nonviral vectors: Overcoming hurdles? *Mol. Ther.*, 20(7):1298–1304, 2012.

[19] S. Akhtar and I. Benter. Toxicogenomics of non-viral drug delivery systems for RNAi: Potential impact on siRNA-mediated gene silencing activity and specificity. *Adv. Drug Deliver. Rev.*, 59(2-3):164–182, 2007.

[20] K. Bruno. Using drug-excipient interactions for siRNA delivery. *Adv. Drug Deliver. Rev.*, 63(13):1210–1226, 2011.

[21] H. M. Aliabadi, B. Landry, C. Sun, T. Tang, and H. Uludağ. Supramolecular assemblies in functional siRNA delivery: Where do we stand? *Biomaterials*, 33(8):2546–2569, 2012.

[22] L. Huang and Y. Liu. *In vivo* delivery of RNAi with lipid-based nanoparticles. *Annu. Rev. Biomed. Eng.*, 13(1):507–530, 2011.

[23] K. A. Whitehead, R. Langer, and D. G. Anderson. Knocking down barriers: advances in siRNA delivery. *Nat. Rev. Drug Discov.*, 8(2):129–138, 2009.

[24] O. Z. Fisher, T. Kim, S. R. Dietz, and N. A. Peppas. Enhanced core hydrophobicity, functionalization and cell penetration of polybasic nanomatrices. *Pharm. Res.*, 26(1):51–60, 2008.

[25] O. Z. Fisher and N. A. Peppas. Polybasic nanomatrices prepared by UV-initiated photopolymerization. *Macromolecules*, 42(9):3391–3398, 2009.

[26] A. Simakova, S. E. Averick, D. Konkolewicz, and K. Matyjaszewski. Aqueous ARGET ATRP. *Macromolecules*, 45(16):6371–6379, 2012.

[27] S.E. Averick, E. Paredes, A. Irastorza, A. Srinivasan, D.J. Siegwart, A.J.D. Magenau, H.Y. Cho, A.R. Shrivats, E. Hsu, J. Kim, et al. Preparation of cationic nanogels for nucleic acid delivery. *Biomacromolecules*, (11):3445–3449, 2012.

[28] D. C. Forbes, M. Creixell, H. Frizzell, and N. A. Peppas. Polycationic nanoparticles synthesized using ARGET ATRP for drug delivery. *Eur. J. Pharm. Biopharm.*, 84(3):472–478, 2013.

[29] W. B. Liechty. Multi-responsive nanoscale hydrogels for intracellular delivery of siRNA. *Preliminary Oral Examination, Department of Chemical Engineering, The University of Texas at Austin*, 2012.

[30] A.J. Convertine, D.S.W. Benoit, C.L. Duvall, A.S. Hoffman, and P.S. Stayton. Development of a novel endosomolytic diblock copolymer for siRNA delivery. *J. Control. Release*, 133(3):221–229, 2009.

[31] A. Shatkay and I. Michaeli. Potentiometric titrations of polyelectrolytes with separation of phases. *J. Phys. Chem.*, 70(12):3777–3782, 1966.

[32] J. I. Amalvy, E. J. Wanless, Y. Li, V. Michailidou, S. P. Armes, and Y. Duccini. Synthesis and characterization of novel pH-responsive microgels based on tertiary amine methacrylates. *Langmuir*, 20(21):8992–8999, 2004.

Chapter 5

Polycationic Nanoparticles for siRNA Delivery: Comparing ARGET ATRP and UV-initiated Formulations

5.1 Introduction

Drug delivery systems for siRNA have been extensively studied; however, the challenges associated with safe and effective delivery continue to prevent widespread translation of the new technology from the bench to the clinic.[1–9] Oligonucleotides such as siRNA are susceptible to degradation by endogenous nucleases, and as a result, require a protection mechanism. Other delivery challenges include effective cellular uptake and endosomal escape; siRNA must be inside the cytosol (rather than sequestered in a sub-cellular compartment) to have a therapeutic effect.

Some cell types, such as primary cells,[10] cells of the central nervous system,[11] and macrophage-type cell lines[12] are considered difficult to transfect, while other cell types such as HEK293T are widely used for siRNA screen experiments. For examples of siRNA knockdown in the literature for represen-

tative “easy” and “difficult” cell types see Table 5.1 and Table 5.2 (HEK293T and RAW264.7, respectively). Note that since a brief search for articles referencing siRNA in a major literature search service reveals 100,000s of articles, and these articles likely represent 1,000s-10,000s distinct delivery strategies to 10s-100s of cell types, the types listed in the tables represent only a small fraction of the siRNA delivery experiments reported in the literature.

Effective drug delivery vehicles must demonstrate siRNA binding, low cytotoxicity, effective cellular uptake, and most importantly, evidence of siRNA-induced knockdown. This work evaluates polycationic nanoparticles synthesized by either ARGET ATRP (activators regenerated by electron transfer atom transfer radical polymerization) or UV-initiated polymerization and examines their suitability as siRNA delivery vehicles to HEK293T and RAW264.7 cells.

5.2 Materials and methods

5.2.1 Chemicals

Poly(ethylene glycol) methyl ether methacrylate (PEGMA) solution (M_n 2000 for PEG chain, 50 wt% in water), 2-(diethylamino)ethyl methacrylate (DEAEMA), *tert*-butyl methacrylate (tBMA), tetraethylene glycol dimethacrylate (TEGDMA), ethyl 2-bromoisobutyrate (EBIB), tris (2-pyridylmethyl) amine (TPMA), ascorbic acid (AA), trypsin-EDTA solution, and Dulbecco’s Phosphate Buffered Saline (DPBS, Sigma-Aldrich) were pur-

chased from Sigma-Aldrich. 1 N Hydrochloric acid (HCl) was purchased from Fisher Scientific. Copper(II) bromide was purchased from Acros Organics. Ultrapure water was used for all studies. All chemicals were used as received.

5.2.2 Nanoparticle synthesis and purification

P(DEAEMA-*co*-tBMA-*co*-PEGMA-*co*-TEGDMA) polycationic nanoparticles were synthesized using a previously reported activators regenerated by electron transfer atom transfer radical polymerization (ARGET ATRP) technique[13;14] or a UV-initiated polymerization technique previously developed by Fisher and colleagues[15]. Briefly, reagents DEAEMA:PEGMA:TEGDMA:$CuBr_2$:TPMA:EBIB at molar ratios of 100:10:4:0.5:0.5:4 (with tBMA with a molar ratio of 30 or 45 depending on the formulation) were combined with 8 mg/ml Brij® 30 (Acros Organics) and 1.35 mg/ml myristyltrimethylammonium bromide (MyTab, Sigma-Aldrich) in water for a 0.1 weight ratio of monomer to solvent. For the UV-initiated polymerization, Irgacure® 2959 (Ciba) was added at a 0.005 mass ratio of initiator to monomer in place of $CuBr_2$:TPMA:EBIB.

Following probe sonication (S-4000 Misonix Ultrasonicator, Misonix Inc.) and nitrogen purge, the ARGET ATRP and UV-initiated polymerizations were reacted at ambient temperature for 3 h by the addition of degassed ascorbic acid solution as a reducing agent (AA: DEAEMA::0.5:100) or for 2.5 h by exposure to UV light (Dymax BlueWave^{TM}200 UV), respectively. Purification was done by a technique described previously by Fisher and Peppas[16]

with repeated precipitation/resuspension with acetone/0.5 N HCl. Following dialysis (12,000-14,000 molecular weight cut off regenerated cellulose tubing, Spectra/Por®), polymer was recovered by freeze-drying.

5.2.3 Binding of siRNA

Nanoparticles were loaded with AllStars Negative Control siRNA (Qiagen) in 1x PBS pH 5.5 (0.125 mg/ml nanoparticles and 500nM siRNA). Nuclease free 10x PBS was prepared by dissolving sodium chloride, potassium chloride, monosodium phosphate monohydrate, and disodium phosphate heptahydrate (Fisher Scientific) in water, treating with 0.1% v/v diethylpyrocarbonate (DEPC, Fisher Scientific) overnight, and then autoclaving to remove DEPC. The bound siRNA was determined within 10 min of combining the siRNA with the nanoparticles and then again after 70 min and 160 min in order to evaluate the effect of loading time. The siRNA binding was also evaluated at 0.025 mg/ml nanoparticles and 100 nM siRNA in 0.2x PBS pH 5.5, 1x PBS pH 5.5, 1x PBS pH 7.4, and Opti-MEM® (Reduced Serum Medium, no Phenol Red, Life Technologies) at approximately 30 minutes after combining the siRNA with the nanoparticles in order to evaluate the amount of siRNA released in conditions prior to uptake by cells.

The fraction of bound siRNA was determined using a Quant-iT™ RiboGreen® RNA Assay Kit (Life Technologies) that was adapted for 384-well low volume plates. Briefly, a 10 µl sample was combined with 10 µl RiboGreen® assay solution (RiboGreen® reagent diluted 200x in 1x TE buffer) in

a black 384-well low volume plate. The fluorescence intensity (F) was measured using a microplate reader (Synergy HT, BioTek Instruments, Inc.) 2-5 min after adding the RiboGreen® assay solution with 485 nm excitation and 528 nm emission. The RiboGreen® reagent is sensitive to components other than RNA present in the assay (although the importance of these contributions diminished for increasing siRNA concentrations), so these contributions to the fluorescence were subtracted from the measured fluorescence signal to calculate the percent of loading (L) in Equation 5.1:

$$\text{L}=100\times\left(1-\frac{F_{nanoparticle+siRNA\,complex}-F_{nanoparticle\,only}}{F_{siRNA\,only}-F_{buffer\,only}})\right) \tag{5.1}$$

5.2.4 Cell Culture

Human Embryonic Kidney 293T cells (HEK293T) and murine macrophage RAW264.7 cells (obtained from American Type Culture Collection) were maintained in Dulbecco's Modified Eagle's Medium high glucose without L-glutamine (Sigma-Aldrich) supplemented with with 1% L-glutamine (MediaTech), 1% penicillin (Sigma-Aldrich), 1% streptomycin (Sigma-Aldrich), and 10% HyClone USDA Tested Fetal Bovine Serum (FBS, Thermo Scientific). Opti-MEM® Reduced Serum Medium, no Phenol Red (Life Technologies) was used for all cytotoxicity and transfection experiments. Lipofectamine and Lipofectamine2000 (Life Technologies) were used as controls in transfection experiments.

5.2.4.1 Nanoparticle cytotoxicity

HEK293T cells were seeded at 5,000 cells/well on fibronectin (Sigma-Aldrich) coated 96 well plates (0.4 µg/well in 75 µl/well DPBS for 45 min) and RAW264.7 cells were seeded at 10,000 cells per well in 96 well plates without fibronectin coating (Nunc, Thermo Scientific). After 18 h incubation, the media was replaced with Opti-MEM®. The nanoparticles were prepared at 5x concentration in 1x PBS pH 5.5 and then added to cells at a final concentration of 1x in the wells following 1 h incubation with Opti-MEM®.

Following 48 h incubation, media was removed and cells were incubated for 90 min with CellTiter 96® AQ_{ueous} Non-Radioactive Cell Proliferation Assay (MTS, Promega) with serum-free DMEM without phenol red (Sigma-Aldrich). The absorbance (A) at 690 nm (background) and 490 nm (MTS assay) was measured using a microplate reader (Synergy HT, BioTek Instruments, Inc.), and cell relative viability (V) was calculated as shown in Equation 5.2:

$$\mathrm{V} = \frac{A_{490,\,sample} - A_{690,\,sample} - (A_{490,\,no\,cells} - A_{690,\,no\,cells})}{A_{490\,media} - A_{690,\,media} - (A_{490,\,no\,cells} - A_{690,\,no\,cells})} \qquad (5.2)$$

5.2.4.2 Flow cytometry to quantify uptake of fluorescently-labeled siRNA

Flow cytometry was used to quantify siRNA internalization. Flow cytometry measurements were collected using a BD Fortessa Flow Cytometer and analyzed using FACSDiva software (BD Biosciences). 120,000 HEK293T cells or 240,000 RAW264.7 cells were plated in 6 well plates (Nunc, Thermo Scientific) and incubated for 40 h. Next, cells were incubated for 2 h with 0.05 mg/ml polycationic nanoparticles or appropriate controls with 200 nM fluorescently-labeled DY647 siRNA (Thermo Scientific). Controls included Lipofectamine and Lipofectamine 2000 (5 µl/well) as well as siRNA-only and untreated controls. Following incubation, cells were rinsed twice with cold 1xDPBS pH 7.4 prior to treating with trypsin (HEK293T) or scraping (RAW264.7) to form a cell suspension. The cell suspension was centrifuged, the supernatant discarded, pellet resuspended in flow cytometry buffer (1% FBS in DPBS), centrifuged again, supernatant discarded, and finally the pellet resuspended in flow cytometry buffer. The samples were stored in darkness at 4 °C before measurement. The results are reported in two ways: as the average percent of cells (taken over a large number of cells, typically 10,000) containing fluorescently-labeled DY647 siRNA and as the mean fluorescence intensity of the sample normalized to the fluorescence intensity of the blank control. All results are reported as the average plus/minus the standard deviation of three independent experiments.

5.2.4.3 Confocal microscopy to verify siRNA internalization

Cover slips (18 mm round, no. 1.5 thickness) were acid washed overnight with 1 N HCl at 60 °C, rinsed with ethanol/water mixtures with successively increasing volume ratios of ethanol, and then the cover slips were placed in a 12 well plate. Prior to plating the HEK293T cells, the acid-washed cover slips in a 12 well plate were coated with fibronectin (4 μg fibronectin/well in 750 μl/well DPBS); no fibronectin coating was used for the RAW264.7 cells. HEK293T and RAW264.7 cells were added at 40,000 cells/well and 80,000 cells/well, respectively. Cells were incubated for 40 h prior to 2 h incubation with 0.05 mg/ml polycationic nanoparticles or appropriate controls with 200 nM siRNA. Controls included Lipofectamine and Lipofectamine 2000 (2.5 μl/well) as well as siRNA-only and untreated controls. Following incubation, cells were rinsed three times with 1xPBS pH 7.4 and fixed with 4% paraformaldehyde in 1xDPBS for 10 min prior to washing three times with HBSS (BioWhittaker) and once with DI water (autoclaved). Cover slips were mounted to glass slides using Prolong® Gold anti-fade reagent with DAPI (Life Technologies) and stored in the freezer prior to imaging.

Confocal images were acquired using a Zeiss LSM 710 confocal microscope with a 63x objective. The gain and offset for the different channels were kept constant for the full series of images of each cell type (with the settings for the HEK293T and RAW264.7 cell types optimized separately) to permit image comparisons. Images were collected in 16 bit format, and all images underwent identical post-processing (γ=0.45 for red and blue channels, γ=0.1.3

for brightfield, and brightfield scale adjusted to max/min using ZEN Blue).

5.2.4.4 Transfection with AllStars Death siRNA

Transfection conditions were matched to those used for cytotoxicity. HEK293T cells were seeded at 5,000 cells/well on fibronectin (Sigma-Aldrich) coated 96 well plates (0.4 µg/well fibronectin in 75 µl/well DPBS for 45 min) and RAW264.7 cells were seeded at 10,000 cells per well in 96 well plates without fibronectin coating (Nunc, Thermo Scientific). After 18 h incubation, the media was replaced with Opti-MEM®. The nanoparticles were combined with siRNA (AllStars Hs Cell Death siRNA or AllStars Mm/Tn Cell Death siRNA, Qiagen) in 1xPBS pH 5.5 at 0.125 mg/ml nanoparticles and 5x the final siRNA concentration. The complexes were added to cells at a final concentration of 0.025 mg/ml in the wells (with 100 nM or 200 nM siRNA) following 1 h incubation with Opti-MEM®. Lipofectamine and Lipofectamine2000 wells contained 0.25 µl/well Lipofectamine or Lipofectamine2000. Following 48 h incubation, media was removed and cell death visually confirmed. Viability was evaluated as for cytotoxicity experiments (cells were incubated for 90 min with MTS solution, and the absorbance was measured with a plate reader). The results for viability for the AllStars Death and the Scrambled siRNA were compared by Student's t-test (two-tailed, unequal variance) to check for statistically significant knockdown. The knockdown efficiency was evaluated using the cell viability (V) ratio of cells with Death siRNA and cells with scrambled siRNA as shown in Equation 5.3.

$$\% \text{ Knockdown} = 100 \times \left(1 - \frac{V_{Death}}{V_{Scrambled}}\right) \tag{5.3}$$

5.3 Results and discussion

5.3.1 Binding of siRNA

The loading efficiency of the polycationic nanoparticles is related to the siRNA binding, and the binding of siRNA to polycationic nanoparticles was evaluated using the RiboGreen® assay. The siRNA demonstrates efficient loading even after 10 minutes, with 85-91% loading efficiency for all polycationic nanoparticle formulations (Figure 5.1). After 70 min incubation, the loading efficiency demonstrates a nominal increase to 96-98% efficiency for all polycationic nanoparticle formulations, and this efficiency persists after 160 min. Based on the negligible increase in siRNA from 10 min to 70 min, the siRNA/nanoparticle complexes were used shortly after preparation (approximately 10 minutes after adding the siRNA) rather than after a longer incubation. At all time points, there is no significant difference in siRNA binding among the four formulations.

The siRNA demonstrates very efficient binding (~98% for all formulations) in 0.2x PBS pH 5.5, likely due to positive charge induced by low pH combined with low ionic strength (Figure 5.2). Across all formulations, the siRNA binding follows the following decreasing trend: 0.2xPBS pH 5.5 > 1xPBS pH 5.5 > 1xPBS pH 7.4 > Opti-MEM®. For the 1xPBS pH 7.4 and

the Opti-MEM®, the 30UV and 30ARGET formulations demonstrate slightly higher binding efficiencies than the corresponding 45UV and 45ARGET formulations. The 45ARGET formulation demonstrates the lowest binding efficiency in Opti-MEM® of the four formulations, with 55% of the siRNA bound to the polymer (compared to 74% for 30UV, 70% for 45UV, and 63% for 30ARGET). The reduced binding efficiency for 45ARGET compared to the other formulations may be a factor in determining knockdown efficiency; however, it is one factor among many.

5.3.2 Nanoparticle cytotoxicity

The biocompatibility of the polycationic nanoparticles with HEK293T cells and RAW264.7 cells was evaluated using an MTS assay following 48 h incubation with the nanoparticles (see Figure 5.3). Both cell lines demonstrate high relative viability at low concentrations (greater than 80% viability at 0.025 mg/ml and lower concentrations). In HEK293T cells, formulations 45UV and 45ARGET show increased biocompatibility compared to the 30UV and 30ARGET formulations; for example, at 0.05 mg/ml, the 45UV and 45ARGET formulations demonstrate 60% and 78% viability, respectively, while the 30UV and 30ARGET formulations demonstrate 18% and 21% viability, respectively.

In the RAW264.7 cells, biocompatibility is less dependent on formulation. The biocompatibility of the polycationic nanoparticle formulations with the RAW264.7 cells is indistinguishable at the upper two (0.2 mg/ml and 0.1 mg/ml) and lower two (0.00313 mg/ml and 0.00156 mg/ml) concentrations.

Both 30ARGET and 45ARGET show a slightly increased viability compared to 30UV and 45UV at 0.05 mg/ml and 0.025 mg/ml in RAW264.7 cells. At 0.0625 mg/ml, the 30ARGET shows increased viability compared to the other three formulations (100% versus 74-82% viability. All formulations demonstrated low viability in both cell types at the highest concentration tested (0.2 mg/ml).

5.3.3 Flow cytometry to quantify uptake of fluorescently-labeled siRNA

Flow cytometry was used to evaluate the internalization of fluorescently-labeled siRNA. The percent of cells associated with fluorescently-labeled siRNA and the normalized fluorescent intensity for each formulation are shown in Figure 5.4 and Figure 5.5, respectively, with representative histograms shown in Table 5.3. All polycationic nanoparticles demonstrated efficient uptake with slight differences among formulations in the percentage of cells with fluorescently-labeled siRNA. However, the difference between cell types is more significant. When the siRNA is delivered with polycationic nanoparticles, a greater percentage of RAW264.7 cells than HEK293T cells shows fluorescence of DY647 siRNA. For the polycationic nanoparticle formulations with HEK293T cells, 50.8% to 60.8% of cells are associated with fluorescently-labeled siRNA; likewise, the comparable values for the RAW264.7 cells are 66.0% to 84.5%. In contrast, when the siRNA is delivered with Lipofectamine or Lipofectamine2000, the RAW264.7 cells do not show increased

association compared to HEK293T. Another important difference between the cell types is the no-carrier siRNA-only control, which demonstrates strong association with the HEK293T cells but not the RAW264.7 cells. The cause of this association is unclear, as naked siRNA is negatively charged, and thus tends to resist transport through the negatively charged cell membrane. As flow cytometry cannot distinguish between surface bound and internalized fluorescence signal, it is likely the strong siRNA-only signal is membrane-associated rather than internalized, and this result may be confirmed with confocal microscopy.

For both cell types, 45UV and 45ARGET demonstrate greater normalized fluorescence intensity than the corresponding 30UV and 30ARGET formulations. The formulation 45ARGET demonstrates the largest normalized fluorescence intensity of the four polycationic nanoparticle formulations. Although the difference is slight between the normalized fluorescent intensity for the polycationic nanoparticle formulations between cell types, as a function of normalized fluorescence intensity, the Lipofectamine and Lipofectamine2000 have a much larger signal for the HEK293T cells than for the RAW264.7. Also, the Lipofectamine and Lipofectamine2000 have greater normalized fluorescent intensities than the polycationic nanoparticle formulations.

5.3.4 Confocal microscopy to verify siRNA internalization

Flow cytometry does not distinguish between surface bound and internalized fluorescence signal, so confocal microscopy was used to verify siRNA

internalization. HEK293T cells or RAW264.7 cells were incubated 2 h with DY647 fluorescently-labeled siRNA complexed with polycationic nanoparticles or controls (200 nM siRNA and 0.05 mg/ml polycationic nanoparticles). Cells were rinsed, fixed, stained with DAPI nuclear stain, and then mounted to microscope slides. Settings for image acquisition and processing were kept consistent during the experiment for each cell type to permit direct comparisons within each cell type.

The trends observed with flow cytometry are supported by confocal microscopy. Representative images for the HEK293T and RAW 264.7 confocal microscopy experiments are shown in Figure 5.6 and Figure 5.7, respectively. For the HEK293T cells, visual inspection confirms greater DY647 fluorescence for the 45UV and 45ARGET formulations compared to the corresponding 30UV and 30ARGET formulations. Likewise, the Lipofectamine and Lipofectamine2000 images show more DY647 fluorescence than the polycationic nanoparticles. These microscopy results are consistent with the flow cytometry results. Interestingly, the microscopy results for the 30UV and 45UV suggest a diffuse fluorescence rather than the punctate fluorescence observed for the 30ARGET and 45ARGET formulations. The results of the flow cytometry and confocal microscopy experiments using fluorescently-labeled siRNA indicate evidence of internalization necessary for siRNA-induced knockdown.

5.3.5 Transfection with AllStars Death siRNA

Knockdown efficiency induced by siRNA was evaluated using AllStars Hs Cell Death siRNA or AllStars Mm/Tn Cell Death siRNA. HEK293T cells were transfected for 48 h with 0.025 mg/ml polycationic nanoparticles (or appropriate controls) and 100 nM or 200 nM siRNA following 1 h incubation with Opti-MEM®. Cell death was confirmed visually and viability was evaluated using an MTS assay.

The ability of the polycationic nanoparticles to effectively deliver siRNA was first demonstrated in HEK293T cells with 0.025 mg/ml polycationic nanoparticles and 200 nM AllStars Hs Cell Death siRNA (see Figure 5.8). All of the siRNA delivery carriers demonstrated knockdown, with the greatest efficiency demonstrated by the 30UV, 30ARGET, and 45ARGET formulations (78%, 84%, and 75% knockdown efficiency, respectively). Unfortunately, this increased knockdown efficiency is associated with decreased cell viability.

When the polycationic nanoparticle is kept constant at 0.025 mg/ml and the siRNA concentration is decreased to 100 nM, the HEK293T cells with scrambled siRNA demonstrate improved viability; as a result, later studies used this 100 nM siRNA concentration (see Figure 5.9a and Figure5.10a). While this change results in increased HEK293T cell viability, it also results in decreased knockdown efficiency and increased variation. There was statistically significant knockdown ($p<0.05$) for the 30UV, 30ARGET, and 45ARGET formulations (41%, 51%, and 48%, respectively) as well as the Lipofectamine

commercially available transfection agent (28% knockdown).

Knockdown in RAW264.7 cells using 100 nM AllStars Mm/Tn Cell Death siRNA was evaluated using the four nanoparticle formulations as well as two commercially available transfection agents Lipofectamine and Lipofectamine2000 (see Figure 5.9b and Figure5.10b). Statistically significant knockdown ($p<0.05$) was observed for all four nanoparticle formulations (knockdown efficiency of 27%, 34%, 35%, and 25%, respectively) and also for the Lipofectamine2000 control (41%). The RAW264.7 cells are considered to be more difficult to transfect than HEK293T cells, and this is supported by the decreased transfection efficiency and cell viability with the RAW264.7 cells compared to the HEK293T.

5.4 Conclusion

The purpose of the studies undertaken in this report was to provide an analysis of four formulations of polycationic nanoparticles and examine their suitability as siRNA delivery vehicles to HEK293T and RAW264.7 cells. The polycationic nanoparticles demonstrate effective siRNA loading and good biocompatibility at low concentrations *in vitro*. Uptake experiments using flow cytometry and confocal microscopy confirmed siRNA internalization using fluorescently-labeled siRNA loaded in polycationic nanoparticles. The percent of cells with fluorescently-labeled siRNA uptake was similar across the four formulations, with the RAW264.7 cells demonstrating a greater percent

of cells with fluorescently-labeled siRNA than the HEK293T cells. However, although all four formulations led to approximately the same percent of cells with fluorescently-labeled siRNA, the 45ARGET formulation demonstrated a greater normalized fluorescence intensity than the other polycationic nanoparticle formulations. Knockdown experiments demonstrated knockdown following transfection, with the nanoparticle formulations performing on par with the commercially available carriers. This work indicates that the polycationic nanoparticles may have utility as siRNA delivery vehicles, but additional research is need to improve knockdown at lower concentrations of siRNA.

5.5 Tables

Table 5.1: Examples from the literature: transfection of HEK293 cells with siRNA. DCC: deleted in colorectal cancer, (E)GFP: (enhanced) green fluorescent protein, ELISA: enzyme linked immunosorbent assay, mPEG: methoxy-poly(ethylene glycol), PCL: poly(ε-caprolactone), RT-PCR: reverse transcriptase polymerase chain reaction

Type of carrier	Concentration and type of siRNA	Method of evaluating knockdown	Ref.
Imidazole-4-acetic acid (IAA)-conjugated chitosan	50 nM GAP480 silencer siRNA	KDalert assay kit	[17]
siPORT Amine	20 nM GAPDH siRNA	KDalert assay kit	[18]
Micelle nanoparticles ($mPEG_{45}$-*b*-PCL_{100}-*b*-PCL)	100 nM EGFP siRNA	Flow cytometry to measure GFP expression	[19]
Micelle nanoparticles ($mPEG_{45}$-*b*-PCL_{100}-*b*-PCL)	GL3 luciferase siRNA	Luminescence	[19]
Lipofectamine2000	10 nM of various siRNAs	Luminescence, ELISA, RT-PCR, Western blotting	[20]
Layered double hydroxide nanoparticles	250 nM siRNA DCC gene	Western blotting	[21]

Table 5.2: Examples from the literature: transfection of RAW264.7 cells with siRNA. Unfortunately, macrophage-type cells like like RAW264.7 are difficult to transfect.[12] (E)GFP: (enhanced) green fluorescent protein, ELISA: enzyme linked immunosorbent assay, PEI: polyethylenimine, PLGA: poly(lactide-*co*-glycolide), RT-PCR: reverse transcriptase polymerase chain reaction, TNF-α: tumor necrosis factor-α

Type of carrier	Concentration and type of siRNA	Method of evaluating knockdown	Ref.
PEI-PLGA microparticles	25-30 nM IL-10 siRNA	RT-PCR	18
Dharmafect, Lipofectamine 2000, HiPerfect, and other commercial transfection agents	20 -100 nM EGFP siRNA	Green fluorescence quantified using an automated fluorescence microscope	12
Rabies virus glycoprotein conjugated nona-D-arginine residues (RVG-9dR)	200 nM TNF-α siRNA	TNF-α ELISA, RT-PCR	22
Thioketal nanoparticles	1500-2000 nM TNF-α siRNA	TNF-α ELISA	23
PEI nanoparticles	1 nM TNF-α siRNA	TNF-α ELISA	24
Mannose-modified trimethyl chitosan-cysteine (MTC) conjugate nanoparticles	1-300 nM TNF-α siRNA	TNF-α ELISA, RT-PCR	25
Amphiphilic cationic cyclodextrin	100 nM TNF-α siRNA	TNF-α and IL-6 ELISA, RT-PCR	26
Cationic shell cross-linked knedel-like nanoparticles (cSCKs)	100 nM AllStars Death siRNA	MTS to measure relative cell viability	27

Table 5.3: Representative flow cytometry histograms for uptake of fluorescently-labeled siRNA by HEK293T and RAW264.7 cells. Data collected using a BD Fortessa flow cytometer and analyzed using FACSDiva software. Cells were incubated for 2 h with 0.05 mg/ml polycationic nanoparticles or appropriate controls with 200 nM fluorescently-labeled DY647 siRNA prior to rinsing and suspension.

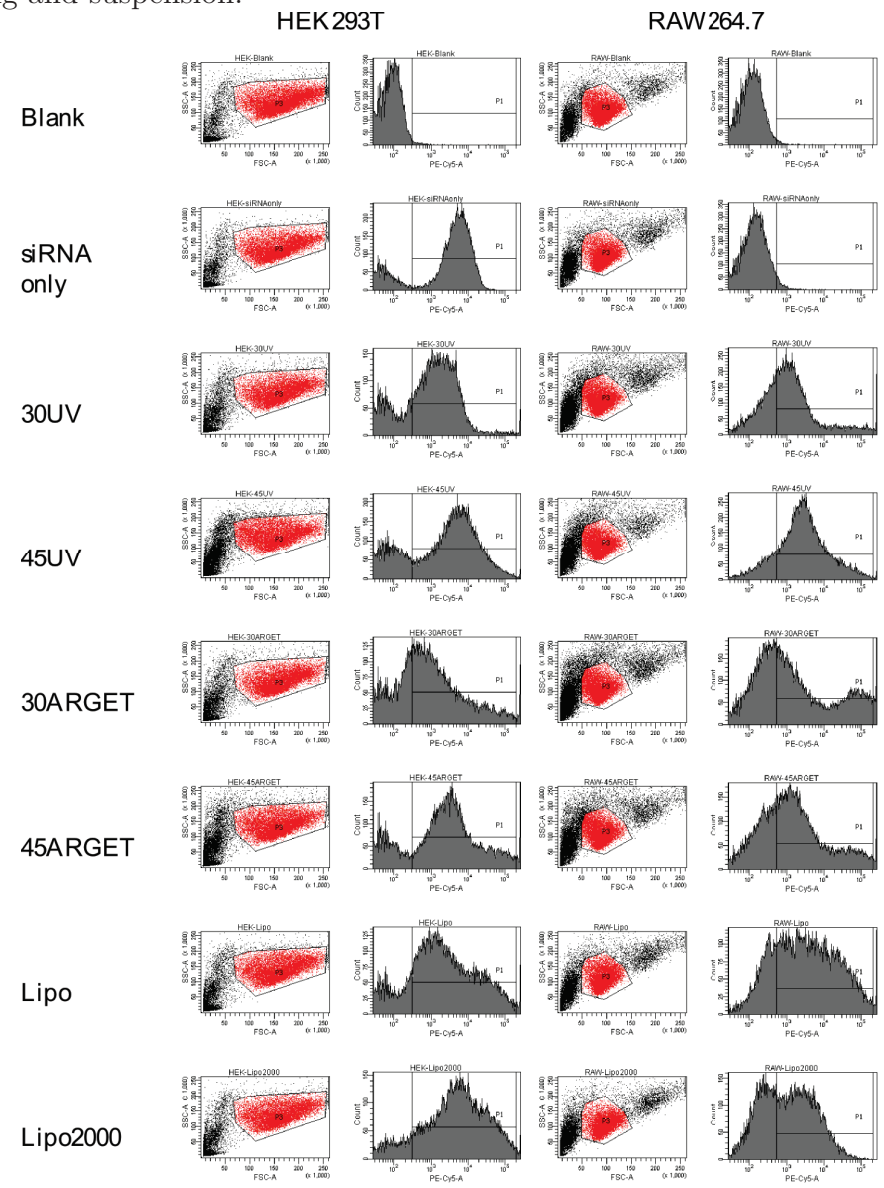

5.6 Figures

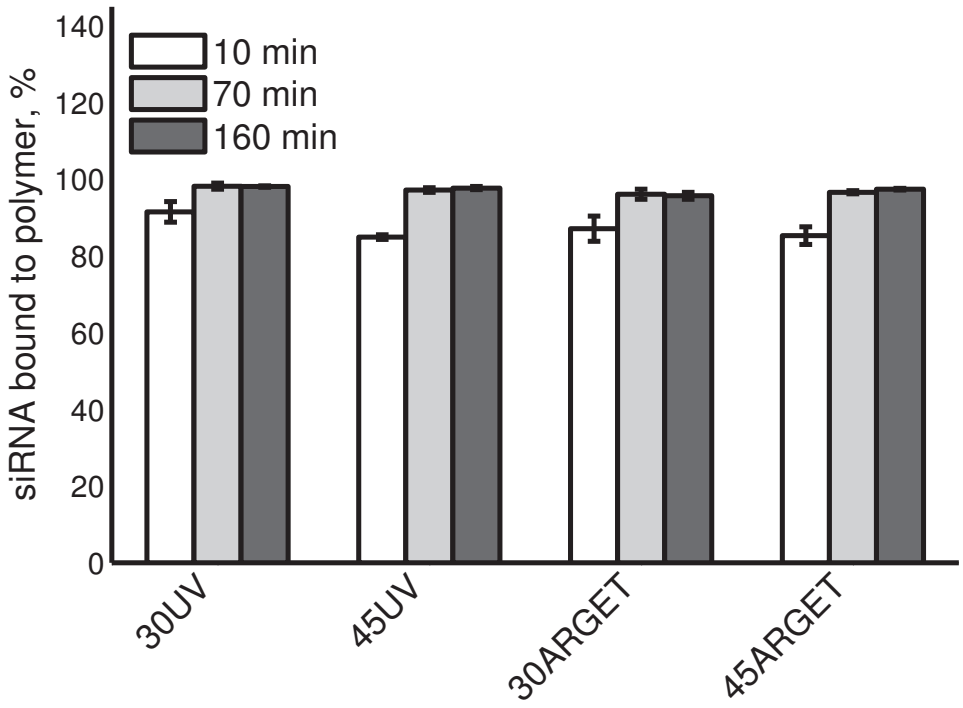

Figure 5.1: Binding of siRNA to polycationic nanoparticles. Nanoparticles were loaded with AllStars Negative Control siRNA in 1x PBS pH 5.5 with 0.125 mg/ml nanoparticles and 500 nM siRNA. Binding of siRNA evaluated at 10 min, 70 min, and 160 min using RiboGreen®.

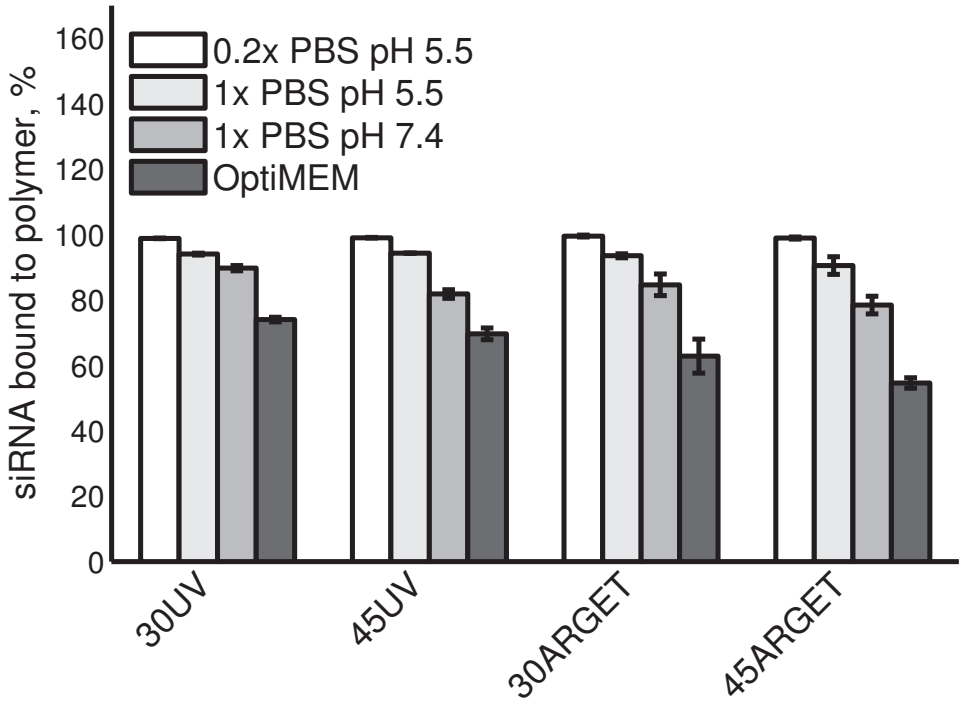

Figure 5.2: Binding of siRNA to polycationic nanoparticles in PBS buffers and Opti-MEM®. Following loading of 0.125 mg/ml nanoparticles with 500 nM siRNA, complexes were diluted 5x in 0.2x PBS pH 5.5, 1x PBS pH 5.5, 1x PBS pH 7.4, and Opti-MEM® prior to evaluating siRNA binding using RiboGreen®.

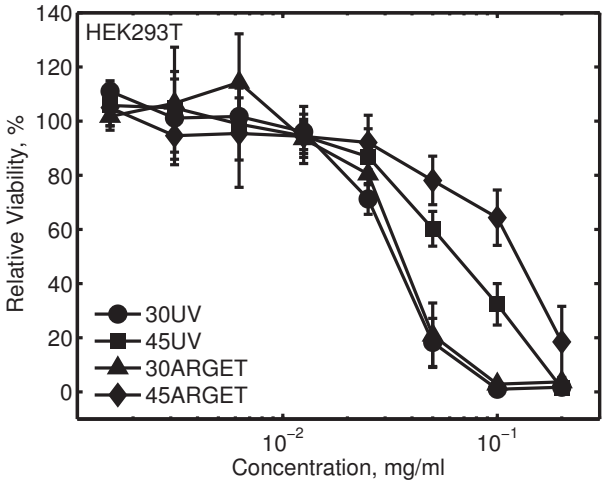

(a) Biocompatibility of HEK293T

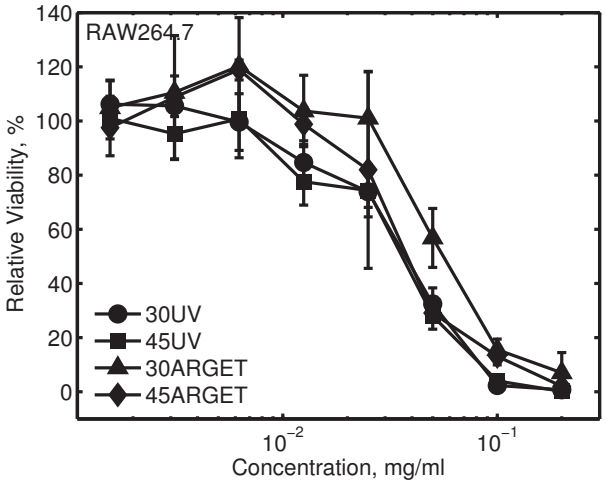

(b) Biocompatibility of RAW264.7

Figure 5.3: Biocompatibility of polycationic nanoparticle formulations with a) HEK293T cells or b) RAW264.7 cells at various concentrations (0.02 mg/ml to 0.00156 mg/ml) evaluated using an MTS assay following 48 h incubation.

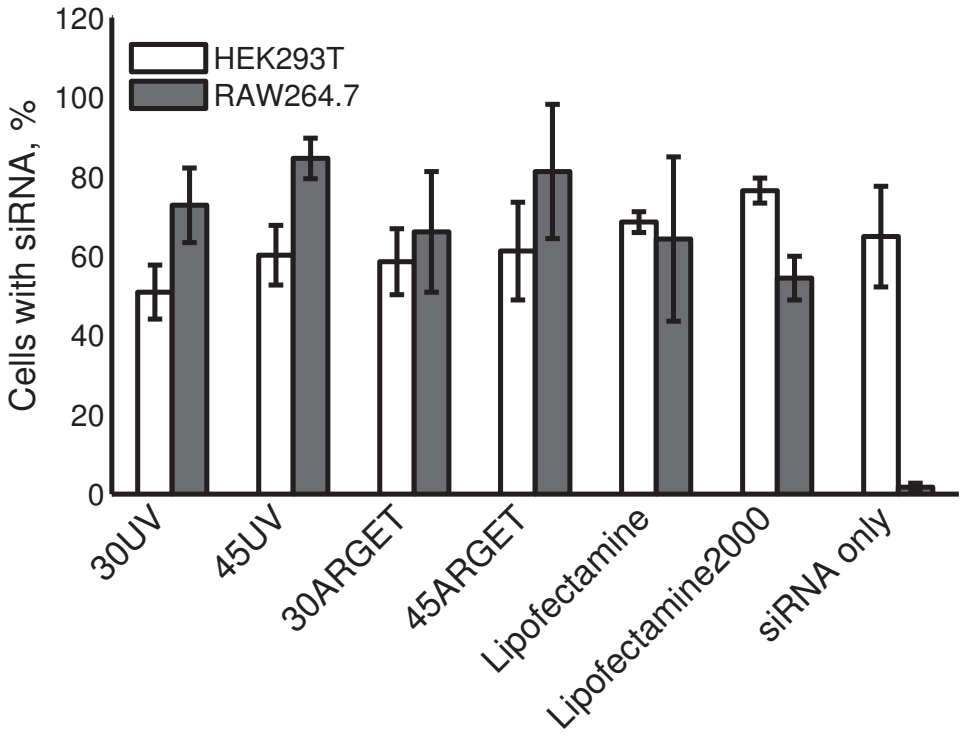

Figure 5.4: HEK293T or RAW264.7 cells associated with fluorescently-labeled DY647 siRNA. Cells were incubated for 2 h with 0.05 mg/ml polycationic nanoparticles or appropriate controls with 200 nM fluorescently-labeled DY647 siRNA. Following incubation, cells were rinsed and suspended for flow cytometry analysis with a BD Fortessa Flow Cytometer. Data are expressed as the mean plus or minus the standard deviation of three independent experiments.

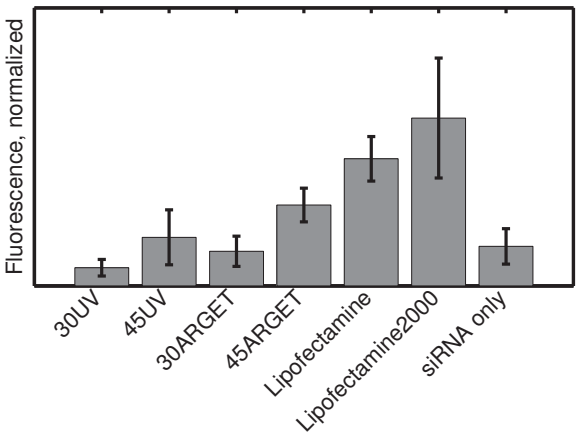

(a) Normalized fluorescent intensity for fluorescently-labeled DY647 siRNA with HEK293T cells

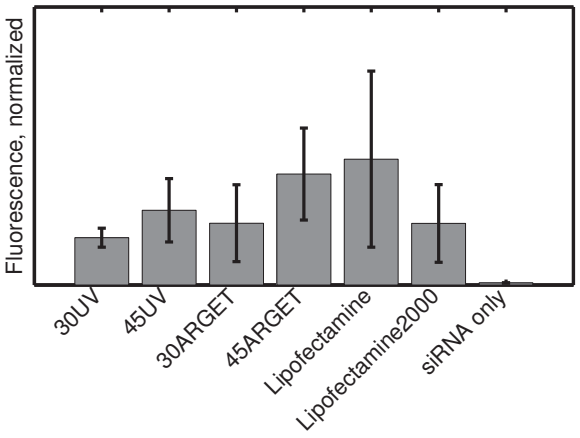

(b) Normalized fluorescent intensity for fluorescently-labeled DY647 siRNA with RAW264.7 cells

Figure 5.5: a) HEK293T or b) RAW264.7 cells associated with fluorescently-labeled DY647 siRNA. Cells were incubated for 2 h with 0.05 mg/ml polycationic nanoparticles or appropriate controls with 200 nM fluorescently-labeled DY647 siRNA. Following incubation, cells were rinsed and suspended for flow cytometry analysis with a BD Fortessa Flow Cytometer. Data are expressed as the mean plus or minus the standard deviation of three independent experiments. The data are normalized by dividing by the fluorescence intensity of the blank PBS-only control.

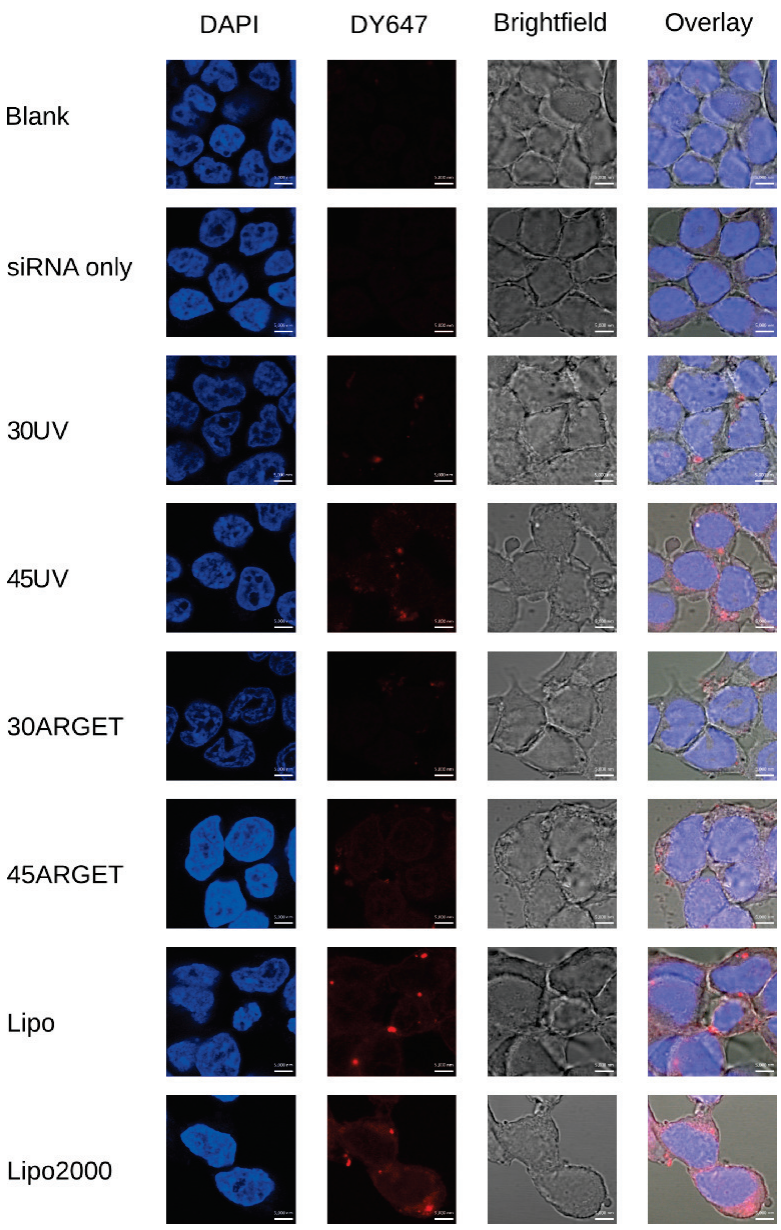

Figure 5.6: Internalization of fluorescently-labeled siRNA in HEK293T cells. Cells were incubated 2 h with 200 nM DY647 fluorescently-labeled siRNA complexed with 0.05 mg/ml polycationic nanoparticles or controls prior to rinsing, fixing, DAPI staining, and mounting. Staining of the cells: blue is DAPI stained nuclei and red is DY647 fluorescently-labeled siRNA. 5000 nm scale bars, 63x magnification, γ_{blue}=γ_{red}=0.45; $\gamma_{brightfield}$=1.3.

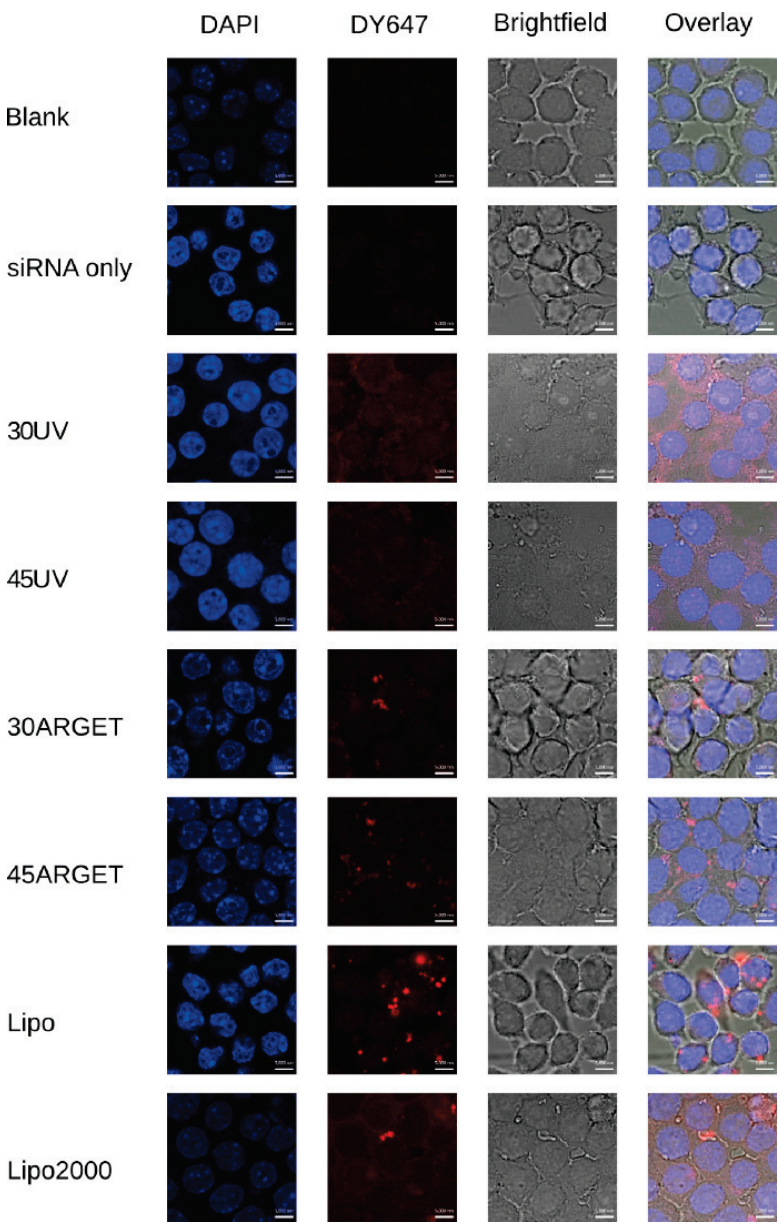

Figure 5.7: Internalization of fluorescently-labeled siRNA in RAW264.7 cells. Cells were incubated 2 h with 200 nM DY647 fluorescently-labeled siRNA complexed with 0.05 mg/ml polycationic nanoparticles or controls prior to rinsing, fixing, DAPI staining, and mounting. Staining of the cells: blue is DAPI stained nuclei and red is DY647 fluorescently-labeled siRNA. 5000 nm scale bars, 63x magnification, γ_{blue}=γ_{red}=0.45; $\gamma_{brightfield}$=1.3.

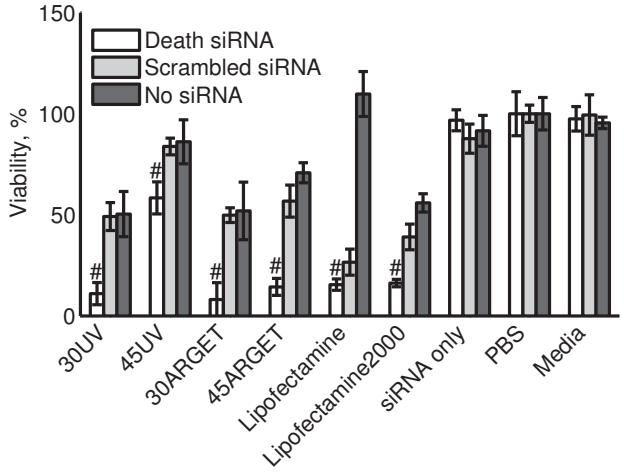

(a) HEK293T knockdown with 200 nM siRNA

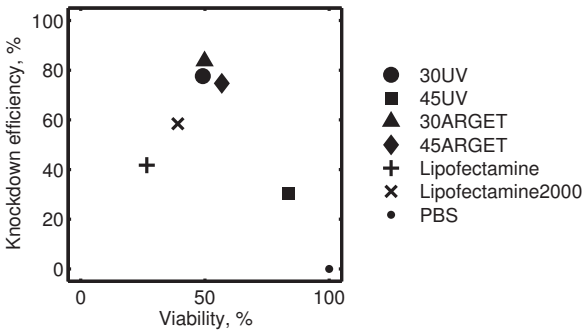

(b) HEK293T knockdown with 200 nM siRNA

Figure 5.8: Delivery of AllStars Death siRNA to HEK293T cells using polycationic nanoparticle carriers. The complexes were added to cells at a final concentration of 0.025 mg/ml and 200 nM in the wells following 1 h incubation with Opti-MEM®. The polycationic nanoparticles were evaluated versus Lipofectamine (0.25 µl/well), Lipofectamine2000 (0.25 µl/well), and no-carrier controls with an MTS assay following 48 h incubation. Pound signs (#) in (a) represent $p<0.015$ as determined using Student's t-test.

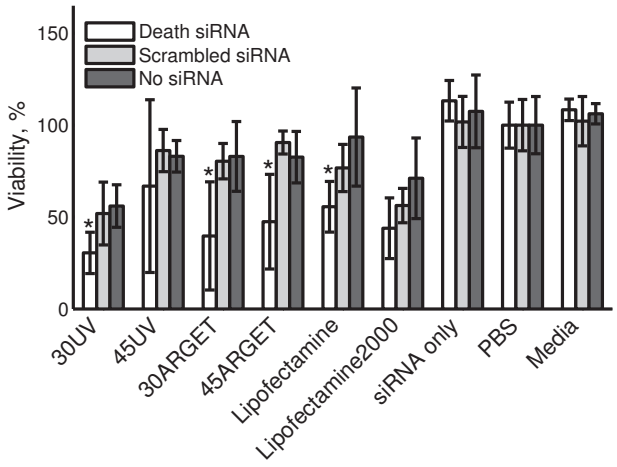

(a) HEK293T knockdown with 100 nM siRNA

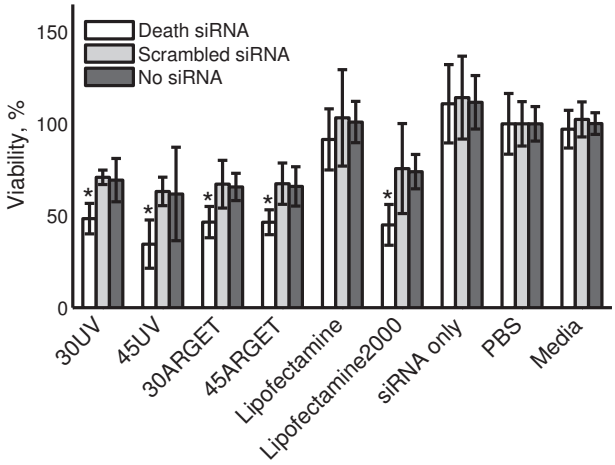

(b) RAW264.7 knockdown with 100 nM siRNA

Figure 5.9: Delivery of AllStars Death siRNA to a) HEK293T or b) RAW 264.7 cells using polycationic nanoparticle carriers. The complexes were added to cells at a final concentration of 0.025 mg/ml and 100 nM in the wells following 1 h incubation with Opti-MEM®. The polycationic nanoparticles were evaluated versus Lipofectamine (0.25 μl/well), Lipofectamine2000 (0.25 μl/well), and no-carrier controls with an MTS assay following 48 h incubation. Asterisks (*) represent $p<0.05$ as determined using Student's t-test.

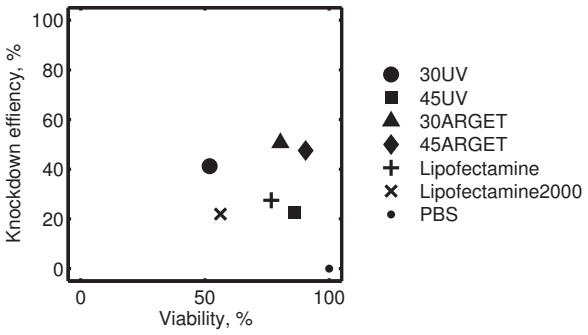

(a) HEK293T knockdown versus viability for 100 nM siRNA

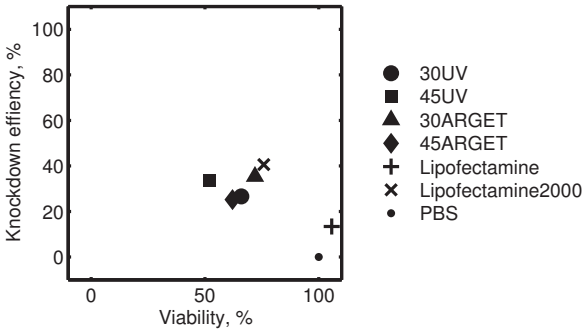

(b) RAW264.7 knockdown versus viability for 100 nM siRNA

Figure 5.10: Knockdown efficiency versus viability for a) HEK293T or b) RAW 264.7 cells. Knockdown efficiency was evaluated following 48 h transfection with 0.025 mg/ml polycationic nanoparticles and 100 nM siRNA following 1 h incubation with Opti-MEM®. The polycationic nanoparticles were evaluated versus Lipofectamine (0.25 µl/well), Lipofectamine2000 (0.25 µl/well), and no-carrier controls.

5.7 References

[1] A. Bouchie. Companies in footrace to deliver RNAi. *Nat. Biotechnol.*, 30 (12):1154–1157, 2012.

[2] H. C. Kang, K. M. Huh, and Y. H. Bae. Polymeric nucleic acid carriers: current issues and novel design approaches. *J. Control. Release*, 164(3): 256–264, 2012.

[3] S. Crunkhorn. Trial watch: Pioneering RNAi therapy shows antitumour activity in humans. *Nat. Rev. Drug Discovery*, 12(3):178–178cru, 2013.

[4] C. Kriegel, H. Attarwala, and M. Amiji. Multi-compartmental oral delivery systems for nucleic acid therapy in the gastrointestinal tract. *Adv. Drug Deliver. Rev.*, 65(6):891–901, 2013.

[5] Z. ur Rehman, I. S. Zuhorn, and D. Hoekstra. How cationic lipids transfer nucleic acids into cells and across cellular membranes: Recent advances. *J. Control. Release*, 166(1):46–56, 2013.

[6] D. Guzman-Villanueva, I. M. El-Sherbiny, D. Herrera-Ruiz, A. V. Vlassov, and H. D. C. Smyth. Formulation approaches to short interfering RNA and MicroRNA: Challenges and implications. *J. Pharm. Sci.*, 101(11): 4046–4066, 2012.

[7] D. C. Forbes and N. A. Peppas. Oral delivery of small RNA and DNA. *J. Control. Release*, 162(2):438–445, 2012.

[8] Y. Zhang, A. Satterlee, and L. Huang. *In vivo* gene delivery by nonviral vectors: Overcoming hurdles? *Mol. Ther.*, 20(7):1298–1304, 2012.

[9] T. Wang, J. R. Upponi, and V. P. Torchilin. Design of multifunctional non-viral gene vectors to overcome physiological barriers: Dilemmas and strategies. *Int. J. Pharm.*, 427(1):3–20, 2012.

[10] S. Marine, J. Freeman, A. Riccio, M. Axenborg, J. Pihl, R. Ketteler, and S. Aspengren. High-throughput transfection of differentiated primary neurons from rat forebrain. *J. Biomol. Screen.*, 17(5):692–696, 2012.

[11] B. Bertram, S. Wiese, and A. von Holst. High-efficiency transfection and survival rates of embryonic and adult mouse neural stem cells achieved by electroporation. *J. Neurosci. Meth.*, 209(2):420–427, 2012.

[12] J. Carralot, T. Kim, B. Lenseigne, A. S. Boese, P. Sommer, A. Genovesio, and P. Brodin. Automated high-throughput siRNA transfection in raw 264.7 macrophages: a case study for optimization procedure. *J. Biomol. Screen.*, 14(2):151–160, 2009.

[13] D. C. Forbes, M. Creixell, H. Frizzell, and N. A. Peppas. Polycationic nanoparticles synthesized using ARGET ATRP for drug delivery. *Eur. J. Pharm. Biopharm.*, 84(3):472–478, 2013.

[14] D. C. Forbes and N. A. Peppas. Differences in molecular structure in cross-linked polycationic nanoparticles synthesized using ARGET ATRP or UV-initiated polymerization. *Polymer*, 54(17):4486–4492, 2013.

[15] O. Z. Fisher, T. Kim, S. R. Dietz, and N. A. Peppas. Enhanced core hydrophobicity, functionalization and cell penetration of polybasic nanomatrices. *Pharm. Res.*, 26(1):51–60, 2008.

[16] O. Z. Fisher and N. A. Peppas. Polybasic nanomatrices prepared by UV-initiated photopolymerization. *Macromolecules*, 42(9):3391–3398, 2009.

[17] B. Ghosn, S. P. Kasturi, and K. Roy. Enhancing polysaccharide-mediated delivery of nucleic acids through functionalization with secondary and tertiary amines. *Curr. Top. Med. Chem.*, 8(4):331–340, 2008.

[18] A. Singh, H. Nie, B. Ghosn, H. Qin, L. W. Kwak, and K. Roy. Efficient modulation of T-cell response by dual-mode, single-carrier delivery of cytokine-targeted siRNA and DNA vaccine to antigen-presenting cells. *Mol. Ther.*, 16(12):2011–2021, 2008.

[19] Tian-Meng Sun, Jin-Zhi Du, Li-Feng Yan, Hai-Quan Mao, and Jun Wang. Self-assembled biodegradable micellar nanoparticles of amphiphilic and cationic block copolymer for siRNA delivery. *Biomaterials*, 29(32):4348–4355, 2008.

[20] N. Charlaftis, D. T. Fearon, A. Schoenemeyer, and P. J. Morley. siRNA high-throughput kinase library screen identifies protein kinase, DNA-activated catalytic polypeptide to play a role in MyD88-induced IFNA2 activation and IL-8 secretion. *Biotechnol. Appl. Biochem.*, 59(1):6–14, 2012.

[21] M. Chen, H. M. Cooper, J. Z. Zhou, P. F. Bartlett, and Z. P. Xu. Reduction in the size of layered double hydroxide nanoparticles enhances the efficiency of siRNA delivery. *J. Colloid Interface Sci.*, 390(1):275–281, 2013.

[22] S. Kim, C. Ye, P. Kumar, I. Chiu, S. Subramanya, H. Wu, P. Shankar, and N. Manjunath. Targeted delivery of siRNA to macrophages for anti-inflammatory treatment. *Mol. Ther.*, 18(5):993–1001, 2010.

[23] D. S. Wilson, G. Dalmasso, L. Wang, S. V. Sitaraman, D. Merlin, and N. Murthy. Orally delivered thioketal nanoparticles loaded with TNF-α siRNA target inflammation and inhibit gene expression in the intestines. *Nat. Mater.*, 9(11):923–928, 2010.

[24] H. Laroui, A. L. Theiss, Y. Yan, G. Dalmasso, H. T. T. Nguyen, S. V. Sitaraman, and D. Merlin. Functional TNFα gene silencing mediated by polyethyleneimine/TNFα siRNA nanocomplexes in inflamed colon. *Biomaterials*, 32(4):1218–1228, 2011.

[25] C. He, L. Yin, C. Tang, and C. Yin. Multifunctional polymeric nanoparticles for oral delivery of TNF-alpha siRNA to macrophages. *Biomaterials*, 34(11):2843–2854, 2013.

[26] J. McCarthy, M.J. O'Neill, L. Bourre, D. Walsh, A. Quinlan, G. Hurley, J. Ogier, F. Shanahan, S. Melgar, R. Darcy, and C.M. O'Driscoll. Gene silencing of TNF-alpha in a murine model of acute colitis using a modified cyclodextrin delivery system. *J. Control. Release*, 168(1):28–34, 2013.

[27] R. Shrestha, M. Elsabahy, S. Florez-Malaver, S. Samarajeewa, and K. L. Wooley. Endosomal escape and siRNA delivery with cationic shell crosslinked knedel-like nanoparticles with tunable buffering capacities. *Biomaterials*, 33(33):8557–8568, 2012.

Chapter 6

Polymeric Nanocarriers for siRNA Delivery to Murine Macrophages

6.1 Introduction

Cationic polymers have been investigated as biomaterials for drug delivery of nucleic acids, and polymers containing DEAEMA (2-(diethylamino)ethyl methacrylate) or the related DMAEMA (2-(dimethylamino)ethyl methacrylate) have been investigated by many groups for the delivery of DNA[1–11] as well as siRNA[5;12–23] to cells (see Table 6.1 and Table 6.2). Effective siRNA delivery depends on complex interactions among the siRNA, carrier, and cells of interest. Undesirable cellular toxicity is a common challenge for polycationic carriers, especially since there seems to be a trade-off between transfection efficiency and cellular toxicity.[24] Another challenge for researchers working to design improved delivery vehicles is that the observed transfection efficiency often does not correlate directly with carrier or siRNA uptake;[25] in other words, the carrier with the best transfection efficiency is not necessarily the one with the most efficient cellular

uptake.

This work investigates the interactions of a polycationic nanoparticle carrier synthesized by activators regenerated ARGET ATRP (activators regenerated by electron transfer atom transfer radical polymerization) with siRNA cargo and RAW264.7 cell delivery sites. The polycationic nanoparticle and siRNA interactions are probed using a fluorescent assay as well as light scattering techniques, and the polycationic nanoparticle and RAW264.7 cell interactions are investigated using fluorescently-labeled nanoparticles combined with confocal microscopy or flow cytometry. Finally, the use of these ARGET ATRP polycationic nanoparticles as siRNA delivery carriers to RAW264.7 cells is investigated through concentration-dependent transfection experiments.

6.2 Experimental section

6.2.1 Chemicals

Reagents poly(ethylene glycol) methyl ether methacrylate (PEGMA) solution (M_n 2000 for PEG chain, 50 wt % in water), 2-(diethylamino)ethyl methacrylate (DEAEMA), *tert*-butyl methacrylate (tBMA), tetraethylene glycol dimethacrylate (TEGDMA), ethyl 2-bromoisobutyrate (EBIB), tris (2-pyridylmethyl) amine (TPMA), and ascorbic acid (AA) were purchased from Sigma-Aldrich. Ethanol, 1 N Hydrochloric acid (HCl), sodium chloride, potassium chloride, monosodium phosphate monohydrate, disodium phosphate heptahydrate, and phosphate buffered saline (PBS) were purchased from Fisher

Scientific. Copper(II) bromide was purchased from Acros Organics. Ultrapure water was used for all studies. All chemicals were used as received.

6.2.2 Nanoparticle synthesis and purification

The polycationic nanoparticles were synthesized using a previously reported technique.[26;27] Monomers (DEAEMA, PEGMA, tBMA), cross-linking agent (TEGDMA), catalyst ($CuBr_2$), ligand (TPMA), and initiator (EBIB) were combined at molar ratios of 100:10:45:4:0.5:0.5:4. The reagents were added to a surfactant solution (8 mg/ml Brij® 30 (Acros Organics) and 1.35 mg/ml myristyltrimethylammonium bromide (MyTab, Sigma-Aldrich) in water) at a 0.1 weight ratio of monomer to solvent. An emulsion was formed using probe sonication (S-4000 Misonix Ultrasonicator, Misonix Inc.) and then purged with nitrogen. Degassed ascorbic acid solution was added as a reducing agent (AA:DEAEMA::0.5:100) to start the reaction and the emulsion was allowed to react for 3 h. Purification was done by a technique described previously by Fisher and Peppas[28] with repeated precipitation/resuspension with acetone/0.5 N HCl. Following dialysis (12,000-14,000 molecular weight cut off regenerated cellulose tubing, Spectra/Por®), polymer was recovered by freeze-drying.

Fluorescently-labeled nanoparticles were synthesized using NBD chloride (NBD-Cl, 7-chloro-4-nitrobenzo-2-oxa-1,3-diazole, also called 4-chloro7-nitrobenzofuran, Sigma-Aldrich). Nanoparticles containing primary amines were synthesized with 2-aminoethyl methacrylate (AEMA, Sigma-Aldrich)

(AEMA:DEAEMA::32:100). Dried, purified nanoparticles were suspended in ethanol and combined with an excess of NBD chloride; a typical reaction was 450 mg of dried nanoparticles with 50 mg NBD chloride in 30 ml ethanol. The mixture was allowed to react overnight to form NBD-labeled nanoparticles (NBD-NPs) (Figure 6.1). Unreacted NBD-Cl was removed by dialysis and the fluorescently-labeled nanoparticles were recovered with freeze-drying. Note that the NBD-Cl becomes strongly fluorescent upon reaction with amines and that NBD-amines are excited by visible light (464 nm) with emission maximum of approximately 512 nm.

6.2.3 Binding of siRNA

Nanoparticles were loaded with AllStars Negative Control siRNA (Qiagen) in 1x PBS pH 5.5. The final concentration of siRNA was maintained at 100 nM as the final concentration of polycationic nanoparticles was decreased by halves from 0.1 mg/ml to 6.1 ng/ml (g polymer/g siRNA from 80 to 0.00488). The siRNA concentration was maintained constant to minimize variation associated with the assay at low or high concentrations of siRNA. Nuclease free 10x PBS was prepared by dissolving sodium chloride, potassium chloride, monosodium phosphate monohydrate, and disodium phosphate heptahydrate (Fisher Scientific) in water, treating with 0.1% v/v diethylpyrocarbonate (DEPC, Fisher Scientific) overnight, and then autoclaving to remove DEPC.

The fraction of bound siRNA was determined using a Quant-iT™ Ri-

boGreen® RNA Assay Kit (Life Technologies) that was adapted for 384-well low volume plates. Briefly, a 10 µl sample was combined with 10 µl RiboGreen® assay solution (RiboGreen® reagent diluted 200x in 1x TE buffer) in a black 384-well low volume plate. The fluorescence intensity (F) was measured using a microplate reader (Synergy HT, BioTek Instruments, Inc.) 2-5 min after adding the RiboGreen® assay solution with 485 nm excitation and 528 nm emission. The RiboGreen® reagent is sensitive to components other than RNA present in the assay (although the importance of these contributions diminished for increasing siRNA concentrations), so these contributions to the fluorescence were subtracted from the measured fluorescence signal to calculate the percent loading (L) as calculated in Equation 6.1:

$$\text{L}=100\times\left(1-\frac{F_{nanoparticle+siRNA\,complex}-F_{nanoparticle\,only}}{F_{siRNA\,only}-F_{buffer\,only}})\right) \tag{6.1}$$

6.2.4 Dynamic light scattering

The z-average diameter and zeta potential were measured using a Malvern ZetaSizer NanoZS instrument (Malvern Instruments Corp.) equipped with a 633 nm laser source. Various polymer nanoparticle to siRNA ratios (g polymer / g siRNA) were prepared in nuclease free 0.1x PBS pH 5.5; the polymer nanoparticle concentration was fixed at 0.0125 mg/ml and the concentration of siRNA varied (0 nM, 12.5 nM, 50 nM, 200 nM, and 800 nM). The polymer concentration was fixed in order to minimize variation in the light

scattering results associated with the concentration of polycationic nanoparticles. Concentrations of siRNA greater than 800 nM were not tested due to the limitations of the stock solution; as a result, the minimum polymer/siRNA mass ratio tested was 1.25.

6.2.5 Cell culture

Murine macrophage RAW264.7 cells (obtained from American Type Culture Collection) were maintained in Dulbecco's Modified Eagle's Medium high glucose without L-glutamine (DMEM, Sigma-Aldrich) supplemented with with 1% L-glutamine (MediaTech), 1% penicillin (Sigma-Aldrich), 1% streptomycin (Sigma-Aldrich), and 10% HyClone USDA Tested Fetal Bovine Serum (FBS, Thermo Scientific). Opti-MEM® Reduced Serum Medium, no Phenol Red (Life Technologies) was used for all cytotoxicity and transfection experiments.

6.2.5.1 Flow cytometry

Flow cytometry measurements were collected using a Accuri flow cytometer and analyzed with Accuri software (BD Biosciences) and also with a BD Fortessa flow cytometer and analyzed using FACSDiva software (BD Biosciences). 240,000 RAW264.7 cells were plated in 6 well plates (Thermo Scientific) and incubated for 50 h. Fluorescently-labeled polycationic nanoparticles were added at 0.05 mg/ml, 0.025 mg/ml, and 0.0125 mg/ml for incubation times of 24 h, 2 h, and 30 min at a temperature of 37C and 2 h at a tem-

perature of 4C. Following incubation, cells were rinsed three times with cold Dulbecco's Phosphate-Buffered Saline (DPBS, Sigma-Aldrich) prior to scraping to form a cell suspension. The cell suspension was centrifuged, the supernatant discarded, and the pellet was resuspended in FACS buffer (1% FBS in DPBS). The samples were stored in darkness at 4 °C before measurement. The results are reported in two ways: as the average percent of cells (taken over a large number of cells, typically 10,000) containing fluorescently-labeled NBD-NPs and as the mean fluorescence intensity of the sample normalized to the fluorescence intensity of the blank control. All results are reported as the average plus/minus the standard deviation of two replicates as measured using the Accuri flow cytometer. The results were confirmed in an independent experiment using the Accuri flow cytometer and an independent experiment using the BD Fortessa flow cytometer.

6.2.5.2 Confocal microscopy

Cover slips (18 mm round, 1.5 thickness) were acid washed overnight with 1 N HCl at 60 °C, rinsed with ethanol/water mixtures with successively increasing volume ratios of ethanol, and then the cover slips were placed in a 12 well plate and UV-sterilized. RAW264.7 cells were plated on the glass cover slips at 80,000 cells/well. Cells were incubated for 40 h prior to 2 h incubation with 0.05 mg/ml polycationic nanoparticles. Following incubation, cells were rinsed three times with 1xPBS pH 7.4 to remove non-internalized nanoparticles. Cells were fixed with 4% para formaldehyde in 1xDPBS for 10 min at

room temperature prior to washing three times with HBSS (BioWhittaker). Cells were stained with 1 μg/ml Wheat Germ Agglutinin (WGA) Alexa Fluor 594 conjugate for 10 min at room temperature. Cells were rinsed twice with cold HBSS and once with DI water (autoclaved). Cover slips were mounted to glass slides using Prolong® Gold anti-fade reagent with DAPI (Life Technologies) and stored in the freezer prior to imaging.

Confocal images were acquired using a Zeiss LSM 710 confocal microscope with a 63x objective. The settings for the green laser were adjusted such that blank cells (no nanoparticles) demonstrated negligible fluorescence. The step size was maintained at 0.8 μm, while the total stack volume was varied to match the cell thickness for each field. Images were collected in 16 bit format, and all images underwent identical post-processing (γ=0.45 for red, blue, and green channels, γ=1.3 for brightfield, and brightfield scale adjusted to max/min using ZEN Blue).

6.2.5.3 Transfection with AllStars Death siRNA

RAW264.7 cells were seeded at 10,000 cells per well in 96 well plates (Nunc, Thermo Scientific). After 18 h incubation, the media was replaced with Opti-MEM®. The nanoparticles were combined with siRNA (AllStars Mm/Tn Cell Death or Negative Control siRNA, Qiagen) in 1xPBS pH 5.5 at various concentrations of polymer nanoparticles and siRNA. The complexes were added to cells following 1 h incubation with Opti-MEM®. Lipofectamine wells contained 0.25 μl/well Lipofectamine. Following 48 h incubation, media was

removed and cells were incubated for 90 min with CellTiter 96® AQ_{ueous} Non-Radioactive Cell Proliferation Assay (MTS, Promega) with serum-free DMEM without phenol red (Sigma-Aldrich). The absorbance at 690 nm (background) and 490 nm (MTS assay) was measured using a microplate reader (Synergy HT, BioTek Instruments, Inc.), and cell viability (V) was calculated as shown in Equation 6.2:

$$\mathrm{V} = \frac{A_{490,\,sample} - A_{690,\,sample} - (A_{490,\,no\,cells} - A_{690,\,no\,cells})}{A_{490\,media} - A_{690,\,media} - (A_{490,\,no\,cells} - A_{690,\,no\,cells})} \tag{6.2}$$

The results for viability for the AllStars Death and the Scrambled siRNA were compared by Student's t-test (two-tailed, unequal variance) to check for statistically significant knockdown. The percent knockdown was calculated from the cell viability for cells transfected with AllStars Death siRNA and Scrambled (negative control) siRNA y as shown in Equation 6.3:

$$\%\ \text{Knockdown} = 100 \times \left(1 - \frac{V_{Death}}{V_{Scrambled}}\right) \tag{6.3}$$

6.3 Results and discussion

The polycationic nanoparticles were synthesized using ARGET ATRP. The interactions between polycationic nanoparticles and siRNA were analyzed using a fluorescent RiboGreen® assay and using dynamic light scattering. The interactions between polycationic nanoparticles and murine macrophage cells

were analyzed using flow cytometry and confocal microscopy. Polycationic nanoparticles loaded with siRNA were used to transfect RAW264.7 cells in order to examine the dependence of knockdown efficiency on the concentration of polycationic nanoparticles and siRNA.

6.3.1 Binding of siRNA

The binding of siRNA was determined from measurements of free siRNA taken using a RiboGreen® RNA Assay Kit for a range of polymer to siRNA mass ratios of 80 to 0.0049 (see Figure 6.2). For all measurements, the siRNA concentration was maintained at 100 nM as the polymer nanoparticle concentration was varied. When the mass ratio of polymer to siRNA decreases below 1, the binding efficiency decreases sharply. The binding efficiency continues to decrease as the mass ratio of polymer to siRNA decreases until it begins to level off (reaching 14% binding) near a mass ratio of polymer to siRNA of 0.0195. This binding curve indicates that the polycationic nanoparticles efficiently bind siRNA at mass ratios of polymer/siRNA greater than 1. For mass ratios less than one, the polycationic nanoparticles quickly reach their maximum binding capacity and the binding efficiency decreases sharply.

6.3.2 Dynamic light scattering

Z-average diameter, polydispersity, and zeta potential were measured using dynamic light scattering with a Malvern ZetaSizer NanoZS instrument

(see Figure 6.3). Samples were prepared with a final concentration of 0.0125 mg/ml polymer nanoparticles in 0.1x PBS pH 5.5 with varying concentrations of siRNA. As the concentration of siRNA increases (and the mass ratio decreases), the diameter of the polycationic nanoparticles decreases from a maximum of 195.4 nm (mass ratio 80) to a minimum of 170.7 nm (mass ratio 1.25). The decrease in diameter may be associated with binding of anionic siRNA to the polycationic nanoparticles, resulting in charge neutralization and a decrease in ion repulsion-driving swelling. If the charge neutralization is at work, it is not apparent from the surface charge measurements; the zeta potential was indistinguishable for the five concentrations of siRNA with 0.025 mg/ml polycationic nanoparticles tested (24.2 mV to 25.5 mV).

6.3.3 Flow cytometry to evaluate uptake of polycationic nanoparticles

The uptake of fluorescently-labeled polycationic nanoparticles was evaluated using flow cytometry (see Figure 6.3). The percent of cells with nanoparticles increased as the incubation time increased, indicating uptake continues after 2 h. The percent of cells with nanoparticles also increased as the concentration of nanoparticles increased, although the difference was slight for the 2 h and 30 min incubation times. The maximum percent of cells containing fluorescently-labeled nanoparticles was 54% for 0.05 mg/ml at 24 h. Likewise, the normalized fluorescence intensity increased as the incubation time and nanoparticle concentration increased. Negligible uptake was observed at 30

min (only 6%, 6%, and 4% for 0.05 mg/ml, 0.025 mg/ml, and 0.0125 mg/ml, respectively)

The NBD-NPs demonstrate a temperature-dependent uptake profile; incubation at 37 °C (versus 4 °C) results in a increase in the percent of cells that have taken-up NBD-NPs (see Figure 6.4). The negligible uptake observed at 4 °C indicates that nanoparticle internalization is dominated by active transport processes (endocytosis) rather than by a method where the cells were passive recipients of membrane-disruption by the nanoparticles.

6.3.4 Confocal microscopy to verify internalization of polycationic nanoparticles

The internalization of nanoparticles was confirmed using confocal microscopy. Confocal images were acquired with a Zeiss LSM 710 confocal microscope with a 63x objective. Z-stacks were used to gain a more complete 3-D picture of the cells (see the orthogonal view in Figure 6.5) in addition to 2-D snapshots (see Figure 6.6). The confocal images show green fluorescently-labeled nanoparticles internalized within the red WGA Alexa Fluor 594 conjugate-stained membrane. Cells without green fluorescently-labeled nanoparticles show negligible green fluorescence (see Figure 6.7).

6.3.5 Transfection with AllStars Death siRNA

The dependence of knockdown on the concentration of polycationic nanoparticles and siRNA was determined by transfection of RAW264.7 cells with AllStars Death siRNA followed by an MTS assay to evaluate viability. RAW264.7 cells were transfected with 0.05 mg/ml, 0.025 mg/ml, 0.0125 mg/ml, and 0 mg/ml polycationic nanoparticles with 200 nM, 100 nM, 50 nM, 10 nM, and 0 nM siRNA (AllStars Death or scrambled). For the two higher concentrations of polycationic nanoparticles (0.05 mg/ml and 0.025 mg/ml), knockdown was observed for all four (non-zero) concentrations of siRNA (see Figure 6.8). Higher concentrations of nanoparticles and siRNA was associated with increased knockdown.

Knockdown was also observed with 0.0125 mg/ml polycationic nanoparticles at the siRNA concentrations of 200 nM, 100 nM, and 50 nM (32%, 35%, 34%, respectively) (see Figure 6.9). Surprisingly, a small but statistically significant percentage of knockdown (<20% knockdown, $p<0.02$) was observed for the highest concentration (200 nM) of naked siRNA. Although surprising because naked siRNA is not efficiently taken-up by cells, early siRNA experiments and clinical trial attempts used naked siRNA without a carrier vehicle and saw sufficient knockdown to motivate further studies.[29] Transfection with Lipofectamine/siRNA complexes failed to result in statistically significant knockdown; the polycationic nanoparticles outperformed the commercially available transfection agent Lipofectamine under the experimental conditions tested (see Figure 6.10).

6.4 Conclusions

A polycationic nanoparticle siRNA carrier was investigated for siRNA delivery to RAW264.7 cell. The polycationic nanoparticle efficiently bound siRNA for polymer/siRNA mass ratios less than 1. Dynamic light scattering indicated that siRNA binding was associated with a decreased diameter but no significant change to the zeta potential. Internalization of fluorescently-labeled nanoparticles was confirmed using confocal microscopy, and flow cytometry indicated that nanoparticle uptake increased with nanoparticle concentration and with incubation time. Knockdown experiments using AllStars Death siRNA and RAW264.7 cells demonstrated increasing knockdown efficiency for higher concentrations of polycationic nanoparticles and siRNA, and this proof of knockdown may motivate additional studies of this siRNA delivery vehicle.

6.5 Tables

Table 6.1: Delivery of siRNA using DEAEMA-containing cationic polymers. B16F10: mouse melanoma, BSC-40: primate kidney epithelial, DMF: dimethylformamide, Dual-Glo: luciferase reporter assay (Promega), EGDMA: ethylene glycol dimethacrylate, FLuc: firefly luciferase, HuH-7: human liver cancer, MSN: mesoporous silica nanoparticles, PEG: poly(ethylene glycol), PEGDMA: PEG dimethacrylate

Carrier	Cell type	siRNA	Ref.
DEAEMA-in-water redox free radical emulsion polymerization with EGDMA cross-linking agent	HuH-7	100 nM GL3 FLuc (Dual-Glo)	[12;30]
DEAEMA with PEGDMA cross-linking agent with redox free radical emulsion polymerization in water	BSC-40	100 nM Cyclophilin B	[14;31]
MSN surface-modified with DEAEMA or DMAEMA polymers, synthesized by free radical polymerization in DMF solvent	B16F10	30 nM GAPDH or luciferase	[18]

Table 6.2: Delivery of siRNA using DMAEMA-containing polymers. B16F10: mouse melanoma, Dual-Glo: luciferase reporter assay (Promega), DMF: dimethylformamide, GFP: green fluorescent protein, HeLa: human cervical cancer, MDA-MB: human breast cancer, MSN: mesoporous silica nanoparticles, nBA: *n*-butyl acrylate, PC3: human prostate cancer, PAA: propylacrylic acid, PEGDMA: PEG dimethacrylate, q-: quaternized with ethyl bromide, RAFT: reversible addition-fragmentation chain-transfer, RLuc: *Renilla* luciferase, S2: fruit fly Schneider 2, VEGF: vascular endothelial growth factor

Carrier	Cell type	siRNA	Ref.
PDMAEMA-*b*-PEG palm-tree-like complexes (solvent-free ATRP) with non-covalent post-PEGylation	PC3	300 nM VEGF	13;32
P(DMAEMA-*b*-(DMAEMA-*co*-PAA-*co*-BMA)) (RAFT in DMF)	HeLa	10-100 nM GAPDH	15;17
Micelles of PDMAEMA-*b*-PCL -*b*-PDMAEMA (RAFT in toluene)	MDA-MB	40 nM GFP	16
	PC3	40 nM VEGF	16
MSN surface-modified with DEAEMA or DMAEMA (free radical polymerization in DMF)	B16F10	30 nM GAPDH/ luciferase	18
Micelles of PEG-*b*-PnBA-*b*-PDMAEMA (ATRP in DMF)	HeLa	30 nM GAPDH	19;21
q-DMAEMA and PEGMA with PEGDMA cross-linking agent (water-in-oil inverse emulsion AGET ATRP)	S2	9 pmol RLuc (Dual-Glo)	20
DMAEMA and PEGMA monomers with EGDMA cross-linking agent (ATRP in methanol/toluene)	S2	90 μM RLuc	23
Micelles of PEG-*b*-P(DMAEMA-*co*-BMA) (RAFT in dioxane)	MDA-MB	100 nM luciferase	22

Table 6.3: Z-average diameter, polydispersity, and zeta potential were measured using dynamic light scattering with a Malvern ZetaSizer NanoZS instrument. Samples were prepared in 0.1x PBS pH 5.5 with 0.0125 mg/ml polymer nanoparticles and varying concentrations of siRNA.

Polymer/ siRNA ratio, g/g	siRNA concentration, nM	Diameter, nm	Zeta potential, mV	PDI
-	0	190.0	25.5	0.270
80	12.5	195.4	25.5	0.277
20	50	193.7	25.2	0.262
5	200	176.3	24.2	0.262
1.25	800	170.7	25.1	0.241

6.6 Figures

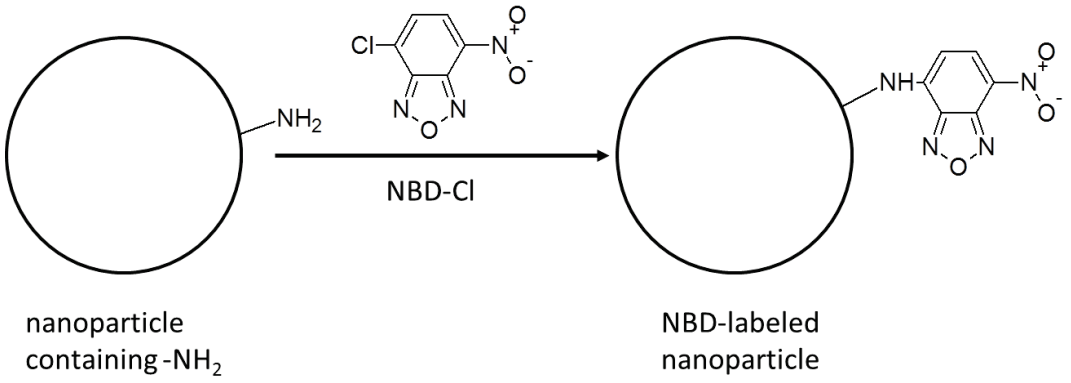

Figure 6.1: Fluorescent labeling of nanoparticles using nanoparticles containing primary amines reacted with 7-chloro-4-nitrobenzo-2-oxa-1,3-diazole (NBD chloride). NBD chloride reacts with primary amines to form fluorescent NBD-amines. Ethanol was used as the solvent. The fluorescent label is covalently attached to the nanoparticle

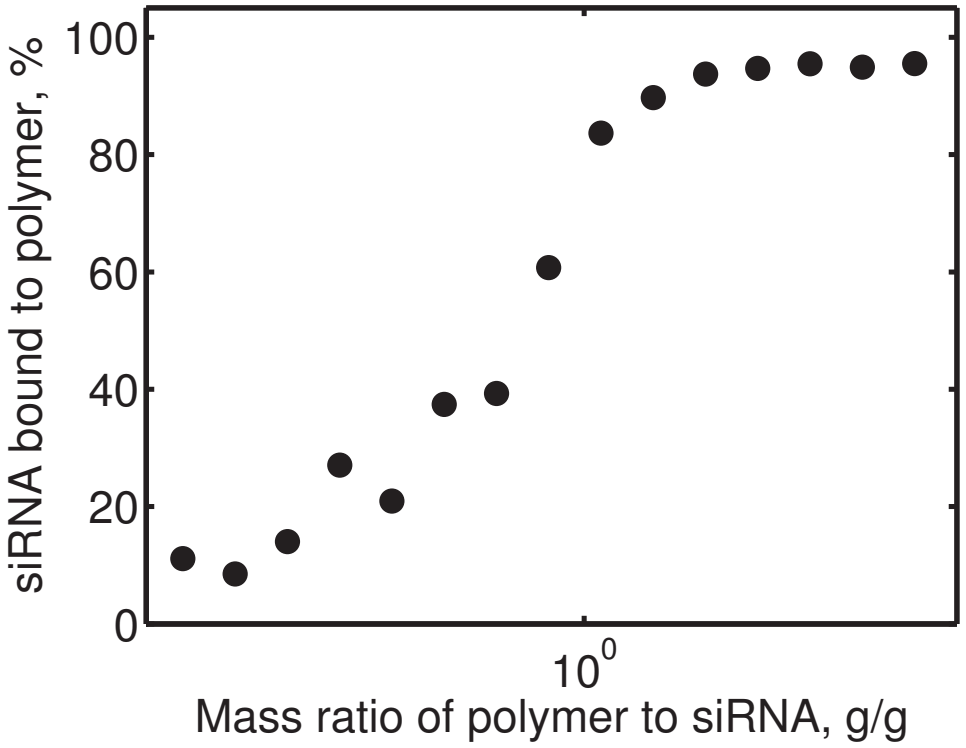

Figure 6.2: Binding curve of siRNA electrostatic binding to polycationic nanoparticles. Free siRNA quantified using a RiboGreen® RNA Assay Kit (fluorescence-based detection). The concentration of siRNA was maintained at 100 nM and the concentration of polycationic nanoparticles was varied to achieve a range of polymer to siRNA ratios.

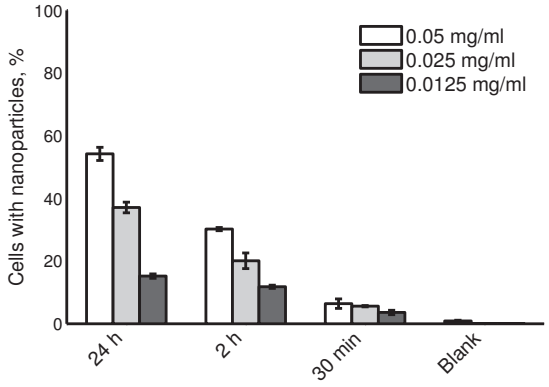

(a) Percent of cells with fluorescently-labeled nanoparticles

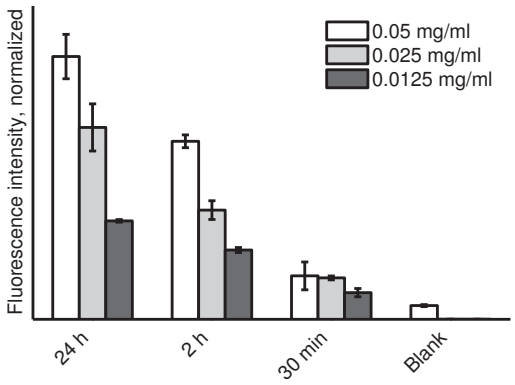

(b) Fluorescence intensity from uptake of fluorescently-labeled nanoparticles

Figure 6.3: Uptake of fluorescently-labeled polycationic nanoparticles at 37 °C by RAW264.7 cells evaluated using flow cytometry. Fluorescently-labeled nanoparticles were added at concentrations of 0.05 mg/ml, 0.025 mg/ml, and 0.0125 mg/ml for incubation times of 24 h, 2 h, and 30 min at 37 °C. The fluorescence intensity was normalized by the fluorescence intensity of the blank sample. All results are reported as the average plus/minus the standard deviation of two replicates as measured using the Accuri flow cytometer and analyzed using the Accuri software.

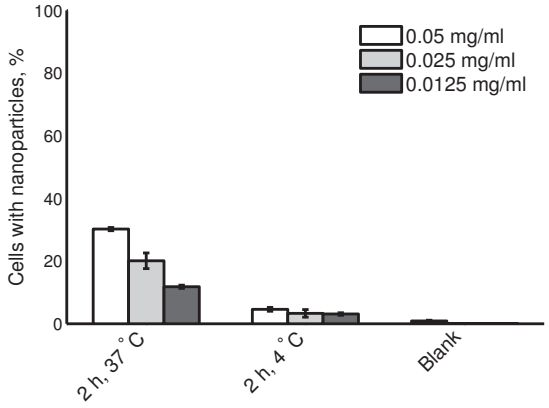

(a) Percent of cells with fluorescently-labeled nanoparticles

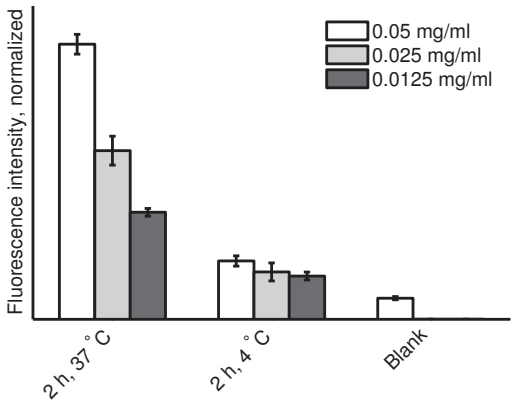

(b) Fluorescence intensity from uptake of fluorescently-labeled nanoparticles

Figure 6.4: Uptake of fluorescently-labeled polycationic nanoparticles by RAW264.7 cells evaluated using flow cytometry. Fluorescently-labeled nanoparticles were added at concentrations of 0.05 mg/ml, 0.025 mg/ml, and 0.0125 mg/ml for 2 h at 4 °C or 37 °C. The fluorescence intensity was normalized by the fluorescence intensity of the blank sample. All results are reported as the average plus/minus the standard deviation of two replicates as measured using the Accuri flow cytometer and analyzed using the Accuri software.

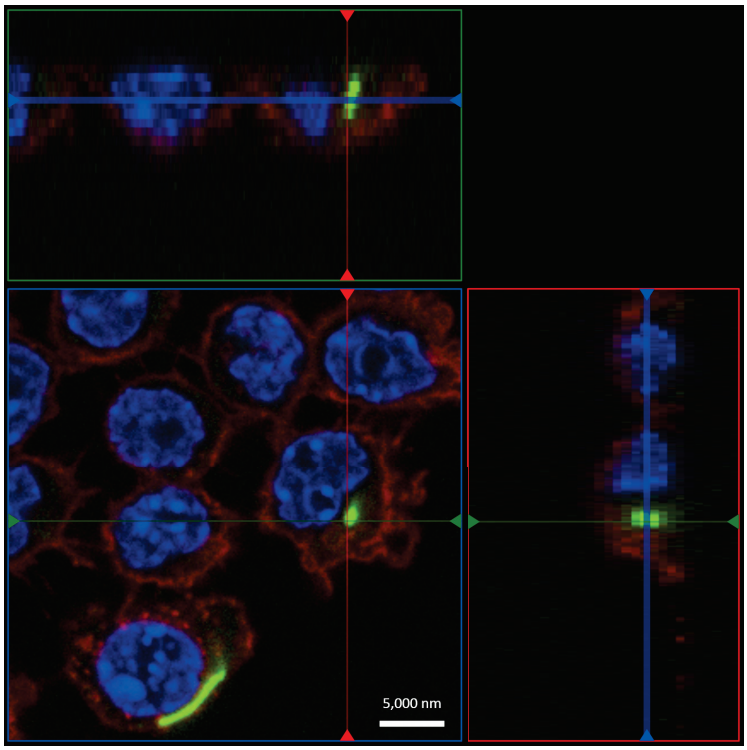

Figure 6.5: Confocal microscopy image of RAW264.7 cells showing internalization of fluorescently-labeled nanoparticles (NBD-NPs). Orthogonal projections represent cross-sectional slices, and they are obtained by taking z-stack images. RAW264.7 cells were incubated with 0.05 mg/ml NBD-NPs for 2 h prior to rinsing, fixing, staining, and mounting. Confocal images were acquired with a Zeiss LSM 710 confocal microscope with a 63x objective. The settings for the green laser were adjusted such that blank cells (no nanoparticles) demonstrated negligible fluorescence. Images were collected in 16 bit format, and all images underwent identical post-processing (γ=0.45 for red, blue, and green channels, γ=1.3 for brightfield, and brightfield scale adjusted to max/min using ZEN Blue). Red: cell membrane stained with Wheat Germ Agglutinin (WGA) Alexa Fluor 594 conjugate, blue: nuclei stained with DAPI, green: fluorescently-labeled nanoparticles

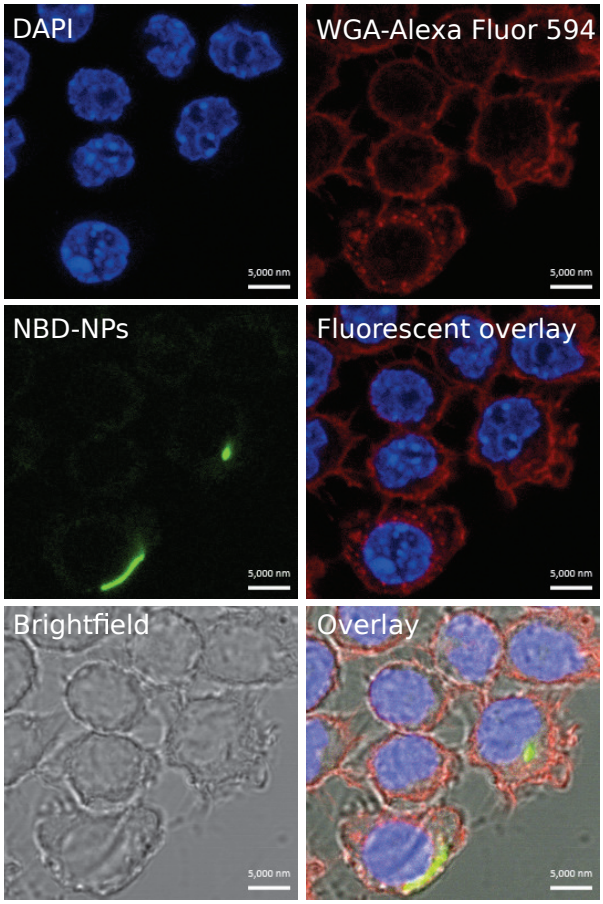

Figure 6.6: Confocal images of cells with fluorescently-labeled nanoparticles (NBD-NPs). RAW264.7 cells were incubated with 0.05 mg/ml NBD-NPs for 2 h prior to rinsing, fixing, staining, and mounting. Confocal images were acquired with a Zeiss LSM 710 confocal microscope with a 63x objective. The settings for the green laser were adjusted such that blank cells (no nanoparticles) demonstrated negligible fluorescence. Images were collected in 16 bit format, and all images underwent identical post-processing (γ=0.45 for red, blue, and green channels, γ=1.3 for brightfield, and brightfield scale adjusted to max/min using ZEN Blue). Red: cell membrane stained with Wheat Germ Agglutinin (WGA) Alexa Fluor 594 conjugate, blue: nuclei stained with DAPI, green: fluorescently-labeled nanoparticles

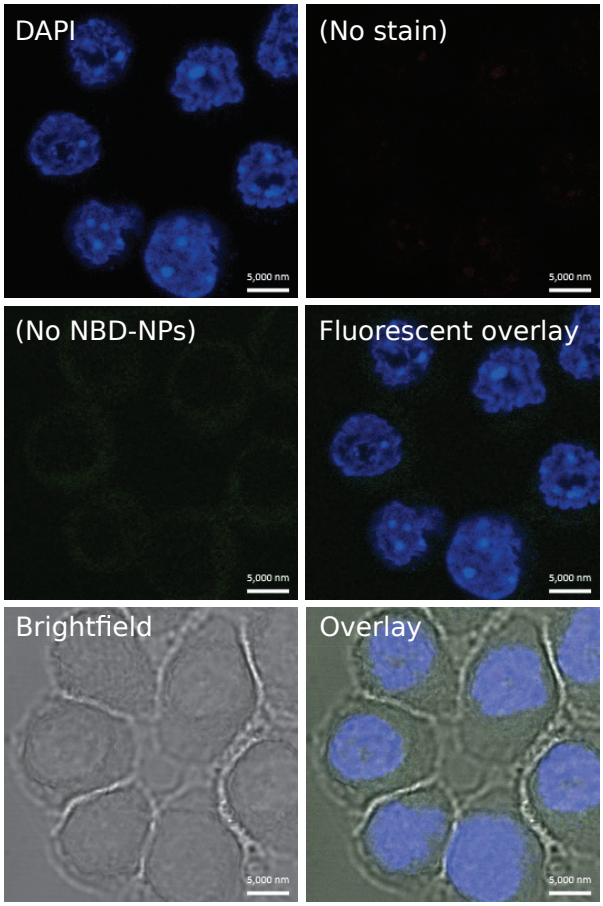

Figure 6.7: Confocal images of blank cells without green fluorescently-labeled nanoparticles (no NBD-NPs) and without red fluorescent membrane stain. Confocal images were acquired with a Zeiss LSM 710 confocal microscope with a 63x objective. The settings for the green laser were adjusted such that blank cells (no nanoparticles) demonstrated negligible fluorescence. Images were collected in 16 bit format, and all images underwent identical post-processing (γ=0.45 for red, blue, and green channels, γ=1.3 for brightfield, and brightfield scale adjusted to max/min using ZEN Blue). Blue: nuclei stained with DAPI

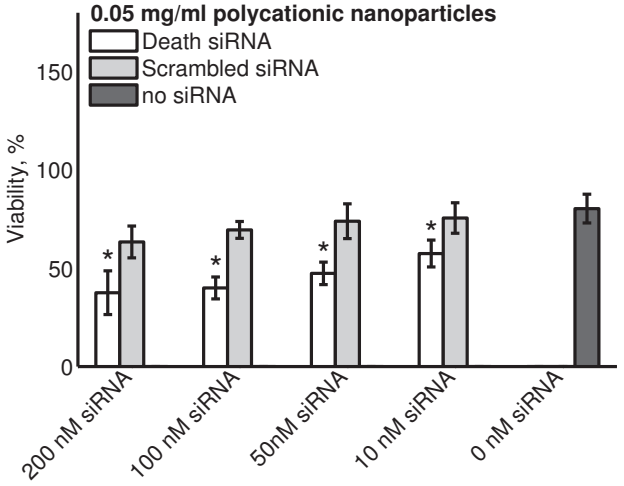

(a) 0.05 mg/ml polycationic nanoparticles

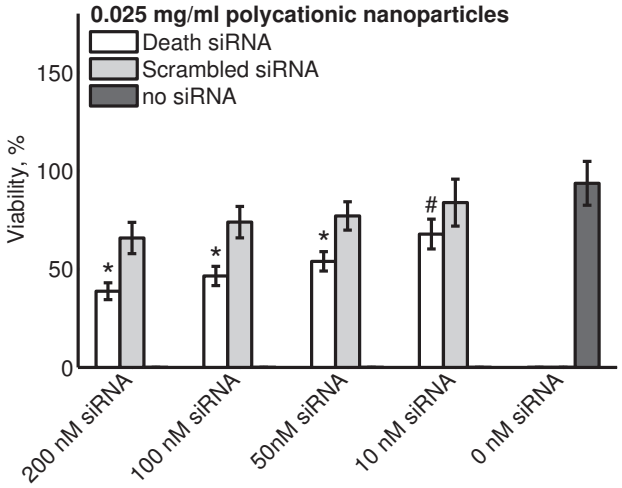

(b) 0.025 mg/ml polycationic nanoparticles

Figure 6.8: Knockdown dependence on polycationic nanoparticle and siRNA concentration. Death siRNA (AllStars Mm/Tn Cell Death) and Scrambled siRNA (negative control) were delivered to RAW264.7 with varying concentrations of polycationic nanoparticle carrier. Following 48 incubation, viability was evaluated using an MTS assay. Asterisk (*) indicates $p<0.003$ and pound sign (#) indicates $p<0.03$.

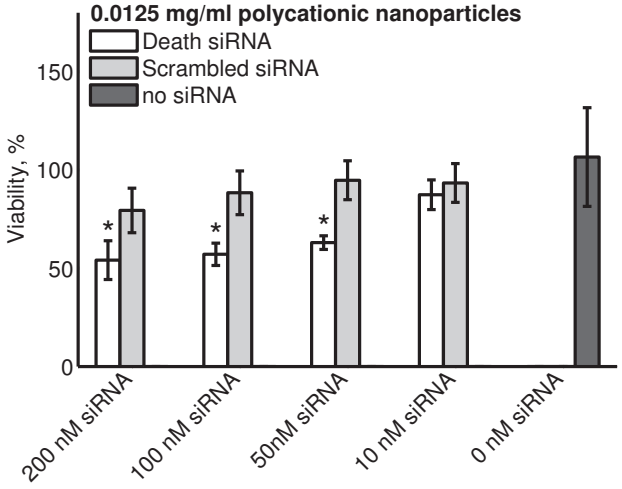

(a) 0.0125 mg/ml polycationic nanoparticles

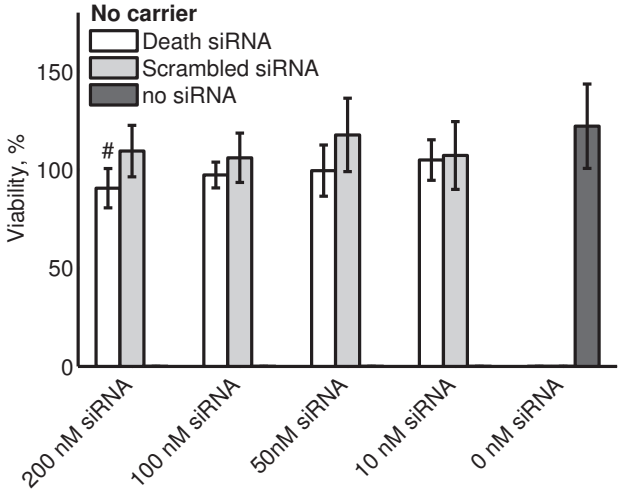

(b) No-carrier, siRNA-only

Figure 6.9: Knockdown dependence on polycationic nanoparticle and siRNA concentration. Death siRNA (AllStars Mm/Tn Cell Death) and Scrambled siRNA (negative control) were delivered to RAW264.7 with varying concentrations of polycationic nanoparticle carrier (0.0125 mg/ml or 0 mg/ml). Following 48 incubation, viability was evaluated using an MTS assay. Asterisk (*) indicates $p<0.003$ and pound sign (#) indicates $p<0.03$.

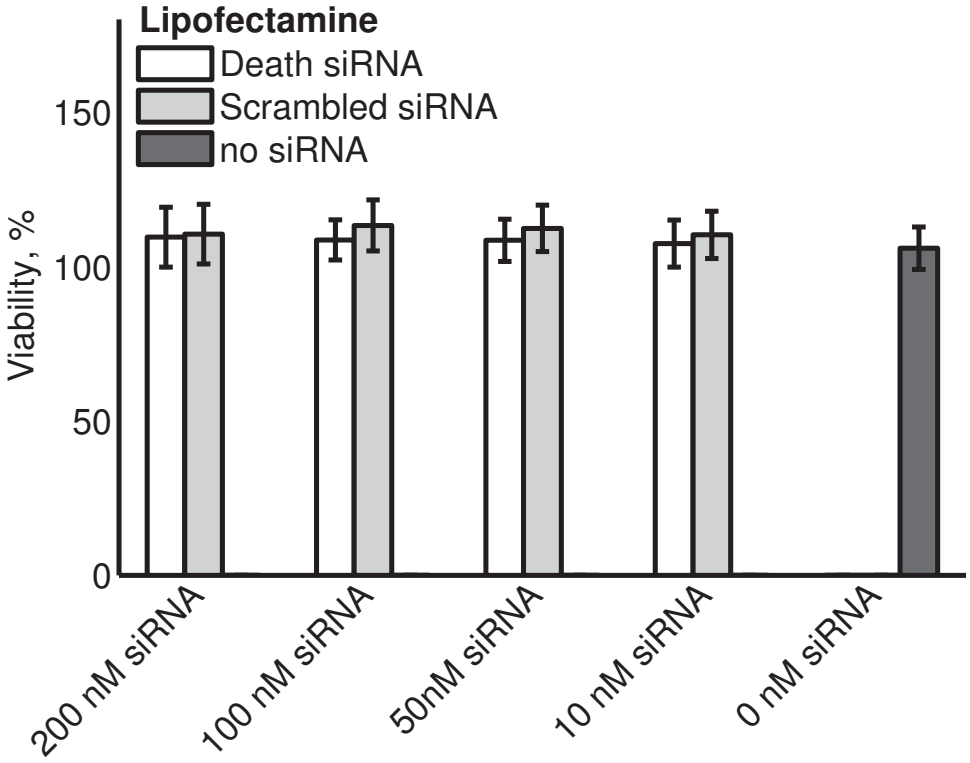

(a) Lipofectamine control

Figure 6.10: Knockdown dependence on polycationic nanoparticle and siRNA concentration. Death siRNA (AllStars Mm/Tn Cell Death) and Scrambled siRNA (negative control) were delivered to RAW264.7 with Lipofectamine. Following 48 incubation, viability was evaluated using an MTS assay.

6.7 References

[1] P. van de Wetering, J. Cherng, H. Talsma, D. J. A. Crommelin, and W. E. Hennink. 2-(Dimethylamino) ethyl methacrylate based (co) polymers as gene transfer agents. *J. Control. Release*, 53(1):145–153, 1998.

[2] X. Jiang, M. C. Lok, and W. E. Hennink. Degradable-brushed pHEMA–pDMAEMA synthesized via ATRP and click chemistry for gene delivery. *Bioconjugate Chem.*, 18(6):2077–2084, 2007.

[3] Y. Qiao, Y. Huang, C. Qiu, X. Yue, L. Deng, Y. Wan, J. Xing, C. Zhang, S. Yuan, A. Dong, and J. Xu. The use of PEGylated poly [2-(N, N-dimethylamino) ethyl methacrylate] as a mucosal DNA delivery vector and the activation of innate immunity and improvement of HIV-1-specific immune responses. *Biomaterials*, 31(1):115–123, 2010.

[4] A. Schallon, V. Jérôme, A. Walther, C.V. Synatschke, A.H.E. Müller, and R. Freitag. Performance of three PDMAEMA-based polycation architectures as gene delivery agents in comparison to linear and branched PEI. *React. Funct. Polym.*, 70(1):1–10, 2010.

[5] F. Dai, P. Sun, Y. Liu, and W. Liu. Redox-cleavable star cationic PDMAEMA by arm-first approach of ATRP as a nonviral vector for gene delivery. *Biomaterials*, 31(3):559–569, 2010.

[6] S. Guo, Y. Huang, T. Wei, W. Zhang, W. Wang, D. Lin, X. Zhang,

A. Kumar, Q. Du, and J. Xing. Amphiphilic and biodegradable methoxy polyethylene glycol-block-(polycaprolactone-graft-poly(2-(dimethylamino)ethyl methacrylate)) as an effective gene carrier. *Biomaterials*, 32(3):879–889, 2011.

[7] C. V. Synatschke, A. Schallon, V. Jérôme, R. Freitag, and A. H. E. Müller. Influence of polymer architecture and molecular weight of poly (2-(dimethylamino) ethyl methacrylate) polycations on transfection efficiency and cell viability in gene delivery. *Biomacromolecules*, 12(12): 4247–4255, 2011.

[8] J. H. Tan, N. A. J. McMillan, E. Payne, C. Alexander, F. Heath, A. K. Whittaker, and K. J. Thurecht. Hyperbranched polymers as delivery vectors for oligonucleotides. *J. Polym. Sci., Part A: Polym. Chem.*, 50 (13):2585–2595, 2012.

[9] Y. Zhang, M. Zheng, T. Kissel, and S. Agarwal. Design and biophysical characterization of bioresponsive degradable poly(dimethylaminoethyl methacrylate) based polymers for in vitro DNA transfection. *Biomacromolecules*, 13:313–322, 2012.

[10] A. P. Majewski, A. Schallon, V. Jérôme, R. Freitag, A. H. E. Müller, and H. Schmalz. Dual-responsive magnetic core–shell nanoparticles for nonviral gene delivery and cell separation. *Biomacromolecules*, 13(3): 857–866, 2012.

[11] Yi Zhang, Achim Aigner, and Seema Agarwal. Degradable and biocompatible poly (*N, N*-dimethylaminoethyl methacrylate-co-caprolactone) s as dna transfection agents. *Macromol. Biosci.*, 13(9):1267–1275, 2013.

[12] A. Tamura, M. Oishi, and Y. Nagasaki. Enhanced cytoplasmic delivery of siRNA using a stabilized polyion complex based on PEGylated nanogels with a cross-linked polyamine structure. *Biomacromolecules*, 10(7):1818–1827, 2009.

[13] W. Kong, D. Sung, Y. Shim, K. H. Bae, P. Dubois, T. G. Park, J. Kim, and S. Seo. Efficient intracellular siRNA delivery strategy through rapid and simple two steps mixing involving noncovalent post-PEGylation. *J. Control. Release*, 138(2):141–147, 2009.

[14] Y. Hu, P. U. Atukorale, J. J. Lu, J. J. Moon, S. H. Um, E. C. Cho, Y. Wang, J. Chen, and D. J. Irvine. Cytosolic delivery mediated via electrostatic surface binding of protein, virus, or siRNA cargos to pH-responsive core- shell gel particles. *Biomacromolecules*, 10(4):756–765, 2009.

[15] A.J. Convertine, D.S.W. Benoit, C.L. Duvall, A.S. Hoffman, and P.S. Stayton. Development of a novel endosomolytic diblock copolymer for siRNA delivery. *J. Control. Release*, 133(3):221–229, 2009.

[16] C. Zhu, S. Jung, S. Luo, F. Meng, X. Zhu, T. G. Park, and Z. Zhong. Co-delivery of siRNA and paclitaxel into cancer cells by biodegradable

cationic micelles based on PDMAEMA-PCL-PDMAEMA triblock copolymers. *Biomaterials*, 31(8):2408–2416, 2010.

[17] A. J. Convertine, C. Diab, M. Prieve, A. Paschal, A. S. Hoffman, P. H. Johnson, and P. S. Stayton. pH-responsive polymeric micelle carriers for siRNA drugs. *Biomacromolecules*, 11(11):2904–2911, 2010.

[18] S. R. Bhattarai, E. Muthuswamy, A. Wani, M. Brichacek, A. L. Castañeda, S. L. Brock, and D. Oupicky. Enhanced gene and siRNA delivery by polycation-modified mesoporous silica nanoparticles loaded with chloroquine. *Pharm. Res.*, 27(12):2556–2568, 2010.

[19] D. J. Gary, H. Lee, R. Sharma, J. Lee, Y. Kim, Z. Y. Cui, D. Jia, V. D. Bowman, P. R. Chipman, L. Wan, Y. Zou, G. Mao, K. Park, B. Herbert, S. F. Konieczny, and Y. Y. Won. Influence of nano-carrier architecture on in vitro siRNA delivery performance and in vivo biodistribution: polyplexes vs micelleplexes. *ACS Nano*, 5(5):3493–3505, 2011.

[20] S.E. Averick, E. Paredes, A. Irastorza, A. Srinivasan, D.J. Siegwart, A.J.D. Magenau, H.Y. Cho, A.R. Shrivats, E. Hsu, J. Kim, et al. Preparation of cationic nanogels for nucleic acid delivery. *Biomacromolecules*, (11):3445–3449, 2012.

[21] D. J. Gary, J. Min, Y. Kim, K. Park, and Y. Y. Won. The effect of N/P ratio on the in vitro and in vivo interaction properties of PEGylated Poly [2-(dimethylamino) ethyl methacrylate]-based siRNA complexes. *Macromol. Biosci.*, 13(8):1059–1071, 2013.

[22] C. E. Nelson, J. R. Kintzing, A. Hanna, J. M. Shannon, M. K. Gupta, and C. L. Duvall. Balancing cationic and hydrophobic content of PEGylated siRNA polyplexes enhances endosome escape, stability, blood circulation time, and bioactivity in vivo. *ACS Nano*, 7(10):8870–8880, 2013.

[23] H. Y. Cho, S. E. Averick, E. Paredes, K. Wegner, A. Averick, S. Jurga, S. R. Das, and K. Matyjaszewski. Star polymers with a cationic core prepared by ATRP for cellular nucleic acids delivery. *Biomacromolecules*, 14(5):1262–1267, 2013.

[24] H. M. Aliabadi, B. Landry, C. Sun, T. Tang, and H. Uludağ. Supramolecular assemblies in functional siRNA delivery: Where do we stand? *Biomaterials*, 33(8):2546–2569, 2012.

[25] J. Carralot, T. Kim, B. Lenseigne, A. S. Boese, P. Sommer, A. Genovesio, and P. Brodin. Automated high-throughput siRNA transfection in raw 264.7 macrophages: a case study for optimization procedure. *J. Biomol. Screen.*, 14(2):151–160, 2009.

[26] D. C. Forbes, M. Creixell, H. Frizzell, and N. A. Peppas. Polycationic nanoparticles synthesized using ARGET ATRP for drug delivery. *Eur. J. Pharm. Biopharm.*, 84(3):472–478, 2013.

[27] D. C. Forbes and N. A. Peppas. Differences in molecular structure in cross-linked polycationic nanoparticles synthesized using ARGET ATRP or UV-initiated polymerization. *Polymer*, 54(17):4486–4492, 2013.

[28] O. Z. Fisher and N. A. Peppas. Polybasic nanomatrices prepared by UV-initiated photopolymerization. *Macromolecules*, 42(9):3391–3398, 2009.

[29] D. C. Forbes and N. A. Peppas. Oral delivery of small RNA and DNA. *J. Control. Release*, 162(2):438–445, 2012.

[30] H. Hayashi, M. Iijima, K. Kataoka, and Y. Nagasaki. pH-sensitive nanogel possessing reactive PEG tethered chains on the surface. *Macromolecules*, 37(14):5389–5396, 2004.

[31] Y. Hu, T. Litwin, A. R. Nagaraja, B. Kwong, J. Katz, N. Watson, and D. J. Irvine. Cytosolic delivery of membrane-impermeable molecules in dendritic cells using pH-responsive core-shell nanoparticles. *Nano Lett.*, 7(10):3056–3064, 2007.

[32] S. Pirotton, C. Muller, N. Pantoustier, F. Botteman, S. Collinet, C. Grandfils, G. Dandrifosse, P. Degée, P. Dubois, and M. Raes. Enhancement of transfection efficiency through rapid and noncovalent post-PEGylation of poly (dimethylaminoethyl methacrylate)/DNA complexes. *Pharm. Res.*, 21(8):1471–1479, 2004.

Chapter 7

Differences in Molecular Structure in Cross-linked Polycationic Nanoparticles Synthesized using ARGET ATRP or UV-initiated Polymerization

7.1 Introduction

Hydrogel nanoparticles and microparticles (nanogels and microgels, respectively) are "physically or chemically cross-linked polymer networks."[1] The increased stability imparted by the cross-linking (compared to self-assembled systems without cross-linking) is important for applications in complex environments (such as physiological fluids with proteins, amino acids, and vitamins).[2] On a microscopic scale, nanogels and microgels "behave much like a conventional hydrogel" in that they can be described by their swelling behavior.[3] There has been much interest in nanogels and microgels for applications such as biomaterials for drug delivery,[1;4] analyte detection (sensors),[5] molecularly imprinted polymers,[6] microreactors,[7;8] chemical/biological separations,[9]

cosmetics,[10–12] food,[13;14] and oil recovery.[3]

The broad range of applications for nanogels and microgels is matched by a broader range of creative synthesis strategies. In addition to traditional free radical polymerization, researchers have also pursued controlled polymerizations, such as ATRP-based techniques, that make it possible to synthesize new types of molecular architecture, such as shell cross-linked micelles assembled from block copolymers. Sometimes the advantages of a new polymerization technique may not come from a new architecture; sometimes an easier route can be more valuable than a new destination. Reverse ATRP techniques such as ARGET ATRP[15–17] use copper(II) catalysts, which are less oxygen-sensitive than the copper(I) catalysts used in forward ATRP techniques such as traditional ATRP. In applications where it is difficult to remove or control the quantity of oxygen, such as miniemulsion polymerization where the high shear mixing (e.g. sonication) tends to entrain air, reverse ATRP can yield better control than forward ATRP[18]. Adapting traditional polymerizations to new controlled techniques may yield advantages in processing while also providing an opportunity to look at the role of heterogeneity in material properties.

An improved understanding of molecular structure, and its connection to synthesis techniques and material properties, may facilitate the design of enhanced materials for a range of applications. Nanoscale heterogeneity, such as heterogeneity of network cross-linking density, hydrophobic component clustering, or local collapse of thermoresponsive macromolecules,[19] is an important aspect of molecular structure because heterogeneity within particles leads to

broad transitions. The "continuous" (rather than discontinuous) transition is a "summation"[9] or "convolution of many transitions"[20] where each contribution has its own characteristic transition. Likewise, heterogeneity within the population of particles also tends to broaden transitions, in the same way that a polydisperse population of linear PNIPAm has a broad transition.[21] Controlled radical polymerizations may reduce heterogeneity compared to traditional free radical polymerization; for example, assuming equal reactivity of monomer and cross-linking agent, densely cross-linked regions resulting from intramolecular cross-linking may form in traditional free radical polymerization but not in controlled radical polymerization where the slower reaction kinetics permit time for chain diffusion and relaxation prior to propagation.[7]

There is no shortage of reports using complex polymer chemistries to make advanced materials, such as pH-responsive nanoparticles for therapeutic delivery, but there are few reports comparing the new techniques to well-established UV-initiated polymerizations. A previous report comparing a panel of polycationic nanoparticles synthesized using ARGET ATRP or UV-initiated polymerization[22] for drug delivery applications prompted interest in elucidating the underlying molecular structural differences responsible for differences in material properties. This report examines the effect of polymerization method on material properties and the connection to molecular structure.

7.2 Materials and methods

7.2.1 Materials

Poly(ethylene glycol) methyl ether methacrylate (PEGMA) solution (M_n 2000 for PEG chain, 50 wt% in water), 2-(diethylamino)ethyl methacrylate (DEAEMA), *tert*-butyl methacrylate (tBMA), tetraethylene glycol dimethacrylate (TEGDMA), ethyl 2-bromoisobutyrate (EBIB), tris (2-pyridylmethyl) amine (TPMA), myristyltrimethylammonium bromide (MyTab), and ascorbic acid (AA) were purchased from Sigma-Aldrich.

1 N Hydrochloric acid (HCl) was purchased from Fisher Scientific; Brij-30®, copper(II) bromide, and D_2O were purchased from Acros Organics; and Irgacure 2959 was purchased from Ciba Specialty Chemicals Corp. Ultrapure water was used for all studies. All chemicals were used as received.

7.2.2 Synthesis and purification

P(DEAEMA-*co*-tBMA-*co*-PEGMA-*co*-TEGDMA) cross-linked polymer nanoparticles were synthesized using a previously reported ARGET ATRP technique[22] or a UV-initiated polymerization previously developed by Fisher and colleagues.[23] Briefly, reagents DEAEMA:PEGMA:TEGDMA:$CuBr_2$:TPMA:EBIB at molar ratios of 100:10:4:0.5:0.5:4 (with tBMA with a molar ratio of 30 or 45 depending on the formulation) were combined with 8 mg/ml Brij® 30 and 1.35 mg/ml MyTab in water for a 0.1 weight ratio of monomer to solvent. For the UV-initiated

polymerization, Irgacure® 2959 was added at a 0.005 weight ratio initiator to monomer in place of $CuBr_2$:TPMA:EBIB. Following probe sonication (S-4000 Misonix Ultrasonicator) and nitrogen purge, the ARGET ATRP and UV-initiated polymerizations were reacted at ambient temperature for 3 h by the addition of degassed ascorbic acid solution as a reducing agent (AA:DEAEMA::0.5:100) or for 2.5 h by exposure to UV light (Dymax BlueWave™200 UV), respectively. Previous work indicates that monomers like DEAEMA can act as an intrinsic reducing agent, but good control in the presence of residual air is achieved after addition of an external reducing agent such as ascorbic acid.[24] Purification was done by a technique described previously by Fisher and Peppas[25] with repeated precipitation/resuspension with acetone/0.5 N HCl. Following dialysis, polymer was recovered by freeze-drying.

P(DEAEMA-*co*-tBMA-*co*-PEGMA) linear polymer chains made without TEGDMA (linear analogs) were synthesized as described previously for cross-linked polycationic nanoparticles except that TEGDMA was omitted. The feed ratio of tBMA is identified in the formulation name (e.g. 30UV and 30ARGET have 30 mol tBMA per 100 mol DEAEMA in the feed); likewise, the synthesis technique (UV or ARGET ATRP) is also indicated in the formulation name. As much as possible, parameters were kept constant across reactions to permit direct comparison.

7.2.3 Instrumentation

Cross-linked nanoparticles and linear analogs were characterized with ^{1}H NMR (nuclear magnetic resonance). Dried polymer was dissolved in D_2O at approximately 25-30 mg/ml. Spectra were obtained using a Varian DirectDrive 400 MHz Nuclear Magnetic Resonance Spectrometer equipped with an automatic sampler and analyzed using SpinWorks 3™ software. The integrated intensity of the DEAEMA 1.17 ppm methyl peak was compared to the oxyethylene proton peak from PEGMA at 3.55 ppm and the *tert*-butyl peak from tBMA at 1.31 ppm. The PEGMA content was corrected by subtracting the contribution from the unreacted PEGMA estimated from the double bond peak at 6.02.

The FTIR spectra were recorded using a Nicolet Avatar 360 FTIR. In all cases, background spectra were subtracted from the sample spectra.

Molecular weight and polydispersity data were collected on an Agilent 1200 Series Iso Pump and Autosampler with an Agilent Technologies 1100 RI detector. One PLgel 5 µm, 100 Å column and one PLgel 5 µm, 10,000 Å column were used with 0.01 M lithium bromide (LiBr) in dimethylformamide (DMF) eluent at 70 °C and a flow rate of 1 ml/min. The elution times were compared to nine poly(methyl methacrylate) (PMMA) standards (1660, 2200, 4250, 6370, 12600, 23500, 41400, 89300, and 201000 Da), which were used to calibrate the instrument by refractive index response (conventional calibration).

The thermal stability of the samples was determined using thermal gravimetric analysis (Mettler-Toledo TGA/DSC 1). A 6-8 mg sample of each polymer was packed tightly into an aluminum oxide crucible. The experiments were performed under nitrogen or air with a heating rate of 10 °C/min from 40 °C to 600 °C.

Thermal transition temperatures were determined using a differential scanning calorimeter (DSC) (Mettler-Toledo DSC1). A 5-10 mg sample of each polymer was packed tightly in an aluminum DSC pan with a 0.1 mm hole in the lid. The samples were dried overnight in a vacuum oven at 30-50 °C. Samples were annealed at 130 °C prior to running DSC to erase the thermal history; the temperature of 130 °C was selected to minimize thermal cleavage of the *tert*-butyl ester linkage.[26] Samples were then cooled to -65 °C before heating to 150 °C. All DSC runs were performed under nitrogen gas atmosphere with 10 °C/min heating rate and 5 °C/min cooling rate.

7.3 Results and discussion

Polycationic nanoparticles (see Figure 7.1) were synthesized with two different feed ratios of hydrophobic monomer tBMA using both ARGET ATRP and UV-initiated polymerization (see Table 7.1). P(DEAEMA-*co*-tBMA-*co*-PEGMA-*co*-TEGDMA) polycationic nanoparticles are statistical copolymers, which means the composition is a function of the feed, but unlike truly random copolymers, the polymer composition is not identical to the feed. The four dif-

ferent formulations demonstrate the effects of composition and synthesis technique on molecular structure and material properties. Linear P(DEAEMA-*co*-tBMA-*co*-PEGMA) chains (analogs of the polycationic nanoparticles, synthesized by omitting the TEGDMA cross-linking agent) were analyzed with GPC and NMR . All other characterization was done using the polycationic nanoparticles.

7.3.1 Polymer composition verified using NMR and FTIR

NMR and FTIR were used to verify that the monomers DEAEMA, tBMA, and PEGMA were incorporated into the polymerization. The polymer composition was evaluated using P(DEAEMA-*co*-tBMA-*co*-PEGMA) linear polymer chains made without TEGDMA; see Figure 7.3 for a schematic of the chemical structure corresponding to peak labeling. NMR spectra indicate that the UV-initiated formulations have greater incorporation of PEGMA and tBMA than the corresponding ARGET ATRP formulations (see Figure 7.4a and Table 7.2). Increased conversion for UV-initiated polymerizations could explain the difference in PEGMA and tBMA incorporation; the Q-e scheme predicts a preference for DEAEMA incorporation at low conversions so that more PEGMA would be incorporated at later times (higher conversion).[27] Reactivity ratios r_1 and r_2 (seem Table 7.3) are calculated using tabulated Q-e values (equation 7.1 and equation 7.2).

$$r_1 = \frac{k_{11}}{k_{12}} = \frac{Q_1}{Q_2} \exp\left(-e_1\left(e_1 - e_2\right)\right) \tag{7.1}$$

$$r_2 = \frac{k_{22}}{k_{21}} = \frac{Q_2}{Q_1} \exp\left(-e_2\left(e_2 - e_1\right)\right) \tag{7.2}$$

The cross-linking has a significant impact on the spectra; the peaks are broadened significantly for the polycationic nanoparticles compared to the linear analogs (see Figure 7.4). The strong peak associated with the PEG oxyethylene protons in the cross-linked spectra suggests a surface brush layer of solvated PEG chains. FTIR spectroscopy studies verified the presence of the methacrylate carboxyl group and the C-N bonds corresponding to the DEAEMA (see Figure 7.5).

7.3.2 Evaluate molecular weight distribution of linear polymer chains using GPC

Gel permeation chromatography (GPC) analysis was used to analyze P(DEAEMA-*co*-tBMA-*co*-PEGMA) linear polymer chains made without TEGDMA to gain insight into the molecular weight distribution of the polymer chains in the cross-linked polycationic nanoparticles (Figure 7.6). The molecular weight and polydispersity index (PDI) were determined using conventional calibration, so values are reported as PMMA equivalents (Table 7.4). The ARGET ATRP formulations have a different curve shape than the UV-initiated formulations; the UV-initiated formulations have a single broad peak

with a shallow shoulder while the ARGET ATRP formulations have a narrow peak with a trailing shoulder. Focusing on the main peak, the PMMA equivalent PDI of the ARGET ATRP formulations is smaller than for the UV-initiated formulations. The narrower main peak is the expected result for a controlled polymerization such as ARGET ATRP rather than an uncontrolled polymerization such as the UV-initiated polymerization. This result for the linear chains suggests a narrower distribution of main chain length for the ARGET ATRP polycationic nanoparticles.

The narrower distribution of molecular weight may explain the previously reported sharper pH-responsive swelling transition for the ARGET ATRP formulations compared to the UV-initiated formulations.[22] Narrower molecular weight distributions have been associated with sharper thermoresponsive transitions in linear PNIPAm while broad molecular weight distributions result in broad transitions,[21] so it seems probable that similar effects may occur in pH-responsive transitions.

The molecular weight distribution of the linear chains is an incomplete picture of molecular structure because it does not provide insight into the cross-linking distribution, which is another important factor in nanoscale heterogeneity contributing to broad transitions.[19] Oh and associates[28] attributed increased swelling ratios of nanogels to increased cross-linking homogeneity with their poly(oligo(ethylene glycol) monomethyl ether methacrylate) (POEOMA) nanogels with a disulfide-methacrylate cross-linking agent synthesized using AGET (activators generated by electron transfer) ATRP or conventional rad-

ical polymerization. Oh and associates found that the AGET ATRP nanogels demonstrated greater swelling (weight swelling ratio of 28.5 in water) than the conventional radical polymerization nanogels (weight swelling ratio of 16.2 in water). In contrast, the P(DEAEMA-*co*-tBMA-*co*-PEGMA-*co*-TEGDMA) polycationic nanoparticles synthesized using both methods had comparable swelling (see Forbes et al.[22] for dynamic light scattering and transmission electron microscopy data), which may indicate the ARGET ATRP did not result in improved cross-linking homogeneity for the polycationic nanoparticles.

7.3.3 Thermal gravimetric analysis (TGA)

The TGA thermal profile describes the degradation behavior of the polymer in air and nitrogen and may also give insights into the polymer composition. Consideration of degradation behavior is particularly important for sample handling during analysis and when considering the use of heat-based processing or sterilization. TGA results in nitrogen atmosphere (Figure 7.7 and Table 7.5) show a small initial weight loss from evaporating water followed by a first degradation step, and then a temperature range without additional degradation followed by a final degradation step. The first weight loss (~40%) occurs from 205 °C - 274 °C, there is negligible weight loss from 274 °C - 402 °C, and the final weight loss (~40%) occurs from 402 °C - 450 °C with negligible additional weight loss at temperatures above 450 °C. The rate of weight loss is the same for the different formulations.

The observed weight loss following the first degradation step is depen-

dent on the feed ratio of tBMA; formulations 30UV and 30ARGET have 48.8 wt% and 48.5 wt% remaining following the initial degradation while 45UV and 45ARGET have 51.6 wt% and 51.1 wt% remaining. This two step degradation is consistent with the two-step degradation profile of methacrylate polymers such as PtBMA[29;30] with the first step consisting of the loss of the ester group,[26;31] and at least in the case of the *tert*-butyl ester, possible formation of an anhydride cross-linking between deprotected acid groups by removing a water molecule.[26] There are also trends in the final weight percent remaining: i) all of the ARGET formulations have a higher remaining weight percent than the UV formulations and ii) increased tBMA content results in a weight percent remaining. Unfortunately, since the range of degradation temperatures for PDEAEMA and PPEGMA (250 ^{o}C - 500 ^{o}C[32] and 75 ^{o}C - 450 ^{o}C[33], respectively) overlaps with the region of PtBMA degradation, it is difficult to translate the curves to quantitative data. Also, since the differences in composition are subtle, the resulting differences in the thermal profile are also subtle.

The differences are even more subtle for the TGA thermogram in air atmosphere (see Figure 7.8). As for the nitrogen atmosphere, each sample experiences a small initial weight loss from evaporating water, followed by a first degradation step. A close look at the derivative plot (rate of weight loss) indicates at least 4 separate degradation steps for the formulations with tBMA, compared to 3 degradation steps for the formulation without tBMA.

7.3.4 Differential scanning calorimeter (DSC)

DSC provides additional information about the thermal properties of the polymer, and it can also be used to infer details about molecular structure such as domains or crystallization. The DSC thermograms for the four different polymer nanoparticle formulations are shown in Figure 7.9. There are two main differences in the UV and the ARGET formulations: i) the presence of a melting peak for the UV but not for the ARGET formulations and ii) a sharper glass transition for the ARGET than for the UV. The glass transition behavior appears to be strongly influenced by the presence of tBMA; if the tBMA is eliminated from the formulation (as in 00ARGET), the resulting thermogram shows a broader, sloping decline in contrast to the clearly defined transition for 30ARGET and 45ARGET (see Figure 7.10).

The 30UV and 45UV formulation demonstrate an endothermic effect at 24 °C which can be attributed to the melting of crystallites resulting from PEG-rich regions containing more than 50% PEG by volume.[34] As with other copolymers,[34–36] the melting temperature for the crystalline PEG domains is less than that of the PEG homopolymer (54 °C[34]) or the PEGMA macromonomer (58 °C from the measured thermal profile of PEGMA, see Figure 7.11). The crystalline regions likely form by segregation rather than by chain folding since the PEG regions will be distributed statistically rather than incorporated as distinct blocks of the polymer backbone.[34] Crystalline regions are not observed for the ARGET formulations, suggesting that the PEG is incorporated with greater homogeneity that cannot phase-separate. Alterna-

tively, a lower incorporation of PEGMA into the polymer structure might also result in an absence of PEG crystallization resulting from insufficient PEG as NMR indicates that the UV-initiated formulations have more incorporated PEGMA than the ARGET ATRP formulations.

Estimating the degree of crystallinity, X_c, for a homopolymer is straightforward; X_c is the ratio between the measured heat of melting and the reported literature values for heat of melting for the 100% crystalline polymer (Equation 7.3). Note that for PEG, $\triangle H_m^0$ values range from 166 to 265 J/g in Brandrup, et al.,[37] with other reported values including 196.8 J/g[38] and 202.41 J/g.[39]

$$X_c = \frac{\triangle H}{\triangle H_m^0} \tag{7.3}$$

For copolymers or polymer blends, evaluating a degree of crystallinity is less straightforward because crystallinity may only exists in domains containing a single component; for the polycationic nanoparticles, the crystallinity is attributed to regions of PEG that were able to crystallize. As a result, crystallinity is an indicator of heterogeneity in the case of the UV-based formulations. The ratio of crystallized PEG to the total PEG requires an additional term; namely, an NMR-determined weight composition ratio (45% and 54% PEG by weight for 30UV-linear and 45UV-linear, respectively) (Equation 7.4 and Table 7.6).

$$X_c = \frac{\triangle H_{m,\,copolymer}}{\triangle H^0_{m,\,PEG}} \times \frac{1}{\frac{m_{PEG}}{m_{copolymer}}} \tag{7.4}$$

The ARGET formulations have sharper glass transitions than the UV-initiated formulations. The high glass transition temperature suggests the presence of tBMA-rich domains since the T_g of PtBMA is 107 °C (compared to 16 °C - 24 °C for PDEAEMA[37;40] and -51 °C for PPEGMA[41]). Despite the sharper transition, closer examination of all the glass transition curves suggests the overall transition is made up of multiple, overlaying glass transition behavior, perhaps from a range of tBMA domains in the nanoparticle population (see Figure 7.12). The separately calculated and overall glass transition temperatures are shown in Table 7.7. The difference in the highest and lowest individual glass transition temperature can serve as a measure of the sharpness of the transition, with a small difference corresponding to a sharper glass transition; UV-initiated formulations have a larger difference in their individual glass transition temperatures than the ARGET ATRP formulations, which demonstrates that the UV-initiated formulations have a less sharp glass transition than the ARGET ATRP formulations.

The sharper glass transition for the ARGET formulations may indicate a narrower size distribution of tBMA-rich domains in contrast to a broader size distribution of tBMA-rich domains in the UV formulations. However, studies using small-angle x-ray scattering of dry and aqueous polycationic nanoparticles to probe molecular structure and orientation did not provide additional

information. The broader distribution for the UV formulations would be consistent with the uncontrolled polymerization reaction where chains are rapidly created and then terminated, such that the composition of each chain would tend to drift with the time of initiation for sufficiently large conversions. In contrast, ARGET ATRP-based reactions impart control by providing for a closer approximation to simultaneous initiation (upon addition of the reducing agent to activate the catalyst), which will result in polymer chains that may each individually have a gradient composition but individual chains in the population will be indistinguishable.

7.3.5 SAXS analysis to investigate the structure of polycationic nanoparticles

SAXS analysis can provide useful information about molecular structure and orientation for structures with highly ordered domains. The SAXS pattern of the dry samples at ambient temperature and at 130 ^{o}C, as well as the aqueous samples, showed scattering at low q values but no distinct peaks (see Figure 7.6 and Figure 7.14). The change in temperature may change not only the structure, but also the x-ray contrast;[34] however, no peaks are present for either ambient or elevated (130 ^{o}C) temperature. The absence of peaks may indicate a) the structure is disordered, b) insufficient x-ray contrast between the domains, c) the domains are too large (greater than ~500 Å) to be detected using SAXS, or d) the domains are too small (less than 5 Å) to be detected using SAXS. Since TEM indicates that dried nanoparticles are on

the order of 50 nm in diameter,[22] it seems most likely that the structure is too disordered, that the domains have low x-ray contrast, or that the domains are too small to detect with SAXS. The crystalline regions compose a small fraction of the total polymer and there is likely a distribution of tBMA-rich regions.

7.4 Conclusion

This work considers the connections among polymerization method, molecular structure, and material properties. Switching from the UV-initiated polymerization to ARGET ATRP resulted in a narrower molecular weight distribution. In addition, a sharper glass transition for the cross-linked nanoparticles was observed, which suggests reduced heterogeneity in tBMA-rich domains. Switching to ARGET ATRP also eliminated a melting endotherm present in the UV-initiated formulations consistent with PEG crystallites. The reduced heterogeneity may explain the discontinuous pH-responsive transitions previously reported for the 30ARGET compared to the continuous transition for 30UV. The sharper transitions present in the ARGET ATRP formulations motivate additional study in responsive materials using this new and potentially powerful chemistry for nanogel applications such as drug delivery.

7.5 Tables

Table 7.1: Guide to formulation nomenclature for the P(DEAEMA-*co*-tBMA-*co*-PEGMA-*co*-TEGDMA) polycationic nanoparticles synthesized with ARGET ATRP or UV-initiated polymerization with 30 or 45 mol tBMA per 100 mol DEAEMA in the feed.

	UV-initiated	ARGET ATRP
30 mol tBMA per 100 mol DEAEMA in the feed	30UV	30ARGET
45 mol tBMA per 100 mol DEAEMA in the feed	45UV	45ARGET

Table 7.2: Molar composition of the feed and the polymer. Polymer composition determined using ^{1}H NMR of the P(DEAEMA-*co*-tBMA-*co*-PEGMA) linear polymer chains made without TEGDMA, which served as linear analogs of the cross-linked nanoparticles.

	mol% in feed			mol% in polymer (from ^{1}H NMR)		
Formulation	tBMA	DEAEMA	PEGMA	tBMA	DEAEMA	PEGMA
30UV - linear	21%	71%	7%	16%	75%	10%
45UV - linear	29%	65%	6%	18%	66%	16%
30ARGET - linear	21%	71%	7%	15%	78%	7%
45ARGET - linear	29%	65%	6%	17%	75%	8%

Table 7.3: Estimates of reactivity ratios determined using the Q-e scheme. Monomer 1 fixed as DEAEMA. Glycidyl methacrylate and EGDMA selected for their resemblance to PEGMA and TEGDMA, respectively, because Q-e data was unavailable. EGDMA: ethylene glycol dimethacrylate

Monomer 2		Q	e	r_1	r_2
DEAEMA	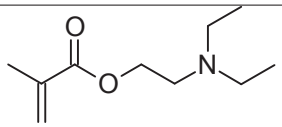	2.08	0.42	1.00	1.00
tBMA	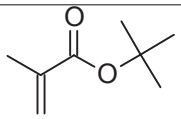	1.18	-0.35	1.28	0.43
PEGMA	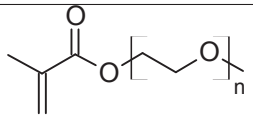	-	-	-	-
Glycidyl methacrylate	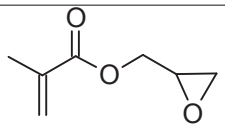	0.85	0.10	2.14	0.42
TEGDMA	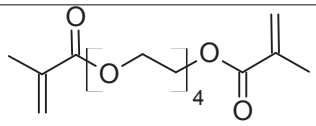	-	-	-	-
EGDMA	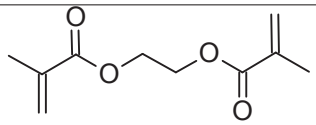	0.88	0.24	2.19	0.44

Table 7.4: GPC was used to determine the molecular weight and the polydispersity index for the P(DEAEMA-*co*-tBMA-*co*-PEGMA) linear polymer chains made without TEGDMA. M_n and PDI were calculated as the PMMA equivalent molecular weight and PMMA equivalent PDI from the main polymer peak.

Formulation	Elution time	M_n	PDI
30UV-linear	12.80 min	27,163 Da	2.53
45UV-linear	12.56 min	27,851 Da	2.07
30ARGET-linear	13.01 min	19,829 Da	1.46
45ARGET-linear	12.98 min	20,300 Da	1.52

Table 7.5: Temperatures associated with the degradation steps of the P(DEAEMA-*co*-tBMA-*co*-PEGMA-*co*-TEGDMA) polycationic nanoparticles, where T_d represents the temperature at the onset of degradation and T_e is the temperature that marks the end of the degradation step.

Formulation	$T_{d,1}$	$T_{e,1}$	wt% at 275 ºC	$T_{d,2}$	$T_{e,2}$	wt% at 600 ºC
30UV	206 ºC	275 ºC	48.8%	401 ºC	450 ºC	2.8%
45UV	206 ºC	274 ºC	51.6%	401 ºC	449 ºC	3.3%
30ARGET	206 ºC	274 ºC	48.5%	404 ºC	450 ºC	5.7%
45ARGET	203 ºC	273 ºC	51.1%	402 ºC	447 ºC	8.1%

Table 7.6: Ratio of crystalline PEG to total PEG in the P(DEAEMA-*co*-tBMA-*co*-PEGMA-*co*-TEGDMA) polycationic nanoparticles calculated using $\triangle H_m^0 = 200$ J/g.

Formulation	$X_{c,\ PEG}$
30UV	0.017
45UV	0.011

Table 7.7: $T_{g,overall}$ describes the overall glass transition value for the multiple overlapping T_g values, while $T_{g,1}$, $T_{g,2}$, and $T_{g,3}$ are the first, second, and third (in the case of 45UV) individual T_g values that can be determined from a careful, closer examination. $T_{g,n}$ represents the highest individual T_g that can be determined.

Formulation	$T_{g,overall}$	$T_{g,1}$	$T_{g,2}$	$T_{g,3}$	$T_{g,n}$-$T_{g,1}$
30UV	124 ºC	114 ºC	125 ºC	-	11 ºC
45UV	116 ºC	106 ºC	115 ºC	120 ºC	14 ºC
30ARGET	107 ºC	107 ºC	111 ºC	-	5 ºC
45ARGET	105 ºC	102 ºC	108 ºC	-	7 ºC

7.6 Figures

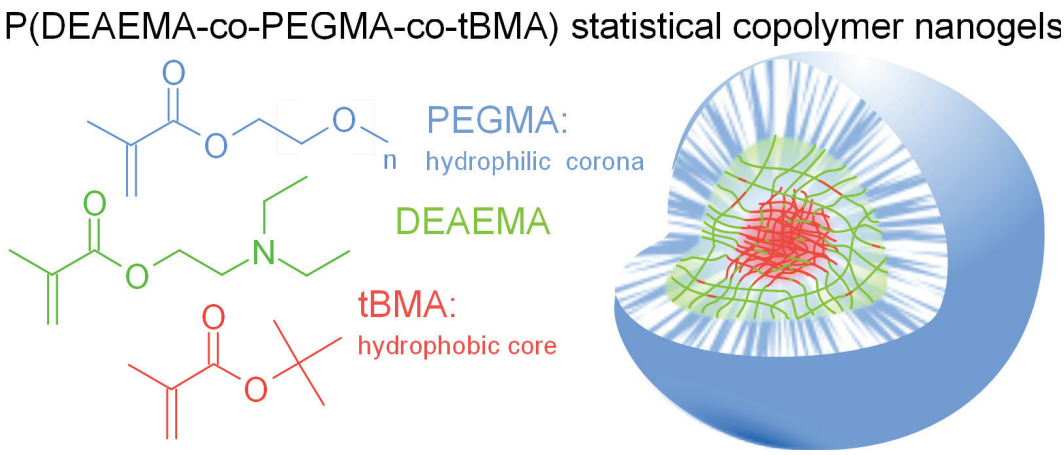

Figure 7.1: Schematic representation of the P(DEAEMA-*co*-tBMA-*co*-PEGMA) statistical copolymer nanogels. The nanogels are cross-linked with TEGDMA. The components tend to segregate based on hydrophobicity, with the hydrophilic PEG forming a corona and the hydrophobic tBMA tending to segregate to the core. The DEAEMA is hydrophilic when positively charged at low pH values.

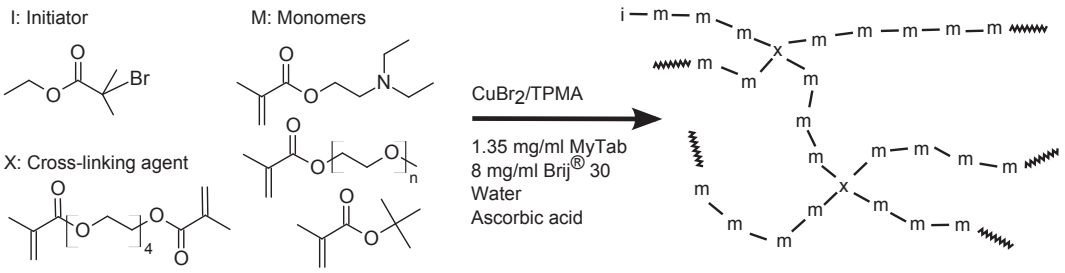

Figure 7.2: Reaction scheme for creating P(DEAEMA-*co*-tBMA-*co*-PEGMA-*co*-TEGDMA) polycationic nanoparticles using ARGET ATRP. EBIB was used as the initiator and TEGDMA was the cross-linking agent. The reacted initiator, monomer, and cross-linking agent are represented by i, m, and x, respectively.

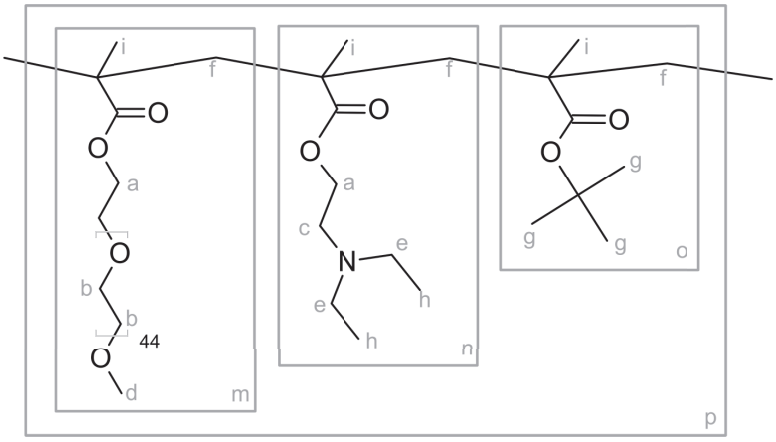

(a) Chemical stucture of linear chains

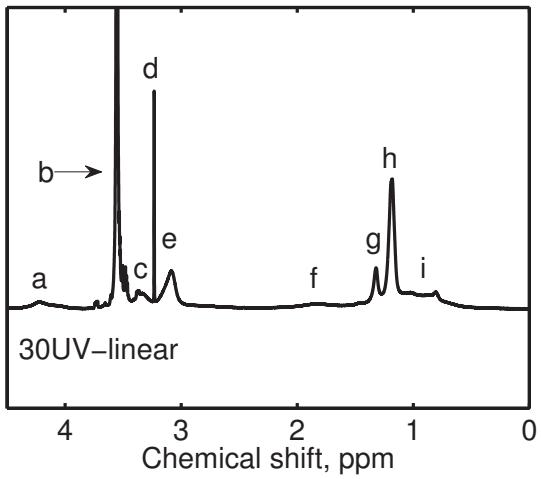

(b) ^1H NMR spectra with labeled peaks

Figure 7.3: Chemical structure of linear chains of P(DEAEMA-*co*-tBMA-*co*-PEGMA) with labeled ^{1}H NMR spectra peaks. Polymers are statistical copolymers, which means the composition is a function of the feed.

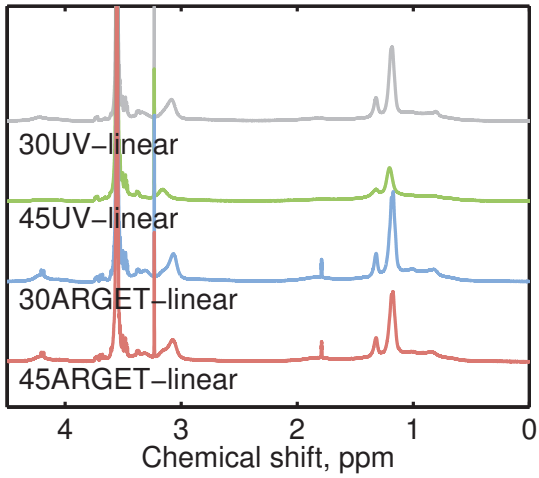

(a) Chemical stucture of linear chains

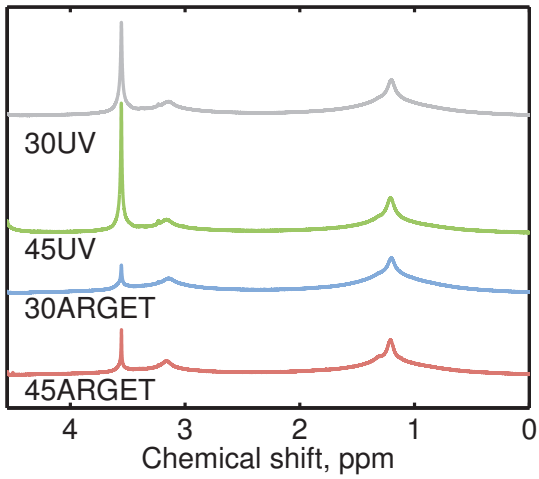

(b) ^{1}H NMR spectra with labeled peaks

Figure 7.4: ^{1}H NMR spectra for the four formulations of a) P(DEAEMA-*co*-tBMA-*co*-PEGMA) linear chains and b) P(DEAEMA-*co*-tBMA-*co*-PEGMA-*co*-TEGDMA) polycationic nanoparticles. Spectra are normalized with respect to the DEAEMA peak at 1.17 ppm and 3.14 ppm for linear and cross-linked polymers, respectively. The compositions of the linear polymers were evaluated by peak integration.

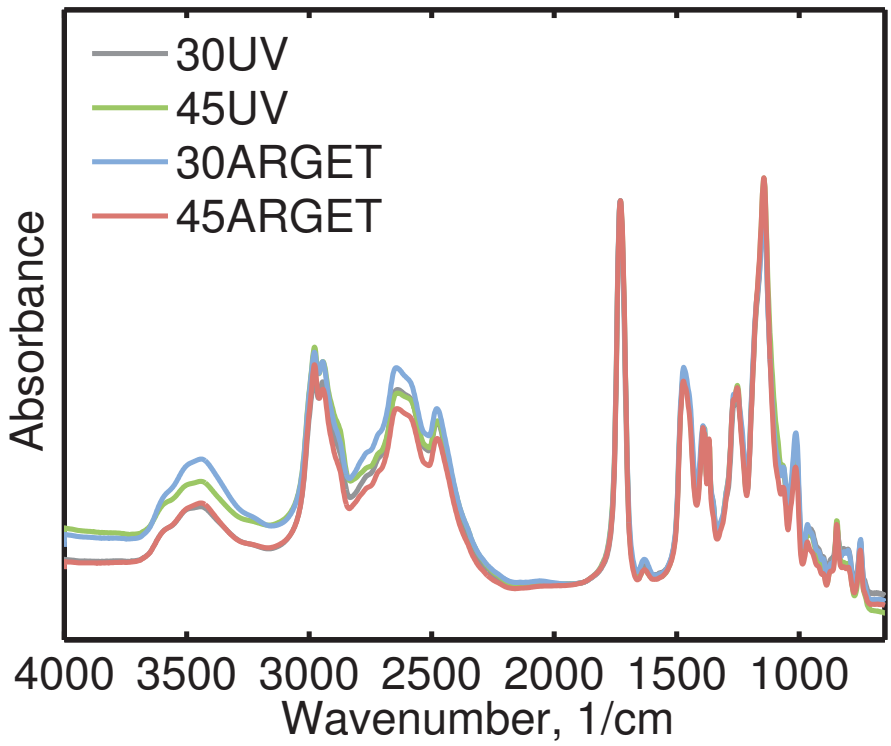

Figure 7.5: FTIR spectra for the P(DEAEMA-*co*-tBMA-*co*-PEGMA-*co*-TEGDMA) polycationic nanoparticles. The spectra were normalized to the carbonyl peak at 1730 cm^{-1}. Dried polymer and potassium bromide were pressed into a pellet for solid phase analysis.

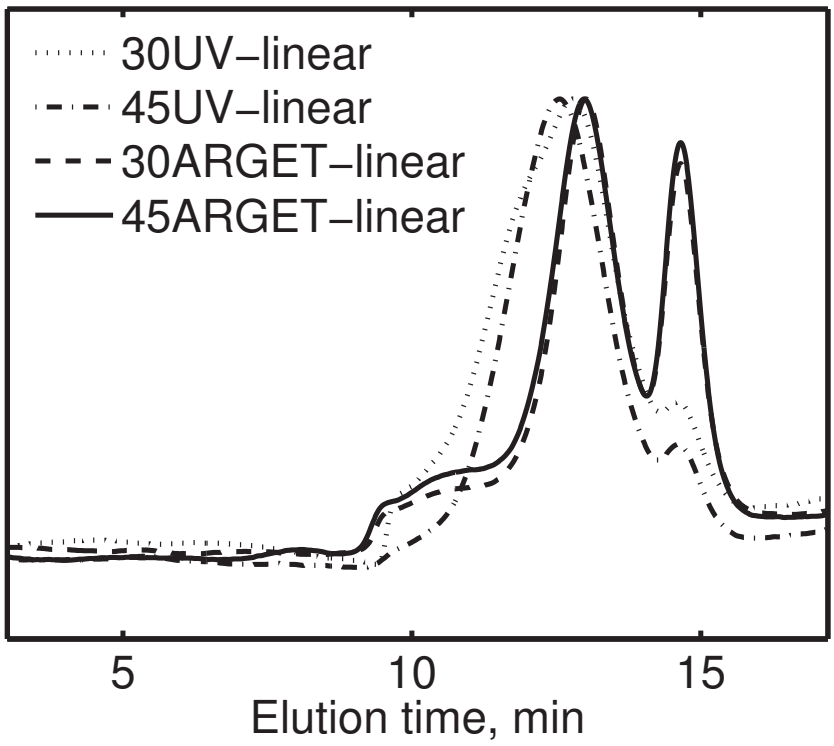

Figure 7.6: GPC curve for the P(DEAEMA-*co*-tBMA-*co*-PEGMA) linear polymer chains made without TEGDMA, which served as linear analogs of the cross-linked nanoparticles. The peak to the right of the polymer peak at 14.61 min is the unreacted macro-monomer PEGMA with molecular weight 2080 that was not removed during purification. The presence of residual unreacted monomer, particularly for the ARGET ATRP formulations, was confirmed using NMR.

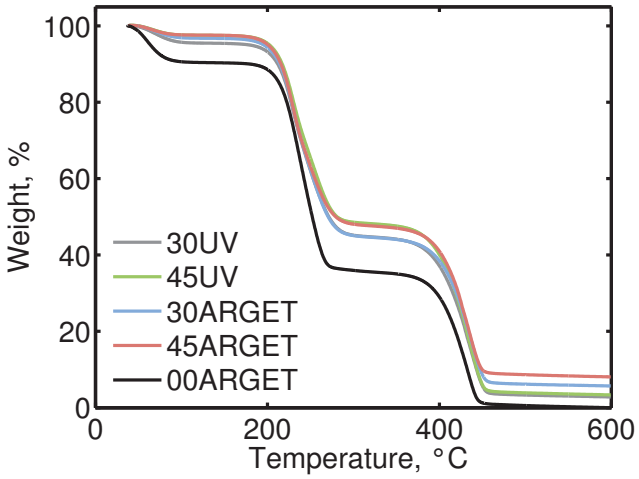

(a) TGA thermogram in N_2 atmosphere

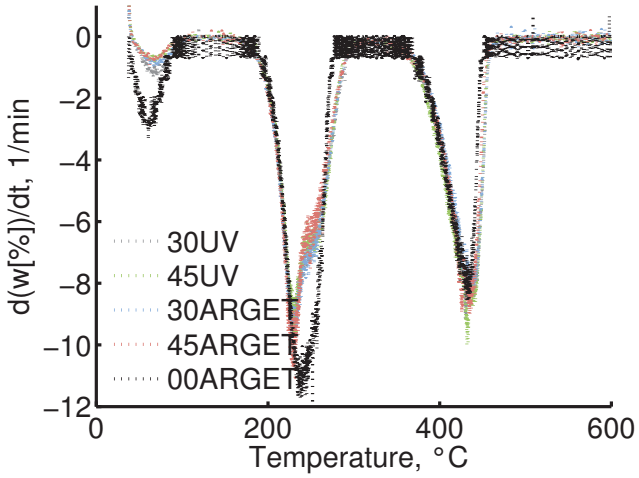

(b) Rate of weight loss in N_2 atmosphere

Figure 7.7: TGA thermograms of the P(DEAEMA-*co*-tBMA-*co*-PEGMA-*co*-TEGDMA) polycationic nanoparticles with nitrogen atmosphere. Formulation 00ARGET (no tBMA in the feed) is shown for comparison. Weight, % given as percent of initial weight. The rate was determined from the derivative of the weight, % versus temperature data. Additional tBMA appears to slow the rate of the first degradation step.

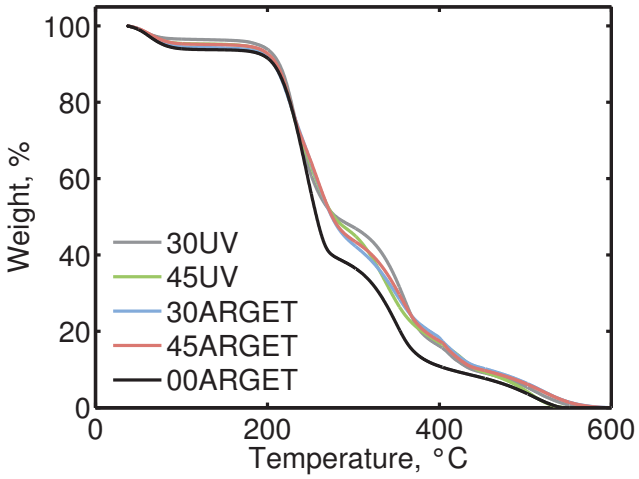

(a) TGA thermogram in air atmosphere

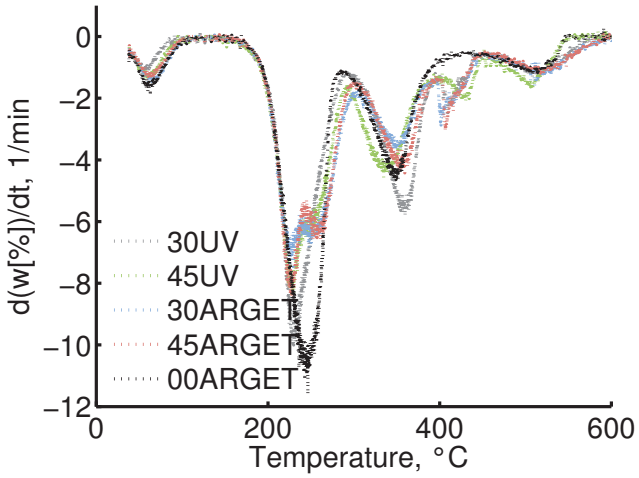

(b) Rate of weight loss in air atmosphere

Figure 7.8: TGA thermograms of the P(DEAEMA-*co*-tBMA-*co*-PEGMA-*co*-TEGDMA) polycationic nanoparticles with air atmosphere. Formulation 00ARGET (no tBMA in the feed) is shown for comparison. Weight, % given as percent of initial weight. The rate was determined from the derivative of the weight, % versus temperature data. Again, additional tBMA appears to slow the rate of the first degradation step.

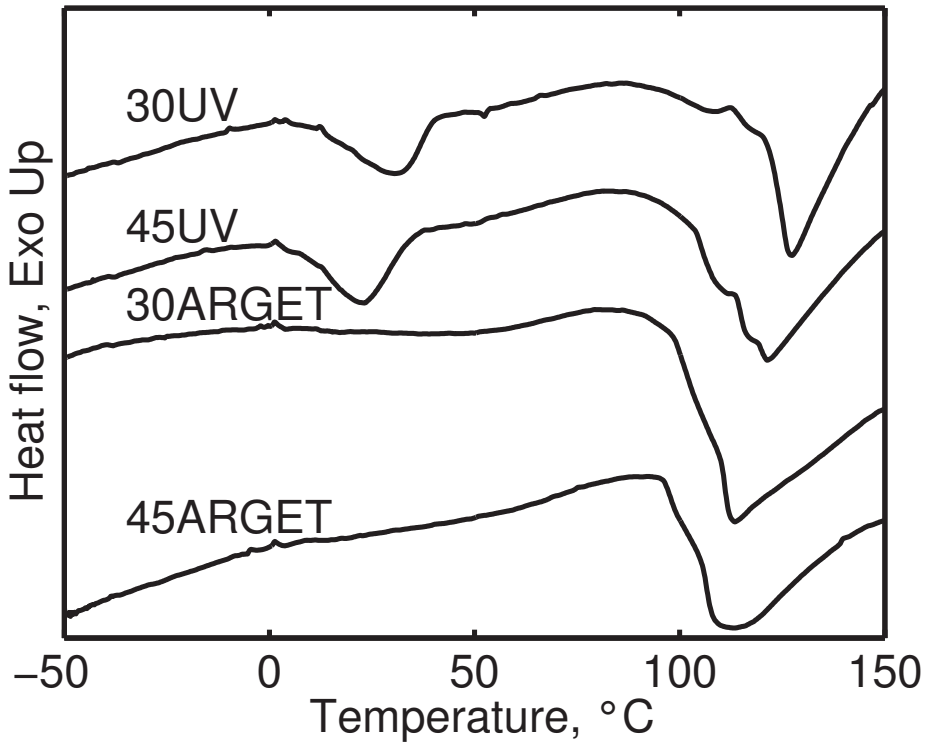

Figure 7.9: DSC curves for the P(DEAEMA-*co*-tBMA-*co*-PEGMA-*co*-TEGDMA) polycationic nanoparticles following annealing at 130 ºC to erase thermal history. Curves are shifted vertically for clarity.

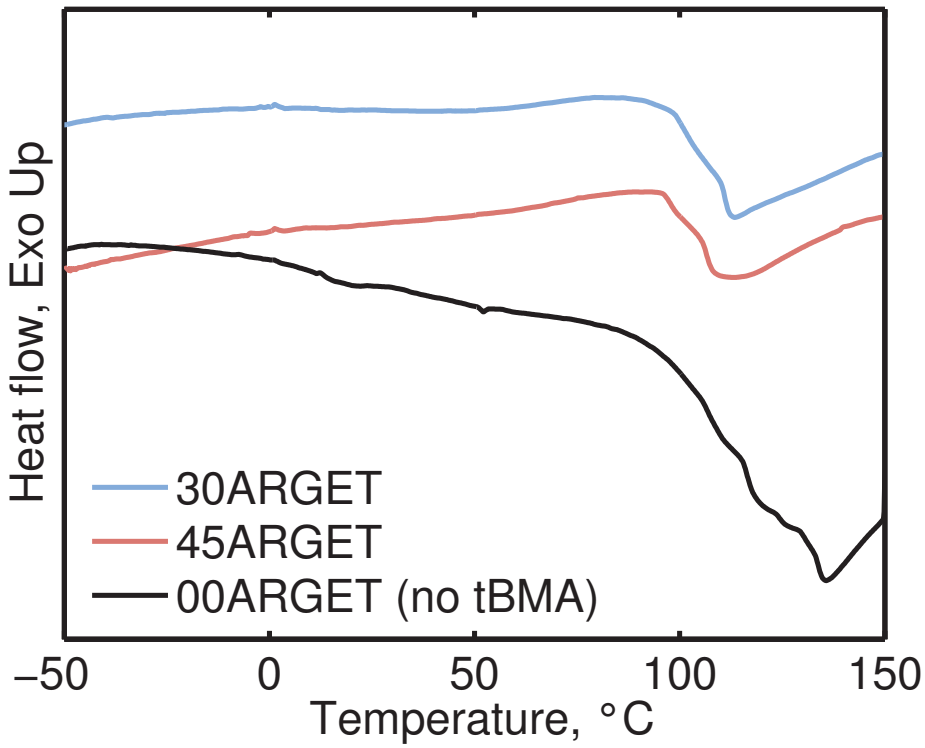

Figure 7.10: DSC curves for the ARGET formulations of P(DEAEMA-*co*-tBMA-*co*-PEGMA-*co*-TEGDMA) polycationic nanoparticles following annealing at 130 ^{o}C to erase thermal history. Note that tBMA strongly influences T_g behavior. If the tBMA is eliminated from the formulation (as in 00ARGET), the resulting thermogram shows a broader, sloping decline in contrast to the clearly defined transition for 30ARGET and 45ARGET.

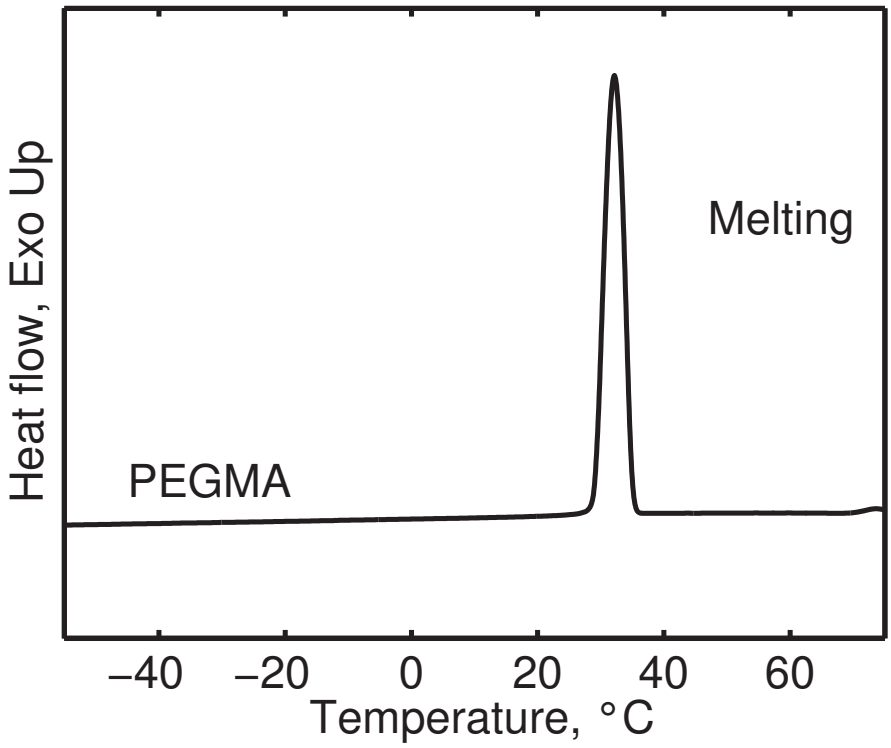

Figure 7.11: DSC curve showing the melting endotherm of PEGMA monomer at 58 °C. The sample was dried in a vacuum oven prior to thermal analysis.

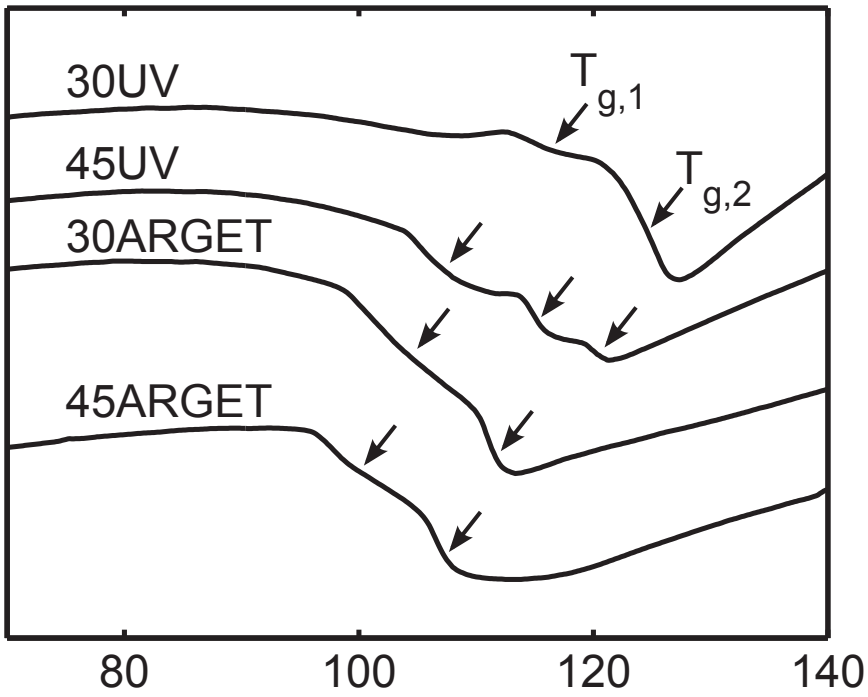

Figure 7.12: Close-up view of glass transition behavior shows multiple T_g values for each P(DEAEMA-*co*-tBMA-*co*-PEGMA-*co*-TEGDMA) polycationic nanoparticle formulation. Curves are shifted vertically for clarity.

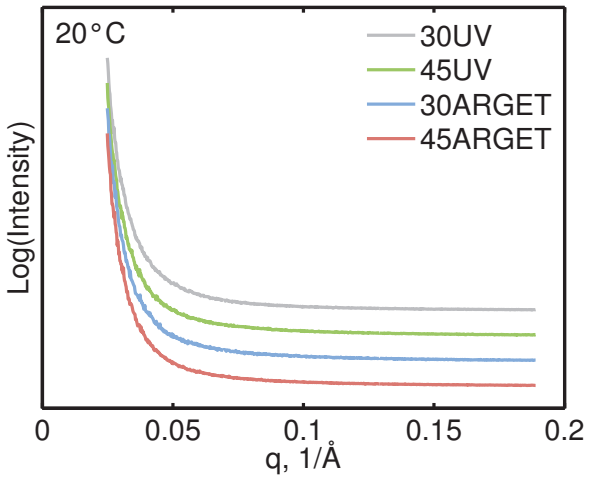

(a) SAXS at ambient temperature

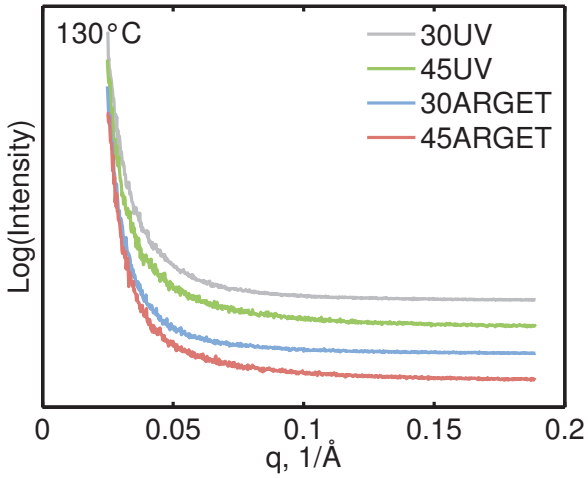

(b) SAXS at 130 °C

Figure 7.13: Integrated SAXS patterns of P(DEAEMA-*co*-tBMA-*co*-PEGMA-*co*-TEGDMA) polycationic nanoparticles collected at ambient temperature or 130 °C after thermal annealing at 130 °C. The patterns are shifted vertically for clarity.

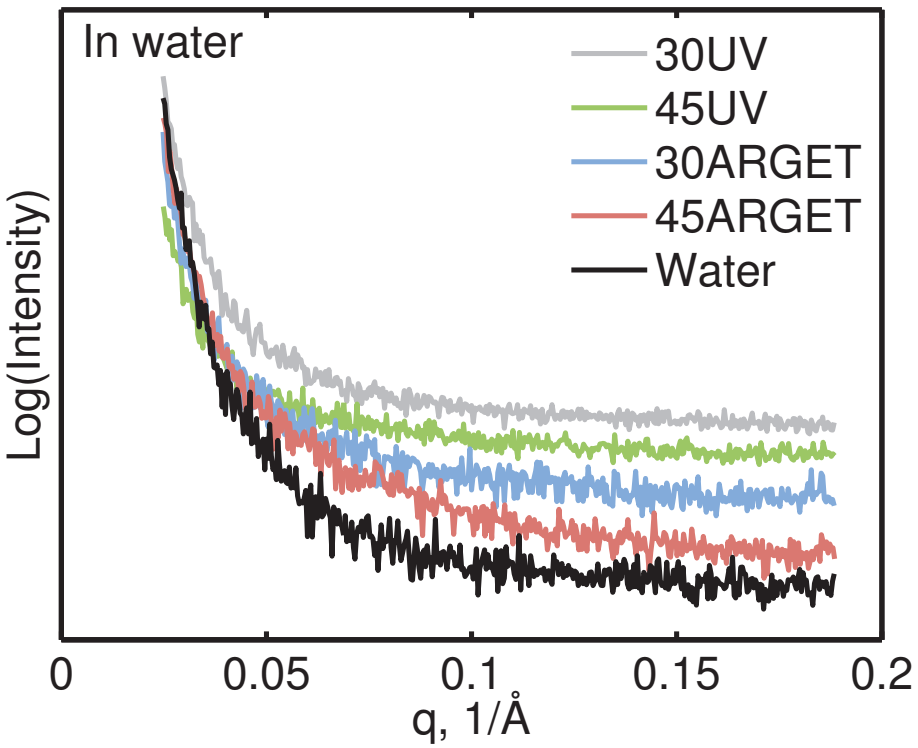

Figure 7.14: Integrated SAXS patterns of P(DEAEMA-*co*-tBMA-*co*-PEGMA-*co*-TEGDMA) polycationic nanoparticles collected at 10 mg/ml polycationic nanoparticles in water at ambient temperature. The patterns are shifted vertically for clarity.

7.7 References

[1] A. V. Kabanov and S. V. Vinogradov. Nanogels as pharmaceutical carriers: finite networks of infinite capabilities. *Angew. Chem., Int. Ed.*, 48 (30):5418–5429, 2009.

[2] Y. Kim, M. H. Pourgholami, D. L. Morris, and M. H. Stenzel. Effect of cross-linking on the performance of micelles as drug delivery carriers: A cell uptake study. *Biomacromolecules*, 13(3):814–825, 2012.

[3] T. Hoare and R. Pelton. Functional group distributions in carboxylic acid containing poly (*N*-isopropylacrylamide) microgels. *Langmuir*, 20 (6):2123–2133, 2004.

[4] W.B. Liechty, M. Caldorera-Moore, M.A. Phillips, C. Schoener, and N.A. Peppas. Advanced molecular design of biopolymers for transmucosal and intracellular delivery of chemotherapeutic agents and biological therapeutics. *J. Control. Release*, 155(2):119–127, 2011.

[5] J. Kim, N. Singh, and L. A. Lyon. Label-free biosensing with hydrogel microlenses. *Angew. Chem., Int. Ed.*, 45(9):1446–1449, 2006.

[6] G. Wulff, B. Chong, and U. Kolb. Soluble single-molecule nanogels of controlled structure as a matrix for efficient artificial enzymes. *Angew. Chem., Int. Ed.*, 45(18):2955–2958, 2006.

[7] N. Sanson and J. Rieger. Synthesis of nanogels/microgels by conventional and controlled radical crosslinking copolymerization. *Polym. Chem.*, 1(7): 965–977, 2010.

[8] D. Palioura, S. P. Armes, S. H. Anastasiadis, and M. Vamvakaki. Metal nanocrystals incorporated within pH-responsive microgel particles. *Langmuir*, 23(10):5761–5768, 2007.

[9] Satish Nayak and L. Andrew Lyon. Soft nanotechnology with soft nanoparticles. *Angew. Chem., Int. Ed.*, 44(47):7686–7708, 2005.

[10] V. B. Patravale and S. D. Mandawgade. Novel cosmetic delivery systems: an application update. *Int. J. Cosmet. Sci.*, 30(1):19–33, 2008.

[11] S. K. Jain and N. K. Jain. Multiparticulate carriers for sun-screening agents. *Int. J. Cosmet. Sci.*, 32(2):89–98, 2010.

[12] W. Abramovits, P. Granowski, and P. Arrazola. Applications of nanomedicine in dermatology: use of nanoparticles in various therapies and imaging. *J. Cosmet. Dermatol.*, 9(2):154–159, 2010.

[13] J. Weiss, P. Takhistov, and D. J. McClements. Functional materials in food nanotechnology. *J. Food Sci.*, 71(9):R107–R116, 2006.

[14] P. Sanguansri and M. A. Augustin. Nanoscale materials development - -a food industry perspective. *Trends Food Sci. Technol.*, 17(10):547–556, 2006.

[15] K. Matyjaszewski, W. Jakubowski, K. Min, W. Tang, J. Huang, W. A. Braunecker, and N. V. Tsarevsky. Diminishing catalyst concentration in atom transfer radical polymerization with reducing agents. *P. Natl. Acad. Sci.*, 103(42):15,309–15,314, 2006.

[16] W. Jakubowski and K. Matyjaszewski. Activators regenerated by electron transfer for atom-transfer radical polymerization of (meth)acrylates and related block copolymers. *Angew. Chem.*, 118(27):4594–4598, 2006.

[17] W. Jakubowski, K. Min, and K. Matyjaszewski. Activators regenerated by electron transfer for atom transfer radical polymerization of styrene. *Macromolecules*, 39(1):39–45, 2006.

[18] M. J. Monteiro and M. F. Cunningham. Polymer nanoparticles via living radical polymerization in aqueous dispersions: Design and applications. *Macromolecules*, 45(12):4939–4957, 2012.

[19] D. Kurzbach, M. J. N. Junk, and D. Hinderberger. Nanoscale inhomogeneities in thermoresponsive polymers. *Macromol. Rapid Commun.*, 34 (2):119–134, 2013.

[20] D. Gan and L. A. Lyon. Interfacial nonradiative energy transfer in responsive core-shell hydrogel nanoparticles. *J. Am. Chem. Soc.*, 123(34): 8203–8209, 2001.

[21] C. Wu and S. Zhou. Volume phase transition of swollen gels: Discontinuous or continuous? *Macromolecules*, 30(3):574–576, 1997.

[22] D. C. Forbes, M. Creixell, H. Frizzell, and N. A. Peppas. Polycationic nanoparticles synthesized using ARGET ATRP for drug delivery. *Eur. J. Pharm. Biopharm.*, 84(3):472–478, 2013.

[23] O. Z. Fisher, T. Kim, S. R. Dietz, and N. A. Peppas. Enhanced core hydrophobicity, functionalization and cell penetration of polybasic nanomatrices. *Pharm. Res.*, 26(1):51–60, 2008.

[24] H. Dong and K. Matyjaszewski. ARGET ATRP of 2-(dimethylamino) ethyl methacrylate as an intrinsic reducing agent. *Macromolecules*, 41 (19):6868–6870, 2008.

[25] O. Z. Fisher and N. A. Peppas. Polybasic nanomatrices prepared by UV-initiated photopolymerization. *Macromolecules*, 42(9):3391–3398, 2009.

[26] Y. H. La, E. W. Edwards, S. M. Park, and P. F. Nealey. Directed assembly of cylinder-forming block copolymer films and thermochemically induced cylinder to sphere transition: a hierarchical route to linear arrays of nanodots. *Nano Lett.*, 5(7):1379–1384, 2005.

[27] G. Ham. *Copolymerization*. Interscience Publishers, 1964. 845-863 pp.

[28] J. K. Oh, C. Tang, H. Gao, N. V. Tsarevsky, and K. Matyjaszewski. Inverse miniemulsion ATRP: a new method for synthesis and functionalization of well-defined water-soluble/cross-linked polymeric particles. *J. Am. Chem. Soc.*, 128(16):5578–5584, 2006.

[29] G. Wallraff, J. Hutchinson, W. Hinsberg, F. Houle, P. Seidel, R. Johnson, and W. Oldham. Thermal and acid-catalyzed deprotection kinetics in candidate deep ultraviolet resist materials. *J. Vac. Sci. Technol. B*, 12 (6):3857–3862, 1994.

[30] J. B. Kim and H. Kim. Effect of acid structure on deprotection of poly (2-trimethylsilyl-2-propyl methacrylate). *Polymer*, 40(14):4055–4061, 1999.

[31] C. Ramireddy, Z. Tuzar, K. Prochazka, S. E. Webber, and P. Munk. Styrene-*tert*-butyl methacrylate and styrene-methacrylic acid block copolymers: synthesis and characterization. *Macromolecules*, 25(9):2541–2545, 1992.

[32] N. Sharifi-Sanjani, A. R. Mahdavian, and P. Bataille. Emulsion polymerization of styrene and DEAEMA with a core–shell structure. *J. Appl. Polym. Sci.*, 78(11):1977–1985, 2000.

[33] C. J. Fristrup, K. Jankova, and S. Hvilsted. Hydrophilization of poly (ether ether ketone) films by surface-initiated atom transfer radical polymerization. *Polym. Chem.*, 1(10):1696–1701, 2010.

[34] N. S. Murthy, W. Wang, and J. Kohn. Microphase separation in copolymers of hydrophilic PEG blocks and hydrophobic tyrosine-derived segments using simultaneous SAXS/WAXS/DSC. *Polymer*, 51(17):3978–3988, 2010.

[35] P. R. Mark, N. S. Murthy, S. Weigand, K. Breitenkamp, M. Kade, and T. Emrick. Microphase separated structures in the solid and molten states of double-crystal graft copolymers of polyethylene and poly (ethylene oxide). *Polymer*, 49(13):3116–3124, 2008.

[36] D. Cohn and A. Hotovely-Salomon. Biodegradable multiblock PEO/PLA thermoplastic elastomers: molecular design and properties. *Polymer*, 46 (7):2068–2075, 2005.

[37] J. Brandrup, E. H. Immergut, E. A. Grulke, A. Abe, and D. R. Bloch. *Polymer Handbook*. Wiley New York, 1999.

[38] K. Pielichowski and K. Flejtuch. Differential scanning calorimetry studies on poly (ethylene glycol) with different molecular weights for thermal energy storage materials. *Polym. Adv. Technol.*, 13(10-12):690–696, 2003.

[39] T. J. Singh and S. V. Bhat. Morphology and conductivity studies of a new solid polymer electrolyte:(PEG) xLiClO4. *Bull. Mater. Sci.*, 26(7): 707–714, 2003.

[40] J. M. Cornejo-Bravo and R. A. Siegel. Water vapour sorption behaviour of copolymers of *N, N*-diethylaminoethyl methacrylate and methyl methacrylate. *Biomaterials*, 17(12):1187–1193, 1996.

[41] S. J. Holder, N. A. A. Rossi, C. T. Yeoh, G. G. Durand, M. J. Boerakker, and N. A. J. M. Sommerdijk. ABA triblock copolymers: from

controlled synthesis to controlled function. *J. Mater. Chem.*, 13(11):2771–2778, 2003.

Chapter 8

Conclusions and Recommendations for Future Research

8.1 Conclusions

The goal of this research was to create and investigate new polymers prepared by ARGET ATRP-based (activators regenerated by electron transfer for atom transfer radical polymerization) reactions in order to understand their utility as biomaterials for drug delivery. Polycationic nanoparticles were synthesized using a new ARGET ATRP-based technique and evaluated as drug delivery biomaterials. A panel of polycationic nanoparticles was prepared using ARGET ATRP or UV-initiated polymerization and characterized in order to examine the effect of polymerization method on material properties and the connection to molecular structure.

This work represents the first report in the literature of an ARGET ATRP-based emulsion in water synthesis method for polycationic nanoparticles.[1] The polycationic nanoparticles were composed of 2-(diethylamino)ethyl methacrylate (DEAEMA) for pH-responsiveness, poly(ethylene glycol) methyl

ether methacrylate (PEGMA) for improved biocompatibility, *tert*-butyl methacrylate (tBMA) to impart hydrophobicity, and a tetraethylene glycol dimethacrylate (TEGDMA) cross-linking agent for enhanced colloidal stability. The polymerization takes 3 h and the reaction takes place at ambient temperature.

The ARGET ATRP synthesis has advantages over UV-initiated polymerizations and traditional ATRP. Avoiding UV-initiation confers advantages including ease of conducting multiple simultaneous reactions, synthesis protocols that can be scaled without account for the UV light source intensity and exposure time, as well as the ability to use photosensitive components such as dyes or biologically-derived components in the polymerization reaction. Compared to traditional ATRP, ARGET ATRP significantly reduces the concentration of copper catalyst and is much less oxygen-sensitive.

The ARGET ATRP synthesis method produces monodisperse, pH-responsive polymer nanoparticles. The polycationic nanoparticles in solution were analyzed with dynamic light scattering, and pH-responsiveness was confirmed. Transmission electron microscopy (TEM) analysis of the dried polycationic nanoparticles demonstrated that the particles are approximately spherical.

The ARGET ATRP polycationic nanoparticles were investigated for use as drug delivery vehicles with a central goal of inducing knockdown in cells through successful siRNA delivery. Prerequisites for successful drug delivery that are independent of the drug type include biocompatibility and the ability

to load and release a drug. Drugs such as siRNA and chemotherapeutic agents require carriers that can be internalized by cells. Effective siRNA delivery also requires endosomal escape so that the siRNA can be released into the cytosol.

The first stage of evaluating the suitability for drug delivery compared an array of polycationic nanoparticles synthesized using UV-initiated polymerization (similar to the method reported by Fisher et al.[2;3]) or ARGET ATRP.[1;4] The molar feed ratio of the hydrophobic component tBMA was set at 30 or 45 mol tBMA per 100 mol DEAEMA in the feed. The four formulations are named based on the synthesis method and the molar feed of tBMA with respect to 100 mol DEAEMA in the feed: 30UV, 45UV, 30ARGET, and 45ARGET.

The array of polycationic nanoparticles was investigated using an MTS assay with cancerous and non-cancerous cell lines. MTS assays provide a measure of relative viability based on the activity of cellular enzymes. For both cell lines at the conditions tested, the ARGET ATRP formulations were more toxic that the UV-initiated formulation with a corresponding feed concentration. Also, formulations containing 45 mol tBMA per 100 mol DEAEMA in the feed were found to be less toxic than the corresponding 30 mol tBMA formulations for both cell lines. The results of the MTS assay were confirmed with an LDH (lactase dehydrogenase) assay which provides a measure of relative viability as a function of the membrane leakage.

Effective siRNA delivery requires cellular internalization as well as endosomal escape, so hemolysis assays were used as a measure of the endoso-

molytic activity for the array of polycationic nanoparticles. All formulations except for 30ARGET demonstrated pH-dependent hemolytic activity, with strong membrane disruption at endosomal conditions (pH 6.5) and small to negligible membrane disruption for extracellular conditions (pH 7.4). The hemolysis assay results correlated with the membrane leakage measured using an LDH assay, providing evidence that the increased toxicity of the 30ARGET formulation was due to membrane disruption at extracellular conditions (pH 7.4).

The siRNA drug loading capability of the polycationic nanoparticles was evaluated using a RiboGreen® siRNA binding assay. The array of polycationic nanoparticles demonstrated efficient binding of siRNA (~98% for all formulations) in 0.2x PBS pH 5.5. The binding efficiency is reduced in Opti-MEM®, particularly for the 45ARGET formulation with 55% of the siRNA bound to the polymer (compared to 74% for 30UV, 70% for 45UV, and 63% for 30ARGET).

Flow cytometry was used to quantify the uptake of fluorescently-labeled siRNA for the array of polycationic nanoparticles. All formulations demonstrated efficient uptake with small differences among formulations but large differences in the percent of cells with siRNA when comparing different cell types (HEK293T and RAW264.7). The RAW264.7 cells have a higher percentage of cells associated with fluorescently-labeled siRNA compared to the HEK293T cells. For both cell types, the 45ARGET formulation demonstrates the largest normalized fluorescence intensity of the four polycationic nanopar-

ticle formulations. The trends observed with flow cytometry were supported by confocal microscopy.

Knockdown efficiency induced by siRNA was evaluated for the array of polycationic nanoparticles using AllStars Death siRNA with HEK293T or RAW264.7 cells. Knockdown was first confirmed in HEK293T cells, with the greatest efficiency demonstrated by the 30UV, 30ARGET, and 45ARGET formulations (78%, 84%, and 75% knockdown efficiency, respectively). Unfortunately, knockdown with these conditions was associated with decreased cell viability for control cells with scrambled siRNA. When the siRNA concentration was decreased from 200 nM to 100 nM, the HEK293T cells with scrambled siRNA demonstrate improved viability with decreased knockdown efficiency. This trade-off between knockdown efficiency and viability is a continuing challenge of siRNA delivery carriers. Knockdown was also evaluated in RAW264.7 cells because they are considered to be more difficult to transfect than HEK293T cells. As expected, the RAW264.7 demonstrated lower knockdown efficiencies than the HEK293T cells when transfected with 100 nM siRNA complexed to polycationic nanoparticles.

The second stage of evaluating the suitability for drug delivery focused on a single polycationic nanoparticle formulation, 45ARGET, to take a closer look at the interactions of the polycationic nanoparticles with siRNA and cells in order to better understand the capabilities and limitations of the carrier. A RiboGreen® siRNA binding assay was used to evaluate the binding profile for a range of polymer/siRNA mass ratios, and the polycationic nanoparticles were

found to efficiently bind siRNA for polymer/siRNA mass ratios less than 1. Dynamic light scattering indicated that siRNA binding was associated with a decreased diameter of the polycationic nanoparticles without a significant change in zeta potential.

A fluorescently-labeled 45ARGET formulation was prepared to investigate cellular internalization. Flow cytometry with RAW264.7 cells indicated that the uptake of fluorescently-labeled nanoparticles increased with nanoparticle concentration and incubation time. Confocal microscopy confirmed internalization of the fluorescently-labeled nanoparticles.

The dependence of knockdown on the concentration of 45ARGET polycationic nanoparticles and siRNA was investigated in RAW264.7 cells. As expected, higher concentrations of nanoparticles and siRNA were associated with increased knockdown. The 45ARGET formulation outperformed the commercially available transfection agent Lipofectamine.

An improved understanding of molecular structure, and its connection to synthesis techniques and material properties, may facilitate the design of enhanced materials. The four formulations of polycationic nanoparticles (30UV, 45UV, 30ARGET, and 45ARGET) were characterized using a variety of techniques designed to probe the molecular structure. Nanoscale heterogeneity is an important aspect of molecular structure, and the analysis demonstrated that the ARGET ATRP polycationic nanoparticle formulations had greater nanoscale homogeneity than the UV-initiated polymerization formulations.

GPC (gel permeation chromatography) was used to analyze P(DEAEMA-co-tBMA-co-PEGMA) linear chains to gain insight into the molecular weight distribution of the polymer chains in the cross-linked polycationic nanoparticles. The ARGET ATRP linear chains have a narrower main elution peak than the UV-initiated linear chains, suggesting a narrower distribution of main chain lengths for the ARGET ATRP polycationic nanoparticles. The narrower distribution of molecular weight may also explain the sharper pH-responsive swelling transition of the ARGET ATRP polycationic nanoparticles compared to the UV-initiated polycationic nanoparticles observed using dynamic light scattering.

Thermal analysis using TGA (thermal gravimetric analysis) and DSC (differential scanning calorimetry) provides additional information about material properties. The polycationic nanoparticle formulations demonstrate subtle differences in their TGA profiles in nitrogen and air. The DSC thermograms show two main differences in the UV and the ARGET ATRP formulations: i) the presence of a melting peak for the UV but not for the ARGET ATRP formulations and ii) a sharper glass transition for the ARGET ATRP formulations than for the UV formulations.

The UV-initiated polycationic nanoparticle formulations demonstrate a melting peak consistent with the melting of crystallites in PEG-rich regions. The ARGET ATRP polycationic nanoparticle formulations do not demonstrate this melting peak, suggesting that the PEG is incorporated with greater homogeneity so it cannot phase-separate. Also, the lack of crystallites

may result from the lower PEGMA incorporation observed for the ARGET ATRP formulations compared to the UV-initiated formulations as observed using NMR (nuclear magnetic resonance) of P(DEAEMA-co-tBMA-co-PEGMA) linear chains.

The ARGET ATRP formulations demonstrate sharper glass transitions than the UV-initiated formulations. This sharpness is consistent with a narrower size distribution of tBMA-rich region for the ARGET ATRP formulations with a broader size distribution of tBMA-rich regions in the UV-initiated formulations. Unfortunately, SAXS (small-angle x-ray scattering) analysis to probe molecular structure did not provide additional information. ARGET ATRP-based reactions impart greater control than UV-initiated polymerizations because of the closer approximation to simultaneous initiation. With simultaneous initiation, individual chains may have a gradient composition, but individual chains in the population are indistinguishable.

8.2 Recommendations for future research

Future investigations of ARGET ATRP polycationic nanoparticles can build on this research. Future work can see if ARGET ATRP may be used for the synthesis of other types of stimuli-responsive nanoparticles composed of different monomers. With respect to siRNA delivery, future work should seek to translate the knockdown behavior observed *in vitro* to a therapeutically relevant *in vivo* model. RT-qPCR (reverse transcriptase quantitative polymerase

chain reaction) may provide an alternative method to detect knockdown by quantifying mRNA expression. Unfortunately, the actual protein expression may only weakly correlate with the mRNA concentration,[5–7] and as a result, mRNA quantification may be an "inappropriate surrogate for protein expression evaluation."[8] An *in vitro* co-culture model may be an important step toward successful *in vivo* studies; for example, a recently reported 3D co-culture model of inflammatory bowel disease may provide a format for experiments that is more therapeutically relevant than mono-culture of epithelial or macrophage cells alone.[9] It is particularly important to account for the role of culture conditions in transfection efficiency; for example, dramatically increased transfection efficiency has been observed in 3D cell culture models compared to 2D models.[10] Simple 2D cell culture models are often unable to represent complex disease states, and so future work must tackle this challenge.

8.3 References

[1] D. C. Forbes, M. Creixell, H. Frizzell, and N. A. Peppas. Polycationic nanoparticles synthesized using ARGET ATRP for drug delivery. *Eur. J. Pharm. Biopharm.*, 84(3):472–478, 2013.

[2] O. Z. Fisher, T. Kim, S. R. Dietz, and N. A. Peppas. Enhanced core hydrophobicity, functionalization and cell penetration of polybasic nanomatrices. *Pharm. Res.*, 26(1):51–60, 2008.

[3] O. Z. Fisher and N. A. Peppas. Polybasic nanomatrices prepared by UV-initiated photopolymerization. *Macromolecules*, 42(9):3391–3398, 2009.

[4] D. C. Forbes and N. A. Peppas. Differences in molecular structure in cross-linked polycationic nanoparticles synthesized using ARGET ATRP or UV-initiated polymerization. *Polymer*, 54(17):4486–4492, 2013.

[5] G. Chen, T. G. Gharib, C. Huang, J. M. G. Taylor, D. E. Misek, S. L. R. Kardia, T. J. Giordano, M. D. Iannettoni, M. B. Orringer, S. M. Hanash, and D. G. Beer. Discordant protein and mRNA expression in lung adenocarcinomas. *Mol. Cell. Proteomics*, 1(4):304–313, 2002.

[6] Q. Tian, S. B. Stepaniants, M. Mao, L. Weng, M. C. Feetham, M. J. Doyle, C. Y. Eugene, H. Dai, V. Thorsson, J. Eng, D. Goodlett, J. P. Berger, B. Gunter, P. S. Linseley, R. B. Stoughton, R. Aebersold, S. J. Collins, W. A. Hanlon, and Hood. L. E. Integrated genomic and proteomic

analyses of gene expression in mammalian cells. *Mol. Cell. Proteomics*, 3 (10):960–969, 2004.

[7] L. Nie, G. Wu, and W. Zhang. Correlation between mRNA and protein abundance in *Desulfovibrio vulgaris*: A multiple regression to identify sources of variations. *Biochem. Biophys. Res. Commun.*, 339(2):603–610, 2006.

[8] J. Carralot, T. Kim, B. Lenseigne, A. S. Boese, P. Sommer, A. Genovesio, and P. Brodin. Automated high-throughput siRNA transfection in raw 264.7 macrophages: a case study for optimization procedure. *J. Biomol. Screen.*, 14(2):151–160, 2009.

[9] F. Leonard, E. Collnot, and C. Lehr. A three-dimensional coculture of enterocytes, monocytes and dendritic cells to model inflamed intestinal mucosa in vitro. *Molecular Pharmaceutics*, 7(6):2103–2119, 2010.

[10] J. Zoldan, A. K. R. Lytton-Jean, E. D. Karagiannis, K. Deiorio-Haggar, L. M. Bellan, R. Langer, and D. G. Anderson. Directing human embryonic stem cell differentiation by non-viral delivery of siRNA in 3D culture. *Biomaterials*, 32(31):7793–7800, 2011.

Appendices

Appendix A

Colon Targeted Delivery Using Nanoparticles Encapsulated in Alginate

The polycationic nanoparticles may have utility as components of an oral siRNA delivery system composed of siRNA-loaded nanoparticles encapsulated in alginate. This two-part system may be able to provide colon targeted delivery of siRNA to the intestines for the treatment of conditions such as inflammatory bowel disease (IBD) or colon cancer. Alginates are well-characterized,[1;2] commercially available[3] biomaterials.

A.1 Colon targeted delivery

Colon targeted delivery may be advantageous for the treatment of diseases of the large intestine where drug delivered directly to the disease site may improve treatment effectiveness and reduce side effects associated with non-specific delivery.[4–6] Traditional oral administration results in drug absorption in the upper part of the gastrointestinal tract, while rectal administration for colon delivery is subject to a high degree of variability.[4] There is an unmet

need for improved colon targeting systems.[7]

Approaches for colon targeting include pH-dependent, time-dependent, pressure-dependent and enzyme-responsive systems, but each system has limitations.[4;7] Premature release in the small intestine or no release in the colon have been reported for pH-dependent colon-targeted systems.[8–11] The pH of the colon (average of 7.0)[12] falls within the range of reported values for the pH of the small intestines: 5-6 as reported by Laroui and colleagues[7] and 6.6 to 7.5 in the proximal small intestine (duodenum, see Figure A.1) to terminal ileum, respectively, as reported by Evans and colleagues[12]), so a pH-dependent approach may be inadequate for colon specific delivery. Time-dependent approaches take advantage of mechanisms such as swelling or erosion that can be modeled as a function of time.[7] However, colon transit may vary from a few hours to 2 days[13] and the system will be susceptible to this variation.[4;11] Pressure-dependent systems use the increased intestinal pressure in the colon from peristalsis to cause rupture of the system resulting in drug release.[7]

Enzyme-responsive systems are designed with degradable components that trigger release. Typically, this degradation is caused by digestion of polysaccharides by colonic bacteria.[5;7] An example of such a system would be using polysaccharide coating to coat a gelatin capsule to favor release in the colon. The colon contains a very high concentration of microflora, with typical concentration values of 10^{11} CFU/ml, compared to typical values of 10^3 CFU/ml elsewhere in the gastric track[13] (note: CFU represents a colony-forming unit and is a measure of viable microorganisms). These microflora

in the colon compose about 400 bacterial species, but the main bacteria for alginate degradation are Bacteroides and Bifidobacteria.[5] Poor control over release kinetics has been reported for some enzyme-responsive polysaccharide systems that are degraded by microflora in the colon.[14;15] The polysaccharides typically used in enzyme-responsive systems are hydrophilic, and as a result, may swell and prematurely release loaded drug prior to enzymatic degradation in the colon.[4]

Several "di-dependent"[4] delivery systems which take advantage of two of the four targeting strategies (time, pH, pressure, or microflora enzymes) have been developed including Pulsincap®, OROS®-CT, PORT®, and Time Clock®.[4] These multi-component systems may be highly effective, but the complexity is a barrier to efficient manufacturing. Defects are an additional concern; if defects cannot be engineered out of these systems, even low failure rates may lead to problems in patients resulting from uncontrolled release. In spite of the challenges, the reported successes of these di-dependent strategies may motivate the use of a dual-responsive system that makes use of simpler fabrication strategies.

A.2 Alginate as a biomaterial for oral delivery

Alginate is composed of linear, non-branched polysaccharides that are copolymers of β-D-mannuronic acid (M) and α-L-guluronic acid (G) linked by α- or β-1,4 glycosidic bonds (see Figure A.2a).[1;16;17] Alginate is a natural an-

ionic polyelectrolyte[18] from brown algae.[16;17] Alginate has many properties that make it attractive for use as a biomaterial. Alginate is biocompatible (although note that ultra-pure grade should be used when biocompatibility is critical[2;17]). Since networks are formed under mild conditions in salt solution,[2;17] alginate gels can be used as biomaterials for drug delivery for traditional small molecular drugs as well as fragile macromolecules such as proteins.[1] Alginate microparticles have been used for oral gene delivery of plasmid DNA.[19] In the food industry, alginate is used as a gelling agent, stabilizer, and emulsifier,[1] and this accepted use in food is a positive indication supporting the use of alginate in an oral delivery system.

The network structure of alginate hydrogels is formed when dissolved alginate is combined with di- or tri-valent metal ions in solution.[20] The alginate is dissolved at 1-8%, with the 1-2% typically used for high molecular weight alginate and 3-8% used for low molecular weight alginate.[21] Large beads (mm size) can be formed by manually pushing alginate solution through a syringe needle, but compressed air automated systems can produce smaller (10-120 μm) alginate particles.[22] While the particles can be stored in water, freeze-drying provides a simple solution for storage, and freeze-drying is reported to produce beads with a smooth surface morphology.[21]

The "egg-box" model is the most accepted model of network formation; in the egg-box model, the calcium cations each bind to two G units to cross-link the alginate chains (see Figure A.2b).[20] The chains are cross-linked in a physical network structure composed of many linear chains stacked together

along multiple G residues.[5]

Alginates are pH-responsive and enzyme-responsive. At neutral pH conditions, the divalent cross-linking cations dissociate and the network dissolves;[1] particles remain intact at low pH but dissociate at high pH.[19;21] Important parameters that influence erosion and release include particle size, viscosity of the alginate solution, and chemical composition (G/M ratio) of the alginate.[16] Alginate is enzyme-responsive (as well as biodegradable) because they are degraded by bacteria found at high concentrations in the colon.[5]

Bodmeier and associates[23] reported a technique for the oral delivery of microparticles and nanoparticles using alginate. Microparticles and nanoparticles are of considerable interest for controlled release, but compression tableting may damage to particles or may require large concentrations of excipient fillers and binders.[23] The reported technique used by Bodmeier and associates[23] relied upon encapsulation of the microparticles or nanoparticles in an alginate matrix formed by dropped alginate/particle dispersions into a calcium chloride solution for cross-linking.[23] The calcium alginate matrix was pH-responsive; the matrix remained intact in 0.1 N hydrochloric acid but "rapidly disintegrated in simulated intestinal fluids" (United States Pharmacopeia XIX, USP XIX).[23] While disintegration may be undesirable for applications where a constant release rate of a small molecule therapeutic is desired,[1] erosion or disintegration may improve release of nanoparticles over diffusion alone.

A.3 Materials and methods

A.3.1 Chemicals

Alginic acid from brown algae, pepsin, pancreatin, poly(ethylene glycol) methyl ether methacrylate (PEGMA) solution (M_n 2000 for PEG chain, 50 wt % in water), 2-(diethylamino)ethyl methacrylate (DEAEMA), *tert*-butyl methacrylate (tBMA), tetraethylene glycol dimethacrylate (TEGDMA), ethyl 2-bromoisobutyrate (EBIB), tris (2-pyridylmethyl) amine (TPMA), and ascorbic acid (AA) were purchased from Sigma-Aldrich. Ethanol, phosphate buffered saline (PBS), 1N hydrochloric acid (HCl), 1N sodium hydroxide (NaOH), monobasic potassium phosphate, and calcium chloride were purchased from Fisher Scientific. All other chemicals were reagent grade. Ultrapure water was used for all experiments. All chemicals were used as received.

A.3.2 Alginate encapsulation of fluorescently-labeled nanoparticles

Fluorescently-labeled nanoparticles were synthesized using NBD chloride (NBD-Cl, 7-chloro-4-nitrobenzo-2-oxa-1,3-diazole, also called 4-chloro7-nitrobenzofuran, Sigma-Aldrich). Nanoparticles containing primary amines were synthesized with 2-aminoethyl methacrylate (AEMA, Sigma-Aldrich) (AEMA:DEAEMA::32:100). Dried, purified nanoparticles were suspended in ethanol and combined with an excess of NBD chloride; a typical reaction was 450 mg of dried nanoparticles with 50 mg NBD chloride in 30 ml ethanol. The mixture was allowed to react overnight to form NBD-labeled

nanoparticles (NBD-NPs). Unreacted NBD-Cl was removed by dialysis and the fluorescently-labeled nanoparticles were recovered with freeze-drying. Note that the NBD-Cl becomes strongly fluorescent upon reaction with amines and that NBD-amines are excited by visible light (464 nm) with emission maximum of approximately 512 nm.

The encapsulation technique of Bodmeier and associates[23] was adapted to encapsulate polycationic nanoparticles in alginate beads. The synthesis is simple and rapid; following dissolution of all components, bead formation takes less than 10 minutes. The reaction conditions are mild and nontoxic; both components (alginate and calcium chloride) are permitted for use in food by the U.S. Food and Drug Administration (FDA).[24] A solution with 2% alginic acid and 1% nanoparticles was prepared and ejected through a 18 gauge syringe needle dropwise into a stirring solution of 2% calcium chloride. The drops form beads immediately upon addition to the calcium chloride solution. The alginate beads loaded with nanoparticles were recovered by filtration, covered with water, and then freeze-dried.

A.3.3 Alginate encapsulation confirmed using fluorescence microscopy

Fluorescently-labeled nanoparticles encapsulated in alginate were imaged using fluorescence microscopy with a Leica SP2 AOBS confocal microscope or Zeiss Axiovert 200 M microscope. Dry beads where place between a microscope slide and a cover slip using a spacer.

A.3.4 Nanoparticle release from alginate matrices

Nanoparticle release from alginate matrices was initially evaluated using simulated gastric (pH 1.2) and intestinal fluid (pH 7.5) test solutions with and without enzymes (United States Pharmacopeia (USP) XIX) as well as in PBS at pH 2 and 7. Drug dissolution in simulated gastrointestinal fluids is the USP standard for characterizing release for oral delivery systems. The residence time of an oral system in the mouth and esophagus is very short and thus not included as part of a USP standard, the system will spend approximately 2.5 h and 3.3 h in the stomach and small bowel, respectively.[25] The proteolytic enzyme pepsin is a major stomach enzyme and pancreatin is representative of intestinal enzyme. Pancreatin is a mixture of amylase, lipase, and trypsin, to degrade starches, triglycerides, and proteins, respectively. Amylase and lipase are also important enzymes present in saliva.

The simulated gastrointestinal solutions were used for static release experiments and the PBS was used for a dynamic release experiment where there was a step change in pH at 90 minutes. Alginate beads were added to the test solutions at 0.5 mg beads/ml test solution and samples were collected (with replacement) to measure release over time. Photo-bleaching of the fluorophore was minimized by avoiding light exposure to the beads, release solution, or samples. The fluorescence intensity was measured with a plate reader (Synergy HT, BioTek Instruments, Inc.) with excitation set to a 20 nm filter at 485 nm and emission set to a 20 nm filter at 528 nm.

A.4 Results and discussion

A.4.1 Alginate encapsulation confirmed using fluorescence microscopy

Fluorescently-labeled nanoparticles encapsulated in alginate were imaged using fluorescence microscopy with a Leica SP2 AOBS confocal microscope (see Figure A.3) or Zeiss Axiovert 200 M microscope (see Figure A.4). Beads without fluorescently-labeled nanoparticles had negligible autofluorescence. The image was used to confirm encapsulation of the nanoparticles by the alginate as the beads show green fluorescence throughout.

A.4.2 Nanoparticle release from alginate matrices

Nanoparticle release from alginate matrices was initially evaluated using simulated gastric (pH 1.2) and intestinal fluid (pH 7.5) test solutions with and without enzymes as well as in PBS at pH 2 and 7. While the limitations of the preliminary calibration curves prevent determination of the exact concentration (see Figure A.5), the concentration can be approximated using the linear regression trend line (see Figure A.6). The calibration curves show scatter at low concentrations; the poor fit to a linear trend line at low concentrations suggests that accurate concentration measurements at such low fluorescence intensities will not be possible. The approximation results in some concentration values that appear negative (although actual concentration values must be greater than zero). The release plots show release at high and

neutral pH but no release at low pH. The release behavior is well defined in simulated gastrointestinal test solutions without enzymes, but the presence of enzymes results in curves that are less well define.

Images of the beads (dried beads, beads in buffers, and beads in simulated gastric fluids) are shown in Figure A.7. The alginate beads used in the dynamic release experiment where the pH was increased from pH 2 to pH 7 are swollen but intact. The alginate beads exposed to simulated gastric fluids (pH 1.2, with and without enzymes) remained intact while the alginate beads exposed to simulated intestinal fluid (pH 7.5, with and without enzymes) disintegrated.

A.5 Conclusion

Alginate encapsulation was investigated as a strategy for oral delivery. Alginate is a biodegradable biopolymer has been approved for use in food, and so it is an attractive candidate for an oral delivery system. pH-dependent release of fluorescently-labeled nanoparticles from the alginate encapsulation was observed. Unfortunately, accurate quantitation at low concentrations was not possible. While alginate encapsulation may be a useful oral delivery strategy, effective translation of this technology would be best achieved by a commercial partnership with access to a wide variety of alginate types in order to find the best type for this oral delivery system.

A.6 Figures

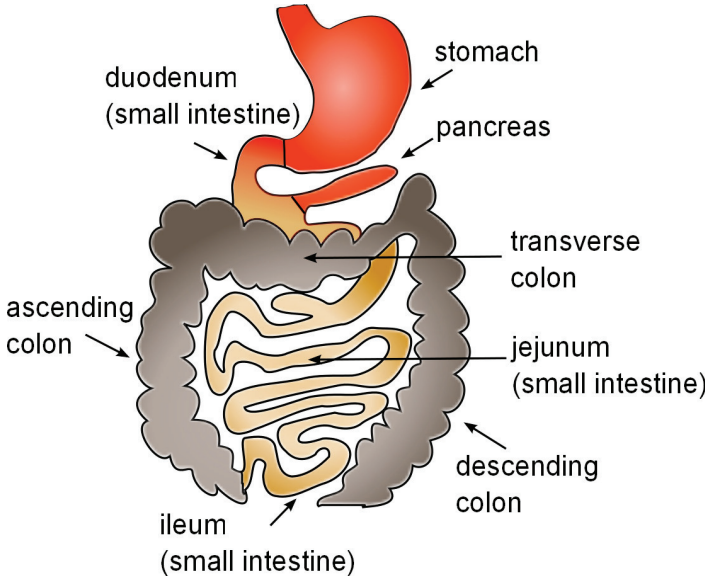

Figure A.1: Gastrointestinal tract, shown from the stomach to the colon. The pH increase from a value of 1.2-2 in the stomach, to 6.6 in the duodenum, to an average pH value of 7 in the colon.[12]

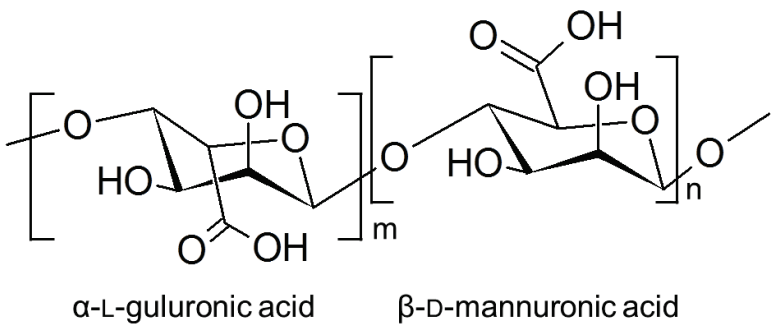

Figure A.2: Alginate is composed of repeating units of α-L-guluronic acid and β-D-mannuronic acid.

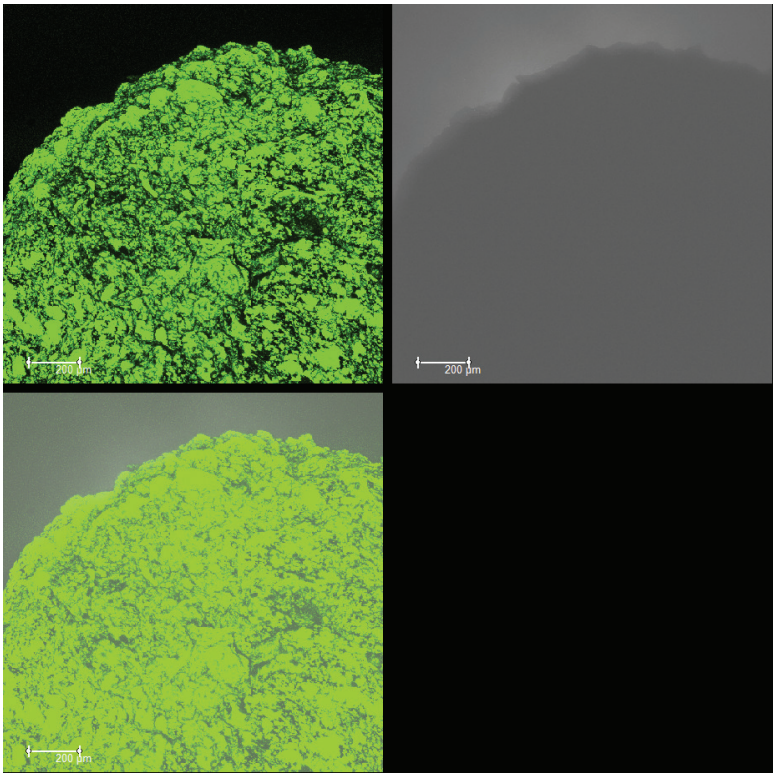

Figure A.3: Alginate bead containing polycationic nanoparticles fluorescently-labeled with NBD. Images taken using the Leica SP2 AOBS confocal microscope and processed using ImageJ software. Alginate does not have detectable autofluorescence.

(a) Brightfield of alginate bead with NBD-NPs

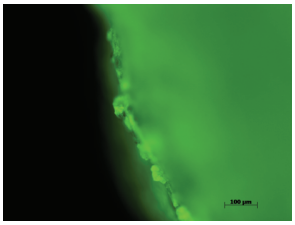

(b) Fluorescence of alginate bead with NBD-NPs

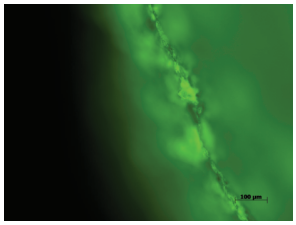

(c) Fluorescence of alginate bead with NBD-NPs

(d) Fluorescence of alginate bead without NPs, normal exposure

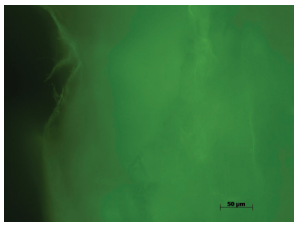

(e) Fluorescence of alginate bead without NPs, near maximum exposure intensity

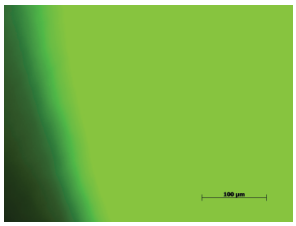

(f) Fluorescence of alginate bead with NBD-NPs, medium exposure intensity

Figure A.4: Alginate bead containing polycationic nanoparticles fluorescently-labeled with NBD. Fluorescence can be detected at all locations observed on the exterior of the bead. Images (b) and (c) show how the line of fluorescence in focus travels up the bead while adjusting focus. Image (d) shows that autofluorescence of the alginate cannot be detected using the exposure settings used for imaging the beads containing NBD-NPs, but image (e) shows that autofluorescence can be detected by greatly increasing exposure up to 10.97 s, 182%. Image (f) shows that for the alginate beads with NBD-NPs, the fluorescence is saturated at exposures much less than those to detect autofluorescence. Images taken using the Zeiss Axiovert 200 M at 10 x. (a-d 92.82 ms, 98% exposure; e 10.97 s, 182% exposure; f 3s, 97% exposure).

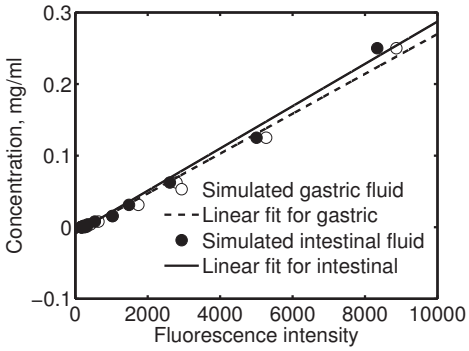

(a) High concentration range in simulated gastrointestinal test solutions without enzymes

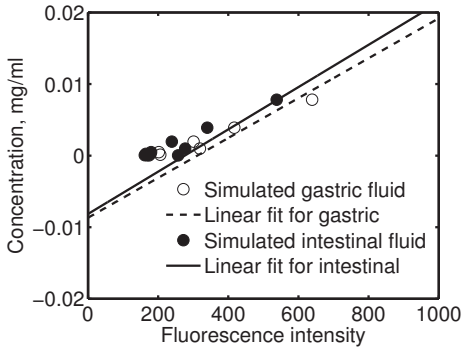

(b) Low concentration range in simulated gastrointestinal test solutions without enzymes

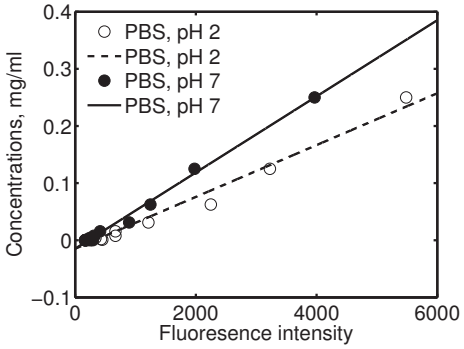

(c) High concentration range in PBS

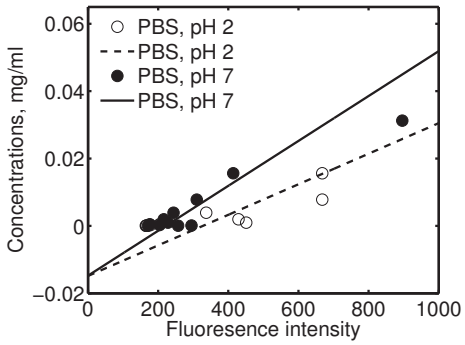

(d) Low concentration range in PBS

Figure A.5: Calibration curves for fluorescently-labeled nanoparticles were prepared in the simulated gastrointestinal solutions without enzymes and in PBS. An additional calibration curve is needed for fluorescently-labeled nanoparticles in simulated gastrointestinal solutions with enzymes.

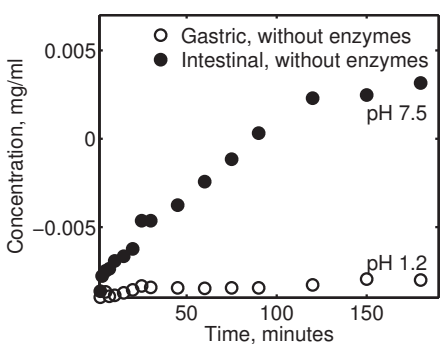

(a) Static release in simulated gastrointestinal test solutions without enzymes

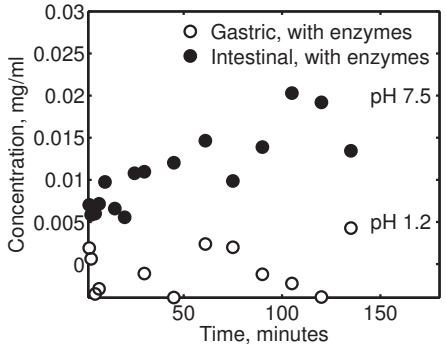

(b) Static release in simulated gastrointestinal test solutions with enzymes

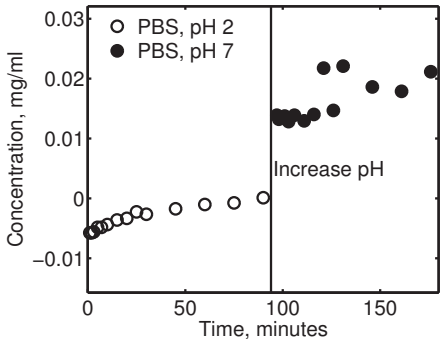

(c) Dynamic release in PBS

Figure A.6: Release of fluorescently-labeled nanoparticles from alginate matrix. The concentration of nanoparticles was determined using a calibration curve as a function of fluorescence intensity. The release with enzymes was approximated using the calibration curve for solutions without enzymes. a) Simulated gastric fluid at pH 1.2 and simulated intestinal fluid at pH 7.5 (USP XIX), prepared without enzymes. b) Simulated gastric fluid at pH 1.2 with pepsin and simulated intestinal fluid at pH 7.5 with pancreatin (amylase, lipase, and protease) (USP XIX). c) Release in PBS buffer at pH 2 and then increased to pH 7 after 90 minutes.

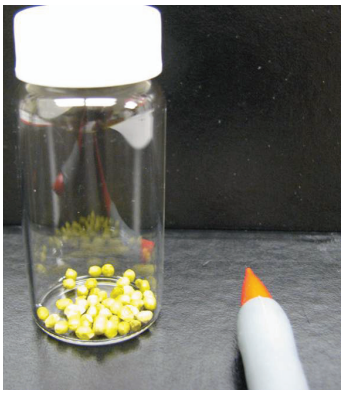

(a) Dried alginate beads containing fluorescently-labeled nanoparticles

(b) Dynamic release in PBS

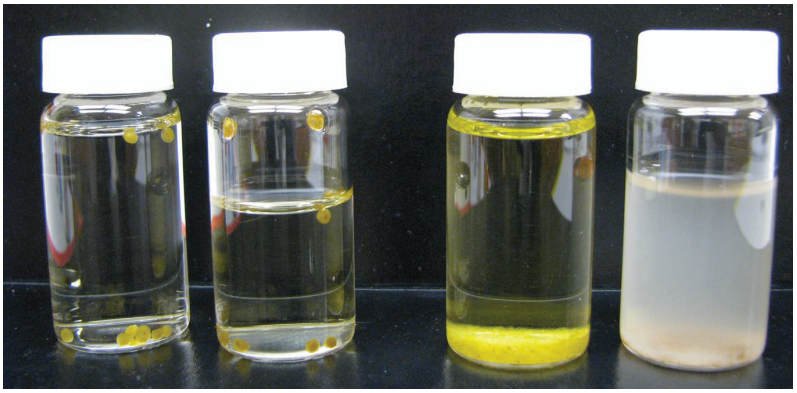

(c) Static release insimulated gastrointestinal fluids (gastric without enzymes, gastric with enzymes, intestinal without enzymes, intestinal with enzymes)

Figure A.7: Alginate beads after nanoparticle release experiment. From left to right: simulated gastric fluid at pH 1.2 without enzymes, simulated intestinal solution at pH 7.5 without enzymes, and PBS at pH 7. Alginate beads remain intact at low pH but disintegrate at pH 7.5 in simulated intestinal fluid without enzymes.

A.7 References

[1] A. D. Augst, H. J. Kong, and D. J. Mooney. Alginate hydrogels as biomaterials. *Macromol. Biosci.*, 6(8):623–633, 2006.

[2] H. H. Tønnesen and J. Karlsen. Alginate in drug delivery systems. *Drug Dev. Ind. Pharm.*, 28(6):621–630, 2002.

[3] FMCBiopolymer. Alginate, 2012. http://www.fmcbiopolymer.com/ othermarkets/OtherMarkets/Products/Alginate.aspx.

[4] M. M. Patel. Cutting-edge technologies in colon-targeted drug delivery systems. *Expert Opin. Drug Del.*, 8(10):1247–1258, 2011.

[5] A. Jain, Y. Gupta, and S. K. Jain. Perspectives of biodegradable natural polysaccharides for site-specific drug delivery to the colon. *J. Pharm. Pharm. Sci.*, 10(1):86–128, 2007.

[6] V. R. Sinha and R. Kumria. Polysaccharides in colon-specific drug delivery. *Int. J. Pharm.*, 224(1):19–38, 2001.

[7] H. Laroui, D. S. Wilson, G. Dalmasso, K. Salaita, N. Murthy, S. V. Sitaraman, and D. Merlin. Nanomedicine in GI. *Am. J. Physiol. Gastrointest. Liver Physiol.*, 300(3):G371–G383, 2011.

[8] M. Ashford, J.T. Fell, D. Attwood, H. Sharma, and P.J. Woodhead. An *in vivo* investigation into the suitability of pH dependent polymers for colonic targeting. *Int. J. Pharm.*, 95(1-3):193–199, 1993.

[9] E. L. McConnell, M. D. Short, and A. W. Basit. An *in vivo* comparison of intestinal pH and bacteria as physiological trigger mechanisms for colonic targeting in man. *J. Control. Release*, 130(2):154–160, 2008.

[10] M. M. Patel and A. F. Amin. Design and optimization of colon-targeted system of theophylline for chronotherapy of nocturnal asthma. *J. Pharm. Sci.*, 100(5):1760–1772, 2011.

[11] V. R. Sinha and R. Kumria. Microbially triggered drug delivery to the colon. *Eur. J. Pharm. Sci.*, 18(1):3–18, 2003.

[12] D. F. Evans, G. Pye, R. Bramley, A. G. Clark, T. J. Dyson, and J. D. Hardcastle. Measurement of gastrointestinal pH profiles in normal ambulant human subjects. *Gut*, 29(8):1035–1041, 1988.

[13] A. Rubinstein. Microbially controlled drug delivery to the colon. *Biopharm. Drug Dispos.*, 11(6):465–475, 1990.

[14] C. Ji, H. Xu, and W. Wu. *In vitro* evaluation and pharmacokinetics in dogs of guar gum and Eudragit FS30D-coated colon-targeted pellets of indomethacin. *J. Drug Targeting*, 15(2):123–131, 2007.

[15] M. M. Patel and A. F. Amin. Process, optimization and characterization of mebeverine hydrochloride loaded guar gum microspheres for irritable bowel syndrome. *Carbohydr. Polym.*, 86(2):536–545, 2011.

[16] C. E. Beneke, A. M. Viljoen, and J. H. Hamman. Polymeric plant-derived excipients in drug delivery. *Molecules*, 14(7):2602–2620, 2009.

[17] C. L. Bayer, É. P. Herrero, and N. A. Peppas. Alginate films as macromolecular imprinted matrices. *J. Biomater. Sci., Polym. Ed.*, 22(11): 1523–1534, 2011.

[18] D. Chang, J. Lei, H. Cui, N. Lu, Y. Sun, X. Zhang, C. Gao, H. Zheng, and Y. Yin. Disulfide cross-linked nanospheres from sodium alginate derivative for inflammatory bowel disease: Preparation, characterization, and *in vitro* drug release behavior. *Carbohydr. Polym.*, 88(2):663–669, 2012.

[19] N. Nograles, S. Abdullah, M. N. Shamsudin, N. Billa, and R. Rosli. Formation and characterization of pDNA-loaded alginate microspheres for oral administration in mice. *J. Biosci. Bioeng.*, 113(2):133–140, 2012.

[20] P. Agulhon, V. Markova, M. Robitzer, F. Quignard, and T. Mineva. Structure of alginate gels: Interaction of diuronate units with divalent cations from density functional calculations. *Biomacromolecules*, 13(6): 1899–1907, 2012.

[21] G. Fundueanu, C. Nastruzzi, A. Carpov, J. Desbrieres, and M. Rinaudo. Physico-chemical characterization of Ca-alginate microparticles produced with different methods. *Biomaterials*, 20(15):1427–1435, 1999.

[22] J. Klein, J. Stock, and K. D. Vorlop. Pore size and properties of spherical Ca-alginate biocatalysts. *Appl. Microbiol. Biotechnol.*, 18(2):86–91, 1983.

[23] R. Bodmeier, H. Chen, and O. Paeratakul. A novel approach to the oral delivery of micro-or nanoparticles. *Pharm. Res.*, 6(5):413–417, 1989.

[24] U.S. Food and Drug Administration. Everything Added to Food in the United States (EAFUS), 2011. http://www.fda.gov/Food/FoodIngredientsPackaging/ucm115326.htm.

[25] L. P. Degen and S. F. Phillips. Variability of gastrointestinal transit in healthy women and men. *Gut*, 39(2):299–305, 1996.

Appendix B

TNF-α Knockdown as a Strategy for the Treatment of Inflammatory Bowel Disease

B.1 Introduction

RNAi-based therapeutics may offer improved treatment strategies to treat and prevent inflammation. Inflammatory bowel disease, a disease characterized by inflammation of the gastrointestinal tract, may benefit from a treatment strategy designed to deliver anti-inflammatory siRNA to the intestines. There are an estimated 1.4 million people in the United States with inflammatory bowel disease (IBD).[1;2] The burden of the disease has been described as "More Than Pain and Diarrhea";[3] the disease has a profound impact on the individual as well as a heavy economic burden ($15.5 billion in direct and indirect costs[4]) for the United States. The disease accounts for an estimated 100,000 hospitalizations per year, and there are an estimated 119,000 people who are disabled and unable to work as a result of inflammatory bowel disease.[1]

Inflammatory bowel disease in children is a huge challenge for physi-

cians; both the disease and the therapeutics used to treat it can interfere with growth and development, and some of the medications are associated with serious or life-threatening cancers in children. There are an estimated 140,000 people under the age of eighteen with inflammatory bowel disease,[1] and the incidence rate in children is increasing.[5]

As its name suggests, inflammatory bowel disease is characterized by inflammation in the gastrointestinal (GI) tract. Symptoms include diarrhea, abdominal pain, GI bleeding, weight loss, fatigue, and fever (see Figure B.1).[1] The exact cause is unknown but is believed to result from a combination of genetic and environmental factors.[6] It is a lifelong disease with periods of remission and relapse. The symptoms of IBD do more than just affect the patient's quality of life; they can also lead to serious and life-threatening complications.

The most common types of inflammatory bowel disease are ulcerative colitis (UC) and Crohn's disease (CD). The most important differences between the types are the location and the extent of the inflammation; for UC, inflammation is restricted to the epithelial lining in the colon and the rectum, and for CD, inflammation may occur anywhere in the gastrointestinal tract (although it most commonly occurs in the intestine) and the inflammation may spread deep into bowel tissue.[7]

There is no curative drug treatment for IBD; instead, treatment is intended to induce and maintain remission. Each of the therapeutics used for the treatment of IBD has limitations (see Table B.1) and for many patients,

medications are not enough and surgery becomes necessary when symptoms are uncontrolled or complications develop. Approximately 30% of people with ulcerative colitis and 70% of people with Crohn's disease will require surgery at some point.[8] Recall that in ulcerative colitis, inflammation is restricted to the colorectal tissue, and so removing all of this tissue will "cure" the patient whereas in the case of Crohn's disease, the inflammation can occur throughout the length of the GI tract and so cannot be "cured" with surgery.

The main focus of both biological and RNA interference (RNAi)-based therapeutics for the treatment of inflammatory bowel disease has been anti-tumor necrosis factor (TNF)-α functionality. Although the pathogenesis of IBD is not well understood, it is acknowledged that TNF-α plays an important role as a pro-inflammatory cytokine.[9] Biological therapeutics that block TNF-α include infliximab (Remicade®, Janssen Biotech, Inc.), adalimumab (Humira®, Abbott Laboratories), and certolizumab (Cimzia®, UCB, Inc.), and etanercept (Enbrel®, Pfizer), and all but etanercept are recommended treatments for Crohn's disease.[10] These biological therapeutics lead to systemic TNF-α repression that can lead to serious side effects; adverse events such as mycobacterial infections (tuberculosis) or allergic responses (anaphylaxis) have been reported.[11] Perhaps even more concerning is the potential carcinogenicity of the treatments, but there is insufficient data to conclude if the reported cases of cancer following infliximab treatment were caused by the infliximab.[11] Unfortunately, up to a third of patients in clinical trials have been unresponsive to infliximab treatment.[4;11] Natalizumab (Tysabri®, Elan Phar-

maceuticals, Inc) is distinct from other biologic treatments for Crohn's disease because it is not an anti-TNF-α antibody but instead is an antibody against the cellular adhesion molecule α4-integrin.[12] Therapeutic siRNAs investigated with oral delivery systems include anti-TNF-α siRNA used by Wilson and associates[13] and Amiji and Kriegel[14] as well as Cyclin D1 (regulates cell cycle progression) used by Amiji and colleagues[14] and Map4k4 (facilitates TNF-α signaling) used by Aouadi and associates.[15]

B.2 Experimental section

B.2.1 Chemicals

Reagents poly(ethylene glycol) methyl ether methacrylate (PEGMA) solution (M_n 2000 for PEG chain, 50 wt% in water), 2-(diethylamino)ethyl methacrylate (DEAEMA), *tert*-butyl methacrylate (tBMA), tetraethylene glycol dimethacrylate (TEGDMA), ethyl 2-bromoisobutyrate (EBIB), tris (2-pyridylmethyl) amine (TPMA), ascorbic acid (AA), and Dulbecco's Phosphate-Buffered Saline (DPBS) were purchased from Sigma-Aldrich. 1 N Hydrochloric acid (HCl) and phosphate buffered saline (PBS) were purchased from Fisher Scientific. Copper(II) bromide was purchased from Acros Organics. Ultrapure water was used for all studies. All chemicals were used as received.

B.2.2 Nanoparticle synthesis and purification

The P(DEAEMA-*co*-PEGMA-*co*-tBMA-*co*-TEGDMA) polycationic nanoparticles were prepared as described previously[16;17] with an ARGET ATRP catalyst/ligand/initiator system ($CuBr_2$/TPMA/EBIB) and 45 mol tBMA and 10 mol PEGMA with respect to 100 mol DEAEMA in the feed. The monomer-in-water emulsion was stabilized with 8 mg/ml Brij® 30 (Acros Organics) and 1.35 mg/ml myristyltrimethylammonium bromide (MyTab, Sigma-Aldrich) at a 0.1 weight ratio monomer to solvent. The mixture was probe sonicated (S-4000 Misonix Ultrasonicator Misonix Inc.) and degassing with nitrogen prior to adding degassed ascorbic acid solution as a reducing agent (AA:DEAEMA::0.5:100) to start the reaction. The reaction was allowed to continue for 3 h and the nanoparticles were purified using a technique described previously by Fisher and Peppas[18] with repeated precipitation/resuspension with acetone/0.5 N HCl followed by dialysis (12,000-14,000 molecular weight cut off regenerated cellulose tubing, Spectra/Por®) and freeze-drying.

Fluorescently-labeled nanoparticles were synthesized using NBD chloride (NBD-Cl, 7-chloro-4-nitrobenzo-2-oxa-1,3-diazole, also called 4-chloro7-nitrobenzofuran, Sigma-Aldrich). Nanoparticles containing primary amines were synthesized with 2-aminoethyl methacrylate (AEMA, Sigma-Aldrich) (AEMA:DEAEMA::32:100). Dried, purified nanoparticles were suspended in ethanol and combined with an excess of NBD chloride; a typical reaction was 450 mg of dried nanoparticles with 50 mg NBD chloride in 30 ml

ethanol. The mixture was allowed to react overnight to form NBD-labeled nanoparticles (NBD-NPs). Unreacted NBD-Cl was removed by dialysis and the fluorescently-labeled nanoparticles were recovered with freeze-drying. Note that the NBD-Cl becomes strongly fluorescent upon reaction with amines and that NBD-amines are excited by visible light (464 nm) with emission maximum of approximately 512 nm.

B.2.3 Cell culture

Murine macrophage RAW264.7 cells (obtained from American Type Culture Collection) were maintained in Dulbecco's Modified Eagle's Medium high glucose without L-glutamine (DMEM, Sigma-Aldrich) supplemented with with 1% L-glutamine (MediaTech), 1% penicillin (Sigma-Aldrich), 1% streptomycin (Sigma-Aldrich), and 10% HyClone USDA Tested Fetal Bovine Serum (FBS, Thermo Scientific). Cells were plated in 2% FBS complete media (no phenol red) or 10% FBS complete media. Opti-MEM® Reduced Serum Medium, no Phenol Red (Life Technologies) was used for transfection experiments.

B.2.4 Internalization of fluorescently-labeled nanoparticles evaluated using flow cytometry and confocal microscopy

Flow cytometry was used to quantify internalization of fluorescently-labeled nanoparticles. Flow cytometry measurements were collected using a

BD Fortessa Flow Cytometer and analyzed using FACSDiva software (BD Biosciences). 1 million RAW264.7 cells were plated in a flask (T25) in 2 % FBS media (complete, no phenol red) and incubated for 18 h. Next, cells were incubated for 2 h with 0.25 mg/ml fluorescently-labeled polycationic nanoparticles in 2 % FBS media. Following this 2 h incubation, cells were rinsed three times with cold DPBS pH 7.4 prior to scraping (RAW264.7) to form a cell suspension. The cell suspension was centrifuged, the supernatant discarded, and the pellet resuspended in flow cytometry buffer (1% FBS in DPBS). The samples were stored in darkness at 4 °C before measurement. The results are reported in two ways: as the average percent of cells (taken over a large number of cells, typically 10,000) containing fluorescently-labeled DY647 siRNA.

Flow cytometry does not distinguish between surface bound and internalized fluorescence signal, so confocal microscopy was used to verify internalization of the fluorescently-labeled nanoparticles. RAW 264.7 cells were seeded at 95,000 cells/well on acid-wash glass cover slips in a 12 well plate. Cells were incubated for 18 h prior to 2 h incubation with 0.25 mg/ml fluorescently-labeled nanoparticles in 2% FBS media. Following incubation, cells were rinsed three times with 1xPBS pH 7.4. Cells were fixed with 4% para formaldehyde in 1xDPBS for 10 min at room temperature prior to washing three times with HBSS (BioWhittaker). Cells were stained with 1 μg/ml Wheat Germ Agglutinin (WGA) Alexa Fluor 594 conjugate for 10 min at room temperature. Cells were rinsed twice with cold HBSS and once with DI water (autoclaved). Cover slips were mounted to glass slides using Prolong® Gold anti-fade reagent with

DAPI (Life Technologies) and stored in the freezer prior to imaging.

Confocal images were acquired using a Zeiss LSM 710 confocal microscope with a 63x objective. The gain and offset for the different channels were kept constant for the full series of images to permit image comparisons. Images were collected in 16 bit format, and all images underwent identical post-processing (γ=0.45 for red and blue channels, γ=0.1.3 for brightfield, and brightfield scale adjusted to max/min using ZEN Blue).

B.2.5 Induce inflammation with LPS in RAW264.7 cells

RAW264.7 cells were seeded at 240,000 cells/well in 6 well plates (Nunc, Thermo Scientific) in 2% FBS complete media (no phenol red). After 18 h incubation, the media was replaced with 2% FBS complete media (no phenol red) or solutions (200 to 3.125 ng/ml in dilutions by halves) of lipopolysaccharide (LPS, Sigma-Aldrich) to induce inflammation. Samples of the supernatant were removed at various times (0 h, 1 h, 2 h, 3 h, 4 h, 6 h, 8 h, 24 h, and 48 h) and stored at -80 °C prior to analysis of the TNF-α expression.

The TNF-α expression in the RAW264.7 cell supernatant was evaluated by TNF-α-induced killing of L929 cells.[19;20] The relative viability of the L929 following incubation with the TNF-α-containing supernatant is correlated with the concentration of the TNF-α. L929 cells were seeded at 35,000 cells per well in 96 well plates (Nunc, Thermo Scientific) in 100 µl of 2% FBS complete media (no phenol red). After 18 h incubation, 50 µl of supernatant sample (or

control) and 50 µl of 8 µg/ml Actinomycin D were added to each well. After 24 h incubation, the media was removed and cells were rinsed once with 100 µl PBS and cells were incubated for 2.5 h with CellTiter 96® AQ_{ueous} Non-Radioactive Cell Proliferation Assay (MTS, Promega) with serum-free DMEM without phenol red (Sigma-Aldrich). The absorbance at 690 nm (background) and 490 nm (MTS assay) was measured using a microplate reader (Synergy HT, BioTek Instruments, Inc.), and cell viability (V) was calculated as shown in Equation B.1:

$$\mathrm{V} = \frac{A_{490,\,sample} - A_{690,\,sample} - (A_{490,\,no\,cells} - A_{690,\,no\,cells})}{A_{490\,media} - A_{690,\,media} - (A_{490,\,no\,cells} - A_{690,\,no\,cells})} \quad \text{(B.1)}$$

B.2.6 Transfect RAW264.7 cells with anti-TNF-α siRNA and induce inflammation with LPS

RAW264.7 cells were transfected with anti-TNF-α siRNA prior to treatment with LPS to induce inflammation to check for knockdown of TNF-α expression. Three different conditions were tested, varying in cell seeding conditions, transfection conditions, transfection incubation time, and LPS treatment incubation time (see Table B.2). The Student's t-test (two-tailed, unequal variance) was used to determine statistical significance. Knockdown was calculated from the TNF-α expression (C) as shown in Equation B.2:

$$\% \text{ Knockdown} = 100 \times \left(1 - \frac{C_{anti-TNF-\alpha}}{C_{Scrambled}}\right) \tag{B.2}$$

Condition 1: RAW264.7 cells were seeded at 95,000 cells per well in 12 well plates in 2% FBS complete media (no phenol red) and incubated for 18 h prior to adding fresh media (2% FBS, complete, no phenol red). After 1 h incubation with fresh media, complexes of polycationic nanoparticles or Lipofectamine2000 with siRNA were added.

The polycationic nanoparticle/siRNA complexes were prepared ahead of time using anti-TNF-α or negative control siRNA (Life Technologies). To prepare the complexes, 1.5 mg/ml polycationic nanoparticles with 150 nM siRNA in 1x PBS pH 5.5 were incubated for 1 h in nuclease-free low-adhesion tubes. Next, acetone was added and the tubes were centrifuged for 15 min at 14,500 rpm to form a pellet. The supernatant was discarded and the tubes allowed to dry for ~20 min in a laminar flow hood so residual acetone could evaporate. The pellets were resuspended and added to cells at 1/6 the concentration of the preparation. Lipofectamine2000/siRNA complexes were added to wells for 0.25 µl/well Lipofectamine2000 with 25 nM siRNA.

The RAW264.7 cells were incubated with the complexes for 4 h prior to removal and replacement with fresh media (2% FBS, complete, no phenol red). After 20 h incubation with the fresh media, samples of supernatant were removed (0 h time point) and cells were incubated with 200 ng/ml LPS in media. Supernatant samples were removed at 1 h and 24 h and the TNF-α

concentration was evaluated using a TNF-α ELISA (eBioscience) according to the manufacturers instructions.

Condition 2: RAW264.7 cells were seeded at 10,000 cells per well in 96 well plates in 10% FBS complete media. After 18 h incubation, the media was replaced with Opti-MEM®. The nanoparticles were combined with siRNA (anti-TNF-α or negative control siRNA) in 1xPBS pH 5.5. The complexes were added to cells following 1 h incubation with Opti-MEM®. The final concentration of polycationic nanoparticles in the wells was 0.025 mg/ml with 100 nM or 200 nM siRNA. Lipofectamine2000 wells contained 0.25 µl/well Lipofectamine2000. Following 42 h incubation, media was removed and cells were incubated with Opti-MEM® or 200 ng/ml LPS in Opti-MEM®. Following 7 h incubation, the supernatant was removed and the TNF-α concentration was evaluated using a TNF-α ELISA (eBioscience) according to the manufacturers instructions.

Condition 3: Condition 3 varies from Condition 2 only in the incubation times for transfection and LPS treatment. In Condition 3, the RAW264.7 cells are incubated with the complexes for 26 h and with 200 ng/ml LPS for 16 h.

B.3 Results and discussion

The ability of polycationic nanoparticles to reduce TNF-α expression in inflamed RAW264.7 cells was evaluated. LPS was used to induce inflam-

mation in RAW264.7 cells. TNF-α is an important target for the treatment of inflammatory diseases, such as inflammatory bowel disease and arthritis.

B.3.1 Internalization of fluorescently-labeled nanoparticles evaluated using flow cytometry and confocal microscopy

The internalization of fluorescently-labeled nanoparticles by RAW264.7 cells was evaluated using flow cytometry. RAW264.7 cells were incubated for 2 h with 0.25 mg/ml fluorescently-labeled nanoparticles. The fluorescently-labeled nanoparticles are efficiently internalized by the RAW264.7 cells, with ~88% of cells associated with fluorescently-labeled nanoparticles (representative histogram shown in Figure B.2). Confocal microscopy confirmed internalization of the fluorescently-labeled nanoparticles (see Figure B.3 and Figure B.4).

B.3.2 Induce inflammation with LPS in RAW264.7 cells

Inflammation was induced in RAW264.7 cells with LPS at various concentrations. The inflammation profile of the RAW264.7 cells for various concentrations of LPS over time was determined using TNF-α-induced killing of L929 cells because the relative viability of the L929 cells can be correlated with the TNF-α expression of the RAW264.7 (see Figure B.5); increased viability is associated with decreased TNF-α. After 1 h of incubation of LPS with RAW264.7 cells, the different concentrations of LPS all produce signifi-

cant TNF-α (see Figure B.6). The 200 ng/ml LPS concentration was selected for future experiments.

B.3.3 Transfect RAW264.7 cells with anti-TNF-α siRNA and induce inflammation with LPS

RAW264.7 cells were transfected with anti-TNF-α siRNA prior to treatment with LPS to induce inflammation. Three different conditions were tested, varying in cell seeding density, transfection conditions, transfection incubation time, and LPS treatment incubation time. The transfection with anti-TNF-α siRNA was intended to induce knockdown of TNF-α expression. Unfortunately, the knockdown of TNF-α was highly variable within and between experiments, and it also dependent on the incubation times used in the experiment.

Some statistically significant knockdown was observed in RAW264.7 cells that had been transfected with Condition 1. The cells had been incubated for 4 h with complexes and then the media was changed. After 20 h, inflammation was induced using 200 ng/ml LPS and samples were analyzed from 0 h, 1 h, and 24 h. The 0 h samples demonstrate that the 45ARGET polycationic nanoparticles induce TNF-α expression while the Lipofectamine2000 TNF-α expression is indistinguishable from the no-carrier control (see Figure B.7). As a result, although the 45ARGET formulation induces TNF-α knockdown at 0 h (14-16%), the TNF-α expression of the RAW264.7 cells treated with 45ARGET/anti-TNF-α siRNA still exceeded that of the no-carrier control.

For cells treated with LPS for 1 h or 24 h, the Lipofectamine2000 outperformed the 45ARGET polycationic nanoparticles (see Figure B.8 and Figure B.9). There was 17% knockdown with Lipofectamine2000 for both 1 h and 24 h and 11% knockdown with the 45ARGET for 24 h. Unfortunately, neither the 45ARGET nor the Lipofectamine2000 was able reduce the TNF-α expression to a value comparable to that of the no LPS, no-carrier control.

Some knockdown was observed in RAW264.7 cells that had been transfected 42 h prior to 7 h treatment with LPS (Condition 2). In one experiment, statistically significant knockdown was only observed after LPS treatment of cells that had been transfected with 100 nM anti-TNF-α siRNA complexed with 0.025 mg/ml polycationic nanoparticles (69% knockdown, see Figure B.10). Unfortunately, when the experiment was repeated, statistically significant knockdown was only observed for 100 nM anti-TNF-α siRNA complexed with Lipofectamine2000 (25% knockdown) and increased TNF-α expression was observed for cells transfected with 45ARGET with 100 nM or 200 nM anti-TNF-α siRNA (see Figure B.11).

No knockdown was observed for RAW264.7 cells that had been transfected with Condition 3 (see Figure B.12). The cells had been incubated for 26 h with complexes followed by 16 h incubation with 200 ng/ml LPS to induce inflammation. The lack of knockdown observed may be a result of the reduced incubation time with the complexes combined with increased incubation time with LPS.

B.4 Conclusions

The proinflammatory cytokine TNF-α is an important target for the treatment of inflammatory diseases, such as inflammatory bowel disease and arthritis. RAW264.7 cells were pre-treated with polycationic nanoparticle/anti-TNF-α siRNA complexes prior to LPS-stimulation to induce inflammation. Unfortunately, the knockdown of TNF-α expression was low in magnitude and highly variable depending on the transfection conditions. Problems with *in vitro* transfection for 2D cell cultures have been reported in the literature, with improved knockdown observed in 3D cell culture models that are better able to represent complex biological systems.[21] As a result, the knockdown may be improved in a more complex model that better represents the inflammatory process. Alternatively, the anti-TNF-α-siRNA delivery strategy with the 45ARGET polycationic nanoparticles may not be sufficient to halt TNF-α expression resulting from the powerful LPS-induced inflammation response.

B.5 Tables

Table B.1: Medications used to treat IBD and their disadvantages. Improved treatment strategies are needed to better control symptoms while minimizing side effects.

Medications	**Problems**
5-Aminosalicylates: mesalamine[22] sulfasalazine[23]	Frequent (3-4 x) daily dosing Side effects: match IBD symptoms Risks: kidney damage
Corticosteroids: prednisone[24;25] methylprednisolone[24;26]	Risks: steroid dependence, infection, osteoporosis Side effects: weight gain, higher blood pressure, mood swings
Immunomodulators: azathioprine[27] 6-mercaptopurine[27]	Risks: decreased blood cells in bone marrow, cancer
Biological Treatments: infliximab[28]	Expensive, injections Risks: infection

Table B.2: Conditions for RAW264.7 transfection with anti-TNF-α siRNA. FBS: fetal bovine serum, NPs: polycationic nanoparticles

Parameter	**Condition 1**	**Condition 2**	**Condition 3**
Plate	12-well	96-well	96-well
Cells/well	95,000	10,000	10,000
Plating media	2% FBS complete media	10% FBS complete media	10% FBS complete media
Transfection media	2% FBS complete media	Opti-MEM®	Opti-MEM®
NPs / siRNA complexes	Complex 1.5 mg/ml NPs + 150 nM siRNA for 1h, precipitate and re-suspend, add to cells at 1/6th concentration	Complex 0.125 mg/ml NPs + 500 nM siRNA for 10 min, add to cells at 1/5th concentration (no acetone precipitation)	Complex 0.125 mg/ml NPs + 500 nM siRNA for 10 min, add to cells at 1/5th concentration (no acetone precipitation)
Lipofectamine2000 / siRNA complexes	25 nM siRNA with 2 µl Lipofec-tamine2000 / well	100 nM siRNA with 0.25 µl Lipofec-tamine2000 / well	100 nM siRNA with 0.25 µl Lipofec-tamine2000 / well
Transfection incubation time	4 h (20 h with fresh media)	42 h	24 h
LPS incubation time	1 h and 24 h	7 h	16 h

B.6 Figures

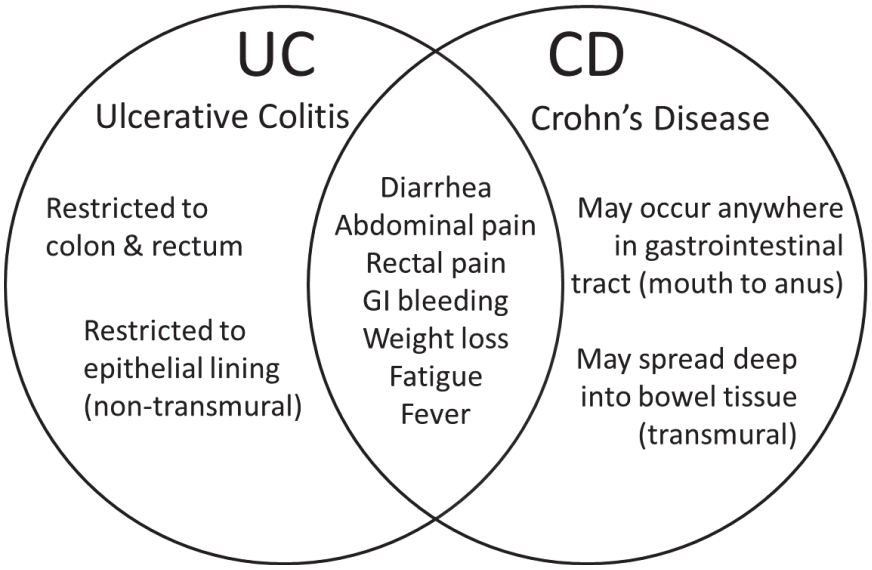

Figure B.1: Comparison of Ulcerative Colitis (UC) and Crohn's Disease (CD), the two main types of inflammatory bowel disease. Many of the symptoms are shared between the two types; the key difference is the location and extent of the inflammation.

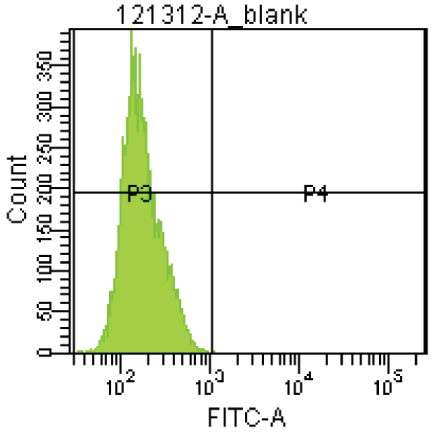

(a) Blank

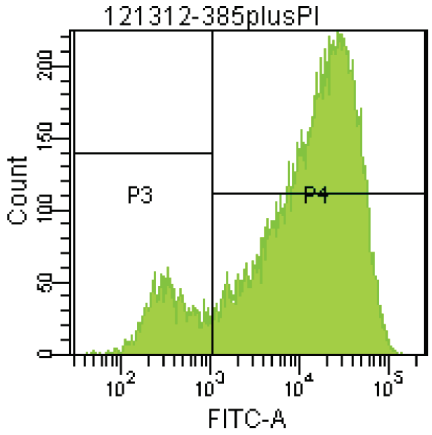

(b) RAW264.7 cells with fluorescently-labeled nanoparticles

Figure B.2: Representative histograms for flow cytometry to quantify uptake of fluorescently-labeled nanoparticles. a) Blank b) RAW264.7 cells incubated for 2 h with 0.25 mg/ml fluorescently-labeled nanoparticles.

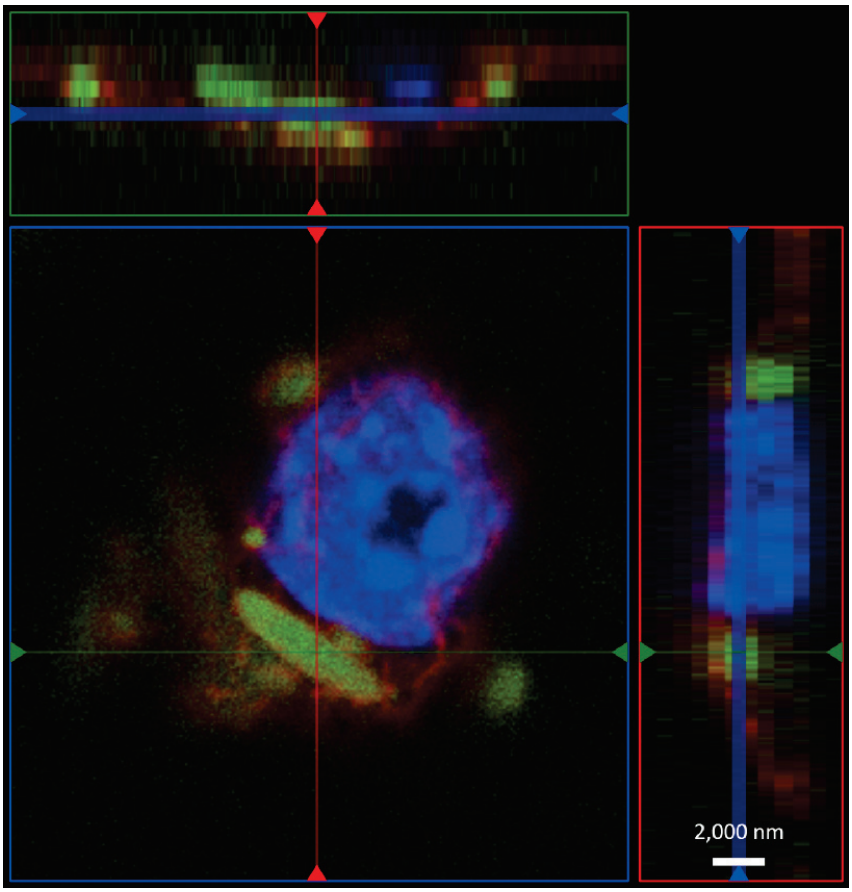

Figure B.3: Confocal microscopy to image internalization of fluorescently-labeled nanoparticles: orthogonal view. Orthogonal projections represent cross-sectional slices, and they are obtained by taking z-stack images. RAW264.7 cells incubated for 2 h with 0.25 mg/ml fluorescently-labeled nanoparticles prior to rinsing, fixing, staining, and mounting. Confocal images were acquired with a Zeiss LSM 710 confocal microscope with a 63x objective. The settings for the green laser were adjusted such that blank cells (no nanoparticles) demonstrated negligible fluorescence. Images were collected in 16 bit format, and all images underwent identical post-processing (γ=0.45 for red, blue, and green channels, γ=1.3 for brightfield, and brightfield scale adjusted to max/min using ZEN Blue). Red: cell membrane stained with Wheat Germ Agglutinin (WGA) Alexa Fluor 594 conjugate, blue: nuclei stained with DAPI, green: fluorescently-labeled nanoparticles

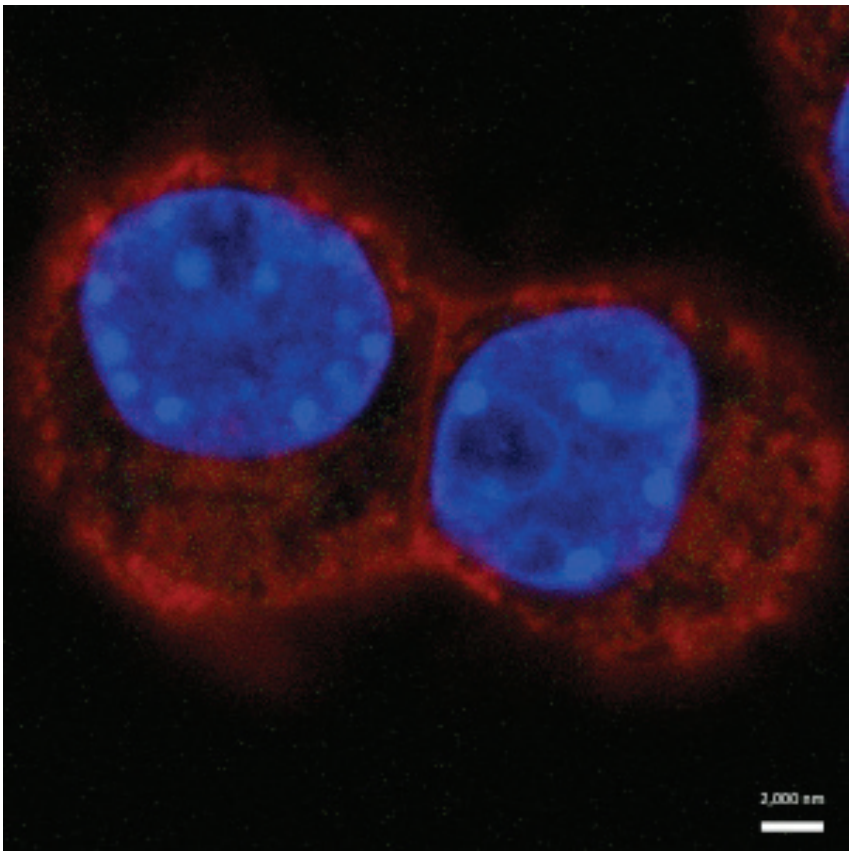

Figure B.4: Confocal microscopy to image internalization of fluorescently-labeled nanoparticles: RAW264.7 cells without fluorescently-labeled nanoparticles. Confocal images were acquired with a Zeiss LSM 710 confocal microscope with a 63x objective. The settings for the green laser were adjusted such that blank cells (no nanoparticles) demonstrated negligible fluorescence. Images were collected in 16 bit format, and all images underwent identical post-processing (γ=0.45 for red, blue, and green channels, γ=1.3 for brightfield, and brightfield scale adjusted to max/min using ZEN Blue). Red: cell membrane stained with Wheat Germ Agglutinin (WGA) Alexa Fluor 594 conjugate, blue: nuclei stained with DAPI, green: fluorescently-labeled nanoparticles

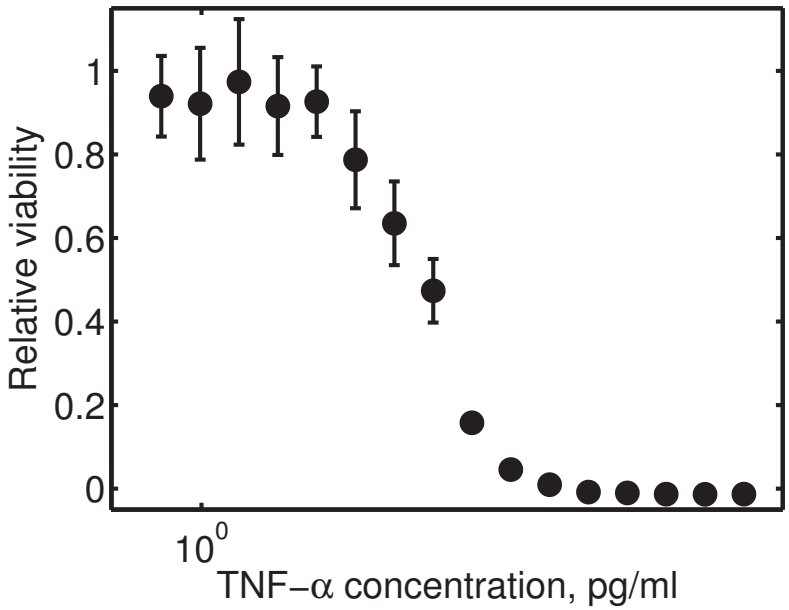

Figure B.5: The relative viability of L929 cells following TNF-α killing is correlated to the concentration of TNF-α. L929 cells were incubated with TNF-α dilutions. Data are represented as the mean plus/minus the standard deviation (n=3). For large concentrations of TNF-α, the standard deviations are smaller than the marker size and so are not visible.

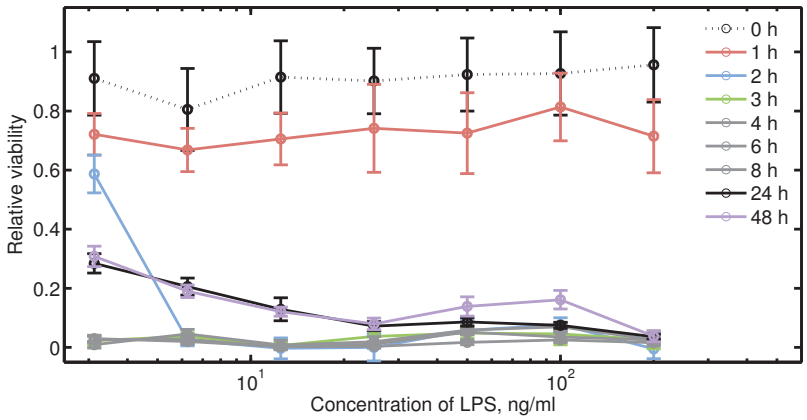

(a) No LPS

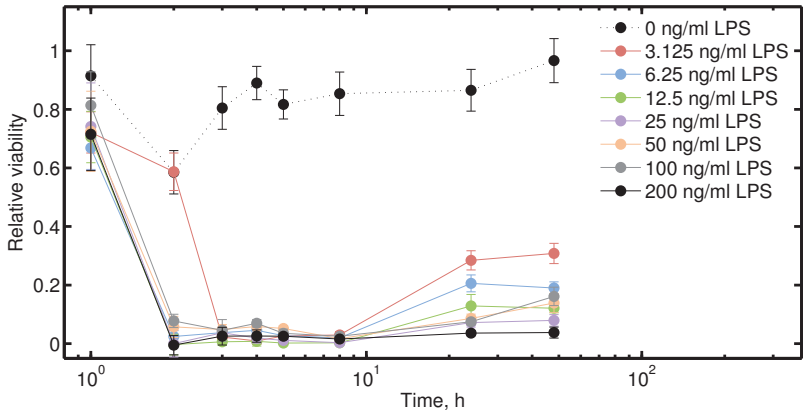

(b) LPS to induce inflammation

Figure B.6: Inflammation profile of RAW264.7 cells following incubation with LPS plotted versus a) concentration of LPS, ng/ml and b) incubation time, h. The relative viability of L929 cells following TNF-α killing is correlated to the concentration of TNF-α. L929 cells were incubated with supernatant from RAW264.7 cells following incubation with LPS. Data are represented as the mean plus/minus the standard deviation (n=3).

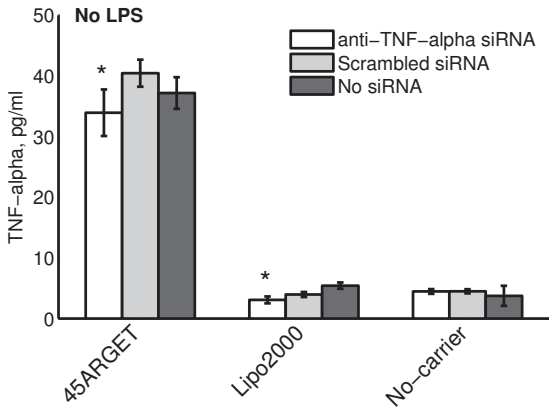

(a) No LPS

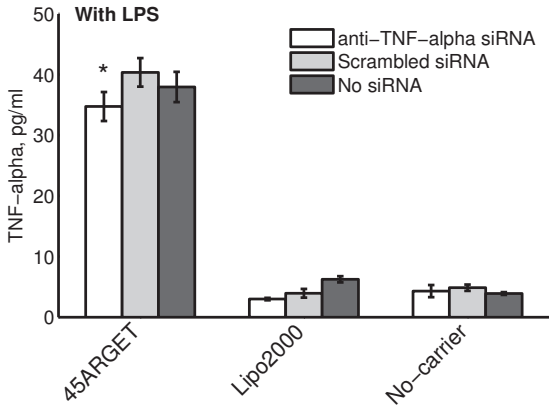

(b) LPS to induce inflammation

Figure B.7: TNF-α expression by RAW264.7 cells a) without LPS and b) with LPS (Condition 1, 0 h). RAW264.7 cells are incubated for 4 h with polycationic nanoparticle/siRNA complexes (acetone precipitate and re-suspend) and then 20 h with fresh media prior to removing supernatant for analysis of TNF-α with ELISA. Data is plotted as the mean plus/minus the standard deviation for n=2 biological replicates and n=2 technical ELISA replicates for each biological replicate. Asterisks (*) indicate $p<0.05$ as determined using a Student's t-test.

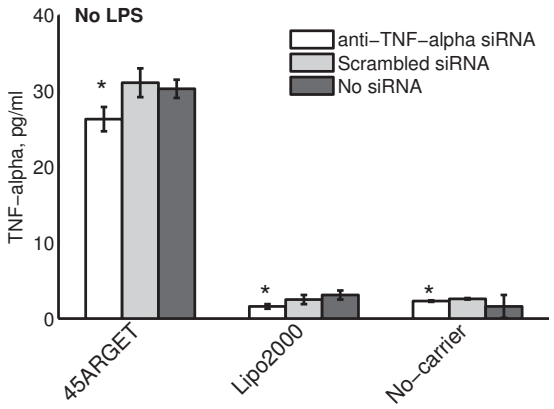

(a) No LPS

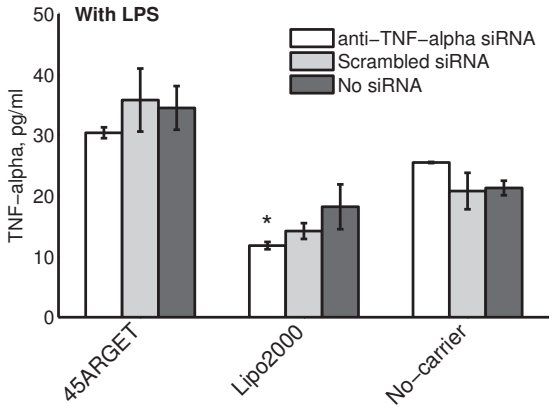

(b) LPS to induce inflammation

Figure B.8: TNF-α expression by RAW264.7 cells a) without LPS and b) with LPS (Condition 1, 1 h). RAW264.7 cells are incubated for 4 h with polycationic nanoparticle/siRNA complexes (acetone precipitate and re-suspend) and then 20 h with fresh media. Next, cells are incubated for 1 h with 200 ng/ml LPS prior to removing supernatant for analysis of TNF-α with ELISA. Data is plotted as the mean plus/minus the standard deviation for n=2 biological replicates and n=2 technical ELISA replicates for each biological replicate. Asterisks (*) indicate $p<0.05$ as determined using a Student's t-test.

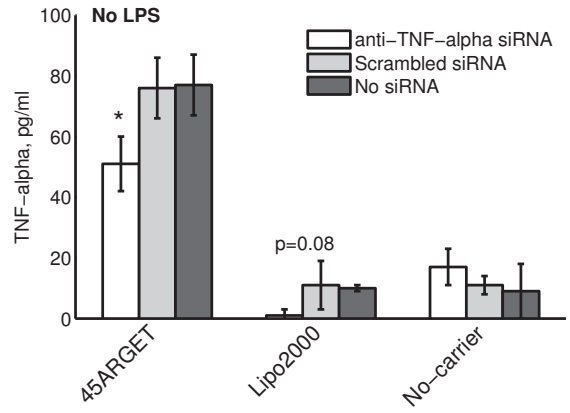

(a) No LPS

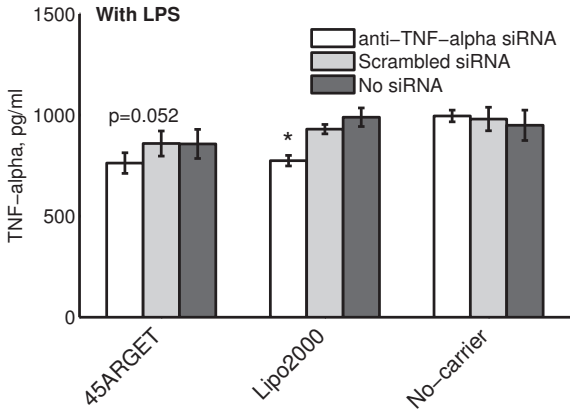

(b) LPS to induce inflammation

Figure B.9: TNF-α expression by RAW264.7 cells a) without LPS and b) with LPS (Condition 1, 24 h). RAW264.7 cells are incubated for 4 h with polycationic nanoparticle/siRNA complexes (acetone precipitate and re-suspend) and then 20 h with fresh media. Next, cells are incubated for 24 h with 200 ng/ml LPS prior to removing supernatant for analysis of TNF-α with ELISA. Data is plotted as the mean plus/minus the standard deviation for n=2 biological replicates and n=2 technical ELISA replicates for each biological replicate. Asterisks (*) indicate $p<0.05$ as determined using a Student's t-test.

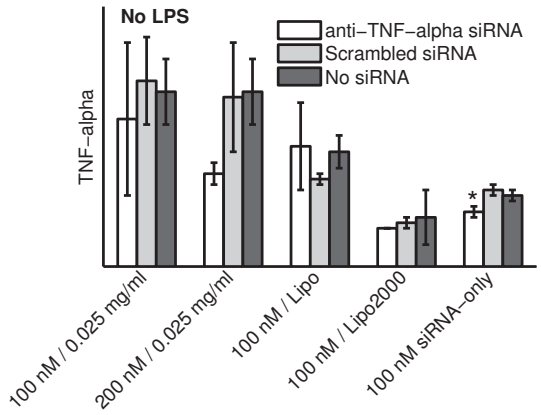

(a) No LPS

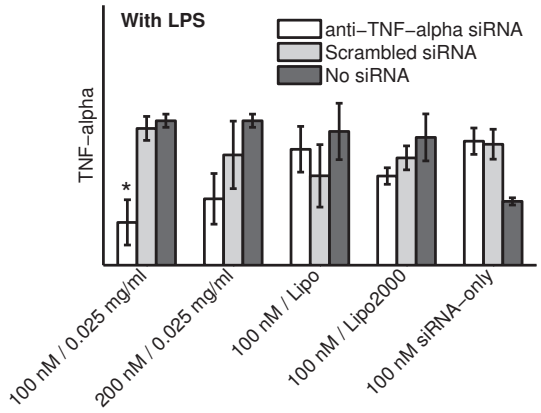

(b) LPS to induce inflammation

Figure B.10: Relative expression of TNF-α by RAW264.7 cells a) without LPS and b) with LPS (Condition 2, experiment 1). RAW264.7 cells are incubated for 42 h with 0.025 mg/ml polycationic nanoparticles with 100 nM or 200 nM siRNA or 0.25 µl/well Lipofectamine2000 (Lipo2000) with 100 nM siRNA. Following this incubation, cells were incubated for 7 h with Opti-MEM® or 200 ng/ml LPS in Opti-MEM®. TNF-α concentration was determined using a TNF-α ELISA. Data is plotted as the mean plus/minus the standard deviation for n=2 biological replicates and n=2 technical ELISA replicates for each biological replicate. Asterisks (*) indicate $p<0.01$ as determined using a Student's t-test.

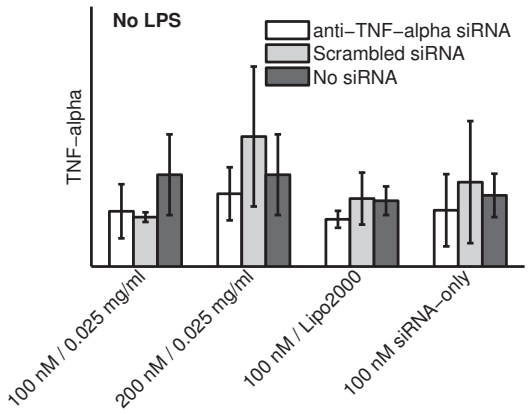

(a) No LPS

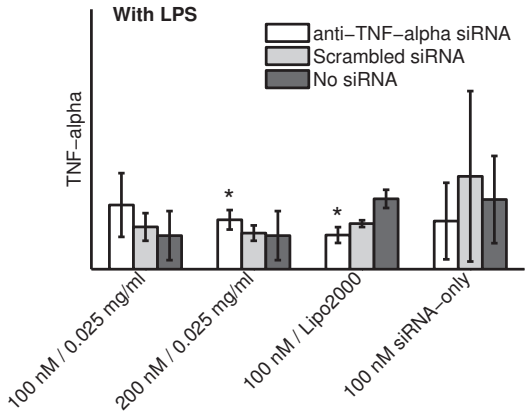

(b) LPS to induce inflammation

Figure B.11: Relative expression of TNF-α by RAW264.7 cells a) without LPS and b) with LPS (Condition 2, experiment 2). RAW264.7 cells are incubated for 42 h with 0.025 mg/ml polycationic nanoparticles with 100 nM or 200 nM siRNA or 0.25 µl/well Lipofectamine2000 (Lipo2000) with 100 nM siRNA. Following this incubation, cells were incubated for 7 h with Opti-MEM® or 200 ng/ml LPS in Opti-MEM®. TNF-α concentration was determined using a TNF-α ELISA. Data is plotted as the mean plus/minus the standard deviation for n=3 biological replicates and n=2 technical ELISA replicates for each biological replicate. Asterisks (*) indicate $p<0.05$ as determined using a Student's t-test.

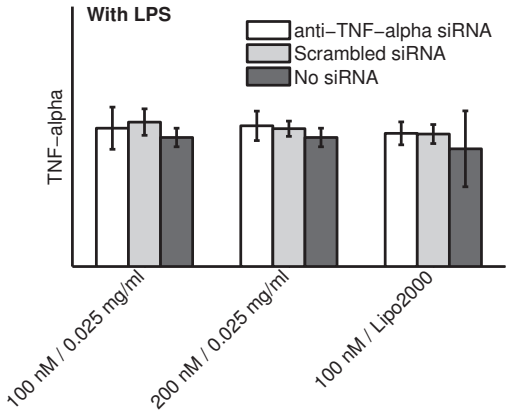

(a) LPS to induce inflammation

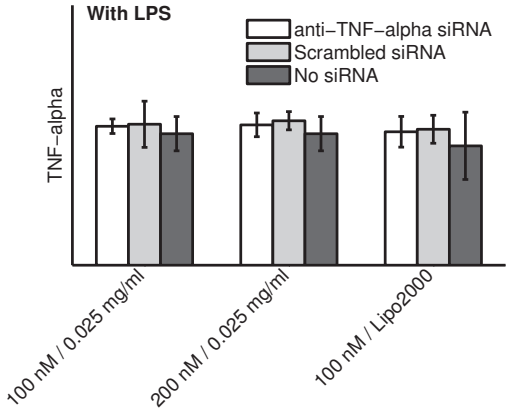

(b) LPS to induce inflammation

Figure B.12: Relative expression of TNF-α by RAW264.7 cells a) without LPS and b) with LPS (Condition 3). RAW264.7 cells are incubated for 26 h with 0.025 mg/ml polycationic nanoparticles with 100 nM or 200 nM siRNA or 0.25 µl/well Lipofectamine2000 (Lipo2000) with 100 nM siRNA. Following this incubation, cells were incubated for 16 h with Opti-MEM® or 200 ng/ml LPS in Opti-MEM®. TNF-α concentration was determined using a TNF-α ELISA. Data is plotted as the mean plus/minus the standard deviation for n=6 biological replicates and n=2 technical ELISA replicates for each biological replicate. The a) and b) plots represent two independent experiments.

B.7 References

[1] Centers for Disease Control and Prevention (CDC). Inflammatory bowel disease, 2011. http://www.cdc.gov/ibd/.

[2] E. V. Loftus. Clinical epidemiology of inflammatory bowel disease: incidence, prevalence, and environmental influences. *Gastroenterology*, 126 (6):1504–1517, 2004.

[3] Y. Lu and A. Bousvaros. Healthcare burden of inflammatory bowel disease in the United States: More than pain and diarrhea. *Inflamm. Bowel Dis.*, 15(11):1767–1768, 2009.

[4] K. Bodger. Cost effectiveness of treatments for inflammatory bowel disease. *Pharmacoeconomics*, 29(5):387–401, 2011.

[5] H. M. Malaty, X.N Fan, A. R. Opekun, C. Thibodeaux, and G. D. Ferry. Rising incidence of inflammatory bowel disease among children: a 12-year study. *J. Pediatr. Gastr. Nutr.*, 50(1):27–31, 2010.

[6] S. Vermeire, D. P. McGovern, G. Van Assche, and P. Rutgeerts. *Genetics of Inflammatory Bowel Disease: How Modern Genomics Informs Basic, Clinical and Translational Science, Inflammatory Bowel Disease: Translating basic science into clinical practice*. Wiley Online Library, 2010. 16-24 pp.

[7] D. C. Baumgart and W. J. Sandborn. Inflammatory bowel disease: clinical aspects and established and evolving therapies. *Lancet*, 369(9573): 1641–1657, 2007.

[8] L. Langmead and P. Irving. *Inflammatory bowel disease: The Facts*. Oxford University Press, Oxford, UK, 2008.

[9] M. V. A. Pichai and L. R. Ferguson. Potential prospects of nanomedicine for targeted therapeutics in inflammatory bowel diseases. *World J. Gastroenterol.*, 18(23):2895–2901, 2012.

[10] National Center for Biotechnology Information (NCBI), PubMed Health. Crohn's disease, 2012. http://www.ncbi.nlm.nih.gov/pubmedhealth/PMH0001295/.

[11] G. D'Haens. Anti-TNF therapy for Crohn's disease. *Curr. Pharm. Des.*, 9(4):289–294, 2003.

[12] S.B. Hanauer. Positioning biologic agents in the treatment of Crohn's disease. *Inflamm. Bowel Dis.*, 15(10):1570–1582, 2009.

[13] D. S. Wilson, G. Dalmasso, L. Wang, S. V. Sitaraman, D. Merlin, and N. Murthy. Orally delivered thioketal nanoparticles loaded with TNF-α siRNA target inflammation and inhibit gene expression in the intestines. *Nat. Mater.*, 9(11):923–928, 2010.

[14] C. Kriegel and M. M. Amiji. Dual *TNF-α/Cyclin D1* gene silencing with an oral polymeric microparticle system as a novel strategy for the

treatment of inflammatory bowel disease. *Clin. Transl. Gastroenterol.*, 2 (3):e2, 2011.

[15] M. Aouadi, G. J. Tesz, S. M. Nicoloro, M. Wang, M. Chouinard, E. Soto, G. R. Ostroff, and M. P. Czech. Orally delivered siRNA targeting macrophage Map4k4 suppresses systemic inflammation. *Nature*, 458 (7242):1180–1184, 2009.

[16] D. C. Forbes, M. Creixell, H. Frizzell, and N. A. Peppas. Polycationic nanoparticles synthesized using ARGET ATRP for drug delivery. *Eur. J. Pharm. Biopharm.*, 84(3):472–478, 2013.

[17] D. C. Forbes and N. A. Peppas. Differences in molecular structure in cross-linked polycationic nanoparticles synthesized using ARGET ATRP or UV-initiated polymerization. *Polymer*, 54(17):4486–4492, 2013.

[18] O. Z. Fisher and N. A. Peppas. Polybasic nanomatrices prepared by UV-initiated photopolymerization. *Macromolecules*, 42(9):3391–3398, 2009.

[19] M. J. Baarsch, M. J. Wannemuehler, T. W. Molitor, and M. P. Murtaugh. Detection of tumor necrosis factor α from porcine alveolar macrophages using an L929 fibroblast bioassay. *J. Immunol. Methods*, 140(1):15–22, 1991.

[20] M. Shiau, H. Chiou, Y. Lee, T. Kuo, and Y. Chang. Establishment of a consistent L929 bioassay system for TNF-α quantitation to evaluate the effect of lipopolysaccharide, phytomitogens and cytodifferentiation agents

on cytotoxicity of TNF-α secreted by adherent human mononuclear cells. *Mediat. Inflamm.*, 10(4):199–208, 2001.

[21] J. Zoldan, A. K. R. Lytton-Jean, E. D. Karagiannis, K. Deiorio-Haggar, L. M. Bellan, R. Langer, and D. G. Anderson. Directing human embryonic stem cell differentiation by non-viral delivery of siRNA in 3D culture. *Biomaterials*, 32(31):7793–7800, 2011.

[22] National Center for Biotechnology Information (NCBI), PubMed Health. Mesalamine, 2012. http://www.ncbi.nlm.nih.gov/pubmedhealth/PMH0000880.

[23] National Center for Biotechnology Information (NCBI), PubMed Health. Sulfasalazine, 2011. http://www.ncbi.nlm.nih.gov/pubmedhealth/PMH0000610.

[24] Mayo Clinic. Prednisone and other corticosteroids: Balance the risks and benefits, 2011. http://www.mayoclinic.com/health/steroids/HQ01431.

[25] National Center for Biotechnology Information (NCBI), PubMed Health. Prednisone, 2011. http://www.ncbi.nlm.nih.gov/pubmedhealth/PMH0000091/.

[26] National Center for Biotechnology Information (NCBI), PubMed Health. Methylprednisolone oral, 2011. http://www.ncbi.nlm.nih.gov/pubmedhealth/PMH0000776/.

[27] National Center for Biotechnology Information (NCBI), PubMed Health. Azathioprine, 2011. http://www.ncbi.nlm.nih.gov/pubmedhealth/PMH0000602.

[28] National Center for Biotechnology Information (NCBI), PubMed Health. Infliximab, 2011. http://www.ncbi.nlm.nih.gov/pubmedhealth/PMH0000267.

Appendix C

Diblock Copolymers

C.1 Introduction

Block copolymers are macromolecules composed of "two or more chemically distinct polymer blocks."[1] Block copolymers, as well as certain types of graft copolymers, can combine properties of the constituent polymers. If the polymer blocks are thermodynamically incompatible, they may phase segregate to form complex nanostructures. In solution, amphiphilic block copolymers can self assemble to form structures like micelles with a hydrophobic core and a hydrophilic corona.[2–4] These self-assembled structures formed from block copolymers are of great interest to researchers designing drug delivery vehicles.[5] The hydrophobic core may be loaded with hydrophobic chemotherapeutic agents[6–8] and stimuli-responsive components that are pH-responsive,[9–11] photo-responsive,[12] temperature-responsive,[13] or multi-responsive[14] may be incorporated in order to achieve controlled drug release. Advanced structures such as core or shell cross-linked micelles may represent an improvement over uncross-linked systems because the cross-linking imparts enhanced stability.[15–17]

C.2 Experimental section

C.2.1 Chemicals

Reagents poly(ethylene glycol) methyl ether methacrylate (PEGMA) (M_n 300 for PEG chain), 2-(dimethylamino)ethyl methacrylate (DMAEMA), ethyl 2-bromoisobutyrate (EBIB), tris (2-pyridylmethyl) amine (TPMA), ascorbic acid (AA), and tin(II) 2-ethylhexanoate were purchased from Sigma-Aldrich. 2-Propanol (IPA) was purchased from Fisher Scientific. Copper(II) bromide was purchased from Acros Organics. Ultrapure water was used for all studies. All chemicals were used as received.

C.2.2 Synthesis

PPEGMA and PPEGMA-*b*-PDMAEMA linear polymer chains were synthesized in a two-step ARGET ATRP synthesis reaction. In the first step, reagents were combined at molar ratios of $CuBr_2$:TPMA:EBIB:PEGMA::0.04:0.4:1:50 in a mixed solvent of 95/5 v/v IPA/W at a ratio of 1.75 v/v solvent/monomer. After a nitrogen purge, the reaction was started by adding a reducing agent solution of tin(II) 2-ethylhexanoate in IPA (10 mg/ml) at a molar ratio of EBIB:tin(II) 2-ethylhexanoate::1:0.25. The mixture was allowed to react overnight and then 25% of the reaction volume was removed for analysis. In the second step, DMAEMA was added at molar ratios PEGMA:DMAEMA::50:60, the mixture was purged with nitrogen, and the reaction was started by adding

a reducing agent solution of tin(II) 2-ethylhexanoate in IPA (10 mg/ml) at a molar ratio of EBIB:tin(II) 2-ethylhexanoate::1:0.25. The mixture was allowed to react overnight.

C.2.3 Instrumentation

Molecular weight and polydispersity data were collected on an Agilent 1200 Series Iso Pump and Autosampler with an Agilent Technologies 1100 RI detector. One PLgel 5 µm, 100 Å column and one PLgel 5 µm, 10,000 Å column were used with 0.01 M lithium bromide (LiBr) in dimethylformamide (DMF) eluent at 70 °C and a flow rate of 1 ml/min. The elution times were compared to nine poly(methyl methacrylate) (PMMA) standards (1660, 2200, 4250, 6370, 12600, 23500, 41400, 89300, and 201000 Da), which were used to calibrate the instrument by refractive index response (conventional calibration).

The polymers were characterized with ^{1}H NMR (nuclear magnetic resonance). Dried polymer was dissolved in deuterated chloroform ($CDCl_3$) at approximately 15 mg/ml. Spectra were obtained using a Varian DirectDrive 400 MHz Nuclear Magnetic Resonance Spectrometer equipped with an automatic sampler and analyzed using SpinWorks 3™ software. The molar ratio of the PEGMA and the DMAEMA was determined by comparing the integrated intensity of the methoxy proton peak of PEGMA at 3.32 ppm and to that of the methyl proton peak of DMAEMA at 2.23 ppm.

C.3 Results and discussion

The linear homopolymers were analyzed with GPC to determine molecular weight distribution and with NMR to determine the composition. Chain extension of the first block confirmed with GPC combined with NMR data to confirm the addition of monomers in the second block is needed to demonstrate the synthesis of a block copolymer.

C.3.1 Analysis of molecular weight distribution with GPC

Gel permeation chromatography (GPC) analysis was used to analyze PPEGMA and PPEGMA-*b*-PDMAEMA linear polymer chains to determine the molecular weight distribution (see Figure C.1). The molecular weight and polydispersity index (PDI) were determined using conventional calibration, so values are reported as PMMA equivalents (see Table C.1). A comparison of the molecular weight of the first block (15,900 Da) to the molecular weight of the diblock (19,400 Da) confirms chain extension. The polydispersity of the linear chains increases upon chain extension (1.58 to 1.99), and these polydispersity values indicate incomplete control over termination reactions in the polymerization.

C.3.2 Analysis of polymer composition with NMR

NMR (nuclear magnetic resonance) was used to evaluate the polymer composition (see Figure C.2). As expected, the NMR spectra for the first

block showed peaks characteristic of PPEGMA, and the NMR spectra for the diblock showed peaks characteristic for both PPEGMA and PDMAEMA. The relative molar quantities of the PEGMA and DMAEMA can be determined by comparing the relative peak integrations (see Table C.2). In both the feed and the diblock copolymer, PEGMA and DMAEMA are present in near equal-molar quantities.

C.4 Conclusions

Diblock PPEGMA-*b*-PDMAEMA copolymers were synthesized using ARGET ATRP. GPC confirmed an increased molecular weight following chain extension of PPEGMA with DMAEMA. NMR confirmed the presence of functional groups from both the PEGMA and DMAEMA in the final diblock copolymer. Unfortunately, the method did not produce tight control over the molecular weight distribution.

C.5 Tables

Table C.1: GPC was used to determine the molecular weight and the polydispersity index for the PPEGMA-*b*-PDMAEMA linear polymer chains. M_n and PDI were calculated as the PMMA equivalent molecular weight and PMMA equivalent PDI from the main polymer peak.

Polymer	M_n, Da	PDI
Block 1: PPEGMA homopolymer	15,900	1.58
Block 2: PPEGMA-*b*-PDMAEMA	19,400	1.99

Table C.2: The molar composition of the feed versus the molar composition of the polymer as determined by ^{1}H NMR. The molar ratio of the PEGMA and the DMAEMA was determined by comparing the integrated intensity of the methoxy proton peak of PEGMA at 3.32 ppm and to that of the methyl proton peak of DMAEMA at 2.23 ppm.

Polymer	PEGMA	DMAEMA
mol % in feed	45%	55%
mol % in polymer (from ^{1}H NMR)	53%	47%

C.6 Figures

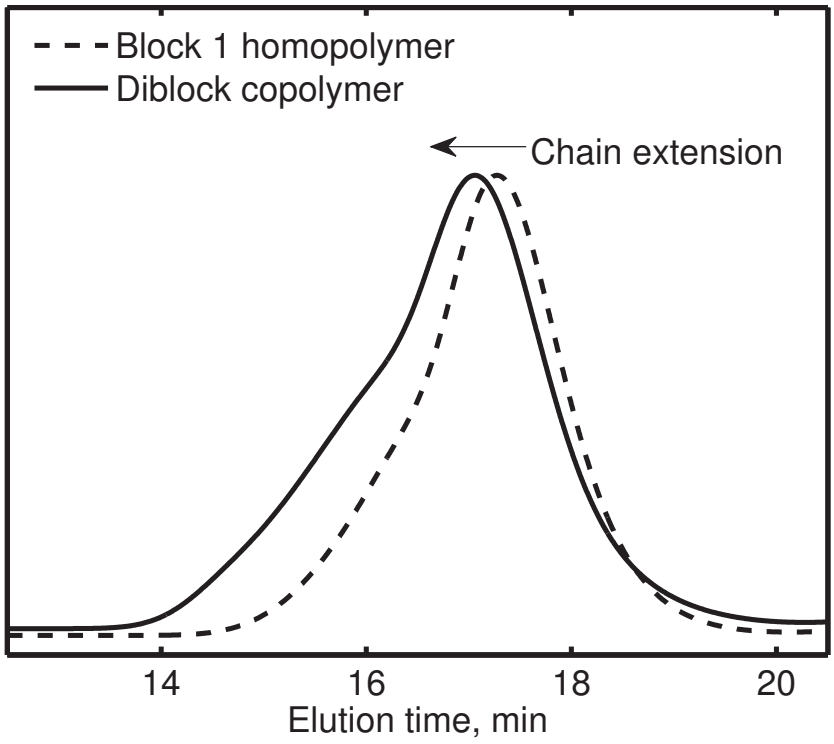

Figure C.1: Chain extension was confirmed with GPC. GPC was used to determine the molecular weight and the polydispersity index for the PPEGMA-*b*-PDMAEMA linear polymer chains. M_n and PDI were calculated as the PMMA equivalent molecular weight and PMMA equivalent PDI from the main polymer peak.

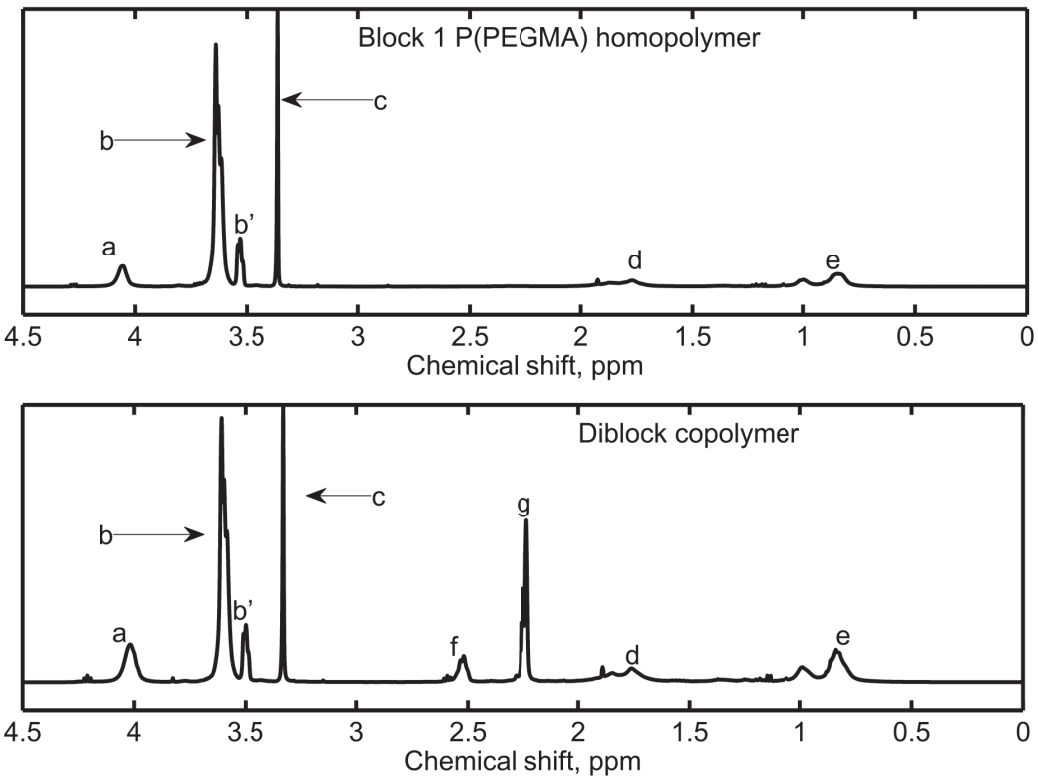

Figure C.2: H NMR spectra for the PPEGMA block and the PPEGMA-*b*-PDMAEMA diblock copolymer chains.

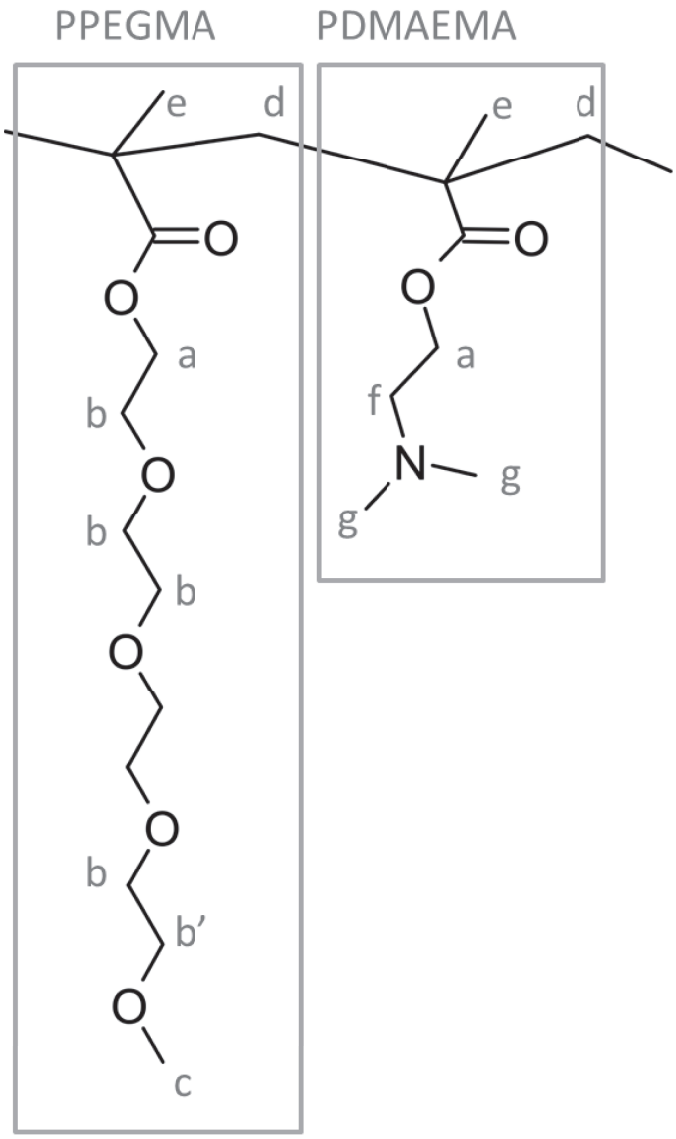

Figure C.3: Chemical structure of the PPEGMA-*b*-PDMAEMA diblock copolymer with labeled peaks corresponding to ^{1}H NMR spectra.

C.7 References

[1] F. S. Bates and G. H. Fredrickson. Block copolymers-designer soft materials. *Phys. Today.*, 38:32–38, 1999.

[2] M. L. Adams, A. Lavasanifar, and G. S. Kwon. Amphiphilic block copolymers for drug delivery. *J. Pharm. Sci.*, 92(7):1343–1355, 2003.

[3] C. Lo, C. Huang, K. Lin, and G. Hsiue. Mixed micelles formed from graft and diblock copolymers for application in intracellular drug delivery. *Biomaterials*, 28(6):1225–1235, 2007.

[4] M. C. Branco and J. P. Schneider. Self-assembling materials for therapeutic delivery. *Acta. Biomater.*, 5(3):817–831, 2009.

[5] G. S. Kwon and T. Okano. Polymeric micelles as new drug carriers. *Adv. Drug Deliver. Rev.*, 21(2):107–116, 1996.

[6] M. R. Nabid, S. J. Tabatabaei Rezaei, R. Sedghi, H. Niknejad, A. A. Entezami, H. A. Oskooie, and M. M. Heravi. Self-assembled micelles of well-defined pentaerythritol-centered amphiphilic A4 B8 star-block copolymers based on PCL and PEG for hydrophobic drug delivery. *Polymer*, 52 (13):2799–2809, 2011.

[7] T. Ren, W. Xia, H. Dong, and Y. Li. Sheddable micelles based on disulfide-linked hybrid PEG-polypeptide copolymer for intracellular drug delivery. *Polymer*, 52(16):3580–3586, 2011.

[8] T. Ren, Y. Feng, Z. Zhang, L. Li, and Y. Li. Shell-sheddable micelles based on star-shaped poly (ϵ-caprolactone)-SS-poly (ethyl glycol) copolymer for intracellular drug release. *Soft Matter*, 7(6):2329–2331, 2011.

[9] G. Cai, H. Zhang, P. Liu, L. Wang, and H. Jiang. Triggered disassembly of hierarchically assembled onion-like micelles into the pristine core–shell micelles via a small change in pH. *Acta. Biomater.*, 7(10):3729–3737, 2011.

[10] Y. Li, H. J. Heo, G. H. Gao, S. W. Kang, C. T. Huynh, M. S. Kim, J. W. Lee, J. H. Lee, and D. S. Lee. Synthesis and characterization of an amphiphilic graft polymer and its potential as a pH-sensitive drug carrier. *Polymer*, 52(15):3304–3310, 2011.

[11] K. Van Butsele, M. Morille, C. Passirani, P. Legras, J. P. Benoit, S. K. Varshney, R. Jérôme, and C. Jérôme. Stealth properties of poly(ethylene oxide)-based triblock copolymer micelles: A prerequisite for a pH-triggered targeting system. *Acta. Biomater.*, 7(10):3700–3707, 2011.

[12] C. J. Chen, G. Y. Liu, Y. T. Shi, C. S. Zhu, S. P. Pang, X. S. Liu, and J. Ji. Biocompatible micelles based on comb-like PEG derivates: Formation, characterization, and photo-responsiveness. *Macromol. Rapid Commun.*, 32(14):1077–1081, 2011.

[13] J. E. Chung, M. Yokoyama, M. Yamato, T. Aoyagi, Y. Sakurai, and

T. Okano. Thermo-responsive drug delivery from polymeric micelles constructed using block copolymers of poly (*N*-isopropylacrylamide) and poly (butylmethacrylate). *J. Control. Release*, 62(1):115–127, 1999.

[14] X. J. Loh, J. del Barrio, P. P. C. Toh, T. Lee, D. Jiao, U. Rauwald, E. A. Appel, and O. A. Scherman. Triply triggered doxorubicin release from supramolecular nanocontainers. *Biomacromolecules*, 13(1):84–91, 2011.

[15] S. Liu, J. V. M. Weaver, Y. Tang, N. C. Billingham, S. P. Armes, and K. Tribe. Synthesis of shell cross-linked micelles with pH-responsive cores using ABC triblock copolymers. *Macromolecules*, 35(16):6121–6131, 2002.

[16] J. V. M. Weaver, Y. Tang, S. Liu, P. D. Iddon, R. Grigg, N. C. Billingham, S. P. Armes, R. Hunter, and S. P. Rannard. Preparation of shell cross-linked micelles by polyelectrolyte complexation. *Angew. Chem.*, 116(11): 1413–1416, 2004.

[17] Y. Kim, M. H. Pourgholami, D. L. Morris, and M. H. Stenzel. Effect of cross-linking on the performance of micelles as drug delivery carriers: A cell uptake study. *Biomacromolecules*, 13(3):814–825, 2012.

Appendix D

Synthesis of 2-Methacryloylamidophenylalanine (MAPA)

D.1 Introduction

Hydrophobic components incorporated into cationic polymer drug delivery carriers for gene delivery may enhance gene delivery efficiency[1] by tuning pH-responsive properties and by enhancing membrane disruption for endosomal escape.[2;3] Various hydrophobic structures including lipids,[1] cholesterol,[1] and hydrophobic amino acids such as L-valine, L-leucine, and L-phenylalanine[4] have been incorporated into polymer carriers. Unfortunately, many of these hydrophobic components lack the functionality to be incorporated during a vinyl polymerization reaction, and vinyl-modified versions are not commercially available. The hydrophobic amino acid derivative 2-methacryloylamidophenylalanine (MAPA) was synthesized for future investigation as part of a drug delivery carrier.

D.2 Experimental section

D.2.1 Chemicals

Anhydrous triethylamine, methacryloyl chloride, and L-phenylalanine methyl ester hydrochloric acid were purchased from Sigma-Aldrich. Sodium hydroxide solution (NaOH, 1 N), hydrochloric acid solution (HCl, 1 N), methylene chloride, hexanes, and ethyl acetate were purchased from Fisher Scientific. Ultrapure water was used for all experiments.

D.2.2 Synthesis and purification

The 2-methacryloylamidophenylalanine (MAPA) was synthesized by conjugating a methacrylate group to the amine site of the amino acid ester to form a L-phenylalanine-based methacrylamide (see Figure D.1). The synthesis method was based on a technique reported by Sandra et al.[5] (although there are other related methods reported in the literature[6–8]). The L-phenylalanine methyl ester hydrochloric acid was dissolved in 1 N NaOH and extracted into methylene chloride. The solution was cooled in an ice bath, and 2 molar equivalents of triethylamine were added. Methacryloyl chloride was added dropwise to the stirring mixture under nitrogen. The reaction continued under nitrogen for 4 h, and then the vessel was sealed and the reaction continued overnight at room temperature.

The reaction mixture was purified using successive acid, base, and salt washes (1 N HCl, 1 N NaOH, and saturated NaCl solutions). The organic

phase was concentrated by rotary evaporation and purified using a Companion Automated Flash Chromatography Instrument equipped with a 100 g silica column and 254 nm absorbance detector. The flow rate was set to 35 ml/min and the column was equilibrated with 500-1500 ml hexanes before injecting 1 ml of the concentrated organic phase product from the synthesis reaction. A gradient elution was used to separate the MAPA product (Solvent A: hexanes and Solvent B: ethyl acetate). For the first 25 min, the fraction of Solvent B was increased from 0 to 0.4 and then held constant for 10 min during the collection of the MAPA fractions. To clear the column, the fraction of Solvent B was increased from 0.4 to 1 for the last 10 min. The collected MAPA fractions were combined and concentrated by rotary evaporation. Vacuum oven drying produced a crystalline, white powder.

D.2.3 Verify product using ^{1}H NMR

The MAPA product was characterized using ^{1}H NMR (nuclear magnetic resonance). Dried sample was dissolved in deuterated chloroform ($CDCl_3$) with tetramethylsilane (TMS) internal standard. Spectra were obtained using a Varian DirectDrive 400 MHz Nuclear Magnetic Resonance Spectrometer equipped with an automatic sampler and analyzed using SpinWorks 3^{TM} software.

D.3 Results and discussion

The 2-methacryloylamidophenylalanine (MAPA) was synthesized and purified, and the product was verified using ^{1}H NMR.

D.3.1 Synthesis and purification

The 2-methacryloylamidophenylalanine (MAPA) is an L-phenylalanine-based methacrylamide that was synthesized by conjugating a methacrylate group to the amine site of L-phenylalanine methyl ester (see Figure D.1). Side reactions with the unprotected carboxyl group of an amino acid were prevented by using a methyl ester analog. The concentrated reaction product was purified using a Companion Automated Flash Chromatography Instrument, and a sample chromatogram is shown in Figure D.2.

D.3.2 Verify product using ^{1}H NMR

The MAPA product was characterized using ^{1}H NMR. The spectra is shown in Figure D.3 with labeled peaks, and the relative peak integration is shown in Table D.1.

D.4 Conclusions

A hydrophobic L-phenylalanine-based methacrylamide was synthesized and purified, and the chemical structure confirmed with ^{1}H NMR. Amino acid-

derived monomers such as 2-methacryloylamidophenylalanine (MAPA) may have utility for the design of new polycationic nanoparticles with enhanced gene delivery efficiency.

Acknowledgments The MAPA synthesis and purification was completed in collaboration with colleague William B. Liechty.

D.5 Tables

Table D.1: Peak integrations for 2-methacryloylamidophenylalanine (MAPA) ^{1}H NMR. Dried sample was dissolved in deuterated chloroform ($CDCl_3$) with tetramethylsilane internal standard. Spectra were obtained using a Varian DirectDrive 400 MHz Nuclear Magnetic Resonance Spectrometer equipped with an automatic sampler and analyzed using SpinWorks 3™ software.

Peak	Number of hydrogen atoms	δ (ppm)	Relative integration area
a	3	7.28	3.38
b	2	7.09	2.09
c	1	6.22	1.00
d	1	5.66	1.00
d	1	5.34	0.98
e	1	4.93	1.01
f	3	3.75	3.09
g	2	3.18	2.11
h	3	1.93	3.05

D.6 Figures

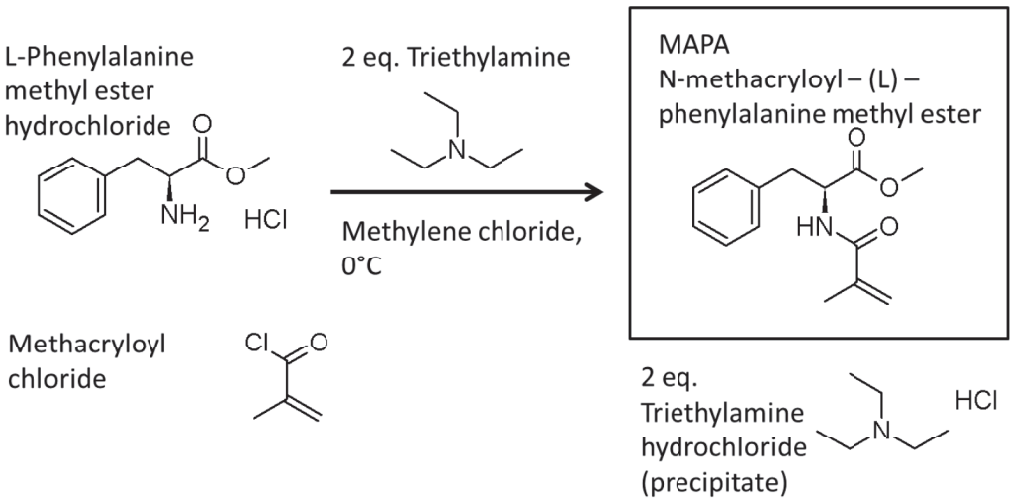

Figure D.1: Reaction scheme for the synthesis of 2-methacryloylamidophenylalanine (MAPA).

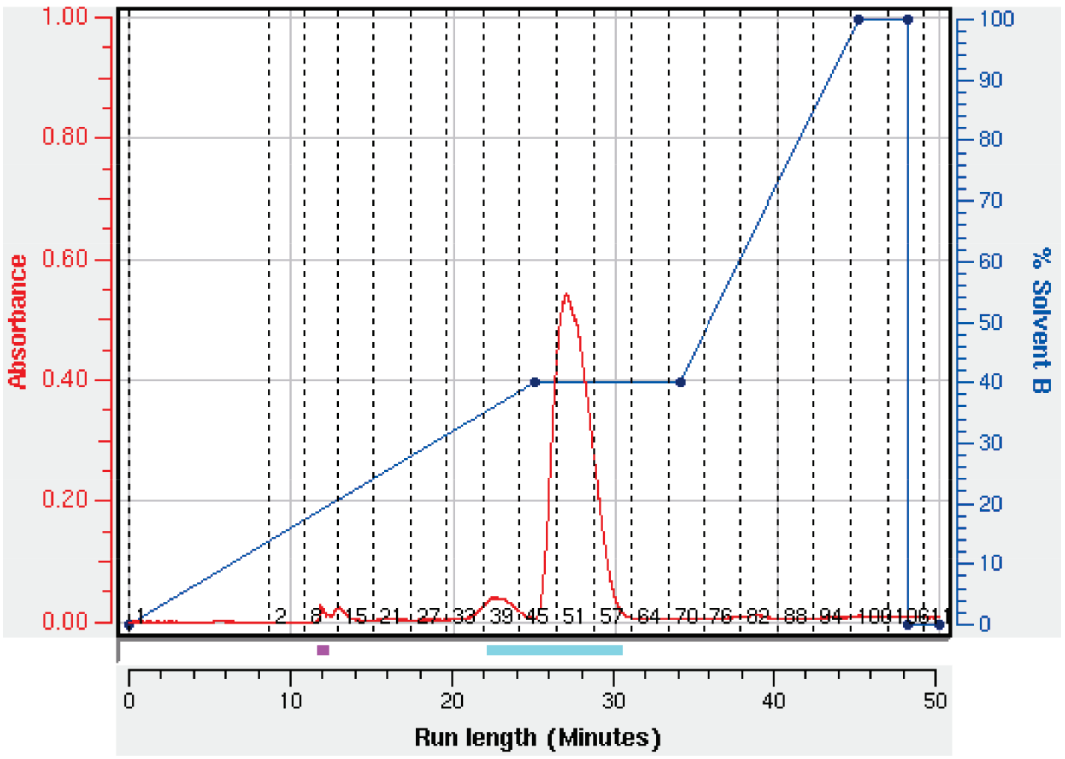

Figure D.2: Purification of 2-methacryloylamidophenylalanine (MAPA) using automated flash chromatography. The organic phase was concentrated by rotary evaporation and purified using a Companion Automated Flash Chromatography Instrument equipped with a 100 g silica column and 254 nm absorbance detector. The flow rate was set to 35 ml/min and the column was equilibrated with 500-1500 ml hexanes before injecting the concentrated organic phase product from the synthesis reaction. A gradient elution was used to separate the MAPA product using Solvent A: hexanes and Solvent B: ethyl acetate. For the first 25 min, the fraction of Solvent B was increased from 0 to 0.4 and then held constant for 10 min during the collection of the MAPA fractions. To clear the column, the fraction of Solvent B was increased from 0.4 to 1 for the last 10 min.

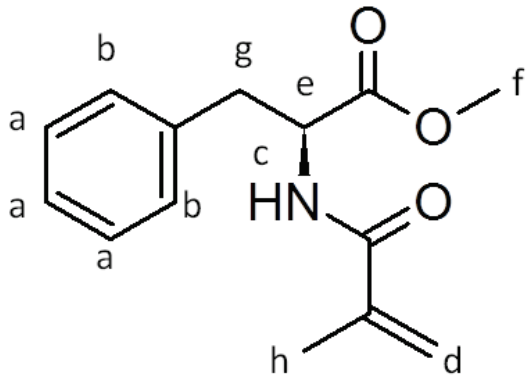

(a) Chemical structure of 2-methacryloylamidophenylalanine (MAPA)

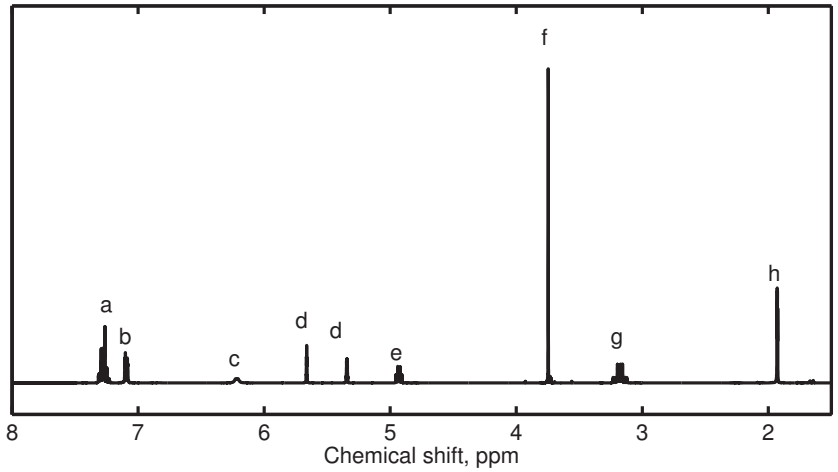

(b) ^{1}H NMR spectra with labeled peaks

Figure D.3: Chemical structure of 2-methacryloylamidophenylalanine (MAPA) with labeled ^{1}H NMR spectra peaks. Dried sample was dissolved in deuterated chloroform ($CDCl_3$) with tetramethylsilane internal standard. Spectra were obtained using a Varian DirectDrive 400 MHz Nuclear Magnetic Resonance Spectrometer equipped with an automatic sampler and analyzed using SpinWorks 3™ software.

D.7 References

[1] Z. Liu, Z. Zhang, C. Zhou, and Y. Jiao. Hydrophobic modifications of cationic polymers for gene delivery. *Prog. Polym. Sci.*, 35(9):1144–1162, 2010.

[2] R. Chen, M. E. Eccleston, Z. Yue, and N. K. H. Slater. Synthesis and pH-responsive properties of pseudo-peptides containing hydrophobic amino acid grafts. *J. Mater. Chem.*, 19(24):4217–4224, 2009.

[3] R. Chen, S. Khormaee, M. E. Eccleston, and N. K. H. Slater. The role of hydrophobic amino acid grafts in the enhancement of membrane-disruptive activity of pH-responsive pseudo-peptides. *Biomaterials*, 30(10): 1954–1961, 2009.

[4] W. B. Liechty, R. Chen, F. Farzaneh, M. Tavassoli, and N. K. H. Slater. Synthetic pH-responsive polymers for protein transduction. *Adv. Mater.*, 21:3910–3914, 2009.

[5] F. Sanda, T. Abe, and T. Endo. Syntheses and radical polymerizations of optically active (meth) acrylamides having amino acid moieties. *J. Polym. Sci., Part A: Polym. Chem.*, 35(13):2619–2629, 1997.

[6] R. Say, S. Emir, B. Garipcan, S. Patir, and A. Denizli. Novel methacryloylamidophenylalanine functionalized porous chelating beads for adsorption of heavy metal ions. *Adv. Polym. Technol.*, 22(4):355–364, 2003.

[7] N. Öztürk, S. Akgöl, M. Arısoy, and A. Denizli. Reversible adsorption of lipase on novel hydrophobic nanospheres. *Sep. Purif. Technol.*, 58(1): 83–90, 2007.

[8] D. Türkmen, N. Öztürk, S. Akgöl, A. Elkak, and A. Denizli. Phenylalanine containing hydrophobic nanospheres for antibody purification. *Biotechnol. Prog.*, 24(6):1297–1303, 2008.

Appendix E

Abbreviations

30ARGET: polycationic nanoparticle formulation synthesized by ARGET ATRP with 30 mol tBMA per 100 mol DEAEMA in the feed

45ARGET: polycationic nanoparticle formulation synthesized by ARGET ATRP with 45 mol tBMA per 100 mol DEAEMA in the feed

30UV: polycationic nanoparticle formulation synthesized by UV-initiated polymerization with 30 mol tBMA per 100 mol DEAEMA in the feed

45UV: polycationic nanoparticle formulation synthesized by UV-initiated polymerization with 45 mol tBMA per 100 mol DEAEMA in the feed

AA: ascorbic acid

AEMA: amino ethyl methacrylate

AGET ATRP: activator generated by electron transfer atom-transfer radical polymerization

ARGET ATRP: activators regenerated by electron transfer atom-transfer radical polymerization

Argo: Argonaute 2

AS-ODN: antisense oligodeoxynucleotide

ATCC: American Type Culture Collection

ATRP: atom-transfer radical polymerization

B16F10: mouse melanoma cell line

BMA: butyl methacrylate

bp: base pairs

BSA: bovine serum albumin

BSC-40: primate kidney epithelial cell line

CCL: core cross-linked

CD: Crohn's disease

$CDCl_3$: deuterated chloroform

cDNA: chromosomal DNA

CRP: controlled radical polymerization

cSCKs: cationic shell cross-linked knedel-like nanoparticles

CS-PLGA NS: Chitosan modified poly(D,L-lactide-co-glycolide) nanospheres

CuBr: copper(I) bromide

$CuBr_2$: copper(II) bromide

Da: Dalton

DAPI: 4',6-diamidino-2-phenylindole

DCC: deleted in colorectal cancer

DEAEMA: 2-(diethylamino)ethyl methacrylate

DLS: dynamic light scattering

DMAEMA: 2-(dimethylamino)ethyl methacrylate

DMEM: Dulbecco's modified eagle medium

DMF: dimethylformamide

DNA: deoxyribonucleic acid

DOTAP: 1,2-dioleoyl-3-trimethylammonium-propane

DPBS: Dulbecco's Phosphate Buffered Saline

DSC: dynamic scanning calorimetry

dsRNA: double-stranded RNA

DSS: dextran sulfate sodium

DY647: DyLight 647 fluorescent dye

EBIB: ethyl 2-bromoisobutyrate

EDTA: ethylenediaminetetraacetic acid

EGDMA: ethylene glycol dimethacrylate

EGFP: enhanced green fluorescent protein

ELISA: enzyme linked immunosorbent assay

EPA: Environmental Protection Agency

ESD: emulsion solvent diffusion method

FACS: fluorescence-activated cell sorting, flow cytometry

FBS: fetal bovine serum

FDA: U.S. Food and Drug Administration

FLuc: firefly luciferase

FTIR: Fourier transform infrared spectroscopy

G: α-L-guluronic acid

GALT: gut-associated lymphatic tissue

GAPDH: glyceraldehyde-3-phospate dehydrogenase

GFP: green fluorescent protein

GI: gastrointestinal

GeRPs: β1,3-D-glucan-encapsulated siRNA particles

GPC: gel permeation chromatography

GTC: galactosylated trimethyl chitosan-cysteine

HBSS: Hank's balanced salt solution

HCl: hydrochloric acid

HEK293T: human embryonic kidney cell line

HeLa: human cervical cancer cell line

HTCC: *N*-((2-hydroxy-3-trimethylammonium) propyl) chitosan chloride

HMIS: hazardous materials identification system

^{1}H NMR: proton nuclear magnetic resonance

HuH-7: human liver cancer cell line

IAA: Imidazole-4-acetic acid

IBD: inflammatory bowel disease

IC50: half maximal inhibitory concentration

IL-10: Interleukin 10

IPS: 2-propanol

IUD: intrauterine device

IUPAC: International Union of Pure and Applied Chemistry

L: ligand

L929: mouse fibroblast cell line

LDH: lactate dehydrogenase

LiBr: lithium bromide

Lipo: Lipofectamine

Lipo2000: Lipofectamine2000

LPS: lipopolysaccharide

M: β-D-mannuronic acid

Map4k4: mitogen-activated protein kinase kinase kinase kinase 4

MAPA: 2-methacryloylamidophenylalanine

MCLG: maximum contaminant level goal

MDA-MB: human breast cancer cell line

Me6TREN: tris[2-(dimethylamino)ethyl]amine

miRNA: microRNA

mPEG: methoxypoly(ethylene glycol)

mRNA: messenger RNA

MSN: mesoporous silica nanoparticles

Mt: transition metal catalyst

MTC: mannose-modified trimethyl chitosan-cysteine

mTERT: mouse telomerase reverse transcriptase

MTS: [3-(4,5-dimethylthiazol-2-yl)-5-(3-carboxymethoxyphenyl)-2-(4-sulfophenyl)-2H-tetrazolium, inner salt used for viability assay

MW: molecular weight

MyTab: myristyltrimethylammonium bromide

NaCl: sodium chloride

NaOH: sodium hydroxide

nBA: *n*-butyl acrylate

NBD chloride: 7-chloro-4-nitrobenzo-2-oxa-1,3-diazole

NBD-NPs: fluorescently-labeled polycationic nanoparticles

NiMOS: nanoparticles-in-microsphere oral system

NCT: national clinical trial

NFPA: National Fire Protection Association

NMR: nuclear magnetic resonance

nt: nucleotides

PAA: propylacrylic acid

PANC-1: pancreatic adenocarcinoma

PBS: phosphate buffered saline

PC3: human prostate cancer cell line

PCL: poly(ε-caprolactone)

PCR: polymerase chain reaction

PDI: polydispersity index

PDMAEMA: poly(2-(dimethylamino) ethyl methacrylate)

PDEAEMA: poly(2-(diethylamino) ethyl meth, Winooski, VTacrylate)

PEG: polyethylene glycol

PEGDMA: PEG dimethacrylate

PEGMA: poly(ethylene glycol) methyl ether methacrylate

PEI: polyethylenimine

PKR: protein kinase R

PLA: polylactide

PLGA: poly(lactic-co-glycolic acid)

PMMA: poly(methyl methacrylate)

POEOMA: poly(oligo(ethylene glycol) monomethyl ether methacrylate)

PPADT: poly(1,4-phenyleneacetone dimethylene thioketal)

PPGDA: poly(propylene glycol) diacrylate

PtBMA: poly(*tert*-butyl methacrylate)

PVA: polyvinyl alcohol

qPCR: quantitative polymerase chain reaction

RA: reducing agent

RAFT: reversible addition−fragmentation chain-transfer polymerization

RAW264.7: murine macrophage cell line

RDRP: reversible-deactivation radical polymerization

RISC: RNA induced silencing complex

RLuc: *Renilla* luciferase

RNA: ribonucleic acid

RNAi: RNA interference

ROS: reactive oxygen species

RT-PCR: reverse transcriptase polymerase chain reaction

RVG-9dR: Rabies virus glycoprotein conjugated nona-D-arginine residues

S2: Drosophila (fruit fly) Schneider 2 cell line

SAXS: small-angle X-ray scattering

SCL: shell cross-linked

SCVCP: self-condensing vinyl copolymerization

shRNA: short hairpin siRNA

siRNA: small interfering RNA

TKN: thioketal nanoparticle

tBMA: *tert*-butyl methacrylate

TE: Tris/EDTA

TEGDMA: tetraethylene glycol dimethacrylate

TEM: transmission electron microscopy

TGA: thermogravimetric analysis

TMS: tetramethylsilane

TNF-α: tumor necrosis factor-alpha

TPMA: tris(2-pyridylmethyl)amine

TPP: thiamine pyrophosphate

TTMC: thiolated trimethyl chitosan

UC: ulcerative colitis

USP: U.S. Pharmacopeia

UV: ultraviolet

VEGF: vascular endothelial growth factor

W: water

WGA: Wheat Germ Agglutinin

Appendix F

List of Coursework

CHE381N Fluid Flow and Heat Transfer

CHE381P Adv Analysis for Chem Engineer

CHE387K Advanced Thermodynamics

CHE392 Polymer Science

CH392N Phys Chem of Macromolec System

CHE384 Adv Engineering Biomaterials

CHE384 Mass Transfer in Polymers

Appendix G

List of Presentations and Publications

G.1 Publications

1. **D. C. Forbes** and N. A. Peppas, Differences in molecular structure in cross-linked polycationic nanoparticles synthesized using ARGET ATRP or UV-initiated polymerization, *Polymer* 54 (17) (2013) 4486-4492.

2. **D. C. Forbes**, M. Creixell, H. Frizzell, and N.A. Peppas, Polycationic nanoparticles synthesized using ARGET ATRP for drug delivery, *European Journal of Pharmaceutics and Biopharmaceutics*, 84 (3) (2013) 472-478.

3. **D. C. Forbes** and N. A. Peppas, Oral delivery of small RNA and DNA, *Journal of Controlled Release* 162 (2) (2012) 438-445.

4. M. Mouton-Johnston and **D. C. Forbes**, Controlled release using an oral drug delivery system designed to improve treatment of conditions such as multiple sclerosis, *JOURNYS: Journal of Youths in Science* 5 (2) (2013) 18-20.

G.2 Presentations

1. **D. C. Forbes** and N. A. Peppas, Therapeutic siRNA delivery using pH-responsive polymer nanoparticles, 2013 AAPS Annual Meeting, San Antonio, Texas, November 2013 (poster).

2. **D. C. Forbes**, H. Frizzell, B. Carillo-Conde, and N. A. Peppas, pH-Responsive polymer nanoparticles synthesized using ARGET ATRP for therapeutic siRNA delivery, Biomaterial's Day, Austin, Texas, May 31, 2013 (poster).

3. **D. C. Forbes**, H. Frizzell, B. Carillo-Conde, and N. A. Peppas, Polycationic Hydrogel Nanoparticles for siRNA Delivery, Society for Biomaterials 2013 Annual Meeting, Boston, Massachusetts, April 11, 2013 (poster).

4. **D. C. Forbes**, M. Creixell, H. Frizzell, and N. A. Peppas, Oral siRNA delivery system for the treatment of colon cancer, CPRIT: Cancer Prevention & Research Institute of Texas Annual Conference, Austin, Texas, October 24, 2012 (poster).

5. **D. C. Forbes** and N. A. Peppas, pH-Responsive, Polycationic Nanoparticles Designed for Intracellular siRNA Delivery, American Institute of Chemical Engineers (AICHE) Annual Meeting, Pittsburgh, Pennsylvania, October 30, 2012 (oral presentation, given by colleague J. Knipe).

6. **D. C. Forbes**, H. Frizzell, and N. A. Peppas, Comparing ARGET ATRP with Traditional Free Radical Polymerization for Versatile Polycationic Hydrogel Nanoparticles, Biomaterial's Day, Houston, Texas, July 27, 2012 (poster).

7. H. Frizzell, **D. C. Forbes**, and N. A. Peppas, Oral Delivery of siRNA Using pH-Responsive Hydrogel Nanoparticles, Biomedical Engineering Society (BMES) Annual Meeting, Seattle, Washington, September 25, 2013 (poster).

8. H. Frizzell, **D. C. Forbes**, and N. A. Peppas, Oral delivery of siRNA using pH-responsive hydrogel nanoparticles, Biomaterial's Day, Austin, Texas, May 31, 2013 (poster).

9. M. Creixell, **D. C. Forbes**, and N. A. Peppas, Nanohydrogels as delivery systems of antineoplastic drugs and siRNA to overcome multidrug resistance in cancer treatment, CPRIT: Cancer Prevention & Research Institute of Texas Annual Conference, Austin, Texas, October 24, 2012 (poster).

10. M. Creixell, **D. C. Forbes**, and N. A. Peppas, Responsive polycationic nanoparticles for co-delivery of siRNA and chemotherapeutical agents to overcome multidrug resistance in cancer therapy, Biomaterial's Day, Houston, Texas, July 27, 2012 (poster).

11. H. Frizzell, **D. C. Forbes**, and N. A. Peppas, Two-part Oral siRNA De-

livery Systems: Polycationic Hydrogel Nanoparticles and Alginate Matrices, Biomaterial's Day, Houston, Texas, July 27, 2012 (poster).

12. **D. C. Brown**, G. Sander, and J. V. Shanks. Alkaloid Extraction and Purification from *Catharanthus roseus* Hairy Root Tissue,

    (a) 5th Annual Research in the Capitol presented by the Iowa Regent Universities, Des Moines, Iowa, March 25, 2010 (poster).

    (b) American Institute of Chemical Engineers (AIChE) Undergraduate Poster Competition, National Convention, Nashville, Tennessee, November 9, 2009 (poster).

    (c) Iowa State University Undergraduate Research Symposium, Ames, Iowa, April 21, 2009 (oral presentation).

    (d) Iowa State University Honors Poster Presentation, Ames, Iowa, April 15, 2009 (poster).

13. **D. C. Brown**, Maize in Mexico, World Food Prize Global Youth Institute, Des Moines, Iowa, October 21, 2006 (paper, poster, and oral presentation).

14. **D. C. Brown**, Students in Asia and Latin America: Making a Difference, Iowa Public Television hosted ICN Video Classroom for middle school students, Johnston, Iowa, October 16, 2006 (oral presentation).

Bibliography

A

[1] W. Abramovits, P. Granowski, and P. Arrazola. Applications of nanomedicine in dermatology: use of nanoparticles in various therapies and imaging. *J. Cosmet. Dermatol.*, 9(2):154–159, 2010.

[2] M. L. Adams, A. Lavasanifar, and G. S. Kwon. Amphiphilic block copolymers for drug delivery. *J. Pharm. Sci.*, 92(7):1343–1355, 2003.

[3] S. Agrawal. *Antisense Therapeutics*. Humana Press, Totowa, NJ, 1996.

[4] P. Agulhon, V. Markova, M. Robitzer, F. Quignard, and T. Mineva. Structure of alginate gels: Interaction of diuronate units with divalent cations from density functional calculations. *Biomacromolecules*, 13(6):1899–1907, 2012.

[5] A. Aigner. Cellular delivery *in vivo* of siRNA-based therapeutics. *Curr. Pharm. Des.*, 14(34):3603–3619, 2008.

[6] S. Akhtar. Oral delivery of siRNA and antisense oligonucleotides. *J. Drug Targeting*, 17(7):491–495, 2009.

[7] S. Akhtar and I. Benter. Toxicogenomics of non-viral drug delivery systems for RNAi: Potential impact on siRNA-mediated gene silencing activity and specificity. *Adv. Drug Deliver. Rev.*, 59(2-3):164–182, 2007.

[8] H. M. Aliabadi, B. Landry, C. Sun, T. Tang, and H. Uludağ. Supramolecular assemblies in functional siRNA delivery: Where do we stand? *Biomaterials*, 33(8):2546–2569, 2012.

[9] J. I. Amalvy, E. J. Wanless, Y. Li, V. Michailidou, S. P. Armes, and Y. Duccini. Synthesis and characterization of novel pH-responsive microgels based on tertiary amine methacrylates. *Langmuir*, 20(21):8992–8999, 2004.

[10] E. K. Anderberg, T. Lindmark, and P. Artursson. Sodium caprate elicits dilatations in human intestinal tight junctions and enhances drug absorption by the paracellular route. *Pharm. Res.*, 10(6):857–864, 1993.

[11] M. Aouadi, G. J. Tesz, S. M. Nicoloro, M. Wang, M. Chouinard, E. Soto, G. R. Ostroff, and M. P. Czech. Orally delivered siRNA targeting macrophage Map4k4 suppresses systemic inflammation. *Nature*, 458(7242):1180–1184, 2009.

[12] M. Ashford, J. Fell, D. Attwood, H. Sharma, and P. Woodhead. An *in vivo* investigation into the suitability of pH dependent polymers for colonic targeting. *Int. J. Pharm.*, 95(1-3):193–199, 1993.

[13] A. D. Augst, H. J. Kong, and D. J. Mooney. Alginate hydrogels as biomaterials. *Macromol. Biosci.*, 6(8):623–633, 2006.

[14] S. Averick, E. Paredes, A. Irastorza, A. Srinivasan, D. Siegwart, A. Magenau, H. Cho, A. Shrivats, E. Hsu, J. Kim, et al. Preparation of cationic nanogels for nucleic acid delivery. *Biomacromolecules*, (11):3445–3449, 2012.

[15] N. Ayres. Atom transfer radical polymerization: a robust and versatile route for polymer synthesis. *Polym. Rev.*, 51(2):138–162, 2011.

B

[16] M. J. Baarsch, M. J. Wannemuehler, T. W. Molitor, and M. P. Murtaugh. Detection of tumor necrosis factor α from porcine alveolar macrophages using an L929 fibroblast bioassay. *J. Immunol. Methods*, 140(1):15–22, 1991.

[17] A. K. Bajpai, J. Bajpai, R. Saini, and R. Gupta. Responsive polymers in biology and technology. *Polym. Rev.*, 51(1):53–97, 2011.

[18] B. Ballarín-González, F. Dagnaes-Hansen, R. A. Fenton, S. Gao, S. Hein, M. Dong, J. Kjems, and K. A. Howard. Protection and systemic translocation of siRNA following oral administration of chitosan/siRNA nanoparticles. *Mol. Ther. Nucleic Acids*, 2(3):e76, 2013.

[19] B. Ballarín-González and K. A. Howard. Polycation-based nanoparticle delivery of {RNAi} therapeutics: Adverse effects and solutions. *Adv. Drug Deliver. Rev.*, 64(15):1717–1729, 2012.

[20] S. C. Balmert and S. R. Little. Biomimetic delivery with micro-and nanoparticles. *Adv. Mater.*, 24(28):3757–3778, 2012.

[21] R. Barbalat, S. E. Ewald, M. L. Mouchess, and G. M. Barton. Nucleic acid recognition by the innate immune system. *Annu. Rev. Immunol.*, 29(1):185–214, 2011.

[22] F. S. Bates and G. H. Fredrickson. Block copolymers-designer soft materials. *Phys. Today.*, 38:32–38, 1999.

[23] D. C. Baumgart and W. J. Sandborn. Inflammatory bowel disease: clinical aspects and established and evolving therapies. *Lancet*, 369(9573):1641–1657, 2007.

[24] C. L. Bayer, É. P. Herrero, and N. A. Peppas. Alginate films as macromolecular imprinted matrices. *J. Biomater. Sci., Polym. Ed.*, 22(11):1523–1534, 2011.

[25] S. A. Bencherif, D. J. Siegwart, A. Srinivasan, F. Horkay, J. O. Hollinger, N. R. Washburn, and K. Matyjaszewski. Nanostructured hybrid hydrogels prepared by a combination of atom transfer radical polymerization and free radical polymerization. *Biomaterials*, 30(29):5270–5278, 2009.

[26] C. E. Beneke, A. M. Viljoen, and J. H. Hamman. Polymeric plant-derived excipients in drug delivery. *Molecules*, 14(7):2602–2620, 2009.

[27] C. F. Bennett and E. E. Swayze. RNA targeting therapeutics: Molecular mechanisms of antisense oligonucleotides as a therapeutic platform. *Annu. Rev. Pharmacol. Toxicol.*, 50(1):259–293, 2010.

[28] S. Y. Berezhna. siRNA in human cells selectively localizes to target RNA sites. *P. Natl. Acad. Sci.*, 103(20):7682–7687, 2006.

[29] B. Bertram, S. Wiese, and A. von Holst. High-efficiency transfection and survival rates of embryonic and adult mouse neural stem cells achieved by electroporation. *J. Neurosci. Meth.*, 209(2):420–427, 2012.

[30] S. R. Bhattarai, E. Muthuswamy, A. Wani, M. Brichacek, A. L. Castañeda, S. L. Brock, and D. Oupicky. Enhanced gene and siRNA delivery by polycation-modified mesoporous silica nanoparticles loaded with chloroquine. *Pharm. Res.*, 27(12):2556–2568, 2010.

[31] M. Bhavsar and M. Amiji. Polymeric nano- and microparticle technologies for oral gene delivery. *Expert Opin. Drug Del.*, 4(3):197–213, 2007.

[32] M. D. Bhavsar and M. M. Amiji. Gastrointestinal distribution and *in vivo* gene transfection studies with nanoparticles-in-microsphere oral system (NiMOS). *J. Control. Release*, 119(3):339–348, 2007.

[33] M. D. Bhavsar and M. M. Amiji. Development of novel biodegradable polymeric nanoparticles-in-microsphere formulation for local plas-

mid DNA delivery in the gastrointestinal tract. *AAPS PharmSciTech*, 9(1):288–294, 2008.

[34] M. D. Bhavsar and M. M. Amiji. Oral IL-10 gene delivery in a microsphere-based formulation for local transfection and therapeutic efficacy in inflammatory bowel disease. *Gene Ther.*, 15(17):1200–1209, 2008.

[35] P. Bielli and L. Calabrese. Structure to function relationships in ceruloplasmin: a 'moonlighting' protein. *Cell. Mol. Life Sci.*, 59(9):1413–1427, 2002.

[36] K. Bodger. Cost effectiveness of treatments for inflammatory bowel disease. *Pharmacoeconomics*, 29(5):387–401, 2011.

[37] R. Bodmeier, H. Chen, and O. Paeratakul. A novel approach to the oral delivery of micro-or nanoparticles. *Pharm. Res.*, 6(5):413–417, 1989.

[38] N. Bodyak, A. Borrelli, J. Fruehauf, J. Harborth, M. B. Vaze, C. Grillot-Courvalin, and A. Silva. Ind-enabling studies for CEQ508 targeting beta-Catenin of GI polyps: First oral RNAi drug. *Gastroenterology (Supplement 1)*, 138(5):S–79, 2010.

[39] L. Bonetta. RNA-based therapeutics: Ready for delivery? *Cell*, 136(4):581–584, 2009.

[40] A. Bouchie. Companies in footrace to deliver RNAi. *Nat. Biotechnol.*, 30(12):1154–1157, 2012.

[41] M. C. Branco and J. P. Schneider. Self-assembling materials for therapeutic delivery. *Acta. Biomater.*, 5(3):817–831, 2009.

[42] J. Brandrup, E. H. Immergut, E. A. Grulke, A. Abe, and D. R. Bloch. *Polymer Handbook*. Wiley New York, 1999.

[43] K. Bruno. Using drug-excipient interactions for siRNA delivery. *Adv. Drug Deliver. Rev.*, 63(13):1210–1226, 2011.

[44] D. Bumcrot, M. Manoharan, V. Koteliansky, and D. W. Y. Sah. RNAi therapeutics: a potential new class of pharmaceutical drugs. *Nat. Chem. Biol.*, 2(12):711–719, 2006.

[45] J. Burnett, J. Rossi, and K. Tiemann. Current progress of siRNA/shRNA therapeutics in clinical trials. *Biotechnol. J.*, 6(9):1130–1146, 2011.

C

[46] G. Cai, H. Zhang, P. Liu, L. Wang, and H. Jiang. Triggered disassembly of hierarchically assembled onion-like micelles into the pristine core–shell micelles via a small change in pH. *Acta. Biomater.*, 7(10):3729–3737, 2011.

[47] M. Caldorera-Moore and N. Peppas. Micro- and nanotechnologies for intelligent and responsive biomaterial-based medical systems. *Adv. Drug Deliver. Rev.*, 61(15):1391–1401, 2009.

[48] L. Cao, T. Man, J. Zhuang, and M. Kruk. Poly (*N*-isopropylacrylamide) and poly (2-(dimethylamino) ethyl methacrylate) grafted on an ordered mesoporous silica surface using atom transfer radical polymerization with activators regenerated by electron transfer. *J. Mater. Chem.*, 22:6939–6946, 2012.

[49] J. Carralot, T. Kim, B. Lenseigne, A. S. Boese, P. Sommer, A. Genovesio, and P. Brodin. Automated high-throughput siRNA transfection in raw 264.7 macrophages: a case study for optimization procedure. *J. Biomol. Screen.*, 14(2):151–160, 2009.

[50] D. Castanotto and J. J. Rossi. The promises and pitfalls of RNA-interference-based therapeutics. *Nature*, 457(7228):426–433, 2009.

[51] D. Cejka, D. Losert, and V. Wacheck. Short interfering RNA (siRNA): tool or therapeutic? *Clin. Sci.*, 110(1):47, 2006.

[52] Centers for Disease Control and Prevention (CDC). Inflammatory bowel disease, 2011. http://www.cdc.gov/ibd/.

[53] D. Chang, J. Lei, H. Cui, N. Lu, Y. Sun, X. Zhang, C. Gao, H. Zheng, and Y. Yin. Disulfide cross-linked nanospheres from sodium alginate derivative for inflammatory bowel disease: Preparation, characterization, and *in vitro* drug release behavior. *Carbohydr. Polym.*, 88(2):663–669, 2012.

[54] N. Charlaftis, D. T. Fearon, A. Schoenemeyer, and P. J. Morley. siRNA high-throughput kinase library screen identifies protein kinase, DNA-activated catalytic polypeptide to play a role in MyD88-induced IFNA2 activation and IL-8 secretion. *Biotechnol. Appl. Biochem.*, 59(1):6–14, 2012.

[55] B. T. Cheesman, A. J. G. Neilson, J. D. Willott, G. B. Webber, S. Edmondson, and E. J. Wanless. Effect of colloidal substrate curvature on pH-responsive polyelectrolyte brush growth. *Langmuir*, 29(20):6131–6140, 2013.

[56] C. J. Chen, G. Y. Liu, Y. T. Shi, C. S. Zhu, S. P. Pang, X. S. Liu, and J. Ji. Biocompatible micelles based on comb-like PEG derivates: Formation, characterization, and photo-responsiveness. *Macromol. Rapid Commun.*, 32(14):1077–1081, 2011.

[57] G. Chen, T. G. Gharib, C. Huang, J. M. G. Taylor, D. E. Misek, S. L. R. Kardia, T. J. Giordano, M. D. Iannettoni, M. B. Orringer, S. M. Hanash, and D. G. Beer. Discordant protein and mRNA expression in lung adenocarcinomas. *Mol. Cell. Proteomics*, 1(4):304–313, 2002.

[58] M. Chen, H. M. Cooper, J. Z. Zhou, P. F. Bartlett, and Z. P. Xu. Reduction in the size of layered double hydroxide nanoparticles enhances the efficiency of siRNA delivery. *J. Colloid Interface Sci.*, 390(1):275–281, 2013.

[59] R. Chen, M. E. Eccleston, Z. Yue, and N. K. H. Slater. Synthesis and pH-responsive properties of pseudo-peptides containing hydrophobic amino acid grafts. *J. Mater. Chem.*, 19(24):4217–4224, 2009.

[60] R. Chen, S. Khormaee, M. E. Eccleston, and N. K. H. Slater. The role of hydrophobic amino acid grafts in the enhancement of membrane-disruptive activity of pH-responsive pseudo-peptides. *Biomaterials*, 30(10):1954–1961, 2009.

[61] K. Cheng and R. I. Mahato. Biological and therapeutic applications of small RNAs. *Pharm. Res.*, 28(12):2961–2965, 2011.

[62] H. Y. Cho, S. E. Averick, E. Paredes, K. Wegner, A. Averick, S. Jurga, S. R. Das, and K. Matyjaszewski. Star polymers with a cationic core prepared by ATRP for cellular nucleic acids delivery. *Biomacromolecules*, 14(5):1262–1267, 2013.

[63] D. S. H. Chu, J. G. Schellinger, J. Shi, A. J. Convertine, P. S. Stayton, and S. H. Pun. Application of living free radical polymerization for nucleic acid delivery. *Acc. Chem. Res.*, 45(7):1089–1099, 2012.

[64] J. E. Chung, M. Yokoyama, M. Yamato, T. Aoyagi, Y. Sakurai, and T. Okano. Thermo-responsive drug delivery from polymeric micelles constructed using block copolymers of poly (*N*-isopropylacrylamide) and poly (butylmethacrylate). *J. Control. Release*, 62(1):115–127, 1999.

[65] D. Cohn and A. Hotovely-Salomon. Biodegradable multiblock PEO/PLA thermoplastic elastomers: molecular design and properties. *Polymer*, 46(7):2068–2075, 2005.

[66] A. Convertine, D. Benoit, C. Duvall, A. Hoffman, and P. Stayton. Development of a novel endosomolytic diblock copolymer for siRNA delivery. *J. Control. Release*, 133(3):221–229, 2009.

[67] A. J. Convertine, C. Diab, M. Prieve, A. Paschal, A. S. Hoffman, P. H. Johnson, and P. S. Stayton. pH-responsive polymeric micelle carriers for siRNA drugs. *Biomacromolecules*, 11(11):2904–2911, 2010.

[68] J. M. Cornejo-Bravo and R. A. Siegel. Water vapour sorption behaviour of copolymers of *N, N*-diethylaminoethyl methacrylate and methyl methacrylate. *Biomaterials*, 17(12):1187–1193, 1996.

[69] M. Cortizo and M. Lorenzo de Mele. Cytotoxicity of copper ions released from metal. *Biol. Trace Elem. Res.*, 102(1):129–141, 2004.

[70] P. Couvreur. Nanoparticles in drug delivery: Past, present and future. *Adv. Drug Deliver. Rev.*, 65(1):21–23, 2013.

[71] M. Creixell and N. A. Peppas. Co-delivery of siRNA and therapeutic agents using nanocarriers to overcome cancer resistance. *Nano Today*, 7(4):367–379, 2012.

[72] G. Crisponi, V. M. Nurchi, D. Fanni, C. Gerosa, S. Nemolato, and G. Faa. Copper-related diseases: from chemistry to molecular pathology. *Coord. Chem. Rev.*, 254(7-8):876–889, 2010.

[73] S. Crunkhorn. Trial watch: Pioneering RNAi therapy shows antitumour activity in humans. *Nat. Rev. Drug Discovery*, 12(3):178–178cru, 2013.

D

[74] F. Dai, P. Sun, Y. Liu, and W. Liu. Redox-cleavable star cationic PDMAEMA by arm-first approach of ATRP as a nonviral vector for gene delivery. *Biomaterials*, 31(3):559–569, 2010.

[75] F. Danhier, E. Ansorena, J. M. Silva, R. Coco, A. Le Breton, and V. Préat. PLGA-based nanoparticles: An overview of biomedical applications. *J. Control. Release*, 161(2 (Special Issue: Drug Delivery Research in Europe)):505–522, 2012.

[76] B. L. Davidson and P. B. McCray. Current prospects for RNA interference-based therapies. *Nat. Rev. Genet.*, 12(5):329–340, 2011.

[77] M. E. Davis, J. E. Zuckerman, C. H. J. Choi, D. Seligson, A. Tolcher, C. A. Alabi, Y. Yen, J. D. Heidel, and A. Ribas. Evidence of RNAi in humans from systemically administered siRNA via targeted nanoparticles. *Nature*, 464(7291):1067–1070, 2010.

[78] S. Davis. Improved targeting of miRNA with antisense oligonucleotides. *Nucleic Acids Res.*, 34(8):2294–2304, 2006.

[79] L. P. Degen and S. F. Phillips. Variability of gastrointestinal transit in healthy women and men. *Gut*, 39(2):299–305, 1996.

[80] G. D'Haens. Anti-TNF therapy for Crohn's disease. *Curr. Pharm. Des.*, 9(4):289–294, 2003.

[81] T. L. Doane and C. Burda. The unique role of nanoparticles in nanomedicine: imaging, drug delivery and therapy. *Chem. Soc. Rev.*, 41(7):2885–2911, 2012.

[82] M. Dominska and D. M. Dykxhoorn. Breaking down the barriers: siRNA delivery and endosome escape. *J. Cell Sci.*, 123(8):1183–1189, 2010.

[83] H. Dong and K. Matyjaszewski. ARGET ATRP of 2-(dimethylamino) ethyl methacrylate as an intrinsic reducing agent. *Macromolecules*, 41(19):6868–6870, 2008.

[84] V. Dubois, S. Breton, M. Linder, J. Fanni, and M. Parmentier. Fatty acid profiles of 80 vegetable oils with regard to their nutritional potential. *Eur. J. Lipid Sci. Technol.*, 109(7):710–732, 2007.

[85] M. Dufresne and J. Leroux. Study of the micellization behavior of different order amino block copolymers with heparin. *Pharm. Res.*, 21(1):160–169, 2004.

E

[86] A. M. Elsen, J. Burdynska, S. Park, and K. Matyjaszewski. Activators regenerated by electron transfer atom transfer radical polymerization in miniemulsion with 50 ppm of copper catalyst. *ACS Macro Lett.*, 2(9):822–825, 2013.

[87] M. L. Etheridge, S. A. Campbell, A. G. Erdman, C. L. Haynes, S. M. Wolf, and J. McCullough. The big picture on nanomedicine: the state of investigational and approved nanomedicine products. *Nanomed.: Nanotechnol.*, 9(1):1–14, 2013.

[88] D. F. Evans, G. Pye, R. Bramley, A. G. Clark, T. J. Dyson, and J. D. Hardcastle. Measurement of gastrointestinal pH profiles in normal ambulant human subjects. *Gut*, 29(8):1035–1041, 1988.

[89] Evonik Industries. EUDRAGIT L 30 D-55, 2012. http://eudragit.evonik.com/product/eudragit/en/products-services/eudragit-products/enteric-formulations/l-30-d-55/pages/default.aspx.

[90] Evonik Industries. EUDRAGIT RS 30 D, 2012. http://eudragit.evonik.com/product/eudragit/en/products-services/eudragit-products/sustained-release-formulations/rs-30-d/pages/default.aspx.

F

[91] G. Faa, C. Liguori, A. Columbano, and G. Diaz. Uneven copper distribution in the human newborn liver. *Hepatology*, 7(5):838–842, 1987.

[92] E. Fattal and A. Bochot. State of the art and perspectives for the delivery of antisense oligonucleotides and siRNA by polymeric nanocarriers. *Int. J. Pharm.*, 364(2):237–248, 2008.

[93] M. G. Ferreiro, L. G. Tillman, G. Hardee, and R. Bodmeier. Alginate/poly-L-lysine microparticles for the intestinal delivery of antisense oligonucleotides. *Pharm. Res.*, 19(6):755–764, 2002.

[94] M. C. Filion and N. C. Phillips. Toxicity and immunomodulatory activity of liposomal vectors formulated with cationic lipids toward immune effector cells. *Biochim. Biophys. Acta, Biomembr.*, 1329(2):345–356, 1997.

[95] A. Fire, S. Q. Xu, M. K. Montgomery, S. A. Kostas, S. E. Driver, and C. C. Mello. Potent and specific genetic interference by double-stranded RNA in *Caenorhabditis elegans*. *Nature*, 391(6669):806–811, 1998.

[96] O. Z. Fisher, T. Kim, S. R. Dietz, and N. A. Peppas. Enhanced core hydrophobicity, functionalization and cell penetration of polybasic nanomatrices. *Pharm. Res.*, 26(1):51–60, 2008.

[97] O. Z. Fisher and N. A. Peppas. Polybasic nanomatrices prepared by UV-initiated photopolymerization. *Macromolecules*, 42(9):3391–3398, 2009.

[98] FMCBiopolymer. Alginate, 2012. http://www.fmcbiopolymer.com/ othermarkets/OtherMarkets/Products/Alginate.aspx.

[99] D. C. Forbes, M. Creixell, H. Frizzell, and N. A. Peppas. Polycationic nanoparticles synthesized using ARGET ATRP for drug delivery. *Eur. J. Pharm. Biopharm.*, 84(3):472–478, 2013.

[100] D. C. Forbes and N. A. Peppas. Oral delivery of small RNA and DNA. *J. Control. Release*, 162(2):438–445, 2012.

[101] D. C. Forbes and N. A. Peppas. Differences in molecular structure in cross-linked polycationic nanoparticles synthesized using ARGET ATRP or UV-initiated polymerization. *Polymer*, 54(17):4486–4492, 2013.

[102] C. J. Fristrup, K. Jankova, and S. Hvilsted. Hydrophilization of poly (ether ether ketone) films by surface-initiated atom transfer radical polymerization. *Polym. Chem.*, 1(10):1696–1701, 2010.

[103] J. Fruehauf, M. Vaze, F. Laroux, and J. Sexton. E. coli mediated gene silencing of beta-catenin. *US Patent 2010/0189691 A1*, 2010.

[104] G. Fundueanu, C. Nastruzzi, A. Carpov, J. Desbrieres, and M. Rinaudo. Physico-chemical characterization of Ca-alginate microparticles produced with different methods. *Biomaterials*, 20(15):1427–1435, 1999.

G

[105] D. Gan and L. A. Lyon. Interfacial nonradiative energy transfer in responsive core-shell hydrogel nanoparticles. *J. Am. Chem. Soc.*, 123(34):8203–8209, 2001.

[106] S. Ganta, H. Devalapally, A. Shahiwala, and M. Amiji. A review of stimuli-responsive nanocarriers for drug and gene delivery. *J. Control. Release*, 126(3):187–204, 2008.

[107] W. Gao, J. M. Chan, and O. C. Farokhzad. pH-responsive nanoparticles for drug delivery. *Mol. Pharm.*, 7(6):1913–1920, 2010.

[108] D. J. Gary, H. Lee, R. Sharma, J. Lee, Y. Kim, Z. Y. Cui, D. Jia, V. D. Bowman, P. R. Chipman, L. Wan, Y. Zou, G. Mao, K. Park, B. Herbert, S. F. Konieczny, and Y. Y. Won. Influence of nano-carrier architecture on in vitro siRNA delivery performance and in vivo biodistribution: polyplexes vs micelleplexes. *ACS Nano*, 5(5):3493–3505, 2011.

[109] D. J. Gary, J. Min, Y. Kim, K. Park, and Y. Y. Won. The effect of N/P ratio on the in vitro and in vivo interaction properties of PEGylated Poly [2-(dimethylamino) ethyl methacrylate]-based siRNA complexes. *Macromol. Biosci.*, 13(8):1059–1071, 2013.

[110] D. J. Gary, N. Puri, and Y. Y. Won. Polymer-based siRNA delivery: Perspectives on the fundamental and phenomenological distinctions from polymer-based DNA delivery. *J. Control. Release*, 121(1-2):64–73, 2007.

[111] B. Ghosn, S. P. Kasturi, and K. Roy. Enhancing polysaccharide-mediated delivery of nucleic acids through functionalization with secondary and tertiary amines. *Curr. Top. Med. Chem.*, 8(4):331–340, 2008.

[112] D. Gitlin, W. Hughes, and C. Janeway. Absorption and excretion of copper in mice. *Nature*, 188(4745):150–151, 1960.

[113] A. Gregory and M. Stenzel. The use of reversible addition fragmentation chain transfer polymerization for drug delivery systems. *Expert Opin. Drug Del.*, 8(2):237–269, 2011.

[114] H. Guo, J. Zhang, and C. Inal. Targeting tumor gene by shRNA-expressing Salmonella-mediated RNAi. *Gene Ther.*, 18(1):95–105, 2010.

[115] S. Guo, Y. Huang, T. Wei, W. Zhang, W. Wang, D. Lin, X. Zhang, A. Kumar, Q. Du, and J. Xing. Amphiphilic and biodegradable methoxy polyethylene glycol-block-(polycaprolactone-graft-poly(2-(dimethylamino)ethyl methacrylate)) as an effective gene carrier. *Biomaterials*, 32(3):879–889, 2011.

[116] D. Guzman-Villanueva, I. M. El-Sherbiny, D. Herrera-Ruiz, A. V. Vlassov, and H. D. C. Smyth. Formulation approaches to short interfering RNA and MicroRNA: Challenges and implications. *J. Pharm. Sci.*, 101(11):4046–4066, 2012.

H

[117] G. Ham. *Copolymerization*. Interscience Publishers, 1964.

[118] S. M. Hammond. MicroRNA therapeutics: a new niche for antisense nucleic acids. *Trends Mol. Med.*, 12(3):99–101, 2006.

[119] S. Hanauer. Positioning biologic agents in the treatment of Crohn's disease. *Inflamm. Bowel Dis.*, 15(10):1570–1582, 2009.

[120] H. Hayashi, M. Iijima, K. Kataoka, and Y. Nagasaki. pH-sensitive nanogel possessing reactive PEG tethered chains on the surface. *Macromolecules*, 37(14):5389–5396, 2004.

[121] C. He, L. Yin, C. Tang, and C. Yin. Multifunctional polymeric nanoparticles for oral delivery of TNF-alpha siRNA to macrophages. *Biomaterials*, 34(11):2843–2854, 2013.

[122] C. He, L. Yin, C. Tang, and C. Yin. Trimethyl chitosan-cysteine nanoparticles for systemic delivery of TNF-α siRNA via oral and intraperitoneal routes. *Pharm. Res.*, 30(10):2596–2606, 2013.

[123] T. He, F. Di Lena, K. C. Neo, and C. L. L. Chai. Direct synthesis of pH-responsive polymer nanoparticles based on living radical polymerization and traditional radical polymerization. *Soft Matter*, 7(7):3358–3365, 2011.

[124] W. He, L. Zhang, J. Miao, Z. Cheng, and X. Zhu. Facile iron-mediated AGET ATRP for water-soluble poly (ethylene glycol) monomethyl ether methacrylate in water. *Macromol. Rapid Commun.*, 33(12):1067–1073, 2012.

[125] N. Hellman and J. Gitlin. Ceruloplasmin metabolism and function. *Annu. Rev. Nutr.*, 22(1):439–458, 2002.

[126] P. C. Hiemenz and T. P. Lodge. *Polymer Chemistry, 2nd.* Boca Raton: CRC Press, 2007.

[127] T. Hoare and R. Pelton. Functional group distributions in carboxylic acid containing poly (*N*-isopropylacrylamide) microgels. *Langmuir*, 20(6):2123–2133, 2004.

[128] A. S. Hoffman. Stimuli-responsive polymers: Biomedical applications and challenges for clinical translation. *Adv. Drug Deliver. Rev.*, 65(1):10–16, 2012.

[129] S. J. Holder, N. A. A. Rossi, C. T. Yeoh, G. G. Durand, M. J. Boerakker, and N. A. J. M. Sommerdijk. ABA triblock copolymers: from controlled synthesis to controlled function. *J. Mater. Chem.*, 13(11):2771–2778, 2003.

[130] Y. Hu, P. U. Atukorale, J. J. Lu, J. J. Moon, S. H. Um, E. C. Cho, Y. Wang, J. Chen, and D. J. Irvine. Cytosolic delivery mediated via electrostatic surface binding of protein, virus, or siRNA cargos to pH-responsive core- shell gel particles. *Biomacromolecules*, 10(4):756–765, 2009.

[131] Y. Hu, T. Litwin, A. R. Nagaraja, B. Kwong, J. Katz, N. Watson, and D. J. Irvine. Cytosolic delivery of membrane-impermeable molecules in dendritic cells using pH-responsive core-shell nanoparticles. *Nano Lett.*, 7(10):3056–3064, 2007.

[132] L. Huang and Y. Liu. *In vivo* delivery of RNAi with lipid-based nanoparticles. *Annu. Rev. Biomed. Eng.*, 13(1):507–530, 2011.

[133] X. Huang, D. Appelhans, P. Formanek, F. Simon, and B. Voit. Tailored synthesis of intelligent polymer nanocapsules: An investigation of controlled permeability and pH-dependent degradability. *ACS Nano*, 6(11):9718–9726, 2012.

J

[134] A. Jain, Y. Gupta, and S. K. Jain. Perspectives of biodegradable natural polysaccharides for site-specific drug delivery to the colon. *J. Pharm. Pharm. Sci.*, 10(1):86–128, 2007.

[135] S. K. Jain and N. K. Jain. Multiparticulate carriers for sun-screening agents. *Int. J. Cosmet. Sci.*, 32(2):89–98, 2010.

[136] W. Jakubowski and K. Matyjaszewski. Activators regenerated by electron transfer for atom-transfer radical polymerization of (meth)acrylates and related block copolymers. *Angew. Chem.*, 118(27):4594–4598, 2006.

[137] W. Jakubowski, K. Min, and K. Matyjaszewski. Activators regenerated by electron transfer for atom transfer radical polymerization of styrene. *Macromolecules*, 39(1):39–45, 2006.

[138] A. D. Jenkins, R. G. Jones, and G. Moad. Terminology for reversible-deactivation radical polymerization previously called "controlled" radi-

cal or "living" radical polymerization (IUPAC Recommendations 2010). *Pure Appl. Chem.*, 82(2):483–491, 2010.

[139] C. Ji, H. Xu, and W. Wu. *In vitro* evaluation and pharmacokinetics in dogs of guar gum and Eudragit FS30D-coated colon-targeted pellets of indomethacin. *J. Drug Targeting*, 15(2):123–131, 2007.

[140] X. Jiang, M. C. Lok, and W. E. Hennink. Degradable-brushed pHEMA–pDMAEMA synthesized via ATRP and click chemistry for gene delivery. *Bioconjugate Chem.*, 18(6):2077–2084, 2007.

[141] R. Juliano, M. Alam, V. Dixit, and H. Kang. Mechanisms and strategies for effective delivery of antisense and siRNA oligonucleotides. *Nucleic Acids Res.*, 36(12):4158–4171, 2008.

[142] R. L. Juliano. The future of nanomedicine: Promises and limitations. *Sci. Publ. Policy*, 39(1):99–104, 2012.

K

[143] A. V. Kabanov and S. V. Vinogradov. Nanogels as pharmaceutical carriers: finite networks of infinite capabilities. *Angew. Chem., Int. Ed.*, 48(30):5418–5429, 2009.

[144] H. C. Kang, K. M. Huh, and Y. H. Bae. Polymeric nucleic acid carriers: current issues and novel design approaches. *J. Control. Release*, 164(3):256–264, 2012.

[145] A. A. Khan, D. Betel, M. L. Miller, C. Sander, C. S. Leslie, and D. S. Marks. Transfection of small RNAs globally perturbs gene regulation by endogenous microRNAs. *Nat. Biotechnol.*, 27:549–555, 2009.

[146] J. Kim, N. Singh, and L. A. Lyon. Label-free biosensing with hydrogel microlenses. *Angew. Chem., Int. Ed.*, 45(9):1446–1449, 2006.

[147] J. B. Kim and H. Kim. Effect of acid structure on deprotection of poly (2-trimethylsilyl-2-propyl methacrylate). *Polymer*, 40(14):4055–4061, 1999.

[148] S. Kim, C. Ye, P. Kumar, I. Chiu, S. Subramanya, H. Wu, P. Shankar, and N. Manjunath. Targeted delivery of siRNA to macrophages for anti-inflammatory treatment. *Mol. Ther.*, 18(5):993–1001, 2010.

[149] Y. Kim, M. H. Pourgholami, D. L. Morris, and M. H. Stenzel. Effect of cross-linking on the performance of micelles as drug delivery carriers: A cell uptake study. *Biomacromolecules*, 13(3):814–825, 2012.

[150] J. Klein, J. Stock, and K. D. Vorlop. Pore size and properties of spherical Ca-alginate biocatalysts. *Appl. Microbiol. Biotechnol.*, 18(2):86–91, 1983.

[151] W. Kong, D. Sung, Y. Shim, K. H. Bae, P. Dubois, T. G. Park, J. Kim, and S. Seo. Efficient intracellular siRNA delivery strategy through rapid and simple two steps mixing involving noncovalent post-PEGylation. *J. Control. Release*, 138(2):141–147, 2009.

[152] C. Kriegel and M. M. Amiji. Dual *TNF-α/Cyclin D1* gene silencing with an oral polymeric microparticle system as a novel strategy for the treatment of inflammatory bowel disease. *Clin. Transl. Gastroenterol.*, 2(3):e2, 2011.

[153] C. Kriegel and M. M. Amiji. Oral TNF-α gene silencing using a polymeric microsphere-based delivery system for the treatment of inflammatory bowel disease. *J. Control. Release*, 150(1):77–86, 2011.

[154] C. Kriegel, H. Attarwala, and M. Amiji. Multi-compartmental oral delivery systems for nucleic acid therapy in the gastrointestinal tract. *Adv. Drug Deliver. Rev.*, 65(6):891–901, 2013.

[155] D. Kurzbach, M. J. N. Junk, and D. Hinderberger. Nanoscale inhomogeneities in thermoresponsive polymers. *Macromol. Rapid Commun.*, 34(2):119–134, 2013.

[156] Y. Kwak, A. J. D. Magenau, and K. Matyjaszewski. ARGET ATRP of methyl acrylate with inexpensive ligands and ppm concentrations of catalyst. *Macromolecules*, 44(4):811–819, 2011.

[157] G. S. Kwon and T. Okano. Polymeric micelles as new drug carriers. *Adv. Drug Deliver. Rev.*, 21(2):107–116, 1996.

L

[158] Y. H. La, E. W. Edwards, S. M. Park, and P. F. Nealey. Directed assembly of cylinder-forming block copolymer films and thermochemically induced cylinder to sphere transition: a hierarchical route to linear arrays of nanodots. *Nano Lett.*, 5(7):1379–1384, 2005.

[159] L. Langmead and P. Irving. *Inflammatory bowel disease: The Facts*. Oxford University Press, Oxford, UK, 2008.

[160] M. R. Lares, J. J. Rossi, and D. L. Ouellet. RNAi and small interfering RNAs in human disease therapeutic applications. *Trends Biotechnol.*, 28(11):570–579, 2010.

[161] H. Laroui, G. Dalmasso, H. T. T. Nguyen, Y. Yan, S. V. Sitaraman, and D. Merlin. Drug-loaded nanoparticles targeted to the colon with polysaccharide hydrogel reduce colitis in a mouse model. *Gastroenterology*, 138(3):843–853.e2, 2010.

[162] H. Laroui, A. L. Theiss, Y. Yan, G. Dalmasso, H. T. T. Nguyen, S. V. Sitaraman, and D. Merlin. Functional TNFα gene silencing mediated by polyethyleneimine/TNFα siRNA nanocomplexes in inflamed colon. *Biomaterials*, 32(4):1218–1228, 2011.

[163] H. Laroui, D. S. Wilson, G. Dalmasso, K. Salaita, N. Murthy, S. V. Sitaraman, and D. Merlin. Nanomedicine in GI. *Am. J. Physiol. Gastrointest. Liver Physiol.*, 300(3):G371–G383, 2011.

[164] F. Leonard, E. Collnot, and C. Lehr. A three-dimensional coculture of enterocytes, monocytes and dendritic cells to model inflamed intestinal mucosa in vitro. *Molecular Pharmaceutics*, 7(6):2103–2119, 2010.

[165] Y. Li, H. J. Heo, G. H. Gao, S. W. Kang, C. T. Huynh, M. S. Kim, J. W. Lee, J. H. Lee, and D. S. Lee. Synthesis and characterization of an amphiphilic graft polymer and its potential as a pH-sensitive drug carrier. *Polymer*, 52(15):3304–3310, 2011.

[166] W. Liechty, M. Caldorera-Moore, M. Phillips, C. Schoener, and N. Peppas. Advanced molecular design of biopolymers for transmucosal and intracellular delivery of chemotherapeutic agents and biological therapeutics. *J. Control. Release*, 155(2):119–127, 2011.

[167] W. Liechty, D. Kryscio, B. Slaughter, and N. Peppas. Polymers for drug delivery systems. *Annu. Rev. Chem. Biomol.*, 1(1):149–173, 2010.

[168] W. Liechty and N. Peppas. Expert opinion: Responsive polymer nanoparticles in cancer therapy. *Eur. J. Pharm. Biopharm.*, 80:241–246, 2012.

[169] W. B. Liechty. Multi-responsive nanoscale hydrogels for intracellular delivery of siRNA. *Preliminary Oral Examination, Department of Chemical Engineering, The University of Texas at Austin*, 2012.

[170] W. B. Liechty, R. Chen, F. Farzaneh, M. Tavassoli, and N. K. H. Slater.

Synthetic pH-responsive polymers for protein transduction. *Adv. Mater.*, 21:3910–3914, 2009.

[171] W. B. Liechty, R. L. Scheuerle, and N. A. Peppas. Tunable, responsive nanogels containing *t*-butyl methacrylate and 2-(*t*-butylamino)ethyl methacrylate. *Polymer*, 54(15):3784–3795, 2013.

[172] M. C. Linder, L. Wooten, P. Cerveza, S. Cotton, R. Shulze, and N. Lomeli. Copper transport. *Am. J. Clin. Nutr.*, 67(5):965S–971S, 1998.

[173] M. Lindow, H. Vornlocher, D. Riley, D. J. Kornbrust, J. Burchard, L. O. Whiteley, J. Kamens, J. D. Thompson, S. Nochur, H. Younis, S. Bartz, J. Parry, N. Ferrari, S. P. Henry, and A. A. Levin. Assessing unintended hybridization-induced biological effects of oligonucleotides. *Nat. Biotechnol.*, 30(10):920–923, 2012.

[174] H. Liu, X. Jiang, J. Fan, G. Wang, and S. Liu. Aldehyde surface-functionalized shell cross-linked micelles with pH-tunable core swellability and their bioconjugation with lysozyme. *Macromolecules*, 40(25):9074–9083, 2007.

[175] Q. Liu and Z. Paroo. Biochemical principles of small RNA pathways. *Annu. Rev. Biochem.*, 79(1):295–319, 2010.

[176] S. Liu, J. V. M. Weaver, Y. Tang, N. C. Billingham, S. P. Armes, and K. Tribe. Synthesis of shell cross-linked micelles with pH-responsive

cores using ABC triblock copolymers. *Macromolecules*, 35(16):6121–6131, 2002.

[177] Z. Liu, Z. Zhang, C. Zhou, and Y. Jiao. Hydrophobic modifications of cationic polymers for gene delivery. *Prog. Polym. Sci.*, 35(9):1144–1162, 2010.

[178] C. Lo, C. Huang, K. Lin, and G. Hsiue. Mixed micelles formed from graft and diblock copolymers for application in intracellular drug delivery. *Biomaterials*, 28(6):1225–1235, 2007.

[179] E. V. Loftus. Clinical epidemiology of inflammatory bowel disease: incidence, prevalence, and environmental influences. *Gastroenterology*, 126(6):1504–1517, 2004.

[180] X. J. Loh, J. del Barrio, P. P. C. Toh, T. Lee, D. Jiao, U. Rauwald, E. A. Appel, and O. A. Scherman. Triply triggered doxorubicin release from supramolecular nanocontainers. *Biomacromolecules*, 13(1):84–91, 2011.

[181] Q. Lou and D. A. Shipp. Recent developments in atom transfer radical polymerization (ATRP): Methods to reduce metal catalyst concentrations. *ChemPhysChem*, 13(14):3257–3261, 2012.

[182] Y. Lu and A. Bousvaros. Healthcare burden of inflammatory bowel disease in the United States: More than pain and diarrhea. *Inflamm. Bowel Dis.*, 15(11):1767–1768, 2009.

M

[183] G. Mack. MicroRNA gets down to business. *Nat. Biotechnol.*, 25(6):631–638, 2007.

[184] S. Maher, T. W. Leonard, J. Jacobsen, and D. J. Brayden. Safety and efficacy of sodium caprate in promoting oral drug absorption: from *in vitro* to the clinic. *Adv. Drug Deliver. Rev.*, 61(15):1427–1449, 2009.

[185] A. P. Majewski, A. Schallon, V. Jérôme, R. Freitag, A. H. E. Müller, and H. Schmalz. Dual-responsive magnetic core–shell nanoparticles for nonviral gene delivery and cell separation. *Biomacromolecules*, 13(3):857–866, 2012.

[186] H. M. Malaty, X. Fan, A. R. Opekun, C. Thibodeaux, and G. D. Ferry. Rising incidence of inflammatory bowel disease among children: a 12-year study. *J. Pediatr. Gastr. Nutr.*, 50(1):27–31, 2010.

[187] A. Malek, O. Merkel, L. Fink, F. Czubayko, T. Kissel, and A. Aigner. *In vivo* pharmacokinetics, tissue distribution and underlying mechanisms of various PEI (-PEG)/siRNA complexes. *Toxicol. Appl. Pharmacol.*, 236(1):97–108, 2009.

[188] M. J. Mann and V. J. Dzau. Therapeutic applications of transcription factor decoy oligonucleotides. *J. Clin. Invest.*, 106(9):1071–1076, 2000.

[189] B. Mao, L. Gan, Y. Gan, X. Li, P. Ravi, and K. Tam. Controlled polymerizations of 2-(dialkylamino)ethyl methacrylates and their block

copolymers in protic solvents at ambient temperature via atrp. *J. Polym. Sci., Part A: Polym. Chem.*, 42(20):5161–5169, 2004.

[190] S. Marine, J. Freeman, A. Riccio, M. Axenborg, J. Pihl, R. Ketteler, and S. Aspengren. High-throughput transfection of differentiated primary neurons from rat forebrain. *J. Biomol. Screen.*, 17(5):692–696, 2012.

[191] P. R. Mark, N. S. Murthy, S. Weigand, K. Breitenkamp, M. Kade, and T. Emrick. Microphase separated structures in the solid and molten states of double-crystal graft copolymers of polyethylene and poly (ethylene oxide). *Polymer*, 49(13):3116–3124, 2008.

[192] K. Matyjaszewski. Atom transfer radical polymerization (ATRP): current status and future perspectives. *Macromolecules*, 45(10):4015–4039, 2012.

[193] K. Matyjaszewski, H. Dong, W. Jakubowski, J. Pietrasik, and A. Kusumo. Grafting from surfaces for everyone: ARGET ATRP in the presence of air. *Langmuir*, 23(8):4528–4531, 2007.

[194] K. Matyjaszewski, W. Jakubowski, K. Min, W. Tang, J. Huang, W. A. Braunecker, and N. V. Tsarevsky. Diminishing catalyst concentration in atom transfer radical polymerization with reducing agents. *P. Natl. Acad. Sci.*, 103(42):15,309–15,314, 2006.

[195] K. Matyjaszewski and J. Xia. Atom transfer radical polymerization. *Chem. Rev.*, 101(9):2921–2990, 2001.

[196] Mayo Clinic. Prednisone and other corticosteroids: Balance the risks and benefits, 2011. http://www.mayoclinic.com/health/steroids/HQ01431.

[197] J. McCarthy, M. O'Neill, L. Bourre, D. Walsh, A. Quinlan, G. Hurley, J. Ogier, F. Shanahan, S. Melgar, R. Darcy, and C. O'Driscoll. Gene silencing of TNF-alpha in a murine model of acute colitis using a modified cyclodextrin delivery system. *J. Control. Release*, 168(1):28–34, 2013.

[198] E. L. McConnell, M. D. Short, and A. W. Basit. An *in vivo* comparison of intestinal pH and bacteria as physiological trigger mechanisms for colonic targeting in man. *J. Control. Release*, 130(2):154–160, 2008.

[199] G. Meister. RNA interference in the nucleus. *Science*, 321(5888):496–497, 2008.

[200] J. Miao, W. He, L. Zhang, Y. Wang, Z. Cheng, and X. Zhu. AGET ATRP of water-soluble PEGMA: Fast living radical polymerization mediated by iron catalyst. *J. Polym. Sci., Part A: Polym. Chem.*, 50(11):2194–2200, 2012.

[201] K. Min, H. Gao, and K. Matyjaszewski. Use of ascorbic acid as reducing agent for synthesis of well-defined polymers by ARGET ATRP. *Macromolecules*, 40(6):1789–1791, 2007.

[202] K. Min, W. Jakubowski, and K. Matyjaszewski. AGET ATRP in the presence of air in miniemulsion and in bulk. *Macromol. Rapid Commun.*, 27(8):594–598, 2006.

[203] S. Moghimi, P. Symonds, J. Murray, A. Hunter, G. Debska, and A. Szewczyk. A two-stage poly(ethylenimine)-mediated cytotoxicity: implications for gene transfer/therapy. *Mol. Ther.*, 11(6):990–995, 2005.

[204] M. J. Monteiro and M. F. Cunningham. Polymer nanoparticles via living radical polymerization in aqueous dispersions: Design and applications. *Macromolecules*, 45(12):4939–4957, 2012.

[205] H. Mori, A. Walther, X. André, M. G. Lanzendörfer, and A. H. E. Müller. Synthesis of highly branched cationic polyelectrolytes via self-condensing atom transfer radical copolymerization with 2-(diethylamino) ethyl methacrylate. *Macromolecules*, 37(6):2054–2066, 2004.

[206] M. Morille, C. Passirani, A. Vonarbourg, A. Clavreul, and J. P. Benoit. Progress in developing cationic vectors for non-viral systemic gene therapy against cancer. *Biomaterials*, 29(24-25):3477–3496, 2008.

[207] R. Morishita, G. H. Gibbons, M. Horiuchi, K. E. Ellison, M. Nakama, L. Zhang, Y. Kaneda, T. Ogihara, and V. J. Dzau. A gene therapy strategy using a transcription factor decoy of the E2F binding site inhibits smooth muscle proliferation *in vivo*. *P. Natl. Acad. Sci.*, 92(13):5855, 1995.

[208] N. S. Murthy, W. Wang, and J. Kohn. Microphase separation in copolymers of hydrophilic PEG blocks and hydrophobic tyrosine-derived segments using simultaneous SAXS/WAXS/DSC. *Polymer*, 51(17):3978–3988, 2010.

N

[209] M. R. Nabid, S. J. Tabatabaei Rezaei, R. Sedghi, H. Niknejad, A. A. Entezami, H. A. Oskooie, and M. M. Heravi. Self-assembled micelles of well-defined pentaerythritol-centered amphiphilic A4 B8 star-block copolymers based on PCL and PEG for hydrophobic drug delivery. *Polymer*, 52(13):2799–2809, 2011.

[210] National Center for Biotechnology Information (NCBI), MedlinePlus. Wilson disease, 2012. http://www.nlm.nih.gov/medlineplus/wilsondisease.html.

[211] National Center for Biotechnology Information (NCBI), PubMed Health. Azathioprine, 2011. http://www.ncbi.nlm.nih.gov/pubmedhealth/PMH0000602.

[212] National Center for Biotechnology Information (NCBI), PubMed Health. Infliximab, 2011. http://www.ncbi.nlm.nih.gov/pubmedhealth/PMH0000267.

[213] National Center for Biotechnology Information (NCBI), PubMed Health. Methylprednisolone oral, 2011. http://www.ncbi.nlm.nih.gov/pubmedhealth/PMH0000776/.

[214] National Center for Biotechnology Information (NCBI), PubMed Health. Prednisone, 2011. http://www.ncbi.nlm.nih.gov/pubmedhealth/PMH0000091/.

[215] National Center for Biotechnology Information (NCBI), PubMed Health. Sulfasalazine, 2011. http://www.ncbi.nlm.nih.gov/pubmedhealth/PMH0000610.

[216] National Center for Biotechnology Information (NCBI), PubMed Health. Crohn's disease, 2012. http://www.ncbi.nlm.nih.gov/pubmedhealth/PMH0001295/.

[217] National Center for Biotechnology Information (NCBI), PubMed Health. Mesalamine, 2012. http://www.ncbi.nlm.nih.gov/pubmedhealth/PMH0000880.

[218] S. Nayak and L. A. Lyon. Soft nanotechnology with soft nanoparticles. *Angew. Chem., Int. Ed.*, 44(47):7686–7708, 2005.

[219] C. E. Nelson, J. R. Kintzing, A. Hanna, J. M. Shannon, M. K. Gupta, and C. L. Duvall. Balancing cationic and hydrophobic content of PEGylated siRNA polyplexes enhances endosome escape, stability, blood circulation time, and bioactivity in vivo. *ACS Nano*, 7(10):8870–8880, 2013.

[220] Y. H. Ng, F. di Lena, and C. L. L. Chai. Metalloenzymatic radical polymerization using alkyl halides as initiators. *Polym. Chem.*, 2(3):589–594, 2011.

[221] Y. H. Ng, F. di Lina, and C. L. L. Chai. PolyPEGA with predeter-

mined molecular weights from enzyme-mediated radical polymerization in water. *Chem. Commun.*, 47(22):6464–6466, 2011.

[222] R. Nicolaÿ and Y. Kwak. ATRP with alkyl pseudohalides acting as initiators and chain transfer agents: When ATRP and RAFT polymerization become one. *Isr. J. Chem.*, 52(3-4):288–305, 2012.

[223] L. Nie, G. Wu, and W. Zhang. Correlation between mRNA and protein abundance in *Desulfovibrio vulgaris*: A multiple regression to identify sources of variations. *Biochem. Biophys. Res. Commun.*, 339(2):603–610, 2006.

[224] N. Nograles, S. Abdullah, M. N. Shamsudin, N. Billa, and R. Rosli. Formation and characterization of pDNA-loaded alginate microspheres for oral administration in mice. *J. Biosci. Bioeng.*, 113(2):133–140, 2012.

O

[225] G. Odian. *Principles of Polymerization.* John Wiley and Sons, Hoboken, NJ, 2004.

[226] J. K. Oh, S. A. Bencherif, and K. Matyjaszewski. Atom transfer radical polymerization in inverse miniemulsion: A versatile route toward preparation and functionalization of microgels/nanogels for targeted drug delivery applications. *Polymer*, 50(19):4407–4423, 2009.

[227] J. K. Oh, H. Dong, R. Zhang, K. Matyjaszewski, and H. Schlaad. Preparation of nanoparticles of double-hydrophilic PEO-PHEMA block copolymers by AGET ATRP in inverse miniemulsion. *J. Polym. Sci., Part A: Polym. Chem.*, 45(21):4764–4772, 2007.

[228] J. K. Oh, R. Drumright, D. J. Siegwart, and K. Matyjaszewski. The development of microgels/nanogels for drug delivery applications. *Prog. Polym. Sci.*, 33(4):448–477, 2008.

[229] J. K. Oh, K. Min, and K. Matyjaszewski. Preparation of poly (oligo (ethylene glycol) monomethyl ether methacrylate) by homogeneous aqueous AGET ATRP. *Macromolecules*, 39(9):3161–3167, 2006.

[230] J. K. Oh, F. Perineau, B. Charleux, and K. Matyjaszewski. AGET ATRP in water and inverse miniemulsion: A facile route for preparation of high-molecular-weight biocompatible brush-like polymers. *J. Polym. Sci., Part A: Polym. Chem.*, 47(7):1771–1781, 2009.

[231] J. K. Oh, F. Perineau, and K. Matyjaszewski. Preparation of nanoparticles of well-controlled water-soluble homopolymers and block copolymers using an inverse miniemulsion ATRP. *Macromolecules*, 39(23):8003–8010, 2006.

[232] J. K. Oh, D. J. Siegwart, H. Lee, G. Sherwood, L. Peteanu, J. O. Hollinger, K. Kataoka, and K. Matyjaszewski. Biodegradable nanogels

prepared by atom transfer radical polymerization as potential drug delivery carriers: synthesis, biodegradation, *in vitro* release, and bioconjugation. *J. Am. Chem. Soc.*, 129(18):5939–5945, 2007.

[233] J. K. Oh, C. Tang, H. Gao, N. V. Tsarevsky, and K. Matyjaszewski. Inverse miniemulsion ATRP: a new method for synthesis and functionalization of well-defined water-soluble/cross-linked polymeric particles. *J. Am. Chem. Soc.*, 128(16):5578–5584, 2006.

[234] Y. K. Oh and T. G. Park. siRNA delivery systems for cancer treatment. *Adv. Drug Deliver. Rev.*, 61(10):850–862, 2009.

[235] N. Öztürk, S. Akgöl, M. Arısoy, and A. Denizli. Reversible adsorption of lipase on novel hydrophobic nanospheres. *Sep. Purif. Technol.*, 58(1):83–90, 2007.

P

[236] D. W. Pack, A. S. Hoffman, S. Pun, and P. S. Stayton. Design and development of polymers for gene delivery. *Nat. Rev. Drug Discov.*, 4(7):581–593, 2005.

[237] D. Palioura, S. P. Armes, S. H. Anastasiadis, and M. Vamvakaki. Metal nanocrystals incorporated within pH-responsive microgel particles. *Langmuir*, 23(10):5761–5768, 2007.

[238] N. Pantoustier, S. Moins, M. Wautier, P. Degée, and P. Dubois. Solvent-free synthesis and purification of poly[2-(dimethylamino)ethyl methacrylate] by atom transfer radical polymerization. *Chem. Commun.*, (3):340–341, 2003.

[239] T. Park, J. Jeong, and S. Kim. Current status of polymeric gene delivery systems. *Adv. Drug Deliver. Rev.*, 58(4):467–486, 2006.

[240] M. M. Patel. Cutting-edge technologies in colon-targeted drug delivery systems. *Expert Opin. Drug Del.*, 8(10):1247–1258, 2011.

[241] M. M. Patel and A. F. Amin. Design and optimization of colon-targeted system of theophylline for chronotherapy of nocturnal asthma. *J. Pharm. Sci.*, 100(5):1760–1772, 2011.

[242] M. M. Patel and A. F. Amin. Process, optimization and characterization of mebeverine hydrochloride loaded guar gum microspheres for irritable bowel syndrome. *Carbohydr. Polym.*, 86(2):536–545, 2011.

[243] S. M. Paterson, D. H. Brown, T. V. Chirila, I. Keen, A. K. Whittaker, and M. V. Baker. The synthesis of water-soluble phema via arget atrp in protic media. *J. Polym. Sci., Part A: Polym. Chem.*, 48(18):4084–4092, 2010.

[244] V. B. Patravale and S. D. Mandawgade. Novel cosmetic delivery systems: an application update. *Int. J. Cosmet. Sci.*, 30(1):19–33, 2008.

[245] K. A. Payne, D. R. D'hooge, P. H. M. Van Steenberge, M. Reyniers, M. F. Cunningham, R. A. Hutchinson, and G. B. Marin. ARGET ATRP of butyl methacrylate: Utilizing kinetic modeling to understand experimental trends. *Macromolecules*, 46(10):3828–3840, 2013.

[246] C. V. Pecot, G. A. Calin, R. L. Coleman, G. Lopez-Berestein, and A. K. Sood. RNA interference in the clinic: challenges and future directions. *Nat. Rev. Cancer*, 11(1):59–67, 2011.

[247] N. A. Peppas. Intelligent therapeutics: biomimetic systems and nanotechnology in drug delivery. *Adv. Drug Deliver. Rev.*, 56(11):1529–1531, 2004.

[248] N. A. Peppas, P. Bures, W. Leobandung, and H. Ichikawa. Hydrogels in pharmaceutical formulations. *Eur. J. Pharm. Biopharm.*, 50(1):27–46, 2000.

[249] N. A. Peppas, J. Z. Hilt, A. Khademhosseini, and R. Langer. Hydrogels in biology and medicine: From molecular principles to bionanotechnology. *Adv. Mater.*, 18(11):1345–1360, 2006.

[250] J. Perkel. RNAi therapeutics: A two-year update. *Science*, 326(5951):454, 2009.

[251] M. Phillips. *Antisense therapeutics*. Springer, Totowa, NJ, 2005.

[252] M. V. A. Pichai and L. R. Ferguson. Potential prospects of nanomedicine for targeted therapeutics in inflammatory bowel diseases. *World J. Gastroenterol.*, 18(23):2895–2901, 2012.

[253] K. Pielichowski and K. Flejtuch. Differential scanning calorimetry studies on poly (ethylene glycol) with different molecular weights for thermal energy storage materials. *Polym. Adv. Technol.*, 13(10-12):690–696, 2003.

[254] T. Pintauer and K. Matyjaszewski. Atom transfer radical addition and polymerization reactions catalyzed by ppm amounts of copper complexes. *Chem. Soc. Rev.*, 37(6):1087, 2008.

[255] S. Pirotton, C. Muller, N. Pantoustier, F. Botteman, S. Collinet, C. Grandfils, G. Dandrifosse, P. Degée, P. Dubois, and M. Raes. Enhancement of transfection efficiency through rapid and noncovalent post-PEGylation of poly (dimethylaminoethyl methacrylate)/DNA complexes. *Pharm. Res.*, 21(8):1471–1479, 2004.

Q

[256] Y. Qiao, Y. Huang, C. Qiu, X. Yue, L. Deng, Y. Wan, J. Xing, C. Zhang, S. Yuan, A. Dong, and J. Xu. The use of PEGylated poly [2-(N, N-dimethylamino) ethyl methacrylate] as a mucosal DNA delivery vector and the activation of innate immunity and improvement of HIV-1-specific immune responses. *Biomaterials*, 31(1):115–123, 2010.

[257] J. Qiu, B. Charleux, and K. Matyjaszewski. Controlled/living radical polymerization in aqueous media: homogeneous and heterogeneous systems. *Prog. Polym. Sci.*, 26(10):2083–2134, 2001.

R

[258] C. Ramireddy, Z. Tuzar, K. Prochazka, S. E. Webber, and P. Munk. Styrene-*tert*-butyl methacrylate and styrene-methacrylic acid block copolymers: synthesis and characterization. *Macromolecules*, 25(9):2541–2545, 1992.

[259] M. Ranger, M. Jones, M. Yessine, and J. Leroux. From well-defined diblock copolymers prepared by a versatile atom transfer radical polymerization method to supramolecular assemblies. *J. Polym. Sci., Part A: Polym. Chem.*, 39(22):3861–3874, 2001.

[260] D. D. Rao, J. S. Vorhies, N. Senzer, and J. Nemunaitis. siRNA vs. shRNA: Similarities and differences. *Adv. Drug Deliver. Rev.*, 61(9):746–759, 2009.

[261] A. A. Raoof, P. Chiu, Z. Ramtoola, I. K. Cumming, C. Teng, S. P. Weinbach, G. E. Hardee, A. A. Levin, and R. S. Geary. Oral bioavailability and multiple dose tolerability of an antisense oligonucleotide tablet formulated with sodium caprate. *J. Pharm. Sci.*, 93(6):1431–1439, 2004.

[262] T. Ren, Y. Feng, Z. Zhang, L. Li, and Y. Li. Shell-sheddable micelles based on star-shaped poly (ϵ-caprolactone)-SS-poly (ethyl glycol)

copolymer for intracellular drug release. *Soft Matter*, 7(6):2329–2331, 2011.

[263] T. Ren, W. Xia, H. Dong, and Y. Li. Sheddable micelles based on disulfide-linked hybrid PEG-polypeptide copolymer for intracellular drug delivery. *Polymer*, 52(16):3580–3586, 2011.

[264] B. D. Riquelme, D. Dumas, A. Fontana, M. Delannoy, J. R. Valverde, D. Sondag, and C. Grandfils. Hemocompatibility and biofunctionality of two poly(2-(dimethylamino)ethyl methacrylate-co-poly(ethyleneglycol) copolymers. *J. Biomed. Mater. Res. Part A*, 99A(3):445–454, 2011.

[265] A. Rubinstein. Microbially controlled drug delivery to the colon. *Biopharm. Drug Dispos.*, 11(6):465–475, 1990.

S

[266] M. Sahnoun, M.-T. Charreyre, L. Veron, T. Delair, and F. D'Agosto. Synthetic and characterization aspects of dimethylaminoethyl methacrylate reversible addition fragmentation chain transfer (RAFT) polymerization. *J. Polym. Sci., Part A: Polym. Chem.*, 43(16):3551–3565, 2005.

[267] F. Sanda, T. Abe, and T. Endo. Syntheses and radical polymerizations of optically active (meth) acrylamides having amino acid moieties. *J. Polym. Sci., Part A: Polym. Chem.*, 35(13):2619–2629, 1997.

[268] P. Sanguansri and M. A. Augustin. Nanoscale materials development - -a food industry perspective. *Trends Food Sci. Technol.*, 17(10):547–556, 2006.

[269] N. Sanson and J. Rieger. Synthesis of nanogels/microgels by conventional and controlled radical crosslinking copolymerization. *Polym. Chem.*, 1(7):965–977, 2010.

[270] R. Say, S. Emir, B. Garipcan, S. Patir, and A. Denizli. Novel methacryloylamidophenylalanine functionalized porous chelating beads for adsorption of heavy metal ions. *Adv. Polym. Technol.*, 22(4):355–364, 2003.

[271] A. Schallon, V. Jérôme, A. Walther, C. Synatschke, A. Müller, and R. Freitag. Performance of three PDMAEMA-based polycation architectures as gene delivery agents in comparison to linear and branched PEI. *React. Funct. Polym.*, 70(1):1–10, 2010.

[272] A. Schmalz, M. Hanisch, H. Schmalz, and A. H. E. Müller. Double stimuli-responsive behavior of linear and star-shaped poly (*N,N*-diethylaminoethyl methacrylate) in aqueous solution. *Polymer*, 51(6):1213–1217, 2010.

[273] G. Schmalz, H. Langer, and H. Schweikl. Cytotoxicity of dental alloy extracts and corresponding metal salt solutions. *J. Dent. Res.*, 77(10):1772–1778, 1998.

[274] N. Sharifi-Sanjani, A. R. Mahdavian, and P. Bataille. Emulsion polymerization of styrene and DEAEMA with a core–shell structure. *J. Appl. Polym. Sci.*, 78(11):1977–1985, 2000.

[275] A. Shatkay and I. Michaeli. Potentiometric titrations of polyelectrolytes with separation of phases. *J. Phys. Chem.*, 70(12):3777–3782, 1966.

[276] M. Shiau, H. Chiou, Y. Lee, T. Kuo, and Y. Chang. Establishment of a consistent L929 bioassay system for TNF-α quantitation to evaluate the effect of lipopolysaccharide, phytomitogens and cytodifferentiation agents on cytotoxicity of TNF-α secreted by adherent human mononuclear cells. *Mediat. Inflamm.*, 10(4):199–208, 2001.

[277] D. A. Shipp. Reversible-deactivation radical polymerizations. *Polym. Rev.*, 51(2):99–103, 2011.

[278] R. Shrestha, M. Elsabahy, S. Florez-Malaver, S. Samarajeewa, and K. L. Wooley. Endosomal escape and siRNA delivery with cationic shell crosslinked knedel-like nanoparticles with tunable buffering capacities. *Biomaterials*, 33(33):8557–8568, 2012.

[279] D. Siegwart, M. Leiendecker, R. Langer, and D. Anderson. Automated ARGET ATRP accelerates catalyst optimization for the synthesis of thiol-functionalized polymers. *Macromolecules*, 45(3):1254–1261, 2012.

[280] D. J. Siegwart, J. K. Oh, and K. Matyjaszewski. ATRP in the design

of functional materials for biomedical applications. *Prog. Polym. Sci.*, 37(1):18–37, 2012.

[281] S. J. Sigg, F. Seidi, K. Renggli, T. B. Silva, G. Kali, and N. Bruns. Horseradish peroxidase as a catalyst for atom transfer radical polymerization. *Macromol. Rapid Commun.*, 32(21):1710–1715, 2011.

[282] Sigma-Aldrich. Material safety data sheet: Tetraethylene glycol dimethacrylate, January 2012.

[283] Sigma-Aldrich. Material safety data sheet: Tris(2-pyridylmethyl)amine, March 2012.

[284] A. Simakova, S. E. Averick, D. Konkolewicz, and K. Matyjaszewski. Aqueous ARGET ATRP. *Macromolecules*, 45(16):6371–6379, 2012.

[285] A. Simakova, M. Mackenzie, S. E. Averick, S. Park, and K. Matyjaszewski. Bioinspired iron-based catalyst for atom transfer radical polymerization. *Angew. Chem. Int. Ed.*, 2013. doi: 10.1002/anie.201306337.

[286] M. R. Simmons, E. N. Yamasaki, and C. S. Patrickios. Cationic amphiphilic model networks: Synthesis by group transfer polymerization and characterization of the degree of swelling. *Macromolecules*, 33(8):3176–3179, 2000.

[287] A. Singh, H. Nie, B. Ghosn, H. Qin, L. W. Kwak, and K. Roy. Efficient modulation of T-cell response by dual-mode, single-carrier delivery of

cytokine-targeted siRNA and DNA vaccine to antigen-presenting cells. *Mol. Ther.*, 16(12):2011–2021, 2008.

[288] T. J. Singh and S. V. Bhat. Morphology and conductivity studies of a new solid polymer electrolyte:(PEG) xLiClO4. *Bull. Mater. Sci.*, 26(7):707–714, 2003.

[289] V. R. Sinha and R. Kumria. Polysaccharides in colon-specific drug delivery. *Int. J. Pharm.*, 224(1):19–38, 2001.

[290] V. R. Sinha and R. Kumria. Microbially triggered drug delivery to the colon. *Eur. J. Pharm. Sci.*, 18(1):3–18, 2003.

[291] C. A. Stein and J. S. Cohen. Oligodeoxynucleotides as inhibitors of gene expression: a review. *Cancer Res.*, 48(10):2659, 1988.

[292] M. Stenzel. RAFT polymerization: an avenue to functional polymeric micelles for drug delivery. *Chem. Commun.*, (30):3486–3503, 2008.

[293] F. Stoffelbach, N. Griffete, C. Bui, and B. Charleux. Use of a simple surface-active initiator in controlled/living free-radical miniemulsion polymerization under AGET and ARGET ATRP conditions. *Chem. Commun.*, (39):4807–4809, 2008.

[294] K. Sui, X. Shan, S. Gao, Y. Xia, Q. Zheng, and D. Xie. Dual-responsive supramolecular inclusion complexes of block copolymer poly (ethylene glycol)-block-poly [(2-dimethylamino) ethyl methacrylate] with α-

cyclodextrin. *J. Polym. Sci., Part A: Polym. Chem.*, 48(10):2143–2153, 2010.

[295] T.-M. Sun, J.-Z. Du, L.-F. Yan, H.-Q. Mao, and J. Wang. Self-assembled biodegradable micellar nanoparticles of amphiphilic and cationic block copolymer for siRNA delivery. *Biomaterials*, 29(32):4348–4355, 2008.

[296] D. V. Svintradze and G. M. Mrevlishvili. Fiber molecular model of atelocollagen-small interfering RNA (siRNA) complex. *Int. J. Biol. Macromol.*, 37(5):283–286, 2005.

[297] C. V. Synatschke, A. Schallon, V. Jérôme, R. Freitag, and A. H. E. Müller. Influence of polymer architecture and molecular weight of poly (2-(dimethylamino) ethyl methacrylate) polycations on transfection efficiency and cell viability in gene delivery. *Biomacromolecules*, 12(12):4247–4255, 2011.

T

[298] K. Tahara, T. Sakai, H. Yamamoto, H. Takeuchi, and Y. Kawashima. Establishing chitosan coated PLGA nanosphere platform loaded with wide variety of nucleic acid by complexation with cationic compound for gene delivery. *Int. J. Pharm.*, 354(1-2):210–216, 2008.

[299] K. Tahara, S. Samura, K. Tsuji, H. Yamamoto, Y. Tsukada, Y. Bando, H. Tsujimoto, R. Morishita, and Y. Kawashima. Oral nuclear factor-κB decoy oligonucleotides delivery system with chitosan modified poly

(D,L-lactide-co-glycolide) nanospheres for inflammatory bowel disease. *Biomaterials*, 32(3):870–878, 2011.

[300] A. Tamura, M. Oishi, and Y. Nagasaki. Enhanced cytoplasmic delivery of siRNA using a stabilized polyion complex based on PEGylated nanogels with a cross-linked polyamine structure. *Biomacromolecules*, 10(7):1818–1827, 2009.

[301] J. H. Tan, N. A. J. McMillan, E. Payne, C. Alexander, F. Heath, A. K. Whittaker, and K. J. Thurecht. Hyperbranched polymers as delivery vectors for oligonucleotides. *J. Polym. Sci., Part A: Polym. Chem.*, 50(13):2585–2595, 2012.

[302] TEVA Pharmaceuticals USA, Inc. Paragard intrauterine copper contraceptive, 2012. http://www.paragard.com/default.aspx.

[303] TEVA Pharmaceuticals USA, Inc. *Prescribing Information: ParaGard T 380A Intrauterine Copper Contraceptive*, 2012.

[304] Q. Tian, S. B. Stepaniants, M. Mao, L. Weng, M. C. Feetham, M. J. Doyle, C. Y. Eugene, H. Dai, V. Thorsson, J. Eng, D. Goodlett, J. P. Berger, B. Gunter, P. S. Linseley, R. B. Stoughton, R. Aebersold, S. J. Collins, W. A. Hanlon, and H. L. E. Integrated genomic and proteomic analyses of gene expression in mammalian cells. *Mol. Cell. Proteomics*, 3(10):960–969, 2004.

[305] K. Tiemann and J. J. Rossi. RNAi-based therapeutics-current status, challenges and prospects. *EMBO Mol. Med.*, 1(3):142–151, 2009.

[306] L. G. Tillman, R. S. Geary, and G. E. Hardee. Oral delivery of antisense oligonucleotides in man. *J. Pharm. Sci.*, 97(1):225–236, 2008.

[307] A. W. Tong, C. M. Jay, N. Senzer, P. B. Maples, and J. Nemunaitis. Systemic therapeutic gene delivery for cancer: Crafting Paris' arrow. *Curr. Gene Ther.*, 9(1):45–60, 2009.

[308] H. H. Tønnesen and J. Karlsen. Alginate in drug delivery systems. *Drug Dev. Ind. Pharm.*, 28(6):621–630, 2002.

[309] N. V. Tsarevsky. Catalytic activity and performance of copper-based complexes mediating atom transfer radical polymerization. *Isr. J. Chem.*, 52(3-4):276–287, 2012.

[310] N. V. Tsarevsky and K. Matyjaszewski. Environmentally benign atom transfer radical polymerization: Towards "green" processes and materials. *J. Polym. Sci., Part A: Polym. Chem.*, 44(17):5098–5112, 2006.

[311] D. Türkmen, N. Öztürk, S. Akgöl, A. Elkak, and A. Denizli. Phenylalanine containing hydrophobic nanospheres for antibody purification. *Biotechnol. Prog.*, 24(6):1297–1303, 2008.

U

[312] M. N. Uddin, N. J. Patel, T. Bhowmik, B. D'Souza, A. Akalkotkar, F. Etzlar, C. W. Oettinger, and M. D'Souza. Enhanced bioavailability of orally administered antisense oligonucleotide to nuclear factor kappa B mRNA after microencapsulation with albumin. *J. Drug Targeting*, 21(5):450–457, 2013.

[313] United States Environmental Protection Agency. Basic information about copper in drinking water, 2012. http://water.epa.gov/drink/contaminants/basicinformation/copper.cfm.

[314] Z. ur Rehman, I. S. Zuhorn, and D. Hoekstra. How cationic lipids transfer nucleic acids into cells and across cellular membranes: Recent advances. *J. Control. Release*, 166(1):46–56, 2013.

[315] U.S. Food and Drug Administration. CFR - Code of Federal Regulations Title 21 Sec. 172.860 Fatty acids, 2011. http://www.accessdata.fda.gov/scripts/cdrh/cfdocs/cfcfr/CFRSearch.cfm?fr=172.863.

[316] U.S. Food and Drug Administration. CFR - Code of Federal Regulations Title 21 Sec. 172.863 Salts of Fatty Acids, 2011. http://www.accessdata.fda.gov/scripts/cdrh/cfdocs/cfcfr/CFRSearch.cfm?fr=172.860.

[317] U.S. Food and Drug Administration. Everything Added to Food in the United States (EAFUS), 2011. http://www.fda.gov/Food/FoodIngredientsPackaging/ucm115326.htm.

[318] U.S. Food and Drug Administration. Everything Added to Food in the United States (EAFUS): Database, 2012. http://www.accessdata.fda.gov/scripts/fcn/fcnNavigation.cfm?rpt=eafusListing.

V

[319] K. Van Butsele, M. Morille, C. Passirani, P. Legras, J. P. Benoit, S. K. Varshney, R. Jérôme, and C. Jérôme. Stealth properties of poly(ethylene oxide)-based triblock copolymer micelles: A prerequisite for a pH-triggered targeting system. *Acta. Biomater.*, 7(10):3700–3707, 2011.

[320] P. van de Wetering, J. Cherng, H. Talsma, D. J. A. Crommelin, and W. E. Hennink. 2-(Dimethylamino) ethyl methacrylate based (co) polymers as gene transfer agents. *J. Control. Release*, 53(1):145–153, 1998.

[321] P. van de Wetering, E. E. Moret, N. M. E. Schuurmans-Nieuwenbroek, M. J. van Steenbergen, and W. E. Hennink. Structure-activity relationships of water-soluble cationic methacrylate/methacrylamide polymers for nonviral gene delivery. *Bioconjugate Chem.*, 10(4):589–597, 1999.

[322] S. Vermeire, D. P. McGovern, G. Van Assche, and P. Rutgeerts. *Genetics of Inflammatory Bowel Disease: How Modern Genomics Informs Basic, Clinical and Translational Science, Inflammatory Bowel Disease: Translating basic science into clinical practice*. Wiley Online Library, 2010.

[323] T. Vickers and S. Crooke. siRNAs targeted to certain polyadenylation sites promote specific, RISC-independent degradation of messenger RNAs. *Nucleic Acids Res.*, 40(13):6223–6234, 2012.

W

[324] G. Wallraff, J. Hutchinson, W. Hinsberg, F. Houle, P. Seidel, R. Johnson, and W. Oldham. Thermal and acid-catalyzed deprotection kinetics in candidate deep ultraviolet resist materials. *J. Vac. Sci. Technol. B*, 12(6):3857–3862, 1994.

[325] T. Wang, J. R. Upponi, and V. P. Torchilin. Design of multifunctional non-viral gene vectors to overcome physiological barriers: Dilemmas and strategies. *Int. J. Pharm.*, 427(1):3–20, 2012.

[326] J. Wataha. Biocompatibility of dental casting alloys: a review. *J. Prosthet. Dent.*, 83(2):223–234, 2000.

[327] J. C. Wataha, C. T. Hanks, and R. G. Craig. The *in vitro* effects of metal cations on eukaryotic cell metabolism. *J. Biomed. Mater. Res.*, 25(9):1133–1149, 1991.

[328] J. K. Watts and D. R. Corey. Silencing disease genes in the laboratory and the clinic. *J. Pathol.*, 226(2):365–379, 2011.

[329] J. V. M. Weaver, Y. Tang, S. Liu, P. D. Iddon, R. Grigg, N. C. Billingham, S. P. Armes, R. Hunter, and S. P. Rannard. Preparation of shell

cross-linked micelles by polyelectrolyte complexation. *Angew. Chem.*, 116(11):1413–1416, 2004.

[330] J. V. M. Weaver, R. T. Williams, B. J. L. Royles, P. H. Findlay, A. I. Cooper, and S. P. Rannard. pH-Responsive branched polymer nanoparticles. *Soft Matter*, 4(5):985–992, 2008.

[331] W. Wei, P. Lv, X. Chen, Z. Yue, Q. Fu, S. Liu, H. Yue, and G. Ma. Codelivery of mTERT siRNA and paclitaxel by chitosan-based nanoparticles promoted synergistic tumor suppression. *Biomaterials*, 34(15):3912–3923, 2013.

[332] J. Weiss, P. Takhistov, and D. J. McClements. Functional materials in food nanotechnology. *J. Food Sci.*, 71(9):R107–R116, 2006.

[333] K. A. Whitehead, J. E. Dahlman, R. S. Langer, and D. G. Anderson. Silencing or stimulation? siRNA delivery and the immune system. *Annu. Rev. Chem. Biomol.*, 2(1):77–96, 2011.

[334] K. A. Whitehead, R. Langer, and D. G. Anderson. Knocking down barriers: advances in siRNA delivery. *Nat. Rev. Drug Discov.*, 8(2):129–138, 2009.

[335] D. S. Wilson, G. Dalmasso, L. Wang, S. V. Sitaraman, D. Merlin, and N. Murthy. Orally delivered thioketal nanoparticles loaded with TNF-α siRNA target inflammation and inhibit gene expression in the intestines. *Nat. Mater.*, 9(11):923–928, 2010.

[336] C. Wu and S. Zhou. Volume phase transition of swollen gels: Discontinuous or continuous? *Macromolecules*, 30(3):574–576, 1997.

[337] L. Wu, J. Zhang, and W. Watanabe. Physical and chemical stability of drug nanoparticles. *Adv. Drug Deliver. Rev.*, 63(6):456–469, 2011.

[338] G. Wulff, B. Chong, and U. Kolb. Soluble single-molecule nanogels of controlled structure as a matrix for efficient artificial enzymes. *Angew. Chem., Int. Ed.*, 45(18):2955–2958, 2006.

X

[339] T. Xing, S. Li, X. Xu, and G. Chen. Structure and properties of silk grafted with *N, N*-dimethylaminoethyl methacrylate via the ARGET ATRP method. *J. Eng. Fiber Fabr.*, Retrieved from http://www.jeffjournal.org/(Special Issue: Fibers), 2012.

[340] Q. Xiong, P. Ni, F. Zhang, and Z. Yu. Synthesis and characterization of 2-(dimethylamino)ethyl methacrylate homopolymers via aqueous RAFT polymerization and their application in miniemulsion polymerization. *Polym. Bull.*, 53(1):1–8, 2004.

[341] F. Xu, K. Neoh, and E. Kang. Bioactive surfaces and biomaterials via atom transfer radical polymerization. *Prog. Polym. Sci.*, 34(8):719–761, 2009.

Y

[342] M. Yang and J. Mattes. Discovery, biology and therapeutic potential of RNA interference, microRNA and antagomirs. *Pharmacol. Ther.*, 117(1):94–104, 2008.

[343] X. Z. Yang, S. Dou, T. M. Sun, C. Q. Mao, H. X. Wang, and J. Wang. Systemic delivery of siRNA with cationic lipid assisted PEG-PLA nanoparticles for cancer therapy. *J. Control. Release*, 156(2):203–211, 2011.

[344] Y. Q. Yang, W. J. Lin, L. J. Zhang, C. Z. Cai, W. Jiang, X. D. Guo, and Y. Qian. Synthesis, characterization and pH-responsive self-assembly behavior of amphiphilic multiarm star triblock copolymers based on PCL, PDEAEMA, and PEG. *Macromol. Res.*, 21(9):1011–1020, 2013.

[345] J. Yoo, D. J. Irvine, D. E. Discher, and S. Mitragotri. Bio-inspired, bioengineered and biomimetic drug delivery carriers. *Nat. Rev. Drug Discov.*, 10(7):521–535, 2011.

[346] J. Yoon, J. Oh, W. Li, T. Kowalewski, and K. Matyjaszewski. *ATRP: A Versatile Tool toward Uniformly Crosslinked Hydrogels with Controlled Architecture and Multifunctionality, Hydrogel Micro and Nanoparticles*. Wiley Online Library, 2012.

[347] E. Yoshii. Cytotoxic effects of acrylates and methacrylates: Relation-

ships of monomer structures and cytotoxicity. *J. Biomed. Mater. Res.*, 37(4):517–524, 1997.

[348] S. Yusa, M. Sugahara, T. Endo, and Y. Morishima. Preparation and characterization of a pH-responsive nanogel based on a photo-cross-linked micelle formed from block copolymers with controlled structure. *Langmuir*, 25(9):5258–5265, 2009.

Z

[349] F. Zeng, Y. Shen, S. Zhu, and R. Pelton. Atom transfer radical polymerization of 2-(dimethylamino) ethyl methacrylate in aqueous media. *J. Polym. Sci., Part A: Polym. Chem.*, 38(20):3821–3827, 2000.

[350] J. Zhang, C. He, C. Tang, and C. Yin. Ternary polymeric nanoparticles for oral siRNA delivery. *Pharm. Res.*, 30(5):1228–1239, 2013.

[351] J. Zhang, C. Tang, and C. Yin. Galactosylated trimethyl chitosan–cysteine nanoparticles loaded with *Map4k4* siRNA for targeting activated macrophages. *Biomaterials*, 34(14):3667–3677, 2013.

[352] W. Zhang, J. He, Z. Liu, P. Ni, and X. Zhu. Biocompatible and ph-responsive triblock copolymer mPEG-b-PCL-b-PDMAEMA: Synthesis, self-assembly, and application. *J. Polym. Sci., Part A: Polym. Chem.*, 48(5):1079–1091, 2010.

[353] Y. Zhang, A. Aigner, and S. Agarwal. Degradable and biocompatible poly (*N, N*-dimethylaminoethyl methacrylate-co-caprolactone) s as dna transfection agents. *Macromol. Biosci.*, 13(9):1267–1275, 2013.

[354] Y. Zhang, A. Satterlee, and L. Huang. *In vivo* gene delivery by nonviral vectors: Overcoming hurdles? *Mol. Ther.*, 20(7):1298–1304, 2012.

[355] Y. Zhang, M. Zheng, T. Kissel, and S. Agarwal. Design and biophysical characterization of bioresponsive degradable poly(dimethylaminoethyl methacrylate) based polymers for in vitro DNA transfection. *Biomacromolecules*, 13:313–322, 2012.

[356] C. Zhu, S. Jung, S. Luo, F. Meng, X. Zhu, T. G. Park, and Z. Zhong. Co-delivery of siRNA and paclitaxel into cancer cells by biodegradable cationic micelles based on PDMAEMA-PCL-PDMAEMA triblock copolymers. *Biomaterials*, 31(8):2408–2416, 2010.

[357] J. Zoldan, A. K. R. Lytton-Jean, E. D. Karagiannis, K. Deiorio-Haggar, L. M. Bellan, R. Langer, and D. G. Anderson. Directing human embryonic stem cell differentiation by non-viral delivery of siRNA in 3D culture. *Biomaterials*, 32(31):7793–7800, 2011.

Vita

Diane Forbes was born in Lawrence, Kansas and grew up in Des Moines, Iowa where she attended Johnston High School and Des Moines Central Academy. After graduation from high school, she participated in biotechnology research in Mexico as a World Food Prize Borlaug-Ruan International Intern. Diane studied chemical engineering as an undergraduate at Iowa State University. As a first-year student, she worked with Dr. Brent Shanks in catalysis research. In following years, Diane worked with plant metabolic engineering researcher Dr. Jacqueline Shanks on an Honors Research Project for alkaloid extraction and purification from *Catharanthus roseus* hairy root tissue. After receiving a B.S. from Iowa State University, Diane joined the Department of Chemical Engineering at the University of Texas at Austin as a National Science Foundation Graduate Research Fellow. She completed the research described in this thesis under the direction of Dr. Nicholas Peppas.

Permanent address: DianeCForbes@gmail.com

This dissertation was typeset with LaTeX[†] by the author.

[†]LaTeX is a document preparation system developed by Leslie Lamport as a special version of Donald Knuth's TeX Program.